STATE OF THE CLIMATE IN 2023

REGIONAL CLIMATES

A. Arguez, P. Bissolli, C. Ganter, R. Martinez, A. Mekonnen, L. Stevens, and Z. Zhu, Eds.

Special Online Supplement to the *Bulletin of the American Meteorological Society*, Vol. 105, No. 8, August 2024

https://doi.org/10.1175/2024BAMSStateoftheClimate_Chapter7.1

Corresponding authors:
North America: Laura Stevens / Laura.Stevens@noaa.gov
Central America and the Caribbean: Anthony Arguez / Anthony.Arguez@noaa.gov
South America: Rodney Martinez / rmartinez@wmo.int
Africa: Ademe Mekonnen / amekonne@ncat.edu
Europe: Peter Bissolli / Peter.Bissolli@dwd.de
Asia: Zhiwei Zhu / zwz@nuist.edu.cn
Oceania: Catherine Ganter / Catherine.Ganter@bom.gov.au

STATE OF THE CLIMATE IN 2023
Regional Climates

Editors

Jessica Blunden
Tim Boyer

Chapter Editors

Anthony Arguez
Josh Blannin
Peter Bissolli
Kyle R. Clem
Howard J. Diamond
Matthew L. Druckenmiller
Robert J. H. Dunn
Catherine Ganter
Nadine Gobron
Gregory C. Johnson
Rick Lumpkin
Rodney Martinez
Ademe Mekonnen
John B. Miller
Twila A. Moon
Marilyn N. Raphael
Carl J. Schreck III
Laura Stevens
Richard L. Thoman
Kate M. Willett
Zhiwei Zhu

Technical Editor

Lukas Noguchi

BAMS Special Editor for Climate

Timothy DelSole

American Meteorological Society

Cover Credit:
Wildfire EWF-031 located southeast of Edson in Alberta, Canada, on 5 May 2023. (Photo credit: Alberta Forestry and Parks)

How to cite this document:
Regional Climates is one chapter from the *State of the Climate in 2023* annual report and is available from https://doi.org/10.1175/2024BAMSStateoftheClimate_Chapter7.1. Compiled by NOAA's National Centers for Environmental Information, *State of the Climate in 2023* is based on contributions from scientists from around the world. It provides a detailed update on global climate indicators, notable weather events, and other data collected by environmental monitoring stations and instruments located on land, water, ice, and in space. The full report is available from https://doi.org/10.1175/2024BAMSStateoftheClimate.1.

Citing the complete report:
Blunden, J. and T. Boyer, Eds., 2024: "State of the Climate in 2023". *Bull. Amer. Meteor. Soc.*, **105** (8), Si–S483 https://doi.org/10.1175/2024BAMSStateoftheClimate.1.

Citing this chapter:
Arguez, A., Bissolli, P., C. Ganter, R. Martinez, A. Mekonnen, L. Stevens, and Z. Zhu, Eds., 2024: Regional Climates [in "State of the Climate in 2023"]. *Bull. Amer. Meteor. Soc.*, **105** (8), S371–S484, https://doi.org/10.1175/2024BAMSStateoftheClimate_Chapter7.1.

Citing a section (example):
Kabidi, K., A. Sayouri, M. ElKharrim, S. Hakmi, and A. E. Mostafa, 2024: North Africa [in "State of the Climate in 2023"]. *Bull. Amer. Meteor. Soc.*, **105** (8), S406–S408, https://doi.org/10.1175/2024BAMSStateoftheClimate_Chapter7.1.

Editor and Author Affiliations (alphabetical by name)

Agyakwah, W., NOAA/NWS National Centers for Environmental Prediction Climate Prediction Center, College Park, Maryland

Ahmadpour, Somayeh, Brandenburg University of Technology (BTU), Cottbus-Senftenberg, Germany

Aldeco, Laura S., Servicio Meteorológico Nacional, Buenos Aires, Argentina

Alfaro, Eric J., Center for Geophysical Research and School of Physics, University of Costa Rica, San José, Costa Rica

Alves, Lincoln M., Centro Nacional de Monitoramento e Alertas de Desastres Naturais CEMADEN, São Paulo, Brazil

Amador, Jorge A., Center for Geophysical Research and School of Physics, University of Costa Rica, San José, Costa Rica

Andrade, B., Seychelles Meteorological Authority, Mahe, Seychelles

Arguez, Anthony, NOAA/NESDIS National Centers for Environmental Information, Asheville, North Carolina

Avalos, Grinia, Servicio Nacional de Meteorología e Hidrología del Perú, Lima, Perú

Bardin, M. Yu., Yu. A. Izrael Institute of Global Climate and Ecology, Institute of Geography, Russian Academy of Sciences, Moscow, Russia

Beauchemin, Marc, Environment and Climate Change Canada, Montreal, Canada

Bekele, E., NOAA/NWS National Centers for Environmental Prediction Climate Prediction Center, College Park, Maryland

Berne, Christine, Météo France, Toulouse, France

Bissolli, Peter, Deutscher Wetterdienst, WMO RA VI Regional Climate Centre Network, Offenbach, Germany

Bochníček, Oliver, Slovak Hydrometeorological Institute, Bratislava, Slovakia

Bukunt, Brandon, NOAA/NWS Weather Forecast Office, Tiyan, Guam

Calderón, Blanca, Center for Geophysical Research, University of Costa Rica, San José, Costa Rica

Campbell, Jayaka, Department of Physics, The University of the West Indies, Kingston, Jamaica

Chandler, Elise, Bureau of Meteorology, Melbourne, Australia

Charlton, Candice S., Department of Physics, The University of the West Indies, Kingston, Jamaica

Chen, Jack, Environment and Climate Change Canada, Ottawa, Canada

Cheng, Vincent Y. S., Environment and Climate Change Canada, Toronto, Canada

Chisholm, Lucy, Environment and Climate Change Canada, Halifax, Canada

Clarke, Leonardo, Department of Physics, The University of the West Indies, Kingston, Jamaica

Correa, Kris, Servicio Nacional de Meteorología e Hidrología del Perú, Lima, Perú

Costa, Felipe, Centro Internacional para la Investigación del Fenómeno de El Niño (CIIFEN), Guayaquil, Ecuador

Cunha, Ana P., Centro Nacional de Monitoramento e Alertas de Desastres Naturais CEMADEN, São Paulo, Brazil

De Bock, Veerle, Royal Meteorological Institute, Ukkel, Belgium

Dindyal, S., Mauritius Meteorological Service, Vacoas, Mauritius

Dulamsuren, Dashkhuu, Institute of Meteorology, Hydrology and Environment, National Agency for Meteorology, Ulaanbaatar, Mongolia

Echeverría Garcés, Paola, Instituto Nacional de Meteorología e Hidrología de Ecuador (INAMHI), Quito, Ecuador

Ekici, Mithat, Turkish State Meteorological Service, Ankara, Türkiye

ElKharrim, M., General Directorate of Meteorology, Rabat, Morocco

Espinoza, Jhan-Carlo, Université Grenoble Alpes, Institut des Géosciences de l'Environnement, IRD, CNRS, Grenoble INP, Grenoble, France

Fenimore, Chris, NOAA/NESDIS National Centers for Environmental Information, Asheville, North Carolina

Fu, Shanshan, Nanjing University of Information Science and Technology, Nanjing, China

Ganter, Catherine, Bureau of Meteorology, Melbourne, Australia

Gevorgyan, Artur, Hydrometeorology and Monitoring Center, Yerevan, Armenia

Gleason, Karin, NOAA/NESDIS National Centers for Environmental Information, Asheville, North Carolina

Gómez Camacho, Julio, National Meteorological Service of Mexico, Mexico City, Mexico

González Hernández, Yolanda, Centro Internacional para la Investigación del Fenómeno de El Niño (CIIFEN), Guayaquil, Ecuador

Hakmi, S., General Directorate of Meteorology, Rabat, Morocco

Heim, Richard R. Jr., NOAA/NESDIS National Centers for Environmental Information, Asheville, North Carolina

Hicks, J., NOAA/NWS National Centers for Environmental Prediction Climate Prediction Center, College Park, Maryland

Hidalgo, Hugo G., Center for Geophysical Research and School of Physics, University of Costa Rica, San José, Costa Rica

Huang, Hongjie, Nanjing University of Information Science and Technology, Nanjing, China

Jadra, Gerardo, Instituto Uruguayo de Meteorología, Montevideo, Uruguay

Jain, Piyush, Natural Resources Canada, Edmonton, Canada

Jumaux, G., Meteo France, Direction Interregionale Pour L'Ocean Indien, Reunion

Kabidi, K., General Directorate of Meteorology, Rabat, Morocco

Kazemi, Amin Fazl, Iran National Meteorology Organization, Tehran, Iran

Kendon, Michael, Met Office Hadley Centre, Exeter, United Kingdom

Kennedy, John, Independent Researcher, Verdun, France

Khalatyan, Yelena, Hydrometeorology and Monitoring Center, Yerevan, Armenia

Khan, Valentina, Hydrometeorological Centre of Russia, World Meteorological Organization (WMO) North EurAsia Climate Center, Moscow, Russia

Khiem, Mai Van, National Center for Hydro-Meteorological Forecasting, Vietnam Meteorological and Hydrological Administration, Hanoi, Vietnam

Kirchmeier-Young, Megan, Environment and Climate Change Canada, Toronto, Canada

Korshunova, Natalia N., All-Russia Research Institute of Hydrometeorological Information, World Data Center, Obninsk, Russia

Kruger, A. C., Climate Service, South African Weather Service, Pretoria, South Africa

Lakatos, Mónika, Climatology Unit, Hungarian Meteorological Service, Budapest, Hungary

Lam, Hoang Phuc, National Center for Hydro-Meteorological Forecasting, Vietnam Meteorological and Hydrological Administration, Hanoi, Vietnam

Lavado-Casimiro, Waldo, Servicio Nacional de Meteorología e Hidrología del Perú, Lima, Perú

Lee, Tsz-Cheung, Hong Kong Observatory, Hong Kong, China

Lu, Rui, Nanjing University of Information Science and Technology, Nanjing, China

Mamen, Jostein, Climate Division, Norwegian Meteorological Institute, Oslo, Norway

Marengo, Jose A., Centro Nacional de Monitoramento e Alertas de Desastres Naturais CEMADEN, São Paulo, Brazil

Marjan, Mohammadi, Iran National Meteorology Organization, Tehran, Iran

Martinez, Rodney, World Meteorological Organization, San Jose, Costa Rica

McBride, C., Climate Service, South African Weather Service, Pretoria, South Africa

Mekonnen, Ademe, North Carolina A&T University, Greensboro, North Carolina

Meyers, Tristan, National Institute of Water and Atmospheric Research (NIWA), Auckland, New Zealand

Minney, Caitlin, Bureau of Meteorology, Melbourne, Australia

Moise, Aurel, Centre for Climate Research Singapore, Meteorological Service Singapore, Singapore

Molina-Carpio, Jorge, Universidad Mayor de San Andrés, La Paz, Bolivia

Moody, Ronald, Meteorological Service Jamaica, Kingston, Jamaica

Mora, Natali, Center for Geophysical Research, University of Costa Rica, San José, Costa Rica

Mostafa, A. E., Department of Seasonal Forecast and Climate Research, Cairo Numerical Weather Prediction, Egyptian Meteorological Authority, Cairo, Egypt

Muharsyah, Robi, Division of Climate Variability Analysis, Meteorological, Climatological, and Geophysical Agency, Jakarta, Indonesia

Editor and Author Affiliations (continued)

Okunaka, Yuka, Tokyo Climate Center, Japan Meteorological Agency, Tokyo, Japan

Orlik, Alexander, GeoSphere, Vienna, Austria

Pascual Ramírez, Reynaldo, National Meteorological Service of Mexico, Mexico City, Mexico

Porat, Amos, Israel Meteorological Service, Bet Dagan, Israel

Quispe, Willy R., Servicio Nacional de Meteorología e Hidrología de Bolivia, La Paz, Bolivia

Ramos, Andrea M., Instituto Nacional de Meteorología, Brasilia, Brazil

Ressl, Hans, GeoSphere, Vienna, Austria

Rivera, Patricia P., Servicio Nacional de Meteorología e Hidrología del Perú, Lima, Perú

Robjhon, M., NOAA/NWS National Centers for Environmental Prediction Climate Prediction Center, College Park, Maryland

Rodriguez Guisado, Esteban, Agencia Estatal de Meteorología, Madrid, Spain

Roebeling, Maarit, Deutscher Wetterdienst, WMO RA VI Regional Climate Centre Network, Offenbach, Germany

Ronchail, Josyane, Laboratoire LOCEAN-IPSL, Paris, France

Rösner, Benjamin, Remote Sensing Section, Deutscher Wetterdienst, Offenbach, Germany

Sabeerali, C. T., India Meteorological Department, Ministry of Earth Sciences, Pune, India

Salinas, Roberto, Dirección de Meteorología e Hidrología / Dirección Nacional de Aeronáutica Civil, Asunción, Paraguay

Sayouri, A., General Directorate of Meteorology, Rabat, Morocco

Segele, Z. T., NOAA/NWS National Centers for Environmental Prediction Climate Prediction Center, College Park, Maryland

Sensoy, Serhat, Turkish State Meteorological Service, Ankara, Türkiye

Seong, Ji-In, Climate Change Monitoring Division, Korea Meteorological Administration, Seoul, South Korea

Serna Cuenca, Julieta, Instituto de Hidrología, Meteorología y Estudios Ambientales de Colombia (IDEAM), Bogotá, Colombia

Shukla, R., ERT, Laurel, Maryland

Smith, Adam, NOAA/NESDIS National Centers for Environmental Information, Asheville, North Carolina

Spence-Hemmings, Jacqueline, Meteorological Service Jamaica, Kingston, Jamaica

Spillane, Sandra, Met Éireann, Dublin, Ireland

Sreejith, O. P., India Meteorological Department, Ministry of Earth Sciences, Pune, India

Srivastava, A. K., India Meteorological Department, Ministry of Earth Sciences, Pune, India

Stella, Jose L., Servicio Meteorológico Nacional, Buenos Aires, Argentina

Stephenson, Tannecia S., Department of Physics, The University of the West Indies, Kingston, Jamaica

Stevens, Laura, Cooperative Institute for Satellite Earth System Studies, North Carolina State University, Asheville, North Carolina

Takahashi, Kiyotoshi, Tokyo Climate Center, Japan Meteorological Agency, Tokyo, Japan

Takemura, Kazuto, Tokyo Climate Center, Japan Meteorological Agency, Tokyo, Japan

Taylor, Michael A., Department of Physics, The University of the West Indies, Kingston, Jamaica

Thiaw, W. M., NOAA/NWS National Centers for Environmental Prediction Climate Prediction Center, College Park, Maryland

Trachte, Katja, Brandenburg University of Technology (BTU), Cottbus-Senftenberg, Germany

Trotman, Adrian, Caribbean Institute for Meteorology and Hydrology, Bridgetown, Barbados

van der Linden, Roderick, Deutscher Wetterdienst, Offenbach, Germany

van der Schrier, Gerard, Royal Netherlands Meteorological Institute (KNMI), De Bilt, The Netherlands

Van Meerbeeck, Cédric J., Caribbean Institute for Meteorology and Hydrology, Bridgetown, Barbados

Vazife, Ahad, Iran National Meteorology Organization, Tehran, Iran

Virasami, R., Mauritius Meteorological Service, Vacoas, Mauritius

Willems, An, Royal Meteorological Institute, Ukkel, Belgium

Wu, Francis, Environment and Climate Change Canada, Vancouver, Canada

Zhang, Peiqun, Beijing Climate Center, Beijing, China

Zhu, Zhiwei, Nanjing University of Information Science and Technology, Nanjing, China

Editorial and Production Team

Allen, Jessicca, Graphics Support, Cooperative Institute for Satellite Earth System Studies, North Carolina State University, Asheville, North Carolina

Camper, Amy V., Graphics Support, Innovative Consulting and Management Services, LLC, NOAA/NESDIS National Centers for Environmental Information, Asheville, North Carolina

Haley, Bridgette O., Graphics Support, NOAA/NESDIS National Centers for Environmental Information, Asheville, North Carolina

Hammer, Gregory, Content Team Lead, Communications and Outreach, NOAA/NESDIS National Centers for Environmental Information, Asheville, North Carolina

Love-Brotak, S. Elizabeth, Lead Graphics Production, NOAA/NESDIS National Centers for Environmental Information, Asheville, North Carolina

Ohlmann, Laura, Technical Editor, Innovative Consulting and Management Services, LLC, NOAA/NESDIS National Centers for Environmental Information, Asheville, North Carolina

Noguchi, Lukas, Technical Editor, Innovative Consulting and Management Services, LLC, NOAA/NESDIS National Centers for Environmental Information, Asheville, North Carolina

Riddle, Deborah B., Graphics Support, NOAA/NESDIS National Centers for Environmental Information, Asheville, North Carolina

Veasey, Sara W., Visual Communications Team Lead, Communications and Outreach, NOAA/NESDIS National Centers for Environmental Information, Asheville, North Carolina

7. Table of Contents

7. Table of Contents

7. REGIONAL CLIMATES

A. Arguez, P. Bissolli, C. Ganter, R. Martinez, A. Mekonnen, L. Stevens, and Z. Zhu, Eds.

a. Overview

This chapter provides summaries of the 2023 temperature and precipitation conditions across seven broad regions: North America, Central America and the Caribbean, South America, Africa, Europe and the Middle East, Asia, and Oceania. In most cases, summaries of notable weather events are also included. Local scientists provided the annual summary for their respective regions and, unless otherwise noted, the source of the data used is typically the agency affiliated with the authors. The base period used for these analyses is 1991–2020, unless otherwise stated. Please note that on occasion different nations, even within the same section, may use unique periods to define their normal. Section introductions typically define the prevailing practices for that section, and exceptions will be noted within the text. In a similar way, many contributing authors use languages other than English as their primary professional language. To minimize additional loss of fidelity through re-interpretation after translation, editors have been conservative and careful to preserve the voice of the author. In some cases, this may result in abrupt transitions in style from section to section.

b. North America

—L. Stevens, Ed.

Above-average temperatures were observed across Canada, large portions of the contiguous United States, and the majority of Mexico in 2023, with record-high annual temperatures in many locations. All other regions were near or slightly below average. Averaged as a whole, North America's annual temperature was 1.13°C above the 1991–2020 base period and was the warmest year in the 114-year continental record (extends back to 1910).

Precipitation varied across North America in 2023. All three countries experienced widespread drought events, with Mexico reporting its driest year on record (since 1950).

Several extreme events occurred during the year, including a record-breaking Canadian wildfire season (Sidebar 7.1). Other notable events included heavy rainfall and flooding in Nova Scotia (NS), heatwaves in both the United States and Mexico, and Hurricane Otis.

Information in this section relates to the geographic continent of North America. Regions of the United States outside the contiguous United States are described in other sections of the report: Alaska (Chapter 5), Puerto Rico (section 7c1), and Guam and the U.S.-Affiliated Pacific Islands (section 7h2). Limited temperature and precipitation data are available for Hawaii but will be included in future reports. Tropical cyclone events affecting all regions are described in Chapter 4.

Anomalies in this section are all with respect to the 1991–2020 base period, unless otherwise noted.

1. CANADA

—V. Y. S. Cheng, F. Wu, M. Beauchemin, and L. Chisholm

Overall, Canada had its second-warmest year on record. National average temperatures for summer and autumn of 2023 were the highest recorded in the nation's 76-year record (1948–2023). National winter and spring temperatures were also above the 1991–2020 average. The temperature records presented in this section are based on adjusted and homogenized Canadian climate data.

(i) Temperature

The annual 2023 average temperature for Canada was 1.8°C above the 1991–2020 average and ranked as the second-warmest year on record, behind only 2010 (Fig. 7.1). Over the past 76 years (1948–2023), the national annual average temperature exhibited a warming of 2.0°C, with 3 of the 10 warmest years occurring since 2015. Spatially, annual anomalies of more than +1.0°C were recorded across most of Canada in 2023, with annual anomalies of more than +2.5°C recorded in most of the Northwest Territories and the western part of Nunavut (Fig. 7.2). Four of the 13 provinces and territories (British Columbia, Alberta, the Yukon, and the Northwest Territories) experienced their highest annual temperatures on record.

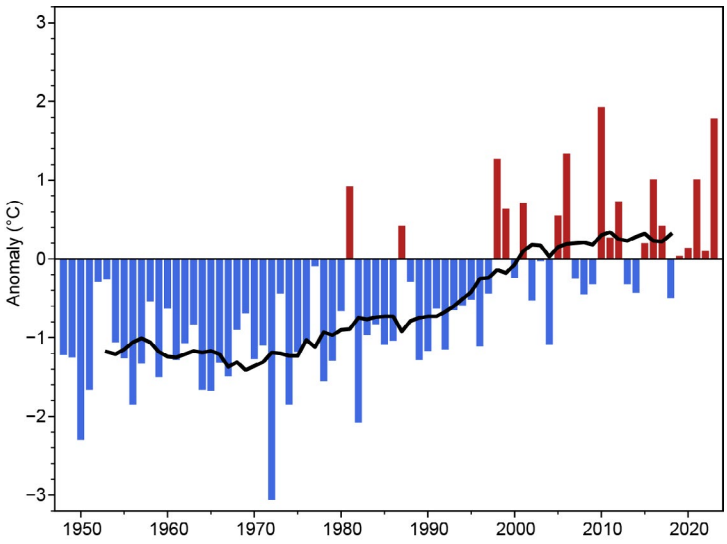

Fig. 7.1. Annual average temperature anomalies (°C; 1991–2020 base period) in Canada for the period 1948–2023. The black line represents an 11-year running mean. (Source: Environment and Climate Change Canada.)

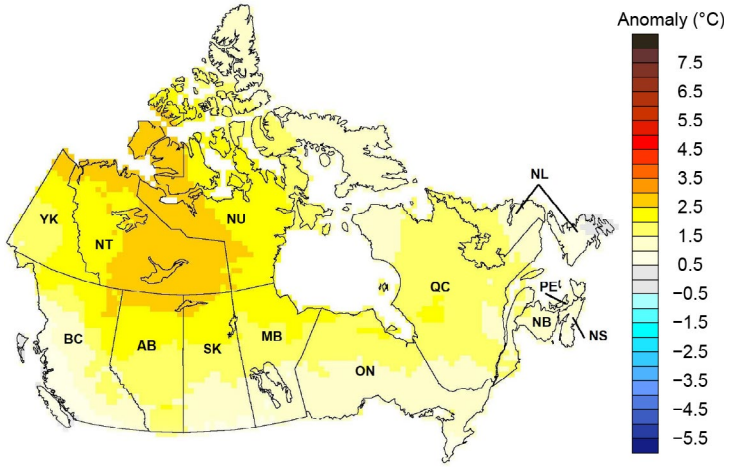

Fig. 7.2. Annual average temperature anomalies (°C; 1991–2020 base period) in Canada for 2023. (Source: Environment and Climate Change Canada.)

Seasonally, the national average temperature for winter (December 2022–February 2023) was 0.3°C above the 1991–2020 average, making it the 19th warmest on record. The highest winter anomalies of +2.5°C were recorded in eastern Ontario and western Quebec.

During spring (March–May), temperature anomalies of at least +0.5°C were observed in most of northern and eastern Canada, while temperature anomalies of at least −0.5°C were observed in the western Yukon, southern Saskatchewan, and Manitoba and western Ontario. The national average temperature for spring 2023 was 1.1°C above average, making it the seventh-warmest spring on record.

The national average temperature for summer (June–August) was 1.2°C above average, the highest on record. Summer anomalies of more than +2.5°C were recorded in the northern region of the Yukon and the Northwest Territories. British Columbia, the Yukon, and the Northwest Territories each had their highest summer temperatures on record.

The national average temperature for autumn (September–November) was 2.4°C above average, making it the warmest autumn on record. Most of the Northwest Territories and Nunavut experienced temperatures 3.0°C or more above average. The Northwest Territories observed their highest autumn temperatures on record, with Nunavut, Quebec, and Alberta each having their second-highest temperatures on record. All provinces and territories had average temperatures among their 10 highest on record for autumn 2023.

(ii) Precipitation

With the evolution of precipitation monitoring technology, Environment and Climate Change Canada (ECCC) and its partners implemented a transition from manual observations to the use of automatic precipitation gauges. Extensive data integration is required to link the current precipitation observations to the long-term historical manual observations. The update and reporting of historical adjusted precipitation trends and variations has been on temporary hiatus pending an extensive data reconciliation, and will be resumed thereafter. ECCC remains committed to providing credible climate data to inform adaptation decision making, while ensuring that the necessary data reconciliation occurs as monitoring technology evolves.

(iii) Notable events and impacts

Canada experienced yet more extremes in 2023. Several heatwaves occurred, and nationwide wildfires set records. A subtropical storm affected the Atlantic Northeast in January, and Hurricane Lee made landfall as a post-tropical cyclone in NS in September. Meanwhile, drought conditions lingered across the country (see the North American Drought Monitor for monthly maps of drought conditions [National Drought Mitigation Center 2024]).

Most notable was the unprecedented wildfire activity across the country (see Sidebar 7.1 for more information). The second most notable was the heavy rainfall in NS that took place on 21–22 July, where a slow-moving trough of low pressure interacted with moist flow from the tropics. Widespread rainfall with totals ranging from 50 mm to 150 mm was observed across NS and eastern Prince Edward Island (Fig. 7.3); locally heavier precipitation of 200 mm to 260 mm fell in parts of Halifax, NS. This event resulted in more than twice the monthly average total rainfall for July (75 mm to 110 mm) in just over two days in the hardest hit areas—the most rain to affect the region in 50 years. Bedford Range, NS, just northwest of Halifax, broke the national rainfall

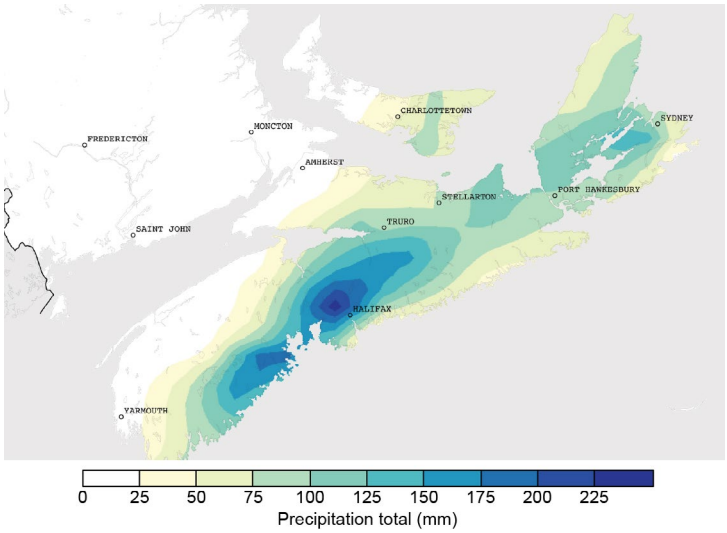

Fig. 7.3. Total precipitation accumulation (mm) during 21–22 July 2023 over Nova Scotia and eastern Prince Edward Island. Darkest blue indicates over 225 mm of rain. (Source: National Laboratory, Meteorological Service of Canada, Environment and Climate Change Canada [ECCC].)

rates record (based on ECCC stations) with 173.4 mm falling over six hours, well exceeding a 1-in-100-year event.

The compounding effect (Singh et al. 2023) of abnormally wet antecedent conditions made this torrential rainfall event even more impactful. Rain had been falling over the region for much of the previous six weeks leading up to the July storm. The already saturated ground led to catastrophic flooding, which damaged infrastructure and led to the loss of four lives when their vehicles were caught in flood waters.

A province-wide state of emergency was declared in NS, with some areas receiving evacuation orders that displaced about 1000 residents (ECCC 2024). Numerous roads and highways were impassable. More than 80,000 homes and businesses lost power. Agricultural losses were also extensive owing to flooded fields, where crops were left submerged for several days (ECCC 2024). In total, this event caused over $236 million Canadian dollars ($179 million U.S. dollars) in insured damage according to the CatIQ database (CatIQ 2024).

2. UNITED STATES

—K. Gleason, C. Fenimore, R. R. Heim Jr., and A. Smith

The annual average temperature for the contiguous United States (CONUS) in 2023 was 12.5°C, which was 0.6°C above the 1991–2020 average, making 2023 the fifth-warmest year in the 129-year record (Fig. 7.4a). Above-average to record-high temperatures were concentrated from the Plains to the East Coast and across portions of the Northwest, while near-average temperatures were observed from California to the central Rockies (Fig. 7.5a). Based on a linear regression of data from 1895 to 2023, the annual CONUS temperature is increasing at an average rate of 0.09°C decade^{-1} (0.27°C decade^{-1} since 1970). Average annual precipitation for the nation totaled 749 mm, which is 94% of the 1991–2020 average (Fig. 7.4b). Overall, the annual precipitation total has been increasing at an average rate of 4 mm decade^{-1} since 1895 (1 mm decade^{-1} since 1970). The average annual temperature across Alaska in 2023 was 0.2°C above average and 17th highest in the 99-year record. Precipitation was 116 mm above average and fifth wettest on record. The annual temperature for Alaska has been increasing at an average rate of 0.17°C decade^{-1} since 1925 (0.44°C decade^{-1} since 1970). Precipitation is increasing at an average rate of 2 mm decade^{-1} since 1925 (21 mm decade^{-1} since 1970).

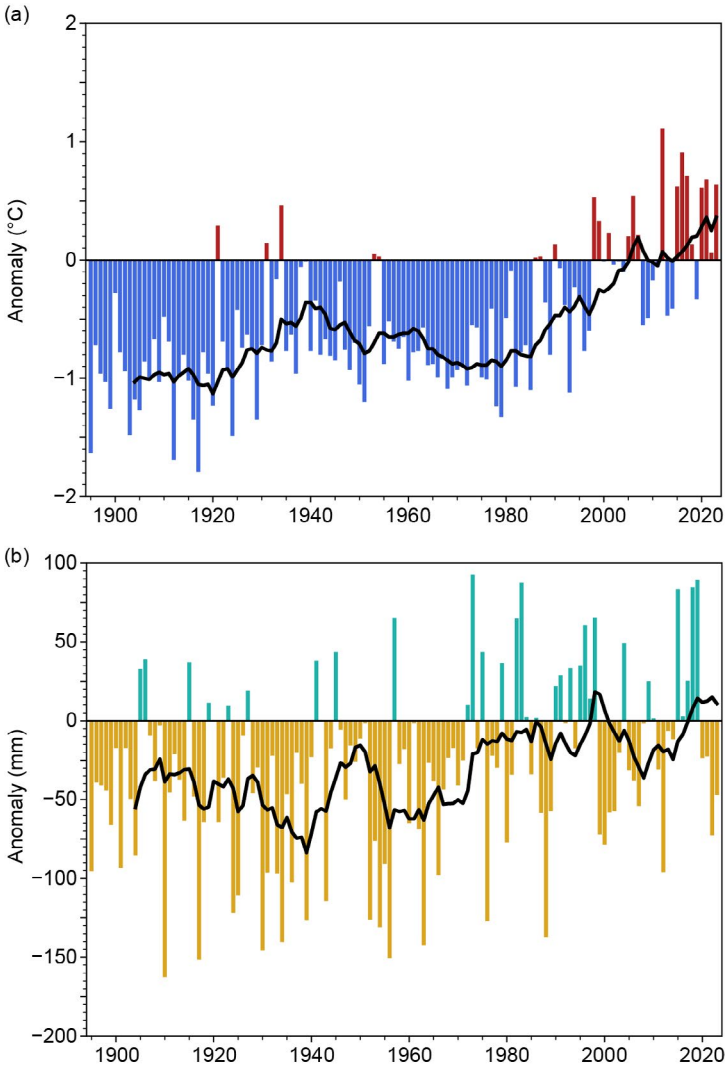

Fig. 7.4. Annual (a) mean temperature anomalies (°C) and (b) precipitation anomalies (mm; 1991–2020 base period) for the contiguous United States during the period 1895–2023. The black lines represent a 10-year running mean. (Source: NOAA/NCEI.)

(i) Temperature

The winter (December 2022–February 2023) CONUS temperature was 0.5°C above average, with anomalous warmth stretching from the southern Plains to the Great Lakes and East Coast. Conversely, the CONUS spring (March–May) temperature was 0.4°C below average with below-average temperatures extending from the West Coast to the northern Plains and above-average temperatures east of a line from southern New Mexico

to the Great Lakes. The summer (June–August) CONUS temperature was 0.4°C above average with record warmth along parts of the Gulf Coast. Louisiana had its warmest summer on record while Texas was second warmest. The autumn (September–November) CONUS temperature was 0.9°C above average, the sixth highest on record. Most of the CONUS experienced above-average temperatures with record heat observed across portions of New Mexico and Texas.

(ii) Precipitation

The climate of the CONUS in 2023 was driven by a broad ridge of high pressure over the central United States, particularly during the second half of the year, which was coincident with a rapid shift from La Niña conditions that lasted for three winters to a strong El Niño by October of 2023 (see section 4b). Louisiana had its ninth-driest year on record while Maine observed its fifth wettest (Fig. 7.5b).

Winter precipitation across the CONUS was 110% of average and ranked in the wettest third of the historical record. Precipitation was above average from California to the Great Lakes and across portions of the Mississippi River Valley and the Northeast. Precipitation totals for Minnesota and Iowa were both third highest on record, and for Wisconsin were the second highest for this winter season. Spring precipitation was near-average (95% of average) for the CONUS, but was below average across portions of the central Plains, Midwest, and Mid-Atlantic. Both Pennsylvania and Maryland had their ninth-driest spring on record. Summer precipitation across the CONUS was 97% of average. Conditions were dry from the Southwest to the central Gulf Coast and in portions of the Northwest and Upper Midwest. Above-average rainfall impacted parts of the West, Plains, and much of the Northeast. Wyoming, Maine, New Hampshire, and Vermont each had their wettest summer on record, while New Mexico and Louisiana both observed their third driest. The autumn CONUS precipitation total was 15th lowest on record at 77% of average. Precipitation was below average across portions of the West, central Plains, and a large portion of the Midwest, Tennessee, and Lower Mississippi River valleys. Tennessee had its third-driest autumn on record.

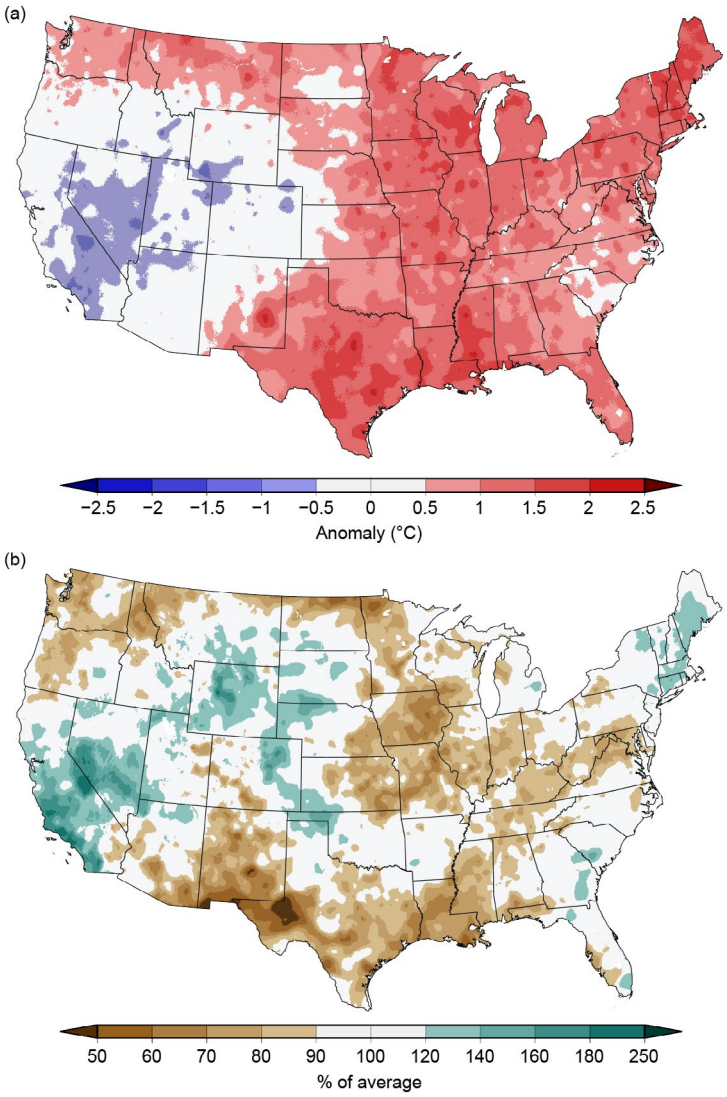

Fig. 7.5. Annual (a) average temperature anomalies (°C) and (b) total precipitation (% of average) in the contiguous United States for 2023 (1991–2020 base period). (Source: NOAA/NCEI.)

Drought coverage across the CONUS remained significant for the fourth consecutive year, beginning with maximum coverage for the year of 46% on 3 January when the most intense areas of drought spanned parts of the West as well as the central and southern Plains. The drought area contracted over the first half of the year, reaching a minimum extent of 19% on 30 May, as drought waned across the West, Midwest, Plains, and Southeast. It expanded throughout the summer and early autumn, reaching a secondary peak of 40% on 3 October, with the epicenter expanding from the central Plains to the Upper Midwest, Deep South, and Pacific Northwest. Warm temperatures and dry conditions led to a flash drought that emerged across portions of the Gulf Coast states and Southeast, with parts of the Mississippi River reaching record-low levels in

October. By the end of 2023, the drought area contracted to 33% of the CONUS, impacting portions of the Southeast, Plains, and Lower Mississippi River Valley. In Hawaii, the lower elevations of Maui saw an expansion of severe drought in early August. These dry conditions, combined with strong, dry winds instigated by Hurricane Dora, contributed to the deadliest wildfire in the United States in more than a century.

(iii) Notable events and impacts

There were a record 28 weather and climate events across the United States during 2023 with losses each exceeding $1 billion: 19 severe storms, 4 flooding, 2 tropical cyclones, and 1 each of drought, wildfire, and winter storm events (Fig. 7.6; Smith 2024). Total disaster costs for these events reached $92.9 billion (note that costs are in U.S. dollars and have been adjusted for inflation; NOAA NCEI 2024). The Southern/Midwestern drought and heatwave that occurred from spring to autumn was the costliest event of the year ($14.5 billion; Smith 2024). Over the last seven years (2017–2023), 137 separate billion-dollar disasters have killed at least 5500 people and incurred costs greater than $1.1 trillion in damage (Smith 2024).

The tornado count for 2023 was 8% above average with 1321 tornadoes reported across the CONUS (SPC 2024). January was an unusually active month with 130 confirmed tornadoes, more than three times the 1991–2020 January average of 39. This was the first time since 2017 and only the third time since 1950 that more than 100 tornadoes occurred during the month of January. Two EF-4 tornadoes were confirmed during the year: the long-lived Rolling Fork, Mississippi, tornado on 24 March that was responsible for 17 fatalities, and the 31 March Keota, Iowa, tornado that destroyed multiple homes. This was the fifth consecutive March with at least one violent tornado (≥EF-4), tying the record streak of five from 1963 to 1967.

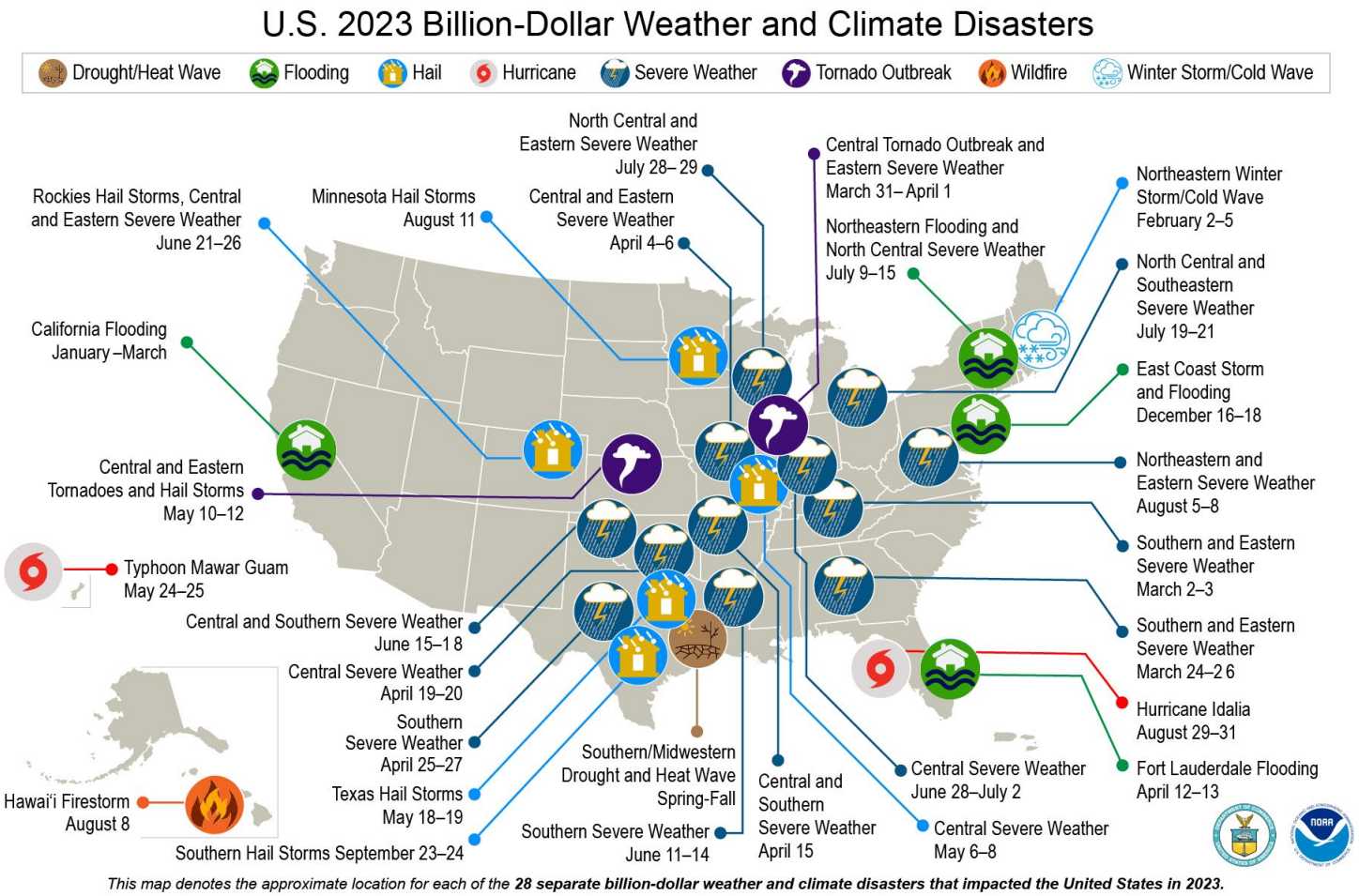

Fig. 7.6. Map depicting date, approximate location, and type of the 28 weather and climate disasters in the United States in 2023 for which losses each exceeded $1 billion (U.S. dollars). (Source: NOAA/NCEI.)

3. MEXICO

—R. Pascual Ramírez and J. Gómez-Camacho

Mexico's annual average temperature for 2023 was the highest since national records began in 1950 (Fig. 7.7a), and the total annual precipitation was the lowest on record (Fig. 7.7b). Only the Baja California Peninsula, the northeast, and southeast recorded above-average annual rainfall throughout the year (Fig. 7.8b); the rest of the country was below average.

(i) Temperature

The 2023 national annual average temperature was 22.7°C, 1.3°C above the 1991–2020 average (Fig. 7.7a) and the highest in the 74-year record. Mexico continues to experience a warming trend, and 2023 marked the 14th consecutive year with an above-average national temperature. Above-average temperatures and persistent heatwaves were prevalent across most of the country, especially during summer; however, regions in the northwest and west experienced near- to below-average annual temperatures (Fig. 7.8a). With the exceptions of February and December, national monthly temperatures were above average, with all months from June to October having been warmest on record for their respective months. From January to March, the northwest and west coast experienced below-average temperatures, while the rest of the country had temperatures much above average. From April through June, below-average temperatures were recorded on the northeast, northwest, and western coasts as the rainy season slowly began; in the central, northern, and southern regions, temperatures were above average.

From July through September, several strong high-pressure systems developed, resulting in very-high temperatures throughout the country. From October to December, above-average temperatures covered the north, central, and south of the country, while slightly below- to near-normal temperatures prevailed along the Gulf of Mexico region.

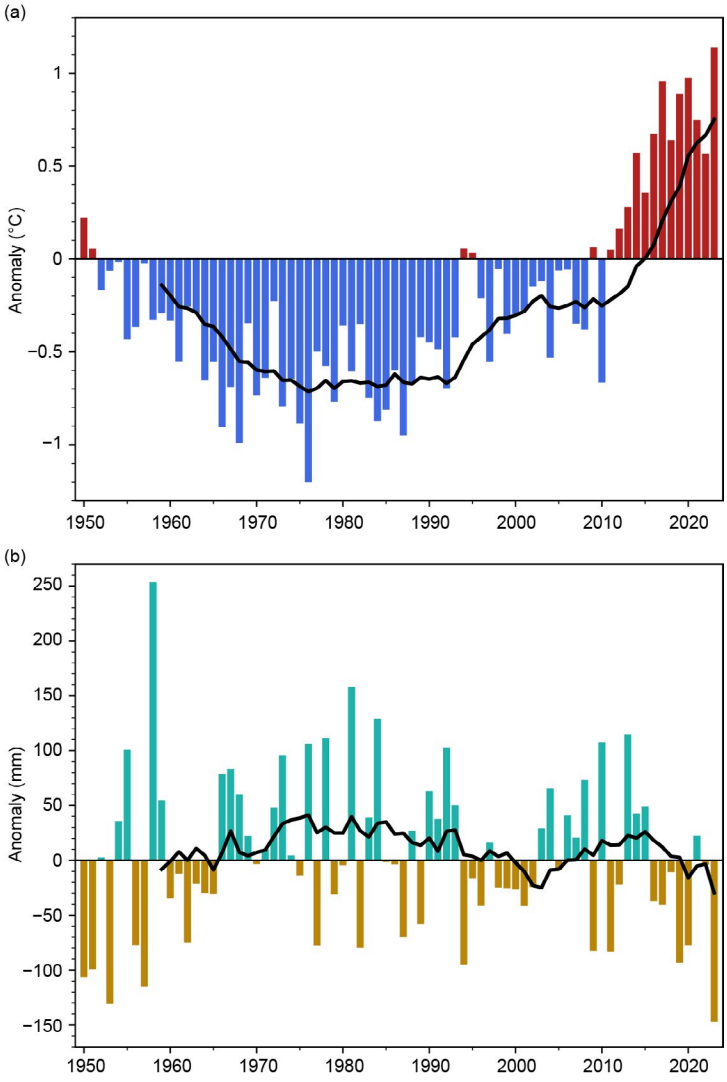

Fig. 7.7. Nationally averaged annual anomalies of (a) temperature (°C) and (b) precipitation (mm) for Mexico from 1950 to 2023 (1991–2020 base period). The black lines represent a 10-year running mean. (Source: National Meteorological Service of Mexico.)

(ii) Precipitation

The national precipitation total for 2023 was 589.9 mm (78.9% of the 1991–2020 average), the lowest annual precipitation total on record for Mexico. Both the dry and wet 2023 seasons recorded below-normal precipitation nationally. Accumulated precipitation for the dry season (November 2022–April 2023) was 115.9 mm, compared to the 1991–2020 average of 133.9 mm. Accumulated precipitation for the wet season (May–October) was 452.0 mm, compared to the 1991–2020 average of 614.0 mm.

Climatologically, September tends to be the country's rainiest month, contributing 18.8% of the annual precipitation; however, for the third year in a row, August contributed more than any other month, with 18.9% of the 2023 annual precipitation. This is a signal of low tropical cyclone activity in September in Mexico over the last two years; September 2023 only provided 11.2% of

the annual rainfall and was the driest September on record. Likewise, June 2023 was the driest June on record. Statistically, March is the driest month of the year, contributing an average of 2.1% of the annual precipitation. In 2023, however, February contributed the least amount of precipitation, with only 2.0% of the annual total. Below-average precipitation fell across most of the country from January to March, with above-average rainfall recorded in the Yucatan Peninsula and the Isthmus of Tehuantepec, as well as in southern and northwest Mexico. The onset of the rainy season in spring was delayed across most of the country, resulting in April–May precipitation deficits, with only the Baja California Peninsula experiencing slightly-above-average precipitation.

Hurricane Beatriz in the Pacific was the only precursor of rainfall in early July, with much less rain occurring during the monsoon season (typically June–September) than in previous years. The 2023 monsoon rainfall was weaker than normal, with 201.9 mm of accumulated precipitation within the region, compared to the 1991–2020 average of 364.9 mm. This was much lower than the 2022 monsoon rainfall, which totaled 453.0 mm.

From July through September, there was less rain than is typically associated with tropical cyclones on both Mexican coasts; in the Atlantic basin, the only two impactful events were Tropical Storm Harold and Hurricane Idalia, both in August. On the Pacific side, Hurricane Hilary, also in August, brought considerable precipitation to the Baja California Peninsula. However, because of minimal moisture transport during these months, widespread drought conditions still occurred, covering up to 75% of the country by the end of September. The last quarter of the year marks the transition between the end of the rainy season and the beginning of the dry season. During this period, it is common to see a combination of tropical and winter systems. From October to December, Tropical Storm Max, three Pacific hurricanes (Lidia, Norma, and Otis), and several cold fronts were the main sources of precipitation in Mexico, thus making it the wettest quarter of the year.

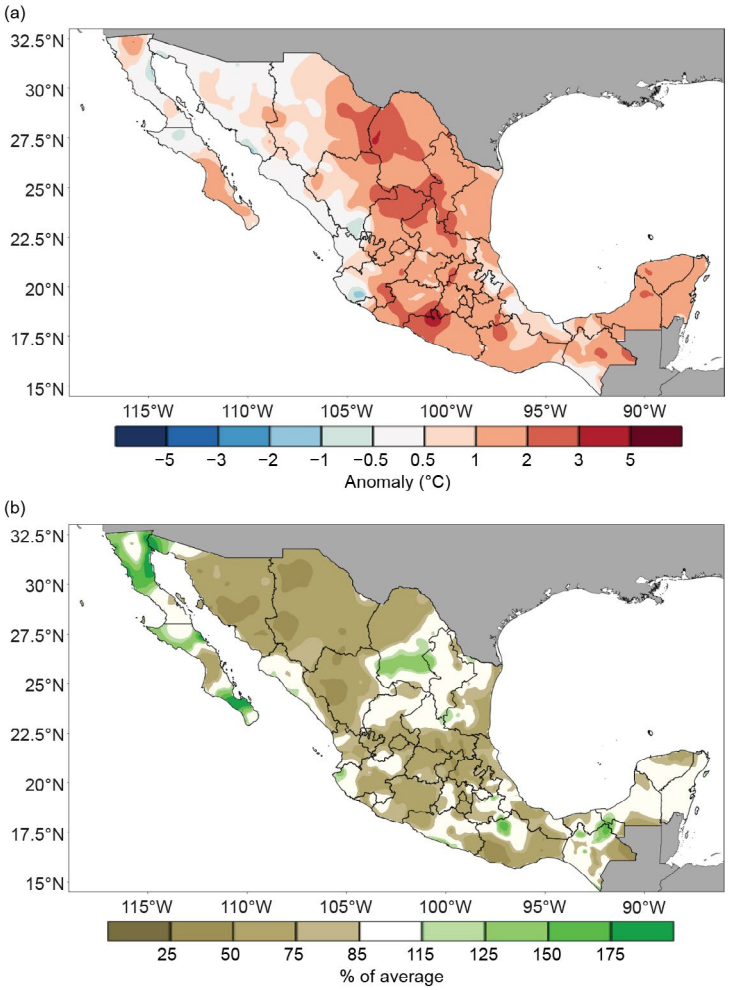

Fig. 7.8. Annual anomalies of (a) mean temperature (°C) and (b) precipitation (% of average) across Mexico in 2023 (1991–2020 base period). (Source: National Meteorological Service of Mexico.)

(iii) Notable events and impacts

From April through June, three heatwaves generated very hot conditions throughout the country, with maximum temperatures surpassing 45°C in places. The heat lasted until September. The heatwave recorded in June was both the most extensive and most intense, with 35 weather observatories or airports across the country reporting record-high temperatures. The highest recorded temperature was 48.0°C at the Ciudad Obregón Observatory in Sonora, which was 9.0°C above the average June high temperature at that location. July 2023 was both the warmest July and the overall warmest month on record for Mexico. According to the Mexican Ministry of Health, 286 deaths associated with heat stroke and dehydration were reported through the end of July, with 35% of these deaths occurring in the state of Nuevo Léon (DGE 2023).

Only two tropical cyclones from the Atlantic basin (Tropical Storm Harold and Hurricane Idalia) affected the eastern coasts of Mexico during 2023. In comparison, the 1991–2020 average number of tropical cyclone impacts is 2.4, with the years 2010 and 2020 each experiencing

impacts from six Atlantic basin tropical cyclones. On the Pacific coast, Tropical Storm Max and Hurricanes Beatriz, Hilary, Lidia, Norma, and Otis all made landfall or tracked near the country and brought significant rainfall to western Mexico. Hurricane Otis had an unprecedented rapid strengthening, intensifying from Category 1 to Category 5 in a record nine hours. Based on records since 1950, Hurricane Otis became the first Category 5 hurricane to make landfall in the state of Guerrero, Mexico, and is one of only two Category 5 hurricanes to make landfall from the Eastern Pacific basin (along with Hurricane Patricia in 2015). The impacts on the city of Acapulco were devastating, with winds of up to 270 km h^{-1} and up to 266 mm of accumulated precipitation in just 24 hours, causing floods and severe damage to infrastructure (see section 4g3 and Sidebar 4.1 for more details on Otis).

Sidebar 7.1: **Record-breaking wildfire season in Canada**

—M. KIRCHMEIER-YOUNG, P. JAIN, J. CHEN, AND F. WU

The 2023 wildfire season in Canada was exceptional. Approximately 15 million hectares (150,000 km^2) burned across the country (Jain et al. 2024), an area more than twice the size of Ireland. The total area burned set a new record for Canada, considering data from the modern satellite era, more than doubling the previous record from 1989 (Fig. SB7.1a). A notable characteristic of this fire season was the extent of the country that experienced record wildfires. The area burned in 2023 was the highest fire-season total for Quebec, Northwest Territories, Alberta, and British Columbia and second highest for Yukon and the Maritimes, based on the satellite record beginning in 1986. The long-range transport of emissions from these fires resulted in high pollutant levels far downwind, including cross-border transport of these pollutants into the United States and overseas. Across the country, approximately 232,000 people were evacuated due to the threat of wildfires, including the entire city of Yellowknife (Northwest Territories) and large populations of Kelowna/West Kelowna (British Columbia) and Halifax (Nova Scotia). Extensive property losses from six large fires led to 17,000 insurance claims for a total of over $1.1 billion Canadian dollars ($815 million U.S. dollars) in damage. The 2023 wildfire season was long, intense, and widespread, and several firefighters died responding to the fires.

Wildfire seasons in Canada typically begin with the loss of snow cover in the spring, and in 2023 the snowmelt was earlier than normal across much of the country. Following snowmelt, the fire season got off to a quick start, with fires of concern occurring in British Columbia, Alberta, and Nova Scotia. In anticipation of nationwide constraints on firefighting capacity, the Interagency Forest Fire Centre set the national preparedness level at its most extreme category on 11 May, the earliest date on record, and kept it at that level for an unprecedented continuous 120 days (CIFFC 2023). Western Canada began the fire season with pre-existing drought conditions that lasted throughout the year. On the other hand, eastern Canada began the fire season with more normal conditions but underwent a

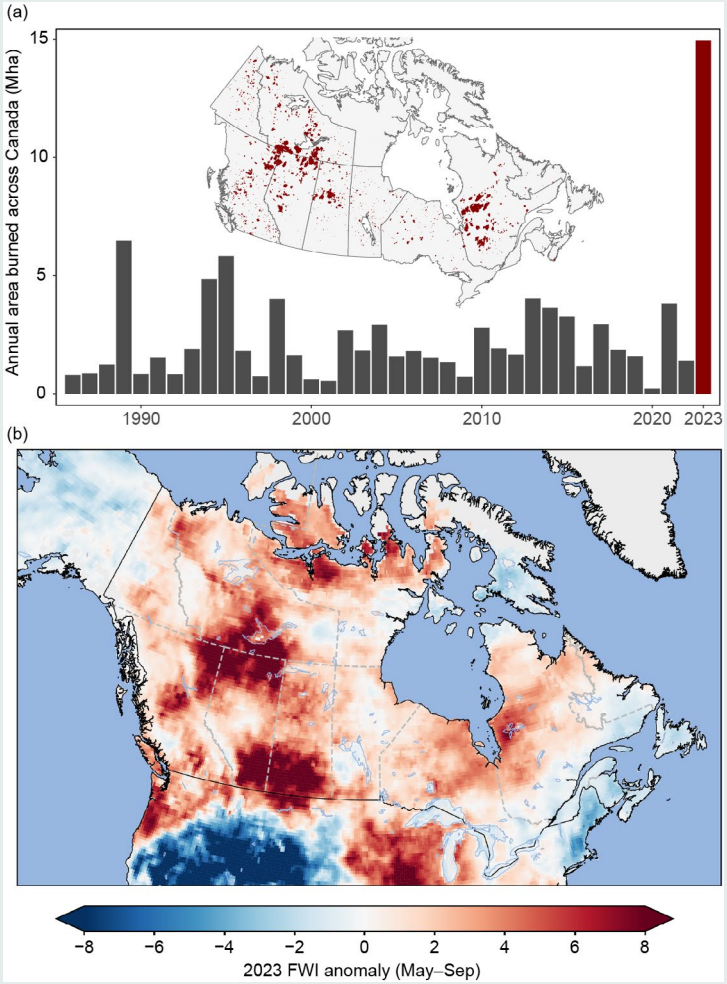

Fig. SB7.1. (a) Annual area burned by wildfires (million ha) in Canada based on data from the National Burned Area Composite (NBAC; Skakun et al. 2022). Inset map: fire perimeters for the 2023 fire season. The data for 2023 were generated from NBAC mapped perimeters and satellite thermal anomalies (Jain et al. 2024). (b) Anomalies of the mean 2023 fire season (May–Sep) value of the Canadian Fire Weather Index relative to 1991–2020. Calculated from the Canadian Forest Fire Danger Rating System and using ERA5 surface weather as inputs.

rapid intensification of drought into June. Southern Quebec, in particular, experienced strong decreases in soil moisture during this time (Jain et al. 2024).

Canada was hot and dry throughout the 2023 fire season. Both summer and autumn were the warmest on record for the country (section 7b1). Much of the area burned in western Canada (Fig. SB7.1a) aligns with the regions that experienced their hottest year on record (see Fig. 7.2), as well as those that experienced prolonged drought conditions (see National Drought Mitigation Center 2024). The Canadian Forest Fire Weather Index System consists of a set of indices that use temperature, precipitation, relative humidity, and wind speed to describe the potential of wildfires to ignite and spread. The system's Fire Weather Index (FWI) largely followed the drought patterns, with local extreme values in western Canada beginning in May and emerging in eastern Canada in June. Considerable portions of the country experienced sustained high FWI values during the fire season, which were driven by well-above-normal temperatures that dried out vegetation through evaporation and a lack of rainfall needed to replenish the moisture. This is confirmed in the 2023 May–September FWI anomaly shown in Fig. SB7.1b, with higher-than-normal FWI conditions occurring throughout the country.

Sustained fire weather conditions primed the landscape, allowing for fire growth following ignition, which was caused by lightning for most of the large fires. Across the country, several days with large increases in area burned occurred with high winds, when already-large fires experienced rapid spread. Another key factor for the extreme fire season was that the established fires tended to burn longer and grow larger than is usually the case. The 20 largest fires in the country contributed to about half of the total area burned (Jain et al. 2024). Many of the fires that ignited during the extreme fire weather conditions in May and June continued to burn through September. This longevity of fires and unusually persistent extreme fire weather helped drive the record fire season.

Smoke from wildfires can impact communities both near and far. In 2023, Environment and Climate Change Canada issued almost 5000 air quality alerts, which is considerably higher than in recent years (compared to about 1800 in 2021, which accompanied the next largest area burned in the last decade). This drastic increase is attributed directly to the extreme poor air quality conditions from wildfires throughout the summer across Canada. The number of smoke hours from May to early September, as defined when visibility is less than 9.7 km, revealed record-breaking smoke conditions across much of western, central, and northern Canada. The city with the highest number of smoke hours was Fort Nelson (British Columbia) with 1054 hours, and several major cities, including Kamloops (British Columbia), Calgary, Edmonton (Alberta), Regina, Saskatoon (Saskatchewan), and Yellowknife (Northwest Territories) experienced more than 200 hours of smoke. Fine particulate matter (PM2.5) measurements are a common indicator of air quality, and high values have been shown to have significant negative impacts on human health. During the fire season in 2023, the most extreme levels of PM2.5 were found in the regions with the most area burned (Fig. SB7.2). Smoke can also be transported hundreds

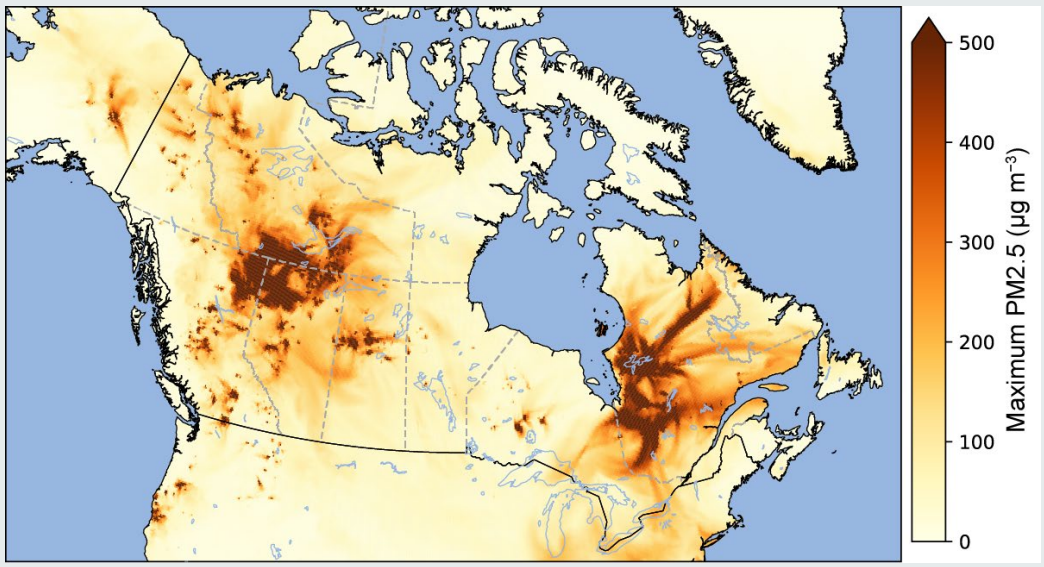

Fig. SB7.2. Maximum daily fine particulate matter (PM2.5) values (µg m^{-3}) across northern North America for May–Sep 2023, calculated from Environment and Climate Change Canada's FireWork model (Chen et al. 2019). The highest values correspond to the locations of the fires in northeastern British Columbia/northern Alberta/southern Northwest Territories and in northwestern Quebec. High-concentration surface plumes extending outward from the fire regions can also be seen.

of kilometers downwind, where it exposes populations to elevated levels of PM2.5 at regional to continental scales. Residents across the country, including those in most of Canada's major cities, experienced numerous days with high smoke and PM2.5 levels, resulting in canceled outdoor events and adverse impacts on physical and mental health from pollutant exposures (Mao et al. 2024; Lowe et al. 2023; Matz et al. 2020). This prompted the immediate release of public health warnings by the Government of Canada in response to the 2023 wildfire season (Public Health Agency of Canada 2023).

Impacts of the wildfires also extended beyond Canada. In early June, cyclonic flow around an area of low pressure over eastern Canada carried smoke from wildfires burning in northern Quebec into the northeastern United States, prompting severe air quality alerts in New York City and other major metropolitan areas (US EPA 2023), and again in late June, impacting Chicago and much of the Great Lakes region. Smoke from the wildfires in Quebec was also transported across the Atlantic to countries in western Europe, further increasing the widespread impacts of Canada's record wildfire season.

c. Central America and the Caribbean

1. CENTRAL AMERICA

—H. G. Hidalgo, J. A. Amador, E. J. Alfaro, B. Calderón, and N. Mora

For this region, nine stations from five countries were analyzed (see Fig. 7.9 for data, station list, and specific data sources). The station distribution is representative of the relevant seasonal and intraseasonal regimes of precipitation (Amador 1998; Magaña et al. 1999; Amador et al. 2016a,b), wind (Amador 2008), and temperature (Hidalgo et al. 2019) on the Caribbean and Pacific slopes of Central America (CA). Precipitation, temperature, and regional wind data for the stations analyzed were provided either by CA National Weather Services (CA-NWS), NOAA, or the University of Costa Rica; in some cases, missing daily precipitation data were filled with the nearest grid point data from the Climate Hazards and Infrared Precipitation with Stations dataset (CHIRPS; Funk et al. 2015). Anomalies are reported using a 1991–2020 base period and were calculated from data provided by CA-NWS. The precise methodologies used for all variables are described by Amador et al. (2011). The Puerto San José station in Guatemala, used in past reports, was substituted with the nearby Montufar station due to lack of data in 2023.

(i) Temperature

The mean temperature (Tm, °C) frequency distributions in 2023 as well as the climatology for all stations analyzed are shown in Fig. 7.9. Most stations across Central America had well-above-normal annual temperatures. Only the station of Liberia, Costa Rica (Tm7), had near-normal temperatures. The two northernmost stations in the Caribbean coast, Philip Goldson International Airport, Belize (Tm1), and Puerto Barrios, Guatemala (Tm2), exhibited a bimodal temperature distribution over the course of the seasonal cycle during the 1991–2020 reference period. This was also reported in the last two yearly climate reports. This feature is also hinted at in the two-peak distribution of Tm in both stations in 2023 (more so in Belize).

(ii) Precipitation

The accumulated pentad precipitation (mm) time series for the nine stations in Central America are presented in Fig. 7.9. Most stations had below-average rainfall totals, with the exceptions of Puerto Barrios (P2) and Montufar (P9) in Guatemala, which presented near-normal conditions, and Tocumen (P5) and David (P6) in Panama, which presented wetter-than-normal conditions. Notably, 2023 showed an atypical precipitation response to the prevailing El Niño–Southern Oscillation event, most likely related to the prevailing above-average sea surface temperature anomalies in the Atlantic/Caribbean basin. Most of the stations on the Pacific and Caribbean side ended the year with below-average annual accumulations (except for the Panama stations) with no contrast between the usual opposite responses in the Pacific and Caribbean slopes. Despite reported problems in the operation of the Panama Canal due to low water levels in Gatun Lake, the Panama stations generally tracked near- to above-normal precipitation throughout 2023, suggesting that rainfall accumulations were not a likely cause of the operational issues in the canal zone. The prevailing wind anomaly pattern (Fig. 7.9) in July implies a light flow from the Caribbean to the Pacific coast from the Nicaragua–Costa Rica border to the north; negative wind anomalies and drier-than-normal Pacific conditions are typical during an El Niño event.

(iii) Notable events and impacts

During 2023, Central America was impacted by various stages of low-pressure systems, including tropical depressions and tropical storms. However, tropical cyclone activity in the Caribbean and eastern tropical Pacific affecting Central America was below normal in 2023. A low-pressure system formed near the southwest coast of Costa Rica in the eastern tropical Pacific on 25 June, becoming Tropical Depression Two-E on 29 June, and eventually developing into Tropical Storm Beatriz. Later, a tropical wave crossed Central America into the eastern tropical Pacific on 29 July off the coast of El Salvador, producing a large area of rain and thunderstorms before becoming Tropical Depression Five-E on 31 July and, later, Tropical Storm Dora. On 12 August, another tropical wave crossed Central America to the eastern tropical Pacific, affecting Guatemala and El Salvador on 14 August. Then, a low-pressure system crossed the isthmus from the eastern tropical Pacific on 24–25 August and persisted offshore of the Caribbean Central America coast, becoming Tropical Depression 10 on 26 August and later becoming Hurricane

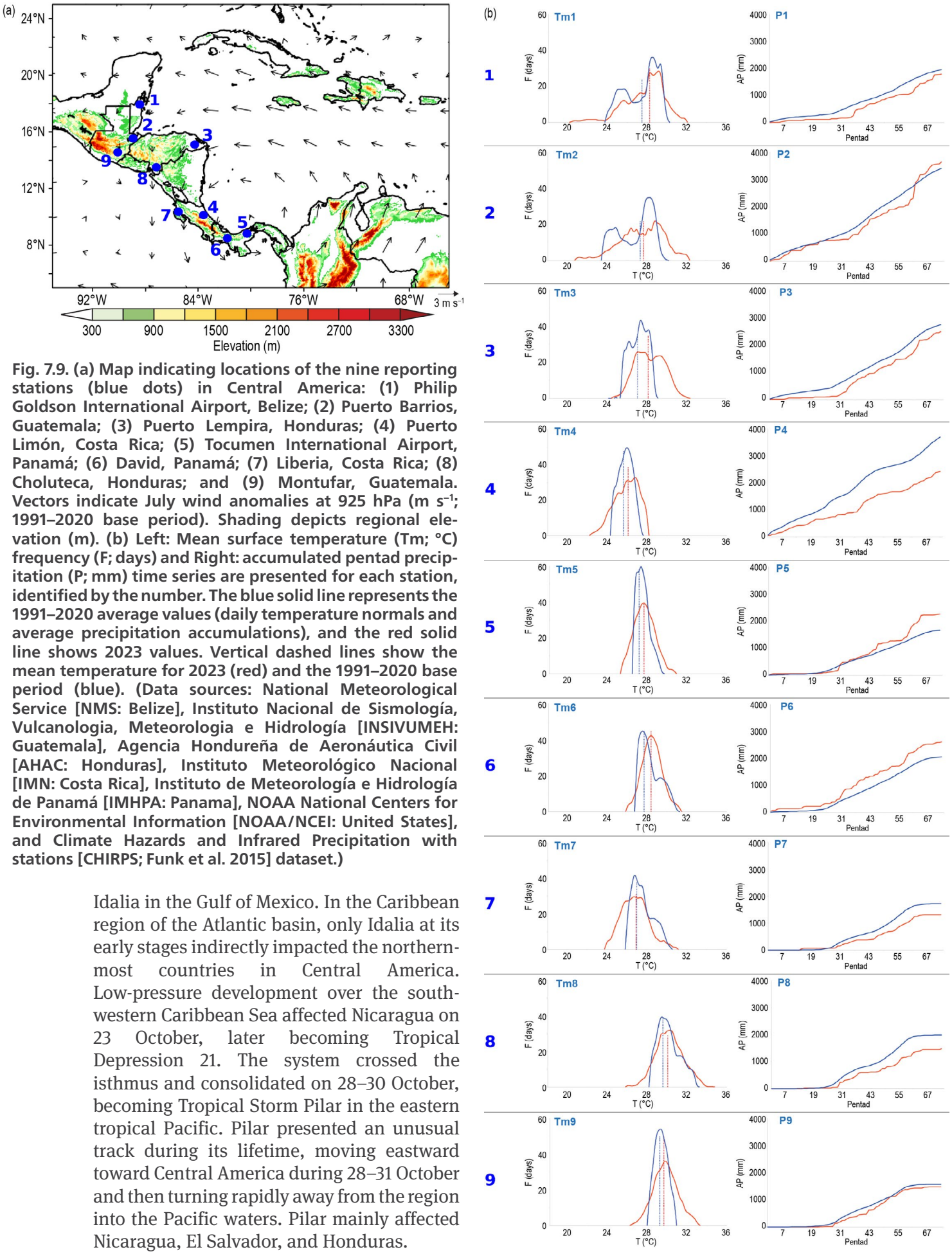

Fig. 7.9. (a) Map indicating locations of the nine reporting stations (blue dots) in Central America: (1) Philip Goldson International Airport, Belize; (2) Puerto Barrios, Guatemala; (3) Puerto Lempira, Honduras; (4) Puerto Limón, Costa Rica; (5) Tocumen International Airport, Panamá; (6) David, Panamá; (7) Liberia, Costa Rica; (8) Choluteca, Honduras; and (9) Montufar, Guatemala. Vectors indicate July wind anomalies at 925 hPa (m s^{-1}; 1991–2020 base period). Shading depicts regional elevation (m). (b) Left: Mean surface temperature (Tm; °C) frequency (F; days) and Right: accumulated pentad precipitation (P; mm) time series are presented for each station, identified by the number. The blue solid line represents the 1991–2020 average values (daily temperature normals and average precipitation accumulations), and the red solid line shows 2023 values. Vertical dashed lines show the mean temperature for 2023 (red) and the 1991–2020 base period (blue). (Data sources: National Meteorological Service [NMS: Belize], Instituto Nacional de Sismología, Vulcanologia, Meteorologia e Hidrología [INSIVUMEH: Guatemala], Agencia Hondureña de Aeronáutica Civil [AHAC: Honduras], Instituto Meteorológico Nacional [IMN: Costa Rica], Instituto de Meteorología e Hidrología de Panamá [IMHPA: Panama], NOAA National Centers for Environmental Information [NOAA/NCEI: United States], and Climate Hazards and Infrared Precipitation with stations [CHIRPS; Funk et al. 2015] dataset.)

Idalia in the Gulf of Mexico. In the Caribbean region of the Atlantic basin, only Idalia at its early stages indirectly impacted the northernmost countries in Central America. Low-pressure development over the southwestern Caribbean Sea affected Nicaragua on 23 October, later becoming Tropical Depression 21. The system crossed the isthmus and consolidated on 28–30 October, becoming Tropical Storm Pilar in the eastern tropical Pacific. Pilar presented an unusual track during its lifetime, moving eastward toward Central America during 28–31 October and then turning rapidly away from the region into the Pacific waters. Pilar mainly affected Nicaragua, El Salvador, and Honduras.

Other rain-producing systems caused landslides and flooding that killed 94 people: 1 each in Panama and Costa Rica, 2 in Nicaragua, 17 in El Salvador, 7 in Honduras, and 66 in Guatemala. Reported lightning strikes caused 24 fatalities in the region during the season (one each in Panama and Costa Rica, six in Nicaragua, seven in El Salvador, five in Guatemala, and four in Honduras). Mortality statistics provided above were obtained from newspaper publications and/or national emergency management agencies such as the following: Guatemala: https://conred.gob.gt/; El Salvador: https://www.proteccioncivil.gob.sv, https://www.gobernacion.gob.sv, https://diario.elmundo.sv; Honduras: https://copeco.gob.hn; Panama: https://www.sinaproc.gob.pa, https://www.panamaamerica.com.pa; Costa Rica: https://www.nacion.com; Nicaragua: https://nicaraguainvestiga.com; https://www.elmundo.es/; https://www.laprensani.com/. Please see sections 4g2 and 4g3 for more details on the 2023 Atlantic basin and eastern Pacific basin tropical cyclones.

2. CARIBBEAN

—T. S. Stephenson, M. A. Taylor, A. Trotman, C. J. Van Meerbeeck, L. Clarke, J. Spence-Hemmings, R. Moody, C. Charlton, and J. Campbell

(i) Temperature

In 2023, the annually averaged 2-m temperature over the Caribbean was 26.68°C, which was 0.73°C above the 1991–2020 average, making it the warmest year since the start of the record in 1950 (Fig. 7.10a). Seasonally, the Caribbean observed its sixth-warmest December–February (0.39°C above normal); fourth-warmest March–May (0.44°C); and record-warmest June–August (0.96°C) and September–November (1.03°C). Overall, the region has been warming at a rate of 0.12°C decade^{-1} since 1950 (0.18°C decade^{-1} since 1970). At the island scale (Fig. 7.11a), the year was characterized by record and near-record mean annual temperatures for 14 of 36 stations archived in the Caribbean Institute for Meteorology and Hydrology CAROGEN database (Table 7.1). The Caribbean heat season, defined here as May–October, was record warm at 18 of 36 stations, with 30 stations measuring values exceeding their 90th percentile.

(ii) Precipitation

Annually averaged rainfall for 2023 over the Caribbean was ~0.16 mm day^{-1} drier than normal, which is ~95% of the 1991–2020 average (3.22 mm day^{-1}; Fig. 7.10b). Normal to below-normal precipitation was observed over the eastern Caribbean, and above-normal precipitation was observed in the north (Fig. 7.11b). December–February rainfall was generally normal to below normal. More intense drying was observed over northern islands, including Jamaica, Haiti, and southeastern Cuba and the Dominican Republic. For March–May, above-normal anomalies were recorded over

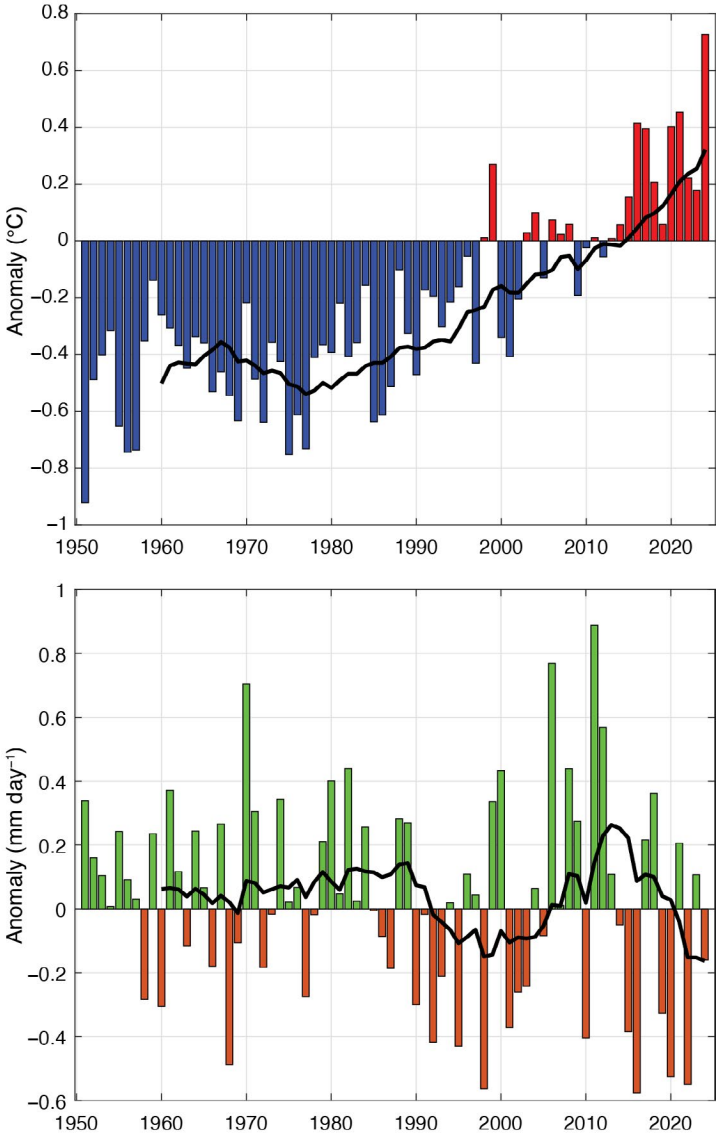

Fig. 7.10. Annually averaged (a) 2-m temperature anomaly (°C) and (b) rainfall anomaly (mm day^{-1}) time series for the Caribbean (9°N–27°N, 58°W–90°W) for the period 1950–2023 relative to the 1991–2020 average. The black line represents the 10-year running mean. (Source: ERA5 from the Copernicus Climate Data Store.)

most of the northern islands, while near-normal to dry conditions continued over the east. During June–August, the region continued to transition to wetter-than-normal conditions in the north and to normal conditions over the rest of the region; however, very-dry conditions were observed over Tobago in the south. An expansion of the drying in the southeast was observed for September–November. Similarly, southeast Cuba and southern Puerto Rico reported drier-than-normal conditions; in contrast, the Bahamas recorded wetter-than-normal conditions during this period.

Since the start of the record in 1971, Jimani, Dominican Republic, recorded its wettest year in 2023 (1105.8 mm, 159% of average); Padre Las Casas, Azua, Dominican Republic, its second wettest (1251.4 mm; 170.9%); Barrah, Dominican Republic, its seventh wettest (1510 mm; 154.0%); and Lynden Pindling International Airport, Bahamas, its fourth-wettest year (1911.0 mm, 133.3%). El Valle, Hato Mayor, Dominican Republic, observed its second-driest year since 1971 (662.4 mm, 47.6%); La Desirade, Guadeloupe, its fifth driest since 1971 (745.9 mm, 65.0%); Lajas, Puerto Rico, its second driest since 1973 (619.8 mm; 56.0%); E.T. Joshua Airport, St. Vincent, its third driest since 1979 (1606.9 mm; 76.0%); and Piarco, Trinidad, its sixth-driest year since 1971 (1498.9 mm; 81.6%).

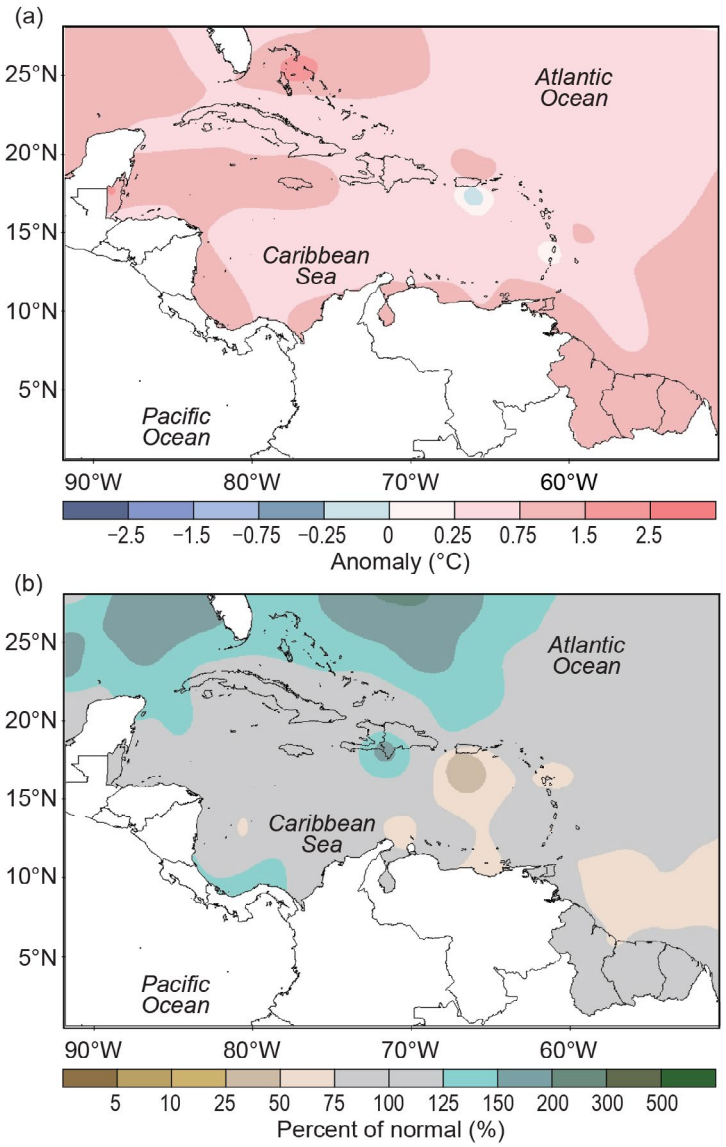

Fig. 7.11. Annual (a) mean temperature anomalies (°C) and (b) total precipitation anomalies (% of normal) relative to 1991–2020. (Source: Caribbean Climate Outlook Forum [CariCOF] and the Caribbean Institute for Meteorology and Hydrology.)

(iii) Notable events and impacts

During 2–6 June, Tropical Storm Arlene caused flooding and landslides in Haiti. Seventy-eight deaths and damage in excess of $420 million (U.S. dollars) were reported (Delforge et al. 2023). During 8–13 June, excessive rainfall due to Tropical Depression Two impacted the central Bahamas, resulting in flooded homes, businesses, and vehicles in the district of Exuma (CCRIF SPC 2023a). Cuba was impacted by heavy rains from the same system on 8–10 June, affecting 18,500 residents (Delforge et al. 2023). On 22–23 June, the center of Tropical Storm Bret passed north of Barbados and over northern St. Vincent and the Grenadines, impacting over 300 people on these islands (Delforge et al. 2023). Bret also impacted St. Lucia, where heavy rains and strong winds downed power lines, flattened banana crops, damaged roofs, and caused flooding and mudslides in some communities (CCRIF SPC 2023b). Tropical Storm Franklin traversed the Dominican Republic during 20–23 August and caused flooding that impacted more than 289,000 residents (Delforge et al. 2023). During 26–29 August, Hurricane Idalia traveled close to the western tip of Cuba, causing flooding in that region. Tropical Storm Philippe impacted Dominica and Antigua and Barbuda on 2–3 October. Excess rainfall from the storm caused flooding and severe landslides in Dominica (CCRIF SPC 2023c). In Antigua and Barbuda, heavy rains and severe flooding impacted low-lying areas, damaged businesses, and caused power

outages (CCRIF SPC 2023d). Many residents were forced to evacuate their homes. On 16–17 November, Jamaica was impacted by a broad area of low pressure over the central Caribbean Sea to the southwest of the island. Sixteen roadways were impacted by the excessive rain, flood waters, and fallen rocks and trees; 22 people marooned in the parish of St. Thomas had to be rescued by the Jamaica Defence Force (CCRIF SPC 2023e).

Table 7.1. Annual temperature extremes for 2023 at Caribbean weather stations contained in CAROGEN (https://carogen.cimh.edu.bb). Included are summary statistics for stations where the annual mean 2-m temperature exceeded the 90th percentile for the reference period 1991–2020. Among the requirements for inclusion are 1) a complete record for 2023, 2) at least 80% of years between 1991 and 2020 being complete, and 3) a period of record spanning at least 30 years since 1971 or the start of station operations, whichever the more recent date may be. Shaded rows with a thermometer icon (🌡) indicate stations registering their warmest years on record in 2023.

Country	Station	Temperature (°C)	Anomaly (°C)	Number of years in data	Rank
Antigua and Barbuda	VC Bird Airport, Antigua	30.1	0.4	53	5
The Bahamas	Freeport, Grand Bahama	29.5	0.9	51	3
The Bahamas	Lynden Pindling International Airport, New Providence	30.3	0.8	53	3
Barbados	Caribbean Institute for Meteorology and Hydrology	30.4	0.4	43	2
Cayman Islands 🌡	Owen Roberts International Airport, Grand Cayman	31.7	1.2	48	1
Cuba	Casa Blanca, Havana	30.9	1.4	53	2
Cuba	National Airport of Camagüey	31.5	1.0	53	2
Cuba	Punta de Maisi	30.9	0.8	53	3
Dominica 🌡	Canefield Airport	32.4	1.2	39	1
Grenada	Maurice Bishop International Airport	30.9	0.4	39	3
Jamaica 🌡	Norman Manley International Airport	32.4	0.5	31	1
Jamaica 🌡	Sangster International Airport	32.9	1.3	50	1
Martinique	Aimé Césaire International Airport	31.2	0.7	53	2
Puerto Rico	Aibonito	26.5	1.0	38	5
Puerto Rico	San Juan	31.0	0.6	53	6
St. Croix	Henry E. Rohlsen Airport	31.5	1.0	52	4
Sint Maarten	Princess Juliana International Airport	31.0	0.7	43	5

d. South America

—R. Martinez, Ed.

1. NORTHERN SOUTH AMERICA

—F. Costa, P. Echeverría, Y. González, and J. Serna

The northern South America region includes Colombia, Ecuador, French Guiana, Guyana, Suriname, and Venezuela. Throughout this section, 1991–2020 is the base period used for both temperature and precipitation unless otherwise specified.

Temperature and precipitation patterns in northern South America during the early months of 2023 showed the influence of the end of the triple La Niña period, which concluded near the start of the year. For the remainder of 2023, the influence of El Niño conditions emerged and strengthened, particularly notable with the excessive rainfall in Ecuador, due to the intense warming of sea surface temperatures in the Niño 1+2 region, known as the Coastal El Niño. By June, when international agencies declared a global El Niño (recorded in the Niño 3.4 region; see section 4b for details), the influence of the positive El Niño–Southern Oscillation (ENSO) phase on air temperatures throughout the region was observed, along with a decrease in precipitation in Venezuela and Colombia.

(i) Temperature

Overall, annual maximum temperatures across northern South America were higher than usual in 2023. In Suriname, recorded values were 1.0°C–1.5°C above the 1991–2020 climatological average. In Venezuela, all records showed anomalies of more than +1.0°C. In Colombia, maximum temperatures had positive anomalies in the range of +1.0°C to +1.5°C. Notably, since El Niño conditions began around mid-2023, most of the country, both continental and insular, recorded above-normal temperatures. The months with warmest temperatures were August, October, and December. In Ecuador, maximum temperatures were also above normal in 2023. The highest anomaly observed in the coastal region was in January with an average maximum temperature of 36.5°C, 4.1°C above normal. In the inter-Andean and Amazon regions, the maximum temperature was recorded in September, at 29°C and 36.9°C, which was 3.4°C and 3.2°C above normal, respectively (Fig. 7.12a).

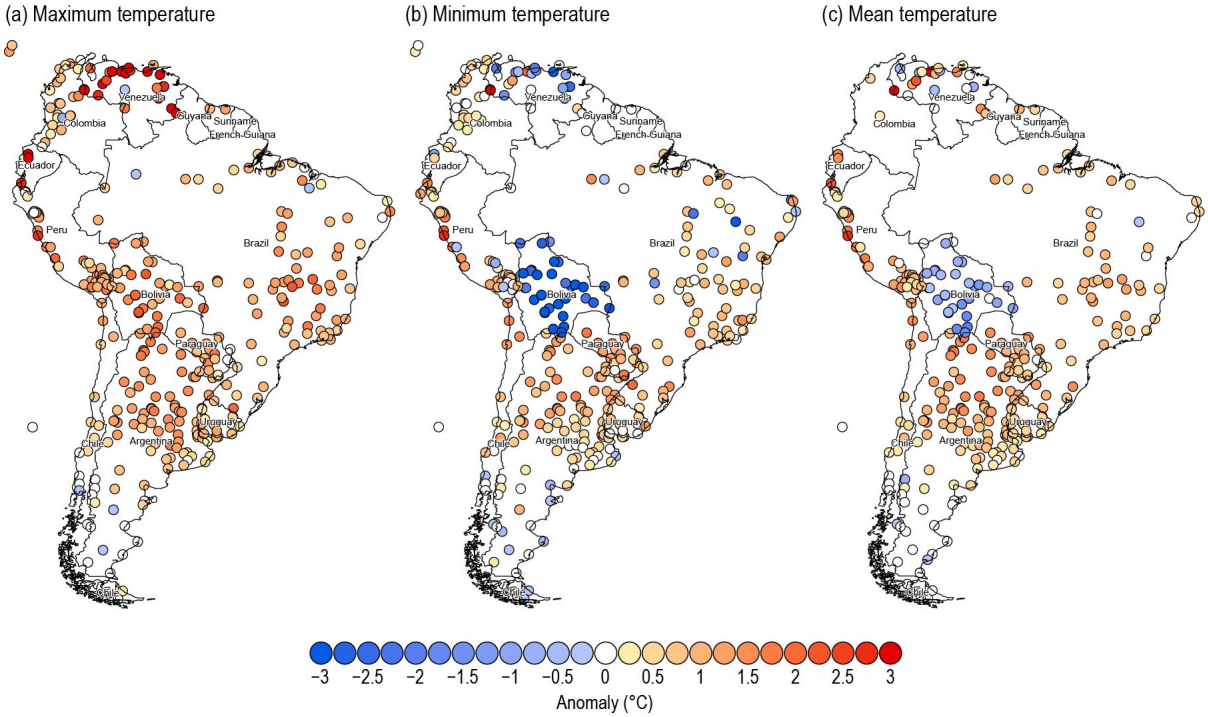

Fig. 7.12. Annual (a) maximum, (b) minimum, and (c) mean temperature anomalies (°C; 1991–2020 base period) for 2023. (Source: data from National Meteorological and Hydrological Services of Argentina, Bolivia, Brazil, Chile, Colombia, Ecuador, Paraguay, Peru, Suriname, Uruguay, and Venezuela. Processed by Centro Internacional para la Investigación del Fenómeno de El Niño [CIIFEN].)

Regarding minimum and mean temperatures, northern South America experienced variable conditions in 2023 (Figs. 7.12b,c). In Suriname, annual minimum temperatures were close to normal, while in Venezuela temperatures ranged from near normal to 3.5°C below normal. The average minimum temperature anomaly from weather stations distributed throughout the country was −0.8°C. In Colombia, minimum temperature anomalies ranged from near normal to +1.0°C. In Ecuador, annual average minimum anomalies were between −1.0°C and +0.5°C. January was the coldest month in the country's coastal region, with a monthly minimum temperature of 20.2°C, which was 1.6°C below normal. In the inter-Andean region, the monthly minimum temperature was −2.1°C in September, which was 3.0°C below normal. In the Amazon, the January minimum temperature was 14.5°C, 4.1°C below normal. The average mean temperature reached its minimum in January in the coastal and Andes region at 25.2°C (normal) and 10°C (0.6°C below normal), respectively. In the Amazon, the average March temperature was 20.9°C, 0.6°C below normal. The highest mean temperature was recorded in May in the coastal region, 28.5°C, which was 1.4°C above normal. In the Andes, the highest mean temperature was 24.1°C in July, 0.3°C above normal, and in the Amazon the July temperature was 29.2°C, 2.3°C above normal.

(ii) Precipitation

Precipitation was variable across northern South America in 2023. Annual totals in Suriname ranged from 30% below normal to 20% above. Venezuela's average precipitation was 30% below normal, with some stations in the north as much as 70% below normal. In Colombia, according to records from Instituto de Hidrología, Meteorología y Estudios Ambientales' meteorological station network, excess rainfall was observed in January, March, and December across much of the country, while deficits were recorded in February, June, and September. Notably, the dry conditions in September were typical of El Niño events. Overall, annual precipitation totals across the country ranged from about 20% below to 20% above normal. In Ecuador, precipitation was generally above normal in 2023. The wettest months were March, April, and May. The coastal region recorded maximum precipitation of 910.4 mm in April and 733.5 mm in May, exceeding normal precipitation levels by 42% and 114%, respectively. In the inter-Andean region, maximum precipitation values of 234.0 mm and 245.3 mm were recorded in March and April, respectively, exceeding normal levels by 29% and 55%, respectively. In the Ecuadorian Amazon, maximum precipitation occurred in April and May, with 588.0 mm and 746.5 mm, exceeding normal levels by 55% and 59%, respectively. The least rainy months in the Ecuadorian Amazon were August and September, with 33.7 mm and 63 mm, corresponding to +14% and +34% of the expected normal precipitation value, respectively (Fig. 7.13).

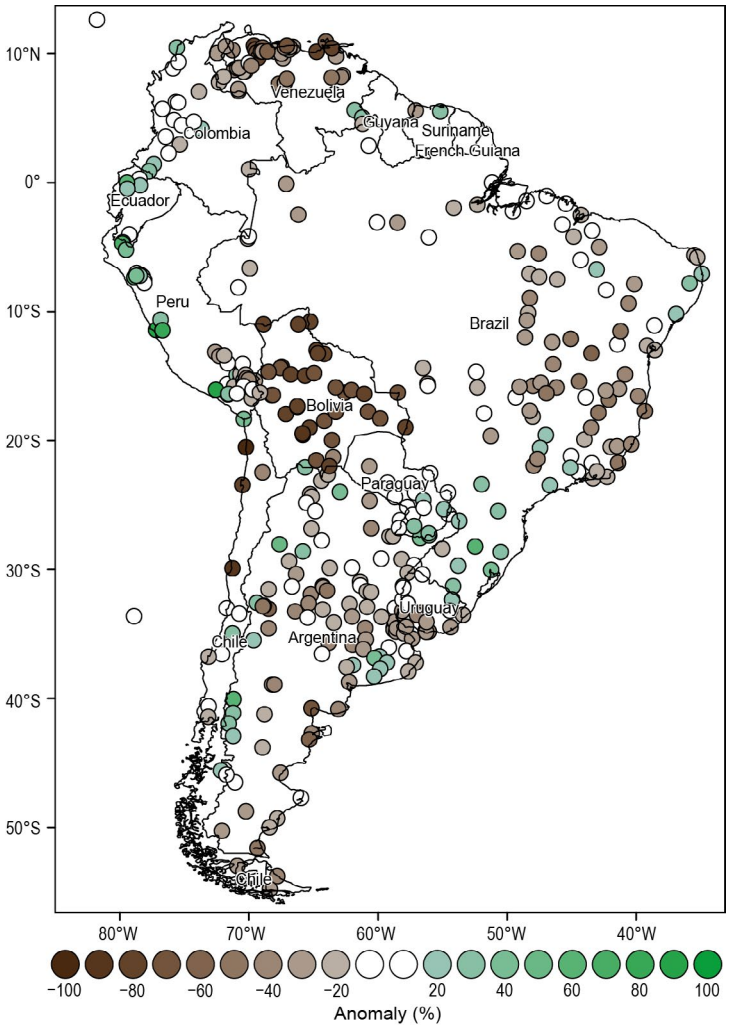

Fig. 7.13. Annual precipitation anomalies (%; 1991–2020 base period) for 2023. (Source: Data from National Meteorological and Hydrological Services of Argentina, Bolivia, Brazil, Chile, Colombia, Ecuador, Paraguay, Peru, Suriname, Uruguay, and Venezuela. Processed by Centro Internacional para la Investigación del Fenómeno de El Niño [CIIFEN].)

(iii) Notable events and impacts

The El Niño phenomenon intensified drought conditions during the second half of 2023 in Colombia. High temperatures and reduced rainfall primarily affected the Caribbean, Andean, and La Guajira regions. Reported impacts included scarcity of drinking water for human consumption and agriculture, crop losses and impacts on livestock, multiple forest fires, deterioration of air quality, water rationing, and decreased energy production.

Ecuador experienced several extreme rainfall events in 2023 with significant impacts, particularly notable in the coastal and Andean regions. On 22–23 March, intense rainfall of 249.5 mm was recorded. This led to flooding in the coastal city of Guayaquil and the overflow of the Guayas River, exacerbated by the high external tide of 5.1 m. The areas most affected by the flooding in the city were Urdesa, Suburbio, Vía Daule, Alborada, Samanes, Guayacanes, and Avenida Tanca Marengo. Structural collapses, disruptions to vehicular traffic, fallen trees, and landslides were reported.

On the night of 26 March, a landslide occurred in Alausí, located in the Andean province of Chimborazo, Ecuador. The landslide was triggered by five days of persistent heavy rains and resulted in seven fatalities, with 16 people injured, 46 missing, and more than 500 affected. The landslide caused significant damage to homes and infrastructure in the area.

On 15 April, 111.2 mm of rain was recorded in 24 hours in Guayaquil, Ecuador, causing flooding in several sectors of the city, including El Fortín, Vía Daule, Mapasingue, La Alborada, and Sauces. The flooding affected roads, homes, and businesses and caused a landslide that killed one person who was trapped inside a vehicle. Several people were also injured, and power outages and disruptions to transportation were reported. The government declared a state of emergency.

2. CENTRAL SOUTH AMERICA

—J. A. Marengo, J. C. Espinoza, J. Ronchail, A. P. Cunha, A. M. Ramos, J. Molina-Carpio, K. Correa, G. Avalos, W. Lavado-Casimiro, R. Salinas, P. P. Rivera, and W. R. Quispe

The central South America region includes Brazil, Peru, Paraguay, and Bolivia. Throughout this section, 1991–2020 is the base period used for both temperature and precipitation unless otherwise specified.

(i) Temperature

The 2023 mean temperature for central South America was 1.62°C above the 1991–2020 average, the highest in the last 50 years and far surpassing the previous record set in 2015 (Fig. 7.14). From January to May, the northern coast of Peru was about 1°C–2°C warmer than normal. As the year progressed, consistent with the intensification of El Niño, the region experienced anomalies of +3°C across western Brazil, northern Paraguay, and Bolivia; these high temperatures were related to six heatwaves that affected the region (See Notable events and impacts).

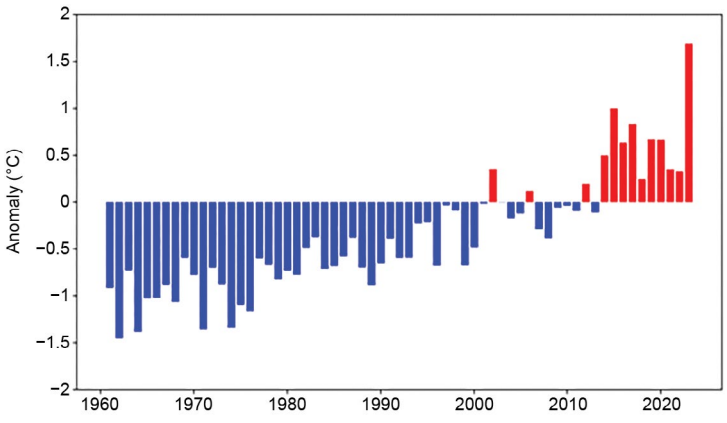

Fig. 7.14. Time series of mean annual regional air temperature anomalies (°C; 1991–2020 base period) for the period 1961–2023 for central South America (Brazil, Bolivia, Paraguay, and Peru). (Source: NOAA National Centers for Environmental Prediction GHCN CAMS data.)

(ii) Precipitation

During January–July, above-average precipitation was observed across northern Peru. During February–May, above-normal rainfall was recorded in western Bolivia and northern Paraguay, while rainfall was below normal in Peru and north-central and southern Brazil. From August to December, rainfall in southern Brazil was 200 mm month^{-1}–300 mm month^{-1} above normal, while dry conditions prevailed over tropical Brazil, Bolivia, and Paraguay. The abundant rainfall in southern Brazil and drought in Amazonia (see Notable events and impacts) were associated with El Niño.

(iii) Notable events and impacts

Several significant extreme events occurred across central South America in 2023 (Fig. 7.15). The Integrated Drought Index (Fig. 7.16) shows drought conditions in the La Plata basin (LPB), in the southern Andes, and the Altiplano during austral summer. During winter and spring, the drought situation was alleviated in the LPB, but drought developed in the Amazon, Pantanal, Bolivian Chiquitania, and parts of northeast Brazil.

With respect to the El Niño–Southern Oscillation, 2023 can be divided in two parts, the first part corresponding with the end of the 2020–23 La Niña and the second to the intensification of El Niño conditions beginning in May.

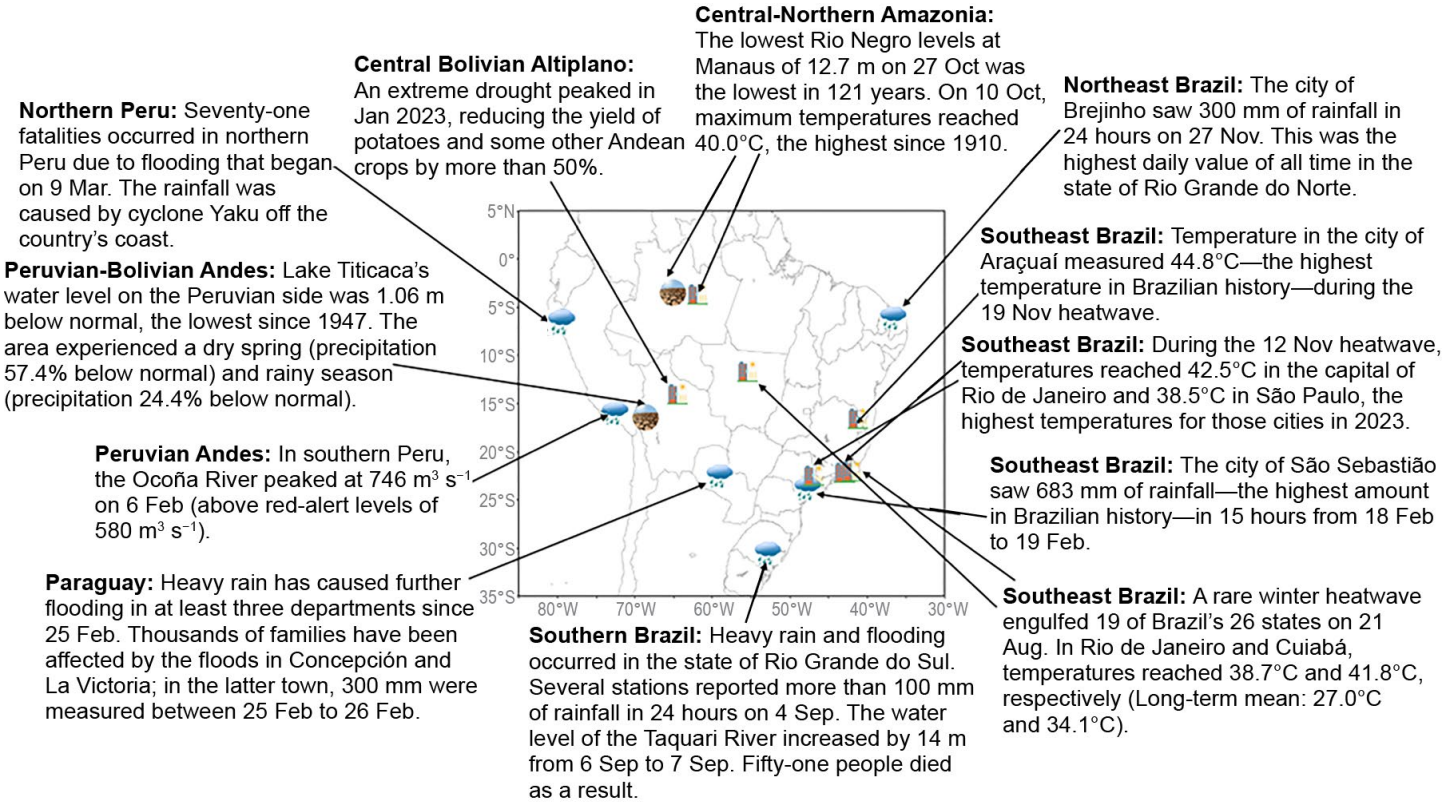

Fig. 7.15. Extreme and notable events across central South America in 2023. (Sources: Peru, Bolivia: Servicio Nacional de Meteorología e Hidrología [SENAMHI]; Paraguay: Dirección de Meteorología e Hidrología [DMH]; Brazil: Instituto Nacional de Meteorologia [INMET], National Center for Monitoring and Early Warning of Natural Disasters [CEMADEN], Instituto Nacional de Pesquisas Espaciais [INPE]; International: UN Office for the Coordination of Humanitarian Affairs [OCHA], Flood list.)

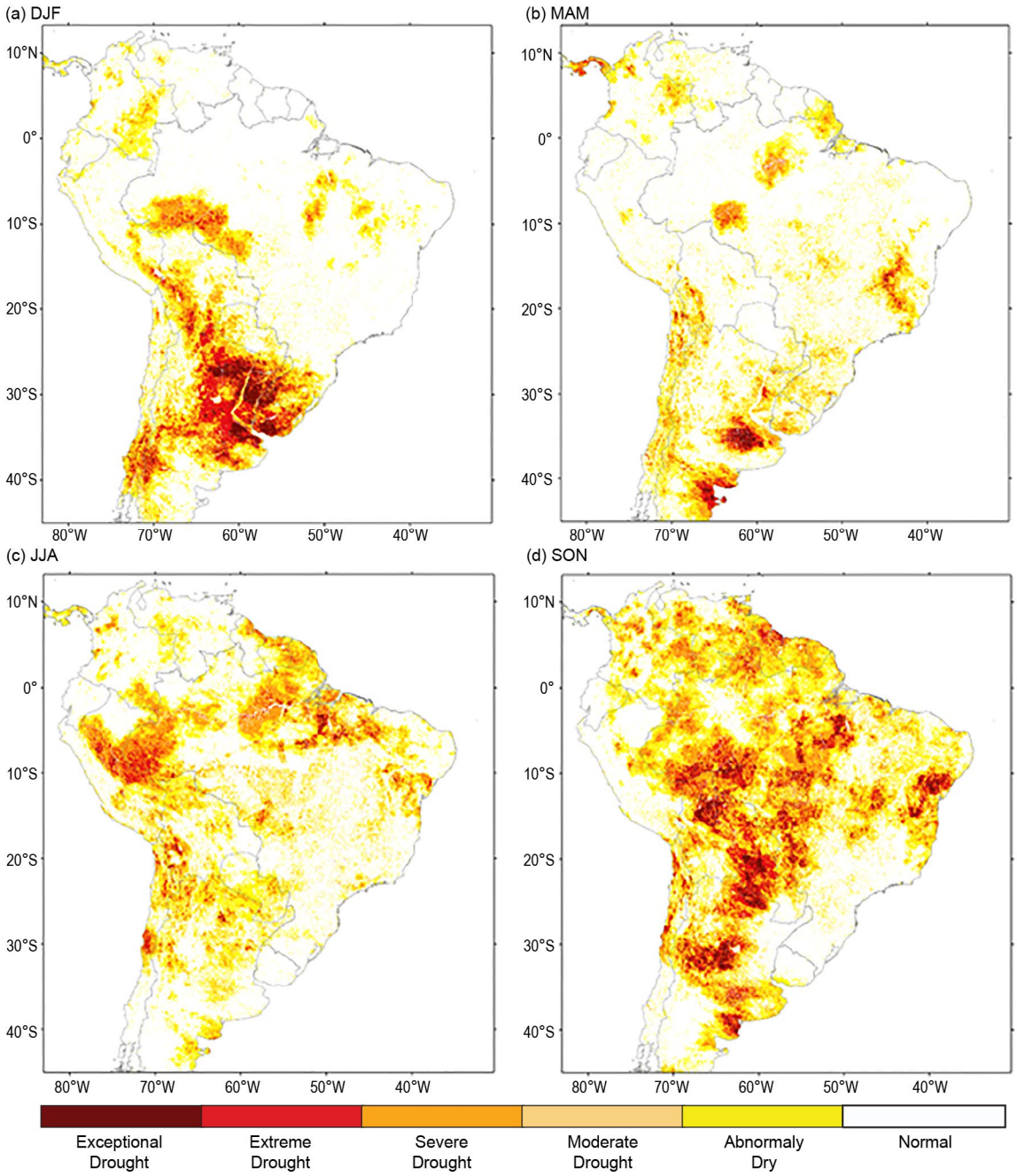

Fig. 7.16. Integrated Drought Index (IDI) maps for central South America during austral (a) summer (DJF) 2022/23, (b) autumn (MAM) 2023, (c) winter (JJA) 2023, and (d) spring (SON) 2023. (Source: Centro Nacional de Monitoramento e Alertas de Desastres Naturais [CEMADEN].)

First half of 2023

During 18–19 February, a cold front over the anomalously warm South Atlantic Ocean that interacted with the Serra de Mar Mountains in southeastern Brazil produced 683 mm rainfall in 15 hours along the coast of the state of São Paulo, and at least 61 people died after floods and landslides impacted the area (Marengo et al. 2024). In southwestern Amazonia on 23 March, heavy rainfall produced flooding in the city of Santa Cruz de la Sierra (Bolivia) and in Rio Branco (Acre-Brazil) where 124.4 mm fell in a 24-hour period; the Acre River rose from 8 m to 15.80 m (critical flood level is 14 m [INMET]). In Southern Peru, a landslide triggered by heavy rains on 5 February destroyed approximately 200 homes and killed 36 people in the Arequipa region. In Paraguay, heavy rain caused flooding in at least three departments at the end of February. Thousands of families were affected by floods in Concepción and La Victoria, with La Victoria receiving 300 mm during 25–26 February (Dirección de Meteorologia e Hidrologia [DMH]; https://www.meteorologia.gov.py/). On the Peruvian coast in early March, Cyclone Yaku caused

flooding, river overflows, and landslides in northern Peru. Seventy-one people died and nearly 113,000 residents were affected, according to the United Nations Office for the Coordination of Humanitarian Affairs (OCHA).

From November 2022 to February 2023, extreme dry conditions were reported over southwestern Amazonia, where rainfall anomalies reached −41 mm month^{-1} (a historical record that was exceeded only during the 1998 El Niño year with −42 mm month^{-1}).

Three cold waves were observed in Brazil in 2023 between May and July. In June, a friagem (cold air outbreak from the south) impacted the Brazilian Amazon. On 13 June, some cities in the Amazon experienced notably below-average temperatures: Cuiabá, 13.1°C (long-term mean [LTM]: 18.0°C), Campo Grande (Mato Grosso do Sul), 8.5°C (LTM: 15.8°C), Vilhena (Rondônia), 9.4°C (LTM: 19.0°C). In Bolivia, Cobija (8.8°C, LTM: 16.8°C) and Santa Ana de Yacuma (7.0°C, LTM: 17°C) recorded their lowest temperatures on record for June.

Second half of 2023

The State of Rio Grande do Sul in southern Brazil was affected by intense precipitation in 2023. On 16 June, torrential rain from an extra-tropical cyclone caused flooding and landslides. As much as 300 mm fell in 24 hours in Maquiné. On 4 September, several stations reported more than 100 mm rainfall totals, leading to a 12-m increase of the Taquari River level on 6–7 September (Alvala et al. 2024). Heavy rain continued to affect the state throughout September and early October, affecting at least 341,000 people across 93 municipalities, with 46 fatalities reported. In certain areas, river levels surged to 17 m above average, obstructing access from the capital city of Porto Alegre and the state's northern regions, according to OCHA. Flash floods on 7–8 October in the Bolivian Andes-Amazon caused severe infrastructure damage, and six people were killed in the Chapare region. On 10 October, 136 municipalities (of 295) in Santa Catarina were affected by rain and floods; 89 of those declared a state of emergency. On 29 October, 300 mm of rain was recorded in Foz do Iguaçu. The Iguaçu Falls recorded a flow of 24,200 m^3 s^{-1} on October 30, its highest flow in recent years (mean flow is 500 m^3 s^{-1} to 10^{00} m^3 s^{-1}).

Drought began in central and northern Amazonia in austral winter (dry season) and spring (pre-rainy season), respectively (see Sidebar 7.2 for details). Coincidentally, a warmer-than-normal winter and spring were observed in southwestern Amazonia due in part to the presence of hot, dry air that developed a heat dome, which occurs when high pressure accumulates over an area and remains for a prolonged period. During August–December, six intense heatwaves impacted central tropical South America on the following dates: 22–29 August, 18–30 September, 3–8 October, 16–25 October, 8–21 November, and 1–19 December (see Appendix Table 7.1 for selected statistics).

At least 27 Bolivian cities recorded their highest (monthly or absolute) temperatures from July to November. Every Andean (Altiplano, valleys, and Yungas) and lowland (Chaco, Chiquitania, Beni savanna, and Amazon rainforest) region was affected. At several locations, maximum temperature records were broken two or more times, even within the same month or heatwave event. El Niño was associated with the extreme temperatures in the Andes but not necessarily with the heatwaves in the lowlands. In August, a rare winter heatwave engulfed 19 of Brazil's 26 states and Bolivia. On 23 September, temperatures reached 31.8°C in Curitiba (LTM: 21.4°C) and 34.8°C in São Paulo (LTM: 24.4°C), and on 24 September reached 41.3°C in the western Amazon in Tingo de Ponaza, Peru (LTM: 33.5°C). The heatwave during 16–25 October led to some all-time records set in the Bolivian Amazon and in the Chaco (Bolivia-Paraguay). At least 10 deaths were attributed to heat in the lowlands of Bolivia as well as 10 in the Paraguayan Chaco. By 12 November, 1120 Brazilian cities recorded their highest temperatures, including 40.4°C in Rio de Janeiro (LTM: 29.4°C). The temperature reached 44.8°C in Araçuaí in Minas Gerais on 20 November (LTM: 32.0°C), potentially the record-highest value observed in Brazil, according to Instituto Nacional de Meteorologia.

Large wildfires raged across the heat-affected regions in Paraguay and Brazil, including in Bahia, Pantanal, and the Amazon where at least 22,050 fires were recorded since October, resulting in heavy smoke that impacted the entire city of Manaus, Brazil (over two million people). More than 3.5 million hectares were burned in Bolivia, including 1 million hectares of forests, causing severe air pollution that affected many Bolivian cities from September to November.

3. SOUTHERN SOUTH AMERICA

—L. S. Aldeco and J. L. Stella

This region includes Argentina, Chile, and Uruguay. Throughout this section, 1991–2020 is the base period used for both temperature and precipitation unless otherwise specified.

(i) Temperature

Above-normal annual temperatures were observed in most parts of the region and during almost every month of the year. Argentina recorded its warmest year on record with an estimated anomaly of +0.83°C. Uruguay had its second-warmest year on record (+0.7°C), and Chile had its third warmest (+0.5°C). Many stations (45 in Argentina and 4 in Uruguay) recorded their highest annual temperatures on record. Temperature anomalies ranged between +1°C and +2°C north of 35°S, where most of these records were set.

Austral summer 2022/23 was extremely hot across most of the region. An unprecedented number of heatwaves occurred between November 2022 and March 2023. It was the warmest summer on record at several locations with seasonal anomalies between +2°C and +3°C, including Paso de Los Libres, Reconquista, Rosario, Junín, Buenos Aires, Santa Rosa, and Neuquén in Argentina; Artigas, Durazno, and Mercedes in Uruguay; and General Bernardo O'Higgins and General Freire in Chile. Following a February heatwave, an unusual polar air irruption produced a significant drop in temperature, and several minimum temperature records were broken across Argentina and Uruguay. Early frosts were recorded with values close to 0°C, severely impacting agricultural areas already affected by drought and extreme heat. On 17–18 February, typical winter conditions occurred in the middle of what would become the warmest summer on record for Argentina.

Austral autumn over southern South America had temperature anomalies similar to summer, with the highest anomalies recorded over central Argentina and Chile. March was extremely warm in Argentina and Uruguay, due in part to a late, prolonged, and intense heatwave. During this heatwave, dozens of daily maximum temperature records were broken. Durazno (+1.8°C), Colonia (+1.8°C), and Prado (+1.7°C) in Uruguay each reported their warmest autumn on record, along with several locations in Argentina.

In accordance with the developing El Niño, austral winter was particularly mild in the central and northern regions of southern South America (SSA), while in southern Argentina and Chile, normal to below-normal temperatures were predominant. During 21–28 July, a cold wave affected extreme southern Argentina and Chile.

During austral spring, below-normal temperatures were observed in central and southern Argentina and Chile and in Uruguay, with anomalies between −0.5°C and −2°C. Above-normal temperatures continued over northern Argentina and Chile. An unusual heatwave affected Misiones province in Argentina during 21–26 September. Extreme high temperatures also severely affected the provinces of Salta, Formosa, and Chaco during spring.

(ii) Precipitation

Most of southern SSA had below-average annual rainfall during 2023, especially during summer and autumn, which were the two seasons that were under the influence of the ending of La Niña (Fig. 7.17). During winter, some cold fronts brought rainfall to different parts of the region, and during spring, precipitation events in Uruguay, northeastern Argentina, and central Chile were consistent with the development of El Niño. Despite high rain totals, the precipitation was not enough to counteract the deficits of the first part of the year in central, northern, and southern Argentina, central Chile, and southern Uruguay, where, overall, annual precipitation was below normal. Northeastern Argentina and Uruguay had above-average annual rainfall, along with some local stations in Patagonia.

During austral summer 2022/23, drier-than-normal conditions were observed in most of southern South America due to the influence of La Niña. The highest deficits were up to 79% below normal in most of Uruguay, northeastern Argentina, and central Patagonia of Chile and Argentina. Some stations recorded their lowest precipitation on record for the season: Florida (Uruguay) was 79% below normal, the lowest since 1980, and Paso de Los Libres (Argentina) was 75% below normal, the lowest since 1961. Agraciada in Uruguay recorded its lowest monthly

precipitation for February since 1980. However, some localized precipitation events led to above-normal rainfall at some stations in central-western Argentina, with totals 64% to 100% above normal.

During autumn, drier-than-average conditions were present across most of the region, with totals 40% to 80% below normal; however, some regions of Argentina and Chile recorded above-average rainfall during this period due to synoptic activity. Santiago del Estero in Argentina recorded its highest rainfall for the season since 1961 (91% above normal) and Teniente Vidal in southern Chile recorded its highest monthly rainfall for March since 1967.

During winter, below-average precipitation was recorded in Uruguay, central Chile, and eastern and southern Argentina, with June having been the driest month of the season (60% to 99% below normal). Nevertheless, in central Argentina, some stations set daily rainfall records for August: 117 mm in San Fernando and 112 mm in Aeroparque on 17 August, the highest daily rainfall totals since 1961. The heavy rain was due to the interaction of an unusual mass of warm and humid air in the region and the advance of cold air, which produced convective development with strong storms that affected extreme northeastern Buenos Aires and southern Uruguay. Central and west Patagonia of Chile and Argentina also recorded above-normal precipitation, setting some monthly and daily records. General Freire in Chile recorded 150.2 mm on 21 August, its highest daily rainfall for August since 1963, which also led to floods. Bariloche in Argentina recorded its highest precipitation total for winter since 1961.

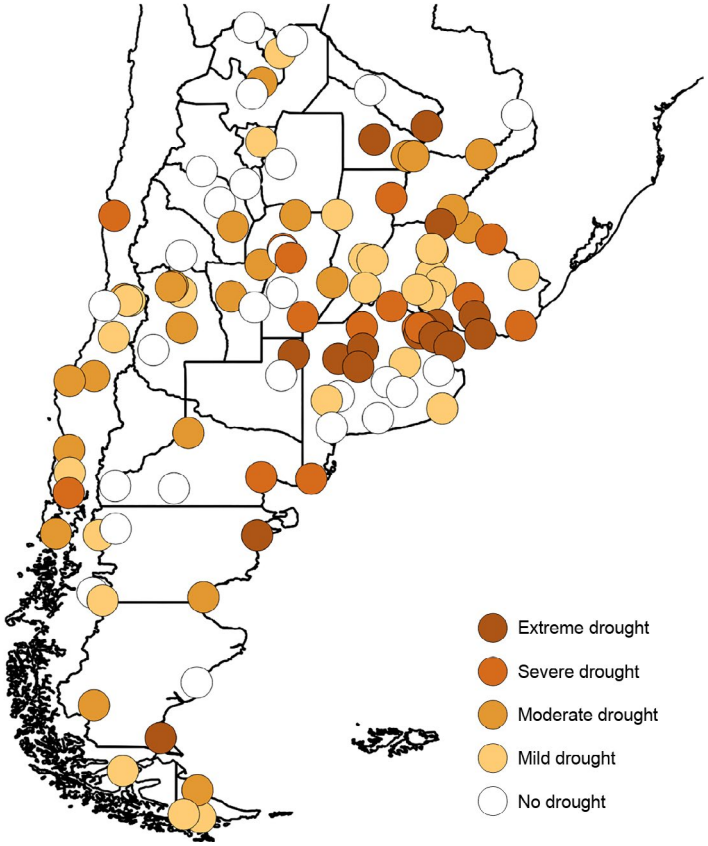

Fig. 7.17. Standardized precipitation index (SPI) for the six-month period 1 Jan–30 Jun 2023. SPI values can be referenced at: https://droughtmonitor.unl.edu/About/AbouttheData/DroughtClassification.aspx.

During austral spring, some regions in central Argentina had below-normal rainfall, but El Niño favored above-normal precipitation in central and northern Uruguay, central Chile, northwestern Patagonia, and northeastern Argentina. On 1 September, heavy rainfall due to a stationary front was observed over northeastern Argentina and Uruguay, and some stations reported new record-high daily totals, including Ituzaingó, Argentina (267 mm), and Bañado Medina, Uruguay (138 mm). Monthly records were set also in Uruguay: Cuchilla Caraguatá Sur, Bañado Medina, and Melo (since 1980), and Posadas and Oberá in Argentina (since 1961). Above-normal rainfall was also observed in Uruguay and eastern Argentina in November.

(iii) Notable events and impacts

Figure 7.18 shows numerous notable events that occurred across the region during 2023. Some of these are discussed in more detail below.

A persistent drought affected several areas in Uruguay, central and northeastern Argentina, and central Chile due to the effects of La Niña. Some of these regions experienced severe or extreme drought, according to the standard precipitation index (Fig. 7.17). In Montevideo, Uruguay's most populous city, there was a lack of water supply between May and June. This situation improved at the beginning of spring as El Niño developed, and precipitation events were favored.

Dry conditions and a blocking pattern with a persistent high-pressure system in the region led to several heatwaves in Uruguay and central-east Argentina. The longest and most intense heatwave occurred during early March in both countries and set new daily records of highest

minimum and maximum temperatures at several stations: Santa Rosa (Argentina) recorded 40.7°C on 3 March, and Nueve de Julio (Argentina) recorded 40°C on 2 March, both the highest on record since 1961; Mercedes (Uruguay) recorded 40.5°C and Durazno (Uruguay) recorded 40.2°C on 11 March, both the highest on record since 1981. In Argentina, the electric energy consumption set a record on 13 March with 29,105 megawatts.

During spring, El Niño favored several precipitation events, mostly convective with different impacts. In northeastern Argentina, heavy precipitation led to river overflows, floods, and the closure of Iguazú Falls National Park; in Paso de Los Libres, a new daily record of 130 mm was set on 22 October, the highest since the start of records in 1961.

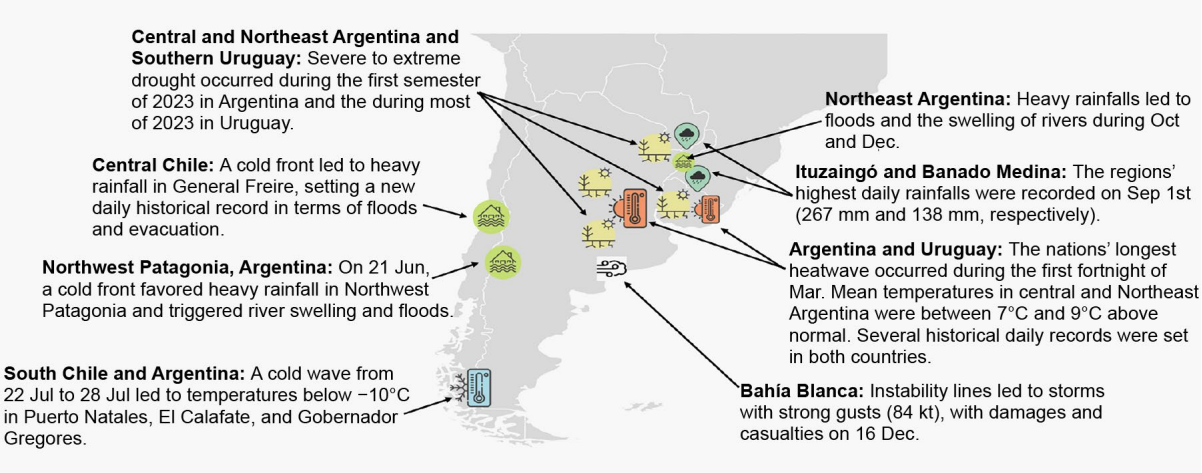

Fig. 7.18. Extreme and notable events in southern South America during 2023.

Sidebar 7.2: Drought in South America in 2023: Amazonia and Altiplano

—J. MARENGO AND J. C. ESPINOZA

Amazonia

A severe drought affected the western Amazon River basin countries and most of northern South America due to a dry period from July 2023 through the end of the year. The spatial-temporal evolution of the drought shows an increase in extent and severity in the Brazilian, Peruvian, and Bolivian Amazon. A series of six heatwaves during winter and spring exacerbated the impact of the precipitation deficits. The average temperature was abnormally high, up to 5°C above normal during austral spring, which is the pre-rainy season in Amazonia (section 7d2). The El Niño event that developed in mid-2023 intensified the drought in Amazonia during austral winter and spring during the low rainfall and pre-rainy seasons, respectively (Espinoza et al. 2024). In September and October, the basin recorded below-average rainfall in the Peruvian and Bolivian Amazonia and northwest and southwest Brazilian Amazonia in the Solimões, Purus, Juruá, and Madeira River basin headwaters. Eight Brazilian states recorded their lowest rainfall totals from July to September in over 40 years, with deficits of 100 mm month^{-1}–300 mm month^{-1} (Toreti et al. 2023).

Due to the warm and dry conditions in spring 2023, most of the main rivers in the Amazon, including the Solimões, Purus, Acre, and Branco, either suffered extreme drops in their levels in some regions, or dried up completely. According to the National Water Agency of Brazil (ANA) and the Brazilian Geological Survey, the level of the Madeira River in Porto Velho reached its lowest level in the 56-year record (15 m on 15 October). According to the Port of Manaus, the Rio Negro recorded a tide of 12.70 m at Manaus on 26 October, its lowest since 1902 (Fig. SB7.3). In the Peruvian Amazon, the flows and levels of the Amazonas, Marañón, Huallaga, and Ucayalí Rivers were

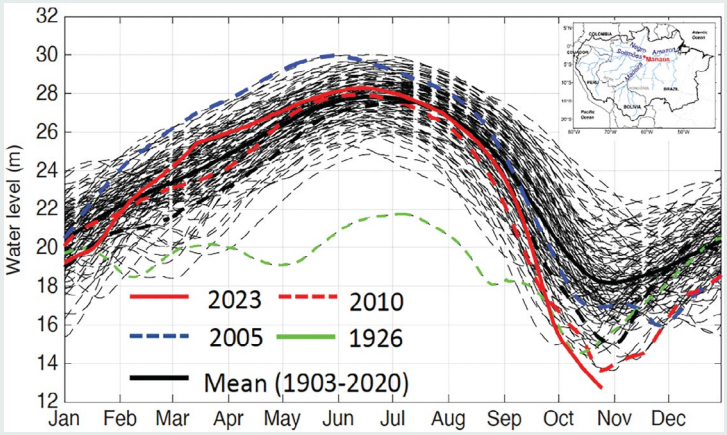

Fig. SB7.3. Rio Negro water levels measured at the Port of Manaus. Solid red line shows the levels in 2023 (Espinoza et al. 2024).

average to much lower than usual. Discharge for the Huallaga River at Tingo María was 45% below normal in October (Servicio Nacional de Meteorología e Hidrología [SENAMHI] 2023b). In Bolivia, the Mamoré-Guaporé and Madeira Rivers were low due to deficient rainfall from July 2022 to June 2023. In Tefé Lake, over 180 botos cor de rosa—an Amazon River dolphin—were found dead after the water reached 40°C, a record-high temperature unprecedented in the region (Costa and Marengo 2023).

Forest vegetation showed signs of wilting during the heatwaves, and high tree mortality increased the risk of wildfire hazard. The drought affected navigation, commerce, and basic food and water supply. The most affected were indigenous communities and the Ribeirinhos (people who live along the shores of the rivers), who are highly vulnerable to changes in the hydrology of the rivers.

Peruvian and Bolivian Altiplano

An extreme drought that started in August–September 2022 peaked in January 2023 in the Peruvian-Bolivian Altiplano, involving most of the Titicaca, Desaguadero, Poopó, and Salar de Coipasa hydrological system (Fig. SB7.4a). The level of Lake Titicaca reported an unusually low rise (0.09 m) between December 2022 and April 2023, representing the fourth-lowest seasonal lake rise since 1940 (Fig. SB7.4b).

Intense El Niño events in this region are related to drought situations during austral summer. However, November–February 2022/23 was characterized by La Niña. Basin wide-averaged precipitation anomalies during austral spring 2022 was 57% below the 1981–2020 September–November normal. From November to the end of austral summer, a historical deficit of atmospheric moisture flux from the southern and western Amazon toward the Altiplano was detected, which favored dry conditions over this region. While this climatic feature was related to La Niña conditions during 2022/23, studies also suggest the potential role of Amazon deforestation in the substantial lack of atmospheric moisture flux reported in this event (Arias et al. 2024; Gutierrez et al. 2024).

Agriculture is the main economic activity in the Peruvian-Bolivian Altiplano and depends directly on precipitation and its variability. The 2022/23 drought in this region reduced the yield of potatoes and some other Andean crops by more than 50%, causing large economic losses to thousands of farmers. According to government figures, the lack of water in Bolivia affected more than 487,000 families. Residents in the La Paz, Cochabamba, Santa Cruz, Oruro, Chuquisaca, Potosí, and Tarija departments in Bolivia all faced drought conditions. In Peru, drought prevailed over the Andean region's northern and southern sections. The city of Puno and surrounding areas experienced its worst drought of the last 60 years, which affected crops, harvest, and the regional economy. It is estimated that the water deficit generated economic losses in Puno, including 80% loss in potatoes and sweet potatoes and 90% loss in Andean grains (Servicio Nacional de Meteorología e Hidrología [SENAMHI] 2023).

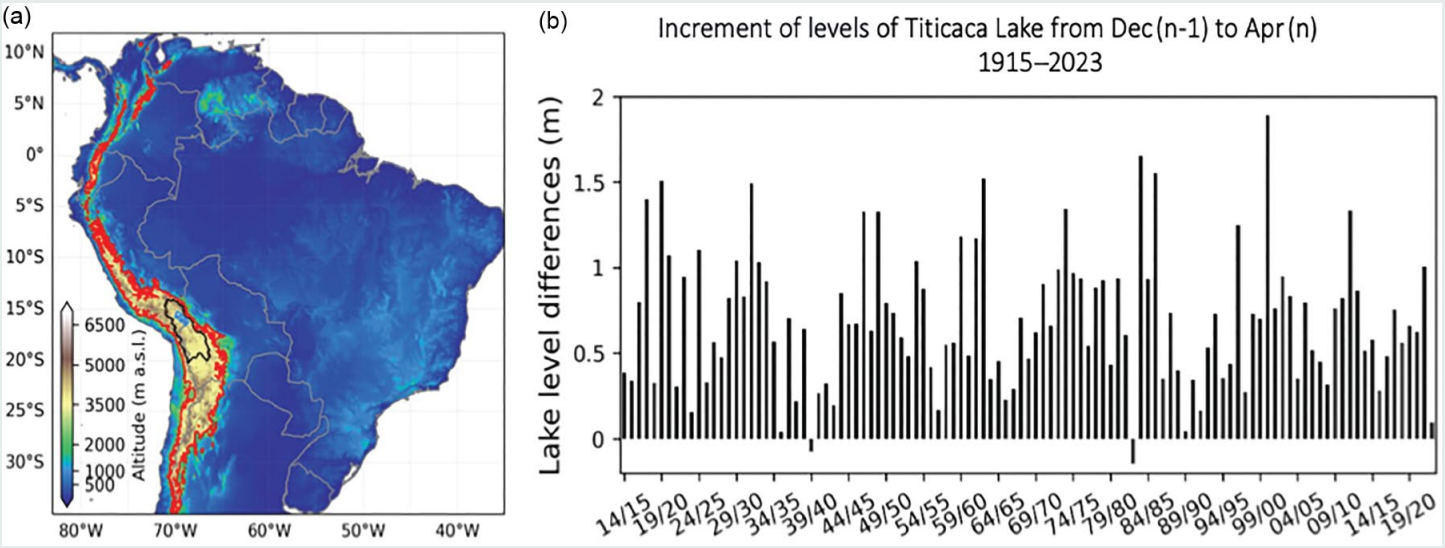

Fig. SB7.4. (a) Location of the Titicaca, Desaguadero, Poopó, and Salar de Coipasa hydrological system (black line) over tropical South America. Red lines in the Andean cordillera denote altitudes of 3000 m a.s.l. (b) Interannual increment of levels of Titicaca Lake from Dec to Apr for the period 1915–2023.

e. Africa

—A. Mekonnen, Ed.

The 2023 analysis for Africa is based on observational records from meteorological and hydrological services including rainfall from the Global Precipitation Climatology Project and reanalysis products from the National Centers for Environmental Prediction/ National Center for Atmospheric Research. Notable events in this year were compiled based on reports from government agencies, regional and international organizations, and research/Early Warning organizations. The climatological base period is 1991–2020, and the terms "normal" and "average" are interchangeably used to refer to this climatology.

Figure 7.19a presents the 2023 mean temperature anomalies for Africa. Above-average annual temperatures were observed over Africa except some areas in central and southern Libya, the southwestern corner of Egypt, and adjoining northwestern Sudan. Anomalies higher than +1.2°C are seen over most of northwest Africa, southwest Africa from Angola to Namibia and Botswana, and across South Sudan, central Africa, the southern half of Cameroon, and southern Nigeria (Fig. 7.19a).

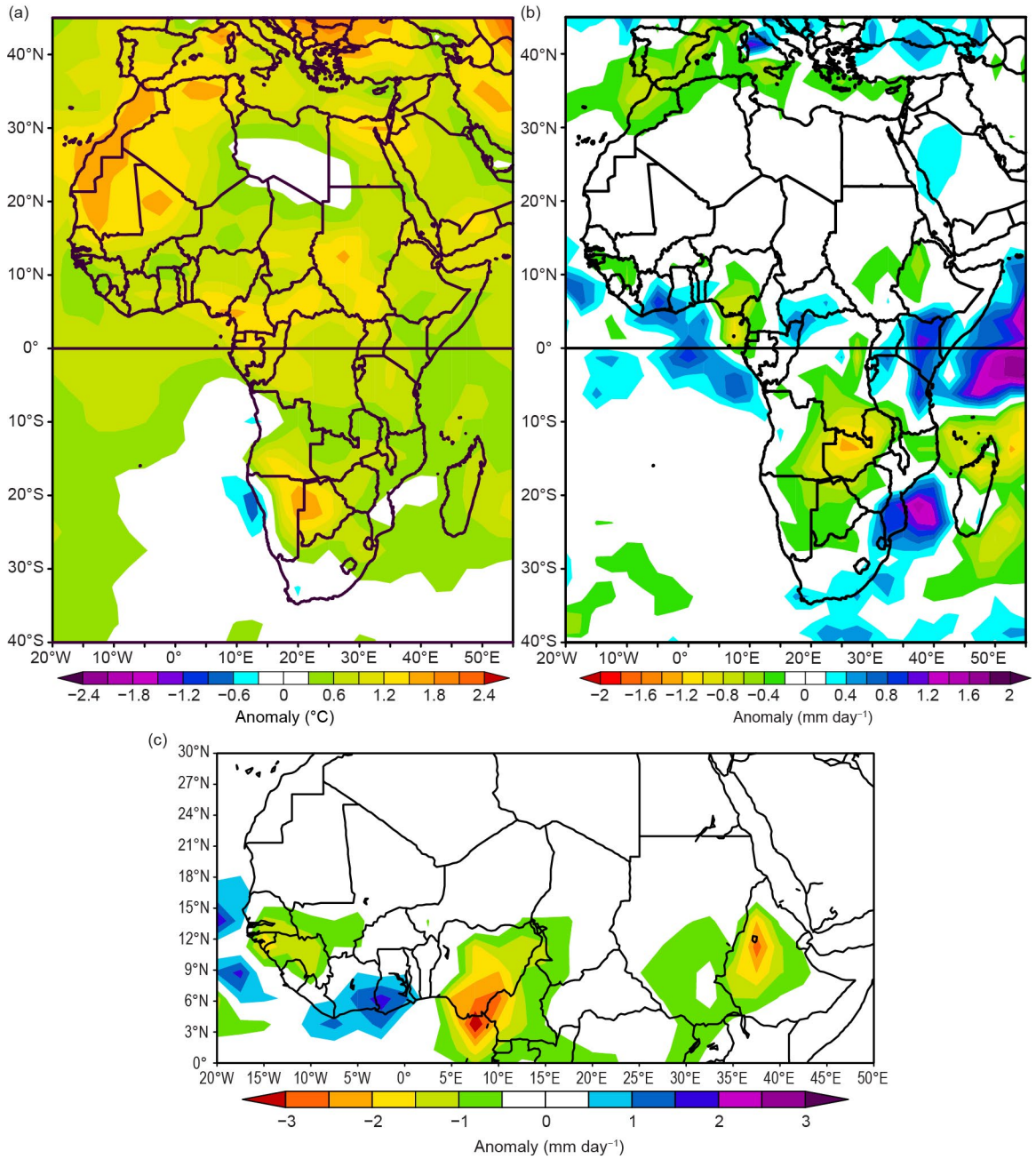

Fig. 7.19. Annual (a) temperature (°C) and (b) rainfall anomalies (mm day^{-1}) over Africa. (c) Jul–Sep rainfall anomalies (mm day^{-1}) over North Africa. Anomalies are with respect to 1991–2010 base period. Temperature is from the National Centers for Environmental Prediction's National Center for Atmospheric Research and rainfall anomalies are based on GPCP.

Above-average rainfall was observed over Kenya, Uganda, southern areas of the Central African Republic, and parts of Ghana and Cote d'Ivoire (Fig. 7.19b). Anomalies of less than −0.4 mm day^{-1} were observed in Zambia, the southeastern part of the Democratic Republic of Congo, and the southeastern corner of Angola as well as in the high rainfall zone of western Ethiopia and adjoining Sudan, southern Nigeria, and southwestern Cameroon (Fig. 7.19b). Significant below-average rainfall over these areas was also observed in 2022. The annual rainfall anomalies over most of the Sahel appears to be within the normal range (−0.2 day^{-1} to +0.2 mm day^{-1}).

The Sahel receives most of its annual rainfall during the July–September (JAS) season. In 2023, significant deficits (1.5 mm day^{-1} to >3 mm day^{-1} below normal) were observed over western Ethiopian highlands, Nigeria, Cameroon, most of Senegal, The Gambia, Guinea-Bissau, and Guinea highlands (Fig. 7.19c). Above-average JAS rainfall is seen over the southern areas of Ghana and Cote d'Ivoire.

High impact weather and climate variabilities were also reported from regions. The details of these are presented below.

1. NORTH AFRICA

—K. Kabidi, A. Sayouri, M. ElKharrim, S. Hakmi, and A. E. Mostafa

The North Africa sub-region includes Mauritania, Morocco, Algeria, Tunisia, Libya, and Egypt. Much of this region is characterized by arid and semi-arid climate, while northern parts exhibit Mediterranean climates. Precipitation over the region in 2023 was highly variable. While above-average precipitation was reported from northern Egyptian meteorological stations, droughts, along with heatwaves, were observed in northwest Africa. In September 2023, a storm and dam collapse in northern Libya caused extensive damage. In contrast, prolonged droughts (extending from past years) and above-normal temperatures were observed in Morocco.

(i) Temperature

During winter (December 2022–February 2023), both above-normal and below-normal temperatures were observed over North Africa north of 10°N (Fig. 7.20a). Anomalies of more than +1°C dominated the North African region, except for Libya. Anomalies of more than 2°C were observed in eastern Mauritania and northern and western Mali. Meteorological stations in Morocco also reported above-average minimum temperatures in January and February. Tunisian stations, on average, had temperatures up to 1.4°C above average in January and February, with anomalies from +0.3°C at Tabarka to +2.4°C at Thala. Minimum temperatures at some Tunisian stations (Mahdia, Thala, Tatouine) were up to 1.4°C above average during this period. January mean temperatures in Algeria were near normal. In northern Egypt, stations indicate above-average temperatures during December 2022 and January 2023 but below-average temperatures in February. Reports from the Egyptian Meteorology and Hydrological Services indicate that winter temperatures were impacted by the positive phase of the North Atlantic Oscillation (NAO). In contrast, the lowest minimum temperature of 0°C on 2 February was recorded at Nekhel in North Sinai, Egypt.

During spring (March–May 2023; Fig. 7.20b), anomalies of more than +2°C were observed across Morocco, western Algeria, Tunisia, and northern Mauritania, while temperatures over Libya and southwestern Egypt were below average. Northern Egypt, however, continued to see above-average temperatures. Tunisia reported monthly anomalies of +1.7°C in March and +0.8°C in May. Minimum and maximum temperatures in April were above average over Morocco, Tunisia, and Algeria. In Tunisia, maximum temperatures of 34.6°C at Bizerte and 37.8°C at Beja and Jendouba were reported.

Summer temperatures (June–August) were more than 2°C above normal over Morocco, northern Algeria, Mauritania, Tunisia, and northern and western Egypt (Fig. 7.20c). The rest of North Africa had mean temperature anomalies between +0.75°C and +2°C. On 7 June in Egypt, the station Sharm-el-sheikh reported an anomaly of +2.5°C, and Dakhla reported a maximum temperature of 48°C. Several Moroccan stations reported new local maximum temperature records during July (Smara, 49.9°C; Bouaarfa, 43.6°C; Errachidia, 44.7°C; Taourirt, 47°C) and August (Agadir, 50.4°C; Essaouira, 48.7°C; Tan-Tan, 48.2°C). Anomalies as high as +5°C were reported from Algerian stations in July, with about 95% of the stations reporting 40°C or higher.

July temperatures over Tunisia were 4°C above normal, making this the country's hottest July since records began in 1950. New records include 49.1°C at Gabes, 49.1°C at Medenine, 49°C at Tunis, 48.9°C at Kebili, and 48.3°C at Monastir. Temperatures in the country returned to near normal in August.

In Autumn (September–November), temperatures were >2°C above normal across most of North Africa, with anomalies of +0.5°C to +1.5°C observed over Libya (Fig. 7.20d). In September and November, temperature anomalies of +2.5°C to +4°C were reported from Moroccan and Algerian stations. In Tunisia, mean temperatures were 1.2°C above normal in September and 2.4°C in October.

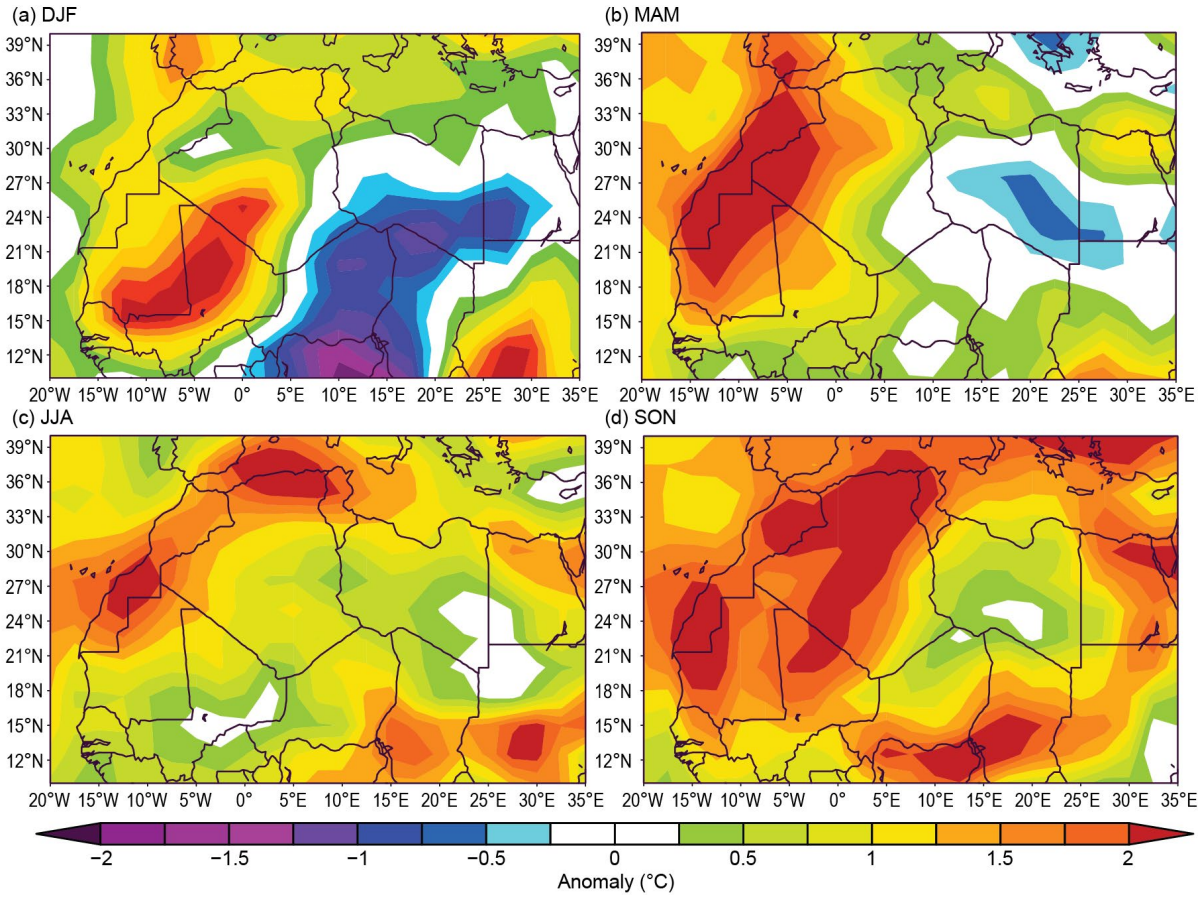

Fig. 7.20. Seasonal temperature anomalies over North Africa for (a) Dec–Feb 2022/23, (b) Mar–May 2023, (c) Jun–Aug 2023, and (d) Sep–Nov 2023. Anomalies are with respect to the 1991–2010 base period. (Source: NCEP/NCAR.)

(ii) Precipitation

Figure 7.21 shows seasonal precipitation variability in 2023. Since summer is not normally a precipitation season over the region, summer precipitation is not presented here.

Winter precipitation was between 0.2 mm day^{-1} and 1 mm day^{-1} below average over much of North Africa and as much as 0.4 mm day^{-1} below average over northeast Libya and northern Egypt (Fig. 7.21a). Moroccan stations largely report drier-than-normal conditions, with stations in the north reporting 13%–60% of their normal precipitation. Near- to above-normal precipitation was reported from Egyptian stations. Heavy rainfalls of about 35 mm were reported from Alexandria on 12 December 2023. Average annual rainfall at this station is 60 mm.

Below-normal precipitation was also observed over northwestern Algeria and northern Morocco during spring (March–May; Fig. 7.21b). In Morocco, stations reported monthly average precipitation in March, April, and May that was 93%, 62%, and 85% of normal, respectively.

Drier-than-normal conditions continued to prevail in autumn (September–November) as well (Fig. 7.21c). Precipitation was about 0.7 mm day^{-1} below normal across Morocco, Tunisia, and the northern half of Algeria. In September, stations in northern Morocco reported about 70% of normal precipitation, while southern stations saw near-normal rainfall and eastern stations above normal. Above-average precipitation was also observed over the Moroccan region

bordering the Atlantic. November and December 2023 were dry, ranging from 96% to 72% of normal. The dryness was associated with the dominance of Azores high pressure and the positive phase of the NAO that lasted several weeks. The prolonged seasonal rainfall deficit, nearly 50% of normal, was also observed over Tunisia. September and October rainfall over Tunisia was about 96% of normal.

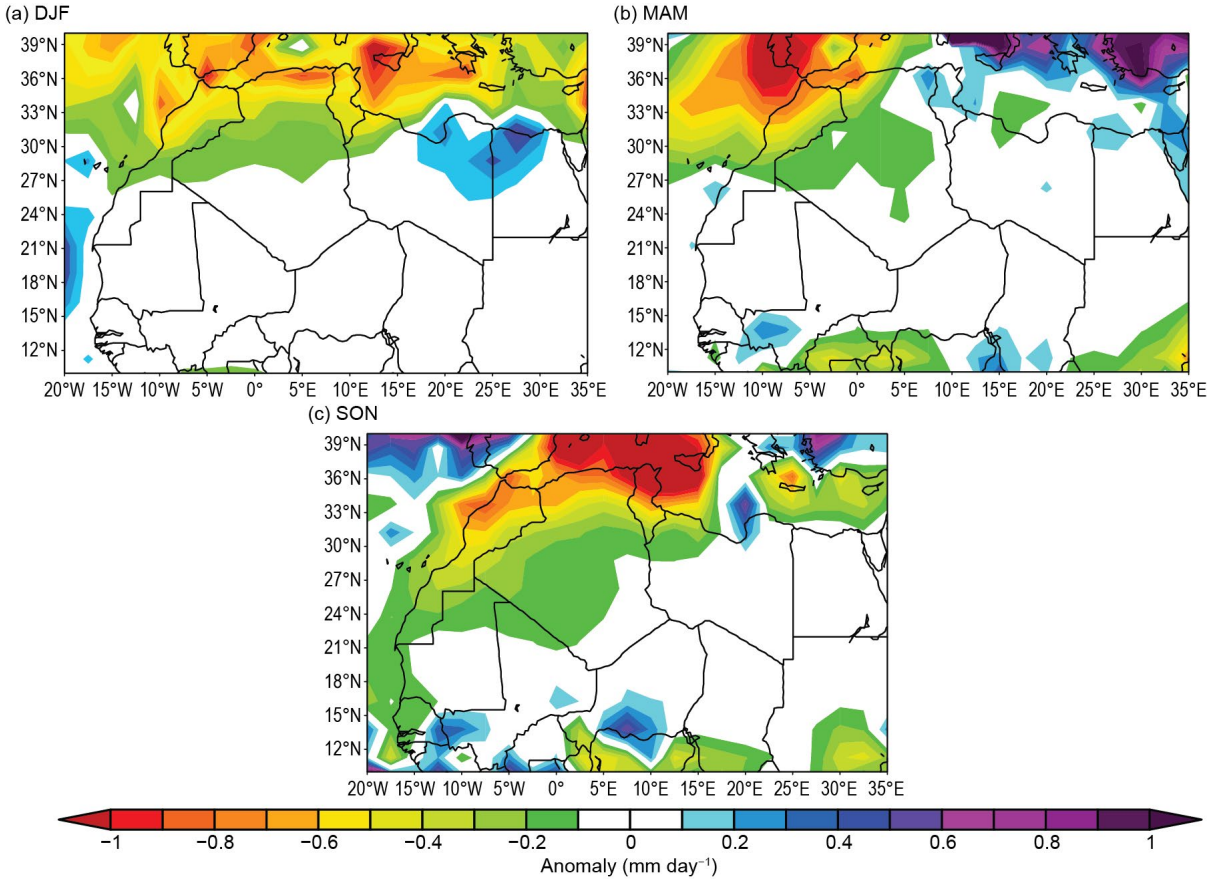

Fig. 7.21. Seasonal precipitation anomalies (mm day^{-1}) over North Africa for (a) Dec–Feb 2022/23, (b) Mar–May 2023, and (c) Sep–Nov 2023. Anomalies are with respect to the 1991–2010 base period. (Source: GPCP.)

(iii) Notable events and impacts

Record-high rainfall was observed over Libya in September, which was associated with Storm Daniel (classified as a "medicane", i.e., a tropical cyclone that forms in the Mediterranean Sea). According to the Libyan National Meteorological Center, rainfall totals ranging from 150 mm to 240 mm were recorded in the first dekad (10 days) of September. The city of Al-Bayda received a total of 414.1 mm during 10–11 September. The storm reached its peak in northeastern Libya on the 10th and brought extreme rainfall that led to devastating floods. The floods killed at least 4352 people and displaced more than 43,000, while another 8000 were missing, according to reports from the United Nations in Libya. Entire neighborhoods disappeared after waters from burst dams flooded the city of Derna.

In May, June, and September, flooding due to torrential rains caused several deaths in many parts of Algeria. During July, flash floods caused by heavy rains affected Moulay Brahim in the region of Alhouz, Morocco, causing material damages.

According to the respective government ministries, forest fires broke out in Morocco, Algeria, and Tunisia during the summer. At least 34 deaths were reported due to the fires in Algeria in July. A total of 41,000 hectares of forest was burnt in Algeria during 2023. In Morocco, 395 forest fires were reported during the year, which burnt 6420 hectares. In Tunisia, 438 forest fires burned 4800 hectares of forests.

2. WEST AFRICA

—W. Agyakwah, J. Hicks, and W. M. Thiaw

West Africa stretches from the Guinean coast to about 20°N and from the eastern Atlantic coast to Niger. It is divided into two sub-regions. The Sahel stretches from Senegal and The Gambia in the west to Niger in the east and is located between 12°N and 17°N. The Gulf of Guinea region is located to the south and runs from approximately 4°N to 10°N. This region covers the Guineas in the eastern Atlantic coast in the west to Nigeria and Cameroon in the east.

(i) Temperature

Mean annual temperatures in the Sahel region were 26°C–30°C, with the highest temperatures recorded in southern Mauritania, central and eastern Senegal, central Mali, northern Burkina Faso, southwestern and southeastern Niger, and northeastern Nigeria (Fig. 7.22). Annual mean temperature anomalies were +0.5°C to +1°C over most of the region; southern Mauritania, eastern Senegal, central Mali, and northeastern Nigeria had anomalies of +1°C to +1.5°C. Mean annual temperatures in the Gulf of Guinea region were 24°C–28°C. Anomalies of +0.5°C to +1°C were observed in many places, except southern Burkina Faso and northern Ghana, which recorded near-normal temperatures. Most of West Africa experienced mean temperatures above the 90th percentile, except for parts of Niger and Burkina Faso (Fig. 7.22).

From January to April, the monthly average temperatures were higher than usual in the far western Sahel region. Positive anomalies started spreading throughout the Sahel region from May onwards. The highest anomalies, +2°C to +3°C, were observed from September to November (SON) over southeastern Niger and northeastern Nigeria. The Gulf of Guinea experienced above-average monthly temperatures from the beginning of the year, much like the Sahel. These above-average anomalies were concentrated along the Gulf of Guinea coastal areas and spread inland over time, reaching their maximum during SON. Central Nigeria experienced the warmest temperatures with anomalies between +1.5°C and +2°C (>90th percentile).

The Sahel experienced mostly near-normal seasonal mean maximum temperatures. However, above-average temperatures dominated the Sahel region during the June–August, June–September (JAS), August–October, and SON seasons. The JAS season saw the highest positive anomalies of +2.5°C to +3°C in northeastern Nigeria (>90th percentile). The mean maximum temperatures in the Gulf of Guinea were higher during January–March (JFM), with the highest anomalies of +4.5°C to +5°C over southwestern Nigeria, which was near a record-breaking level and in the 90th to 97th percentile range.

The coldest minimum temperatures in the Sahel since 1991 occurred from January to April, with anomalies of –1.5°C to –2°C over southeastern Niger and northeastern Nigeria in February. Likewise, in the Gulf of Guinea, the lowest minimum temperatures since 1991 were observed in February, with negative anomalies of up to –3°C over southeastern Nigeria. February's coldest temperatures contributed to JFM 2023 becoming the coldest such period on record throughout both the Sahel and Gulf of Guinea regions.

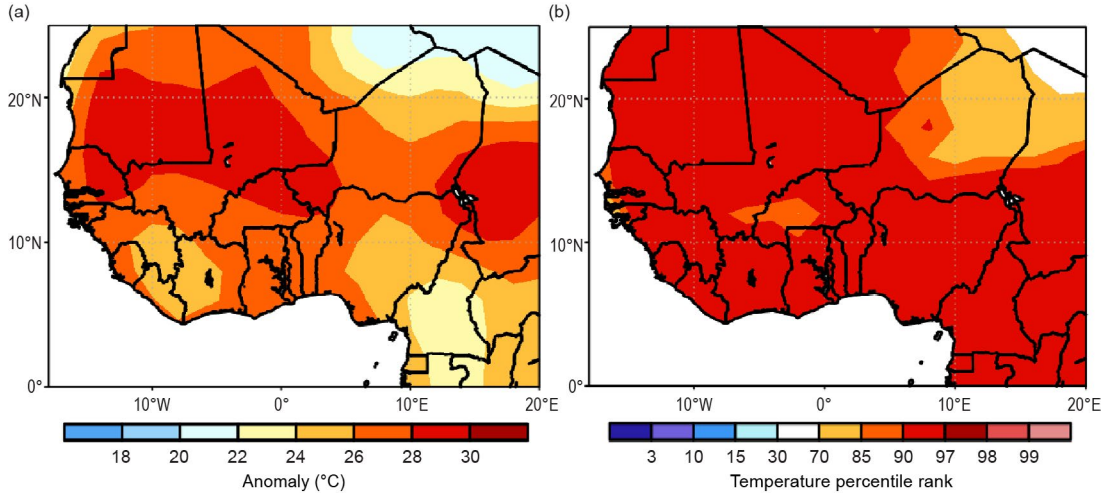

Fig. 7.22. Annual (a) mean temperature (°C; 1991–2020 base period) and (b) percentile ranking in 2023 for West Africa. (Source: NOAA National Centers for Environmental Prediction.)

(ii) Precipitation

In 2023, most of the Sahel experienced below-normal rainfall, with some areas recording deficits ranging from –50 mm to –250 mm. The Gulf of Guinea received above-average rainfall along its coastal regions, with the highest surpluses of +250 mm to +300 mm in southeastern Cote d'Ivoire and southwestern Ghana. The most significant rainfall deficits were observed in eastern Nigeria (<10th percentile).

The onset of the West African monsoon rains occurred in May and June in the southern and northern sectors of the Sahel, respectively. In May, southwestern Mali observed more rainfall than usual (10 mm–20 mm), and this trend continued in June, spreading to much of the Sahel. As the year progressed, rainfall surpluses gradually increased to between +10 mm and +100 mm in southeastern Niger and northern Nigeria. However, rainfall deficits began to appear in July and reached a peak of –100 mm in August over southern Mauritania, eastern Senegal, and southwestern Mali.

The rainy season in the Gulf of Guinea usually starts between March and May. In March, some regions, including Cote d'Ivoire and Nigeria, experienced rainfall surpluses of +10 mm to +30 mm. From April to June, there was an increase in rainfall in the Gulf of Guinea region, resulting in significant rain surpluses of +50 mm to +100 mm in southern Cote d'Ivoire and southwestern Ghana (Fig. 7.23). As the season progressed from June to September, the rain surpluses increased even further, reaching a maximum of over +100 mm in southern Cote d'Ivoire, Ghana, and Togo (Fig. 7.23). This large surplus led to 120%–200% of normal rainfall and contributed to the substantial annual rainfall surplus for those locations. Despite the abundant rainfall in the Gulf of

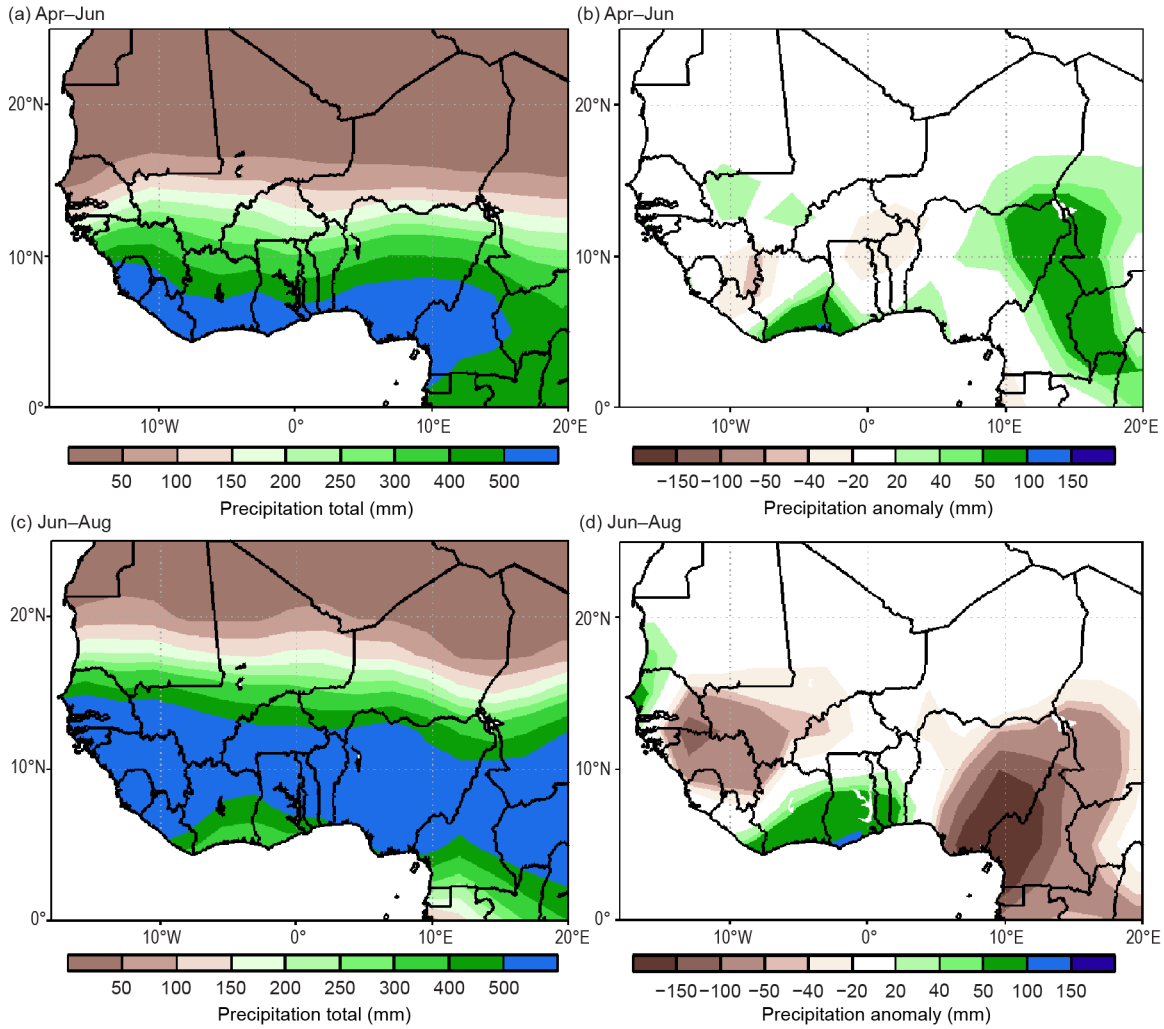

Fig. 7.23. Cumulative Apr–Jun seasonal (a) total precipitation, (b) precipitation anomalies; Jun–Aug seasonal (c) total precipitation, (d) precipitation anomalies in 2023 for West Africa (mm; 1991–2020 base period). (Source: NOAA National Centers for Environmental Prediction.)

Guinea, rainfall deficits started to increase from April (–10 mm to –50mm) and reached a maximum of –50 mm to –100 mm during August. Nigeria experienced below-average rainfall from April to May and again from July to October. Nigeria's central and eastern regions were the most affected, contributing to the annual rainfall deficit. Despite the persistent rainfall deficits, substantial surpluses ranging from +30 mm to +100 mm were recorded over Nigeria in June.

(iii) Notable events

In January, heavy rains that occurred in the previous months led to the overflowing of the Niger River at Dire in Mali, which caused flooding in the regions of Mopti and Tombouctou, according to the UN Office for the Coordination of Humanitarian Affairs. The flooding worsened the destruction already caused by the September 2022 floods in Mopti, affecting over 1000 households and damaging around 620 hectares of fields.

Heavy rainfall and storms hit Freetown on 9–10 May, causing significant damage. The National Disaster Management Agency of Sierra Leone reported seven deaths, mudslides in some parts of Freetown, and damage to the Leone Oil Facility in Kissy.

Heavy rainfall in Cote d'Ivoire on 11 June resulted in flooding, landslides, and significant building damage. Five people died in Yopougon Bel Air, and road closures in Yopougon and Songon isolated some communities.

Niger was impacted by heavy rains and floods since June, which led to 32 fatalities and dozens of injuries, and affected over 88,000 people.

On 6 and 11 August, Guinea was affected by heavy rains that caused severe flooding in Coyah, Conakry, and Siguiri. The flooding made major roads impassable for both vehicles and pedestrians.

Liberia experienced heavy rainfall during 1–4 September that caused severe flooding in the northeast. Around 15,200 people were affected, and infrastructure, houses, and facilities were swept away. Monrovia, Liberia's capital city, and surrounding areas were hardest hit, with around 12,450 people affected by five days of continuous rain beginning on 30 August.

In Ghana, heavy downpours caused flooding in March, June, and December, damaging infrastructure, crops, and homes. In September, the levels of the Lake Volta reservoir rose so high that they led to a spilling at the Akosombo Dam, displacing 30,000 people. Local officials blamed houses built in flood plains and drainage channels for the flooding.

Severe flooding in Nigeria, caused by heavy rainfall and water release from Cameroon's Lagdo Dam on 5 October, led to significant infrastructure damage in 14 of 21 Local Government Areas in Adamawa State. The flood resulted in 33 deaths and affected over 51,000 people across 214 communities, and worsened the humanitarian crisis in the region, with women and children being the most affected.

3. CENTRAL AFRICA

—J. Hicks, W. Agyakwah, and W. M. Thiaw

Central Africa features a unique climate system marked by a strong annual cycle as it spans a wide area of Africa across both the Northern and Southern Hemispheres. The region extends from the southern tip of the Democratic Republic of Congo (DRC) northward into the central areas of Chad. Longitudinally, the region extends from about 5°E to ~35°E. This analysis focuses on the sub-region encompassing Cameroon, Chad, Central Africa Republic (CAR), DRC, Congo (Republic of Congo), Gabon, Equatorial Guinea, and Sao Tome and Principe.

(i) Temperature

Annual mean temperatures were 2°C–4°C above average across much of Chad and CAR in January, with such anomalies persisting through February in southern CAR and northern DRC. During the second half of the year, a larger area of central Africa that extended from Chad to southern DRC observed mean temperatures that were 1.5°C–4°C above average, particularly from July to October. A majority of the region observed mean temperatures above their 90th percentile from May to December. Conversely, southeastern DRC experienced four months (April, May, July, and August) where mean temperatures were as much as 1.5°C below average (<15th

percentile). Monthly maximum temperatures were 4°C–5.5°C above average from southern Cameroon to northern DRC in February and in southwestern DRC during July–August. A majority of Central Africa observed maximum temperatures ranking above their 90th percentile from May to October. The July–September period ranked above the 90th percentile for much of the region outside of southeastern DRC, with maximum temperatures 5°C above average in southwestern DRC (Figs. 7.24a,b). Conversely, central DRC and southern Chad/northern CAR experienced their coldest maximum temperatures since 1991 in January and November, respectively. Despite the anomalously high maximum temperatures between July and September, southwestern DRC also observed some of their coldest minimum temperatures since 1991 during that season.

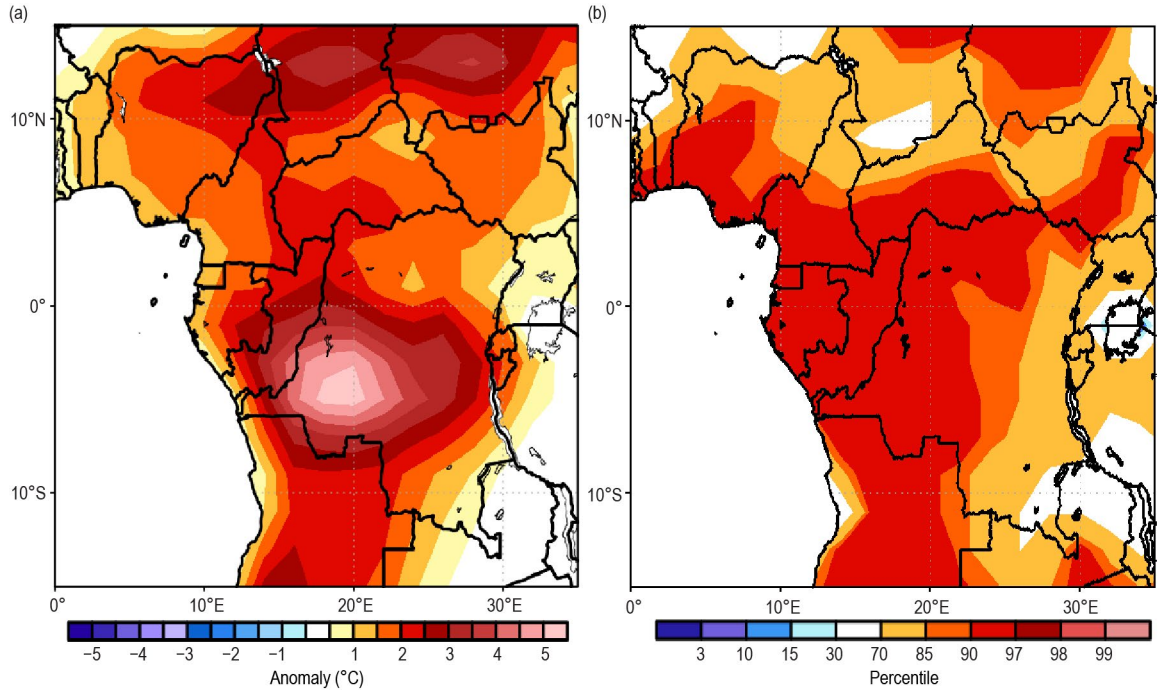

Fig. 7.24. Jul–Sep (a) maximum temperature anomalies (°C; 1991–2020 base period) and (b) maximum temperature percentile rank in 2023 for Central Africa. (Source: NOAA National Centers for Environmental Prediction.)

(ii) Precipitation

Cameroon experienced a rainy start to its wet season after observing rainfall surpluses of 50 mm–100 mm in June, which was up to two times its monthly climatology. Throughout the rest of the rainy season, Cameroon saw monthly rainfall deficits of up to –100 mm. This resulted in one of the driest three-month periods (July–September) since 1991. Monthly rainfall deficits were slightly lower in southwestern Chad over this same period (–30 to –50 mm each month), resulting in accumulations below the 15th percentile. In CAR, rainfall continued past the rainy season and into boreal autumn, resulting in accumulations that were four times higher than the climatological mean in November–December. Southern Cameroon, northern Congo, southern CAR, northern and eastern DRC, and much of Rwanda and Burundi observed rainfall surpluses of over +100 mm in November, with similar surpluses from south-central to southeastern DRC in December. Seasonal rainfall during October–December was 150 mm above the mean from southern CAR to southeastern DRC (>90th percentile; Figs. 7.25a,b). The excess November rainfall over central DRC (50 mm–100 mm) likely contributed to the below-normal maximum temperatures in the region as noted above. Towards the end of the prior wet season (January–March), abnormally dry conditions persisted in southeastern DRC. This region observed rainfall deficits of more than –100 mm in January and 50 mm–100 mm in February. This resulted in accumulations below the 10th percentile in January, while February was one of the driest on record (since 1991).

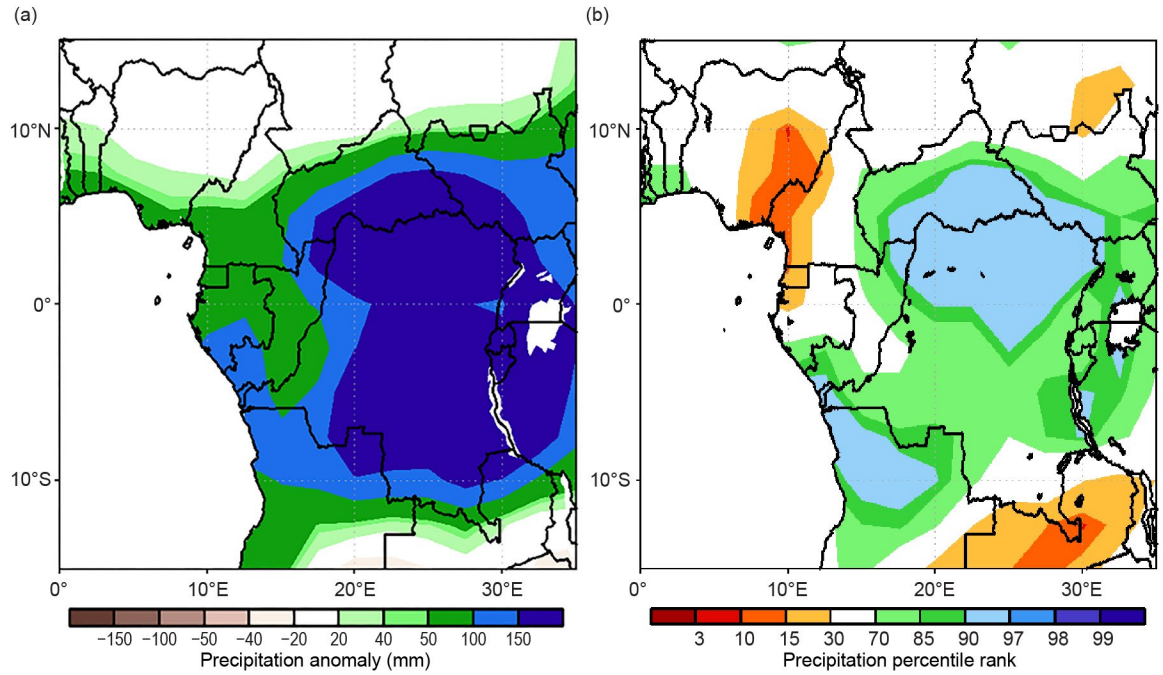

Fig. 7.25. Oct–Dec (a) precipitation accumulation anomalies (mm; 1991–2020 base period) and (b) precipitation percentile rank in 2023 for Central Africa. (Source: NOAA National Centers for Environmental Prediction.)

(iii) Notable events and impacts

Heavy rainfall and landslides during 2–4 May affected ~50,000 people in the South Kivu province of eastern DRC. Over 1500 people were displaced, more than 400 people were killed, more than 3000 houses were destroyed, and multiple health facilities and water, sanitation, and hygiene infrastructure were destroyed in the Kalehe Territory after more than 125 mm of rain fell over the area, according to the NOAA/Climate Prediction Center satellite rainfall estimates version 2 (RFE2). Heavy rainfall throughout November and December also resulted in flooding in DRC's Haut-Uele, South Kivu, and Tshopo provinces. More than 40 people were killed in and around Bukavu, the capital city of South Kivu province, after up to 100 mm of rain fell on 26 December, according to the RFE2. On the same day, 22 people were killed after heavy rainfall (>50 mm) inundated DRC's Kongo-Central province.

Flooding and mudslides in Yaoundé—the capital city of Cameroon—began on 8 October, affecting more than 700 residents, killing 30 people, and destroying 27 houses. According to the RFE2, heavy rainfall of up to 75 mm over a three-day period destroyed a water retention dam at Nkol Etam, triggering the mudslides.

Also according to the RFE2, heavy rainfall of up to 125 mm along with strong winds destroyed 200 homes and impacted 3000 people on 15 May in the Haut Ogooué province of Gabon.

On 11 August, heavy rainfall destroyed villages, houses, and agriculture in Mirvidin, Chad, after the breach of the Bongo-Gamsai dike along the Logone River. Over 2400 people were displaced. Flooding continued in southwestern Chad into September, particularly in the Logone Oriental, Mandoul, Tandjilé, and Mayo Kebbi Est provinces. Overall, during August–September, more than 1000 hectares and 2700 houses were destroyed, 5 people were killed, and over 100 people were injured.

Heavy rainfall that began in October resulted in the flooding of the Congo River, affecting more than 300,000 people in Congo by the end of December. The most impacted departments include Likouala, Sangha, Cuvette, Plateaux, Niari, Brazzaville, and Pointe-Noire. More than 360 villages were submerged, 17 people were killed, and more than 2200 hectares of farmland were flooded.

4. EASTERN AFRICA

—Z. T. Segele, E. Bekele, and W. M. Thiaw

The Greater Horn of Africa, or eastern Africa, covers 11 countries and extends 12°S–24°N and 21°E–52°E. Its northern sector comprises Sudan, South Sudan, the northern two-thirds

of Ethiopia, Eritrea, Djibouti, and northern Somalia. Southern and central Somalia, southern and southeastern Ethiopia, Kenya, northern Tanzania, Uganda, Rwanda, and Burundi are in its equatorial sector, while the southern sector encompasses central and southern Tanzania. The region has a complex terrain, with elevation ranging from about 160 m below sea level at Ethiopia's northern exit of the Rift Valley to more than 5000 m above sea level at glaciated Mount Kilimanjaro. This complex topography is further amplified by the presence of large lakes and reflects multi-faceted climate zones modulated by local and large-scale forcing such as the deep convective and moisture convergence zone, the El Niño–Southern Oscillation, the Indian Ocean dipole, the Madden Julian Oscillation, and tropical-extratropical interactions. Rainfall is bimodal in the equatorial sub-region, with two distinct rainfall seasons in March–May and October–December. Seasonal rainfall is unimodal in the northern and southern sectors, spanning November–April in the south and June–September in the north. The June–September rainfall over Ethiopia–Eritrea is locally known as "Kiremt" rains.

(i) Temperature

Annual mean temperatures in 2023 exceeded 26°C over parts of South Sudan, most of Sudan, Eritrea, and bordering regions of Ethiopia, Djibouti, Kenya, and much of Somalia (Fig. 7.26a). The highest mean annual temperatures of 30°C and above were recorded in localized areas in central Sudan, but mean temperatures above 28°C were widespread in Sudan, southern Somalia, and along the Red Sea coast. Mean annual temperature anomalies were less than +1.5°C across the region, with the largest anomalies being over South Sudan, southwestern Sudan, and along the Red Sea coast and bordering Afar regions of Ethiopia (Fig. 7.26b). Mean annual temperatures in these areas ranked between the 90th and 97th percentiles of historical records. Although anomalously warm (0.5°C to 1°C above the mean), annual mean temperatures were less than 22°C in most of central Ethiopia, southern half of Uganda, Tanzania, Burundi, Rwanda, and southwestern Kenya.

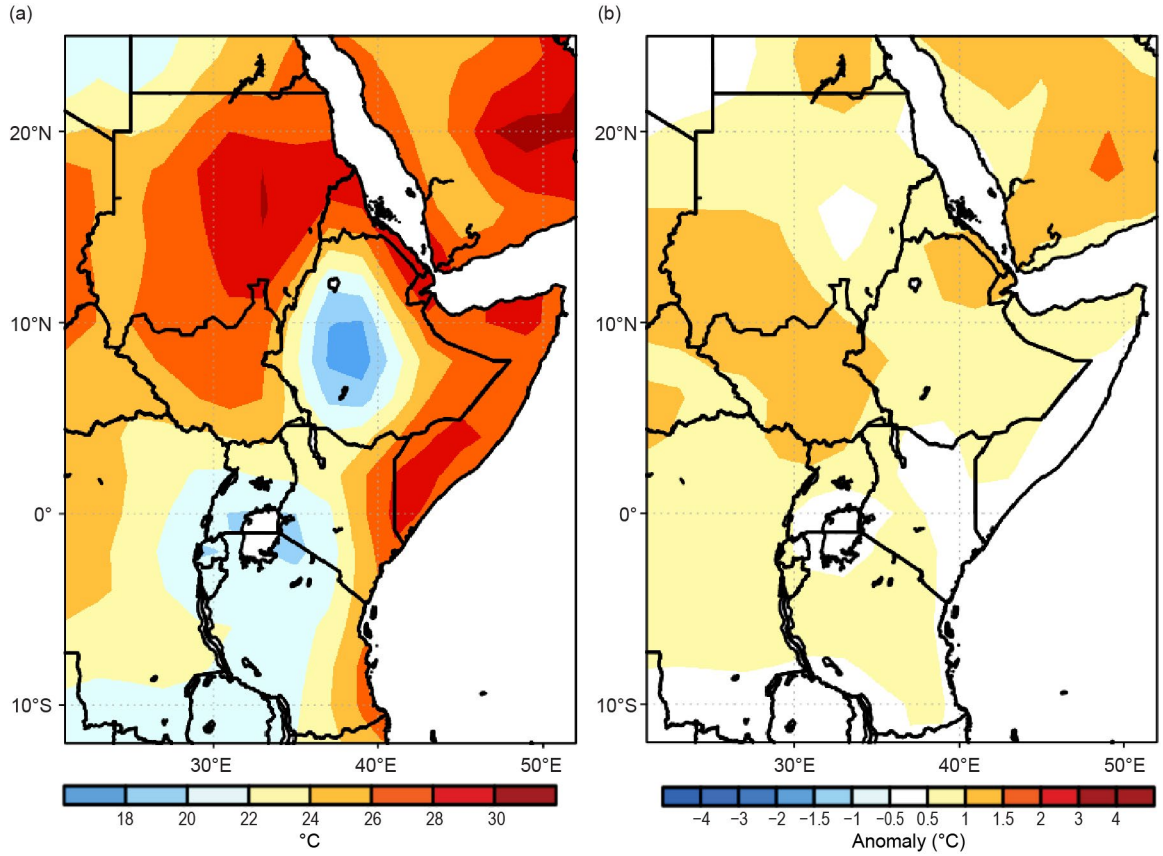

Fig. 7.26. Annual (a) mean temperature and (b) mean temperature anomalies (°C; base period 1991–2020) for eastern Africa in 2023. (Source: NOAA National Centers for Environmental Prediction.)

As the year progressed, a broad region of elevated mean monthly temperatures exceeding 30°C advanced northward from South Sudan in February and reached a peak of 36°C in northern Sudan in September. However, maximum temperatures were much higher (44°C–46°C) in northern Sudan in August and September. Areas in the Red Sea coast, including Djibouti and the Afar region of Ethiopia (northern Somalia), recorded their highest mean temperatures of 32°C–34°C (30°C–32°C) during May–June (May–September). Much of central Ethiopia registered temperatures below 22°C throughout the year. Except for southern Tanzania, which recorded mean temperatures of 24°C–26°C during September–November, most of Tanzania also had cooler temperatures through much of the year. Mean temperature anomalies were highest over South Sudan and Sudan (+3°C to +4°C) in January and over southern Sudan and eastern Ethiopia (+2°C to +3°C) in July. Mean temperatures were >90th percentile in most parts of the equatorial and northern sectors during June–September. Mean temperatures were below average by 2°C–3°C in localized areas over northern Sudan in May (lowest 15th percentile) and in cross-border regions of southeastern Ethiopia and central Somalia in November (lowest 10th percentile).

(ii) Precipitation

Annual rainfall totals in 2023 surpassed 1000 mm across western Ethiopia, South Sudan, most of Uganda, most of Rwanda, Burundi, and western and southern Tanzania (Fig. 7.27a). Western and central Uganda and western Rwanda recorded their highest annual totals in excess of 1500 mm. Most of Kenya, southern and central Ethiopia, northern South Sudan, southern Sudan, and central Tanzania received rainfall totals between 600 mm and 1000 mm. Totals were lower (50 mm–600 mm) over northern Sudan, Eritrea, Djibouti, and northeastern and eastern Ethiopia. Overall, rainfall was below normal over southeastern Sudan and over the Tigray and Wollo regions of Ethiopia, where deficits of –100 mm to –150 mm (<15th percentile) were recorded (Fig. 7.27b). The Garessa, Wajir, and Mandera counties of Kenya and southern Somalia received excessive rainfall, surpassing their normal totals by more than 300 mm (>90th percentile).

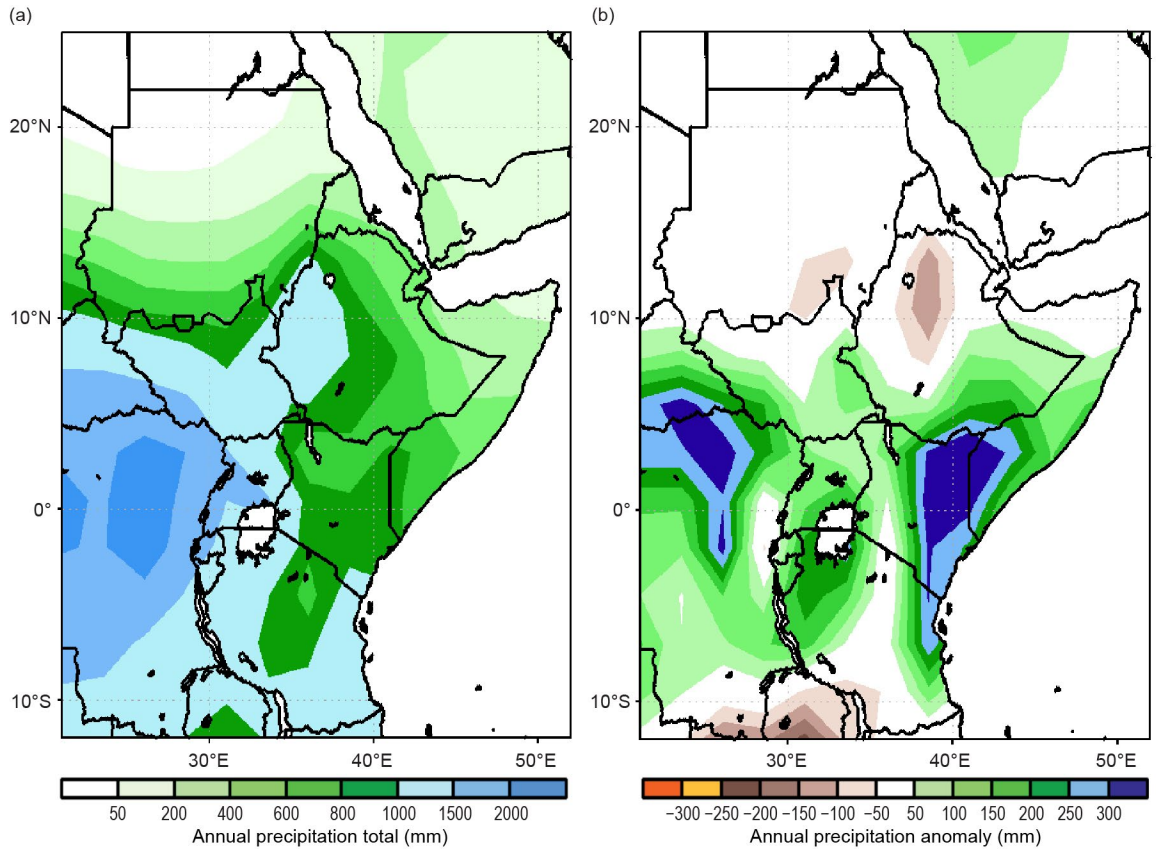

Fig. 7.27. Annual (a) total rainfall and (b) total rainfall anomalies (mm; base period 1991–2020) for eastern Africa in 2023. (Source: GPCP via NOAA National Centers for Environmental Prediction.)

Monthly rainfall totals in 2023 were widespread and in excess of 200 mm over the Lake Victoria regions and southeastern coasts of Kenya and Tanzania in April, over western and northwestern Ethiopia in July, over the equatorial sector in November, and over western Tanzania, Burundi, and Rwanda in December. The Kiremt rains highly underperformed in the northern sector in June and especially in the season's peak month of August. The Kiremt rainfall deficits in Ethiopia may be linked to the influence of anomalously warm eastern Pacific sea surface temperatures (i.e., El Niño), which is known to suppress summer rains in the region (Beltrando and Camberlin 1993). Monthly rainfall surpluses in 2023 exceeded 100 mm in the equatorial sector in March, April, and especially November, where rainfall totals were above the 90th percentiles in each month. Conversely, rainfall deficits exceeded 100 mm during the summer months, especially in August and September, across much of the northern half of Ethiopia, where recorded rainfall totals in August were below the lowest 3rd percentiles of their historical records. Overall, although 2023 rainfall totals in eastern Africa were wetter than average during March–May, October–December, and for the year, there was severe dryness during June–September that led to extensive drought conditions that remained present in Ethiopia through the end of the year.

(iii) Notable events and impacts

The transition from La Niña to El Niño helped bring relief to the prolonged drought conditions in equatorial eastern Africa during the March–May and October–December seasons. However, the 2023/24 El Niño along with positive Indian Ocean dipole conditions also led to excessive rainfall that resulted in devastating floods in many places. Exceptionally heavy rains and severe flooding over southeastern Ethiopia, Somalia, and Kenya during October–December displaced around 1.5 million people, caused human fatalities and livestock deaths, and brought significant damage to critical infrastructure, property, and crops, according to the United Nations Office for the Coordination of Humanitarian Affairs and government agencies. Heavy rains also caused devastating floods in many parts of Ethiopia, Somalia, Rwanda, Uganda, Kenya, and Tanzania during the March–May 2023 season, resulting in hundreds of fatalities, material damages, and displacements of hundreds of thousands of people. Drier-than-average conditions prevailed in the northern and western portions of eastern Africa during the June–September season.

5. SOUTHERN AFRICA

—A. C. Kruger, C. McBride, M. Robjhon, and W. M. Thiaw

Southern Africa is a region that covers a wide area in the southern portion of Africa. It extends from about 5°S to 35°S and comprises Angola, Namibia, Zambia, Botswana, Zimbabwe, Malawi, South Africa, Lesotho, Eswatini, and Mozambique. Southern Africa is characterized by two main seasons: the wet and warm season from November of the previous year to April and the dry and cold season from May to October.

(i) Temperature

Annual mean temperatures ranged from 16°C to 26°C in southern Africa, with warmer conditions in the western, part of central, and eastern sector and colder conditions across the central and southern sector of the region (Fig. 7.28a). Above-average annual mean temperatures extended from eastern Namibia, Botswana, southern and eastern Zambia, Zimbabwe, central and northeastern South Africa, Lesotho, Eswatini, and Malawi to western and northern Mozambique. The largest warm anomalies were observed over west-central Botswana, where annual mean temperatures were 1.5°C–2°C above average (Fig. 7.28b). In contrast, annual mean temperatures were below average in western Namibia.

South Africa experienced a relatively warm year, especially in the central and northern interior; in the south, temperatures were near normal. The annual mean temperature anomaly for 2023, based on the data of 20 climate stations, was on average about 0.4°C above the 1991–2020 normal, making this the eighth-warmest year on record since 1951 (Fig. 7.29). A warming trend of approximately 0.17°C per decade is indicated for the country over the period 1951–2023, statistically significant at the 5% level.

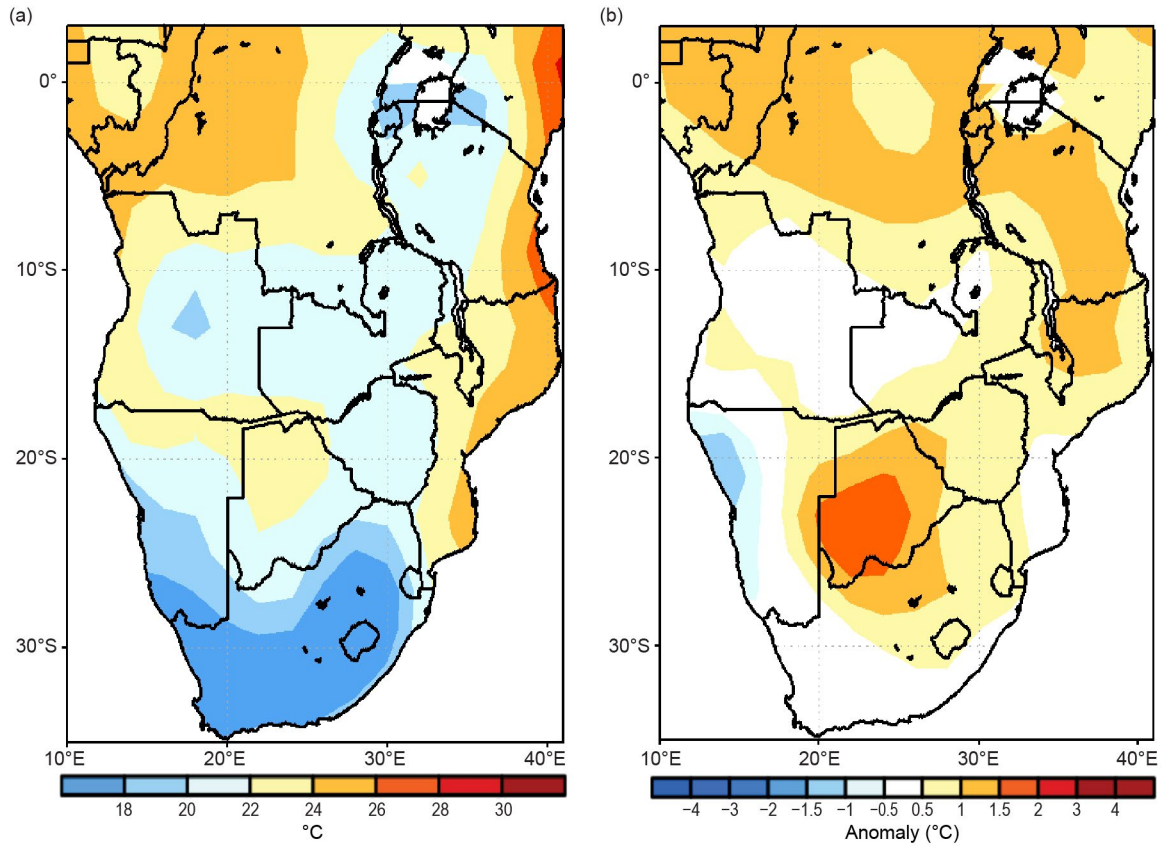

Fig. 7.28. Annual (a) mean temperatures and (b) mean temperature anomalies (°C; 1991–2020 base period) for southern Africa. (Source: NOAA National Centers for Environmental Prediction.)

Annual maximum temperatures were above average over most areas in southern Africa, with the warmest conditions in the western sector. Positive anomalies were +1.5°C to +3°C (90th–97th percentile) across Angola and eastern Namibia. Seasonally, maximum temperatures remained well above average in the western and southeastern parts of southern Africa during June–August and September–November.

Annual minimum temperatures were 1°C–3.5°C above average over the central and eastern portions of southern Africa, including Botswana, central South Africa, Zimbabwe, south-central Malawi, and western and northern Mozambique, whereas annual minimum temperatures dropped to 1°C–3°C below average in the western sector from southwestern Angola to northwestern Namibia. Minimum temperatures were well above average in Botswana during March–May, June–August, and September–November.

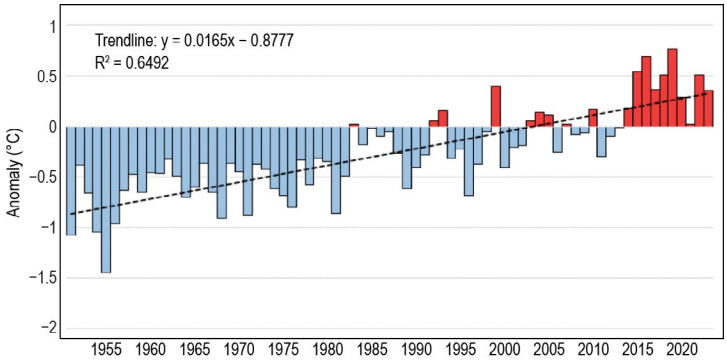

Fig. 7.29. Average surface temperature anomalies (°C; 1991–2020 base period) over South Africa based on 26 climate stations for the period 1951–2023. The linear trend is indicated by the dotted black line. (Source: South African Weather Service.)

(ii) Precipitation

Annual rainfall totals exceeded 1000 mm over the northern and eastern sectors of southern Africa, including northern Angola, northern Zambia, Malawi, the eastern two-thirds of Mozambique, and portions of eastern South Africa (Fig. 7.30a). Annual rainfall totals were below 600 mm across the central and western portions of the region from Botswana and Namibia to western South Africa. Annual rainfall was below average over central southern Africa, encompassing southeastern Angola, Zambia, eastern Namibia, Botswana, northern South Africa, and western Zimbabwe (Fig. 7.30b). The driest area was southwestern Zambia, where annual rainfall

was 200 mm–250 mm below average. Annual rainfall was above average in northern Angola, the southern and eastern tier of South Africa, Lesotho, Eswatini, and southern Mozambique, where rainfall surpluses of over 300 mm were received.

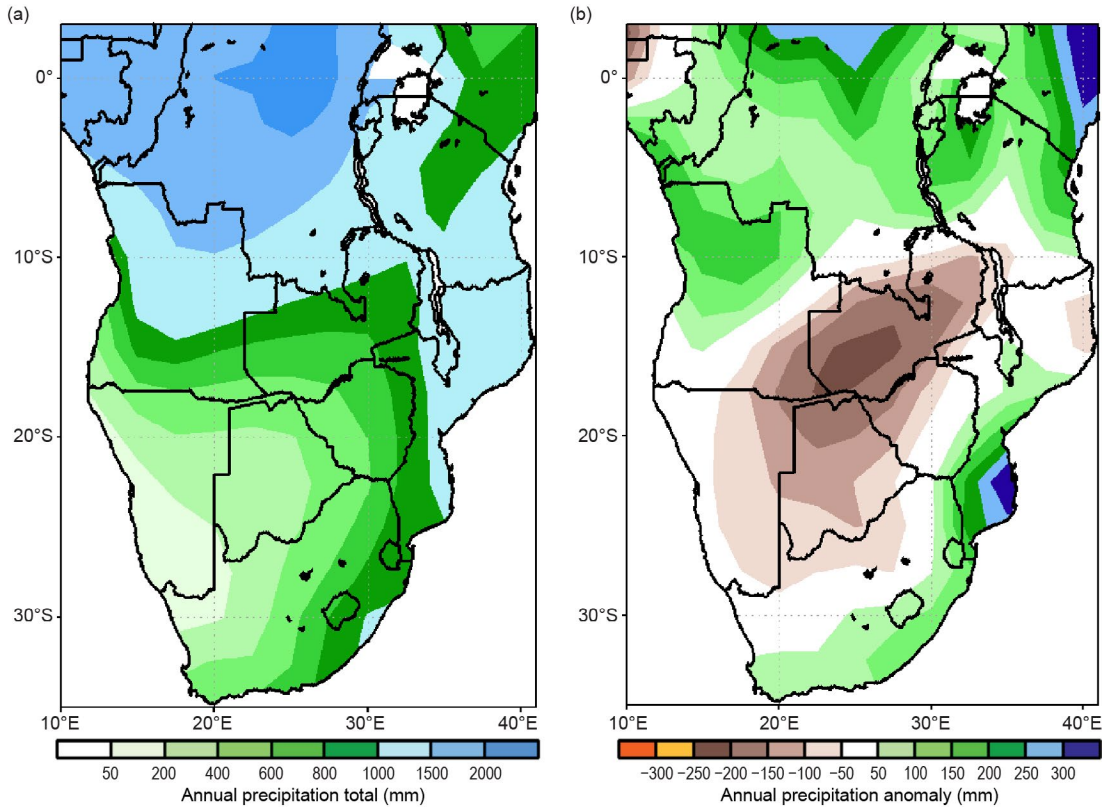

Fig. 7.30. Annual (a) rainfall totals and (b) rainfall anomalies (mm; 1991–2020 base period) for southern Africa. (Source: GPCP, NOAA National Centers for Environmental Prediction.)

In South Africa, most of the country received near-normal rainfall totals, with the exception of the northwestern interior, which received well-below-normal rainfall (Fig. 7.31). In contrast, some regions along the coast and extreme east received well-above-normal rainfall, especially in the Mpumalanga province.

While seasonal rainfall was below average across eastern Angola, Zambia, Botswana, Zimbabwe, northeastern South Africa, and southern Mozambique during December–February and March–May, drier-than-average conditions returned farther south in eastern Botswana, southwestern Zimbabwe, and parts of northern South Africa during September–November.

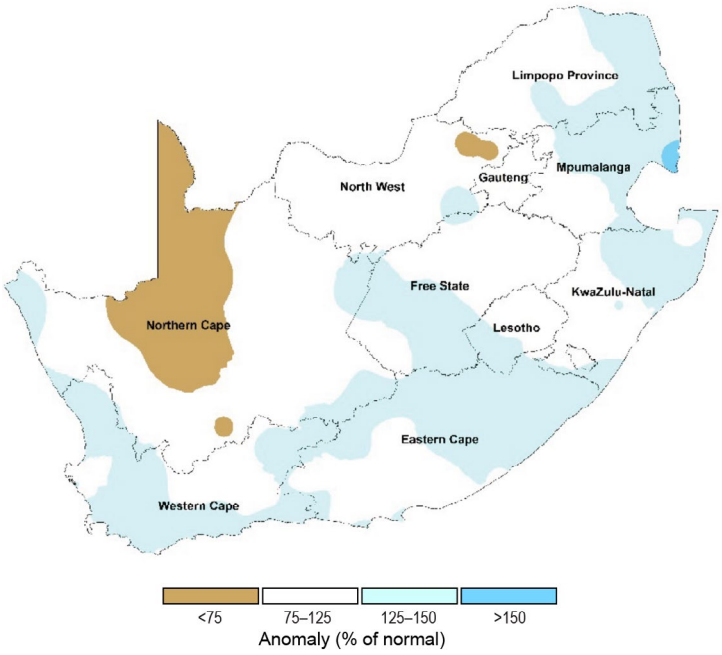

Fig. 7.31. Annual rainfall anomalies (% of normal; 1991–2020 base period) for South Africa for 2023. (Source: South African Weather Service.)

(iii) Notable events and impacts

During 24 February–11 March, Tropical Cyclone Freddy impacted the Niassa, Maputo, Inhambane, Gaza, Manica, Tete, Zambezia, and Sofala Provinces in Mozambique, resulting in 165 deaths, over 500 injuries, and 887,000 people affected. Rainfall totals ranged between 200 mm and 750 mm in central and southern Mozambique, according to the satellite Rainfall Estimates version 2 (RFE2). In Malawi, Cyclone Freddy triggered flooding and landslides in the

Balaka, Blantyre City, Blantyre, Chikwawa, Chiradzulu, Machinga, Mangochi, Mulanje, Neno, Nsanje, Phalombe, Thyolo, Zomba City, Zomb, and Mwanza Districts during 11–13 March, which caused 679 fatalities and 2186 injuries. See Sidebar 4.2 for details on Tropical Cyclone Freddy.

Heavy rains, with totals of 100 mm–300 mm, caused flooding in Luanda, Namibe, Lunda Norte, Lunda Sul, Malanje, Cuanza Norte, and Moxico in Angola during 1–30 April, contributing to 54 fatalities and 450 injuries, and affecting 44,450 people.

Heavy rains totaling 200 mm–750 mm led to flooding in Dar es Salaam, Kigoma, Kagera, Geita, Unguja, Arusha, and Pwani in Tanzania during 15 October–23 November. Twelve people were killed due to impacts from the rain and nearly 2,900,000 residents were affected.

During 2–6 December, heavy rains (75 mm–150 mm) triggered landslides in Katesh, Hanang District, and western Manyara Region (north) in Tanzania, which resulted in 88 fatalities, 139 injuries, and more than 5700 people affected.

In South Africa, the eastern province of KwaZulu-Natal was relatively hot at the start of 2023, and a few highest maximum and minimum temperature records were broken. In February, above-normal rainfall in the east led to several instances of flash floods, causing damage to infrastructure and loss of life. In March, the Western Cape received much above-normal rainfall, which persisted in the Cape Town metropole in April; about 130 residents and 50 shacks were flooded. In May, several major flooding events occurred in the eastern and southeastern coastal region, with more than 1200 residents evacuated from their homes in the Nelson Mandela Bay Municipality in the Eastern Cape after heavy rains on the 13th. In June, much-above-normal rainfall occurred over most of the southwestern half of South Africa; many flooding events were reported with hundreds of people left destitute and traffic disruptions in the main arterials connecting the southwest to the remainder of the country. In the far northeast, it was unusually hot and dry, and maximum temperatures of more than 30°C were reported. In September, floods were once again reported in the Western Cape. Flooding during 24–25 September led to 11 fatalities and the closure of over 200 roads, and over 80,000 people were left without electricity for an extended period. From October, floods were reported in the KwaZulu-Natal province. Several fatalities and extensive damage/destruction to infrastructure and hundreds of homes were reported. On 24 December, more than 20 people were killed in floods in Ladysmith.

6. WESTERN INDIAN OCEAN ISLAND COUNTRIES

—G. Jumaux, B. Andrade, R. Virasami, S. Dindyal, M. Robjhon, and W. M. Thiaw

The Western Indian Ocean island countries consist of Madagascar, Seychelles, Comoros, Mayotte (France), Réunion (France), Mauritius, and Rodrigues (Mauritius). There are two distinct main seasons: a warm and wet period spanning from November of the antecedent year to April and a cold and dry season lasting from May to October. Overall, above-normal temperatures in 2023 (Fig. 7.32) were associated with large-scale prevailing environmental conditions of El Niño and a positive Indian Ocean dipole. Annual rainfall was above normal in Mauritius and Seychelles and below normal in Mayotte and Réunion (Fig. 7.32).

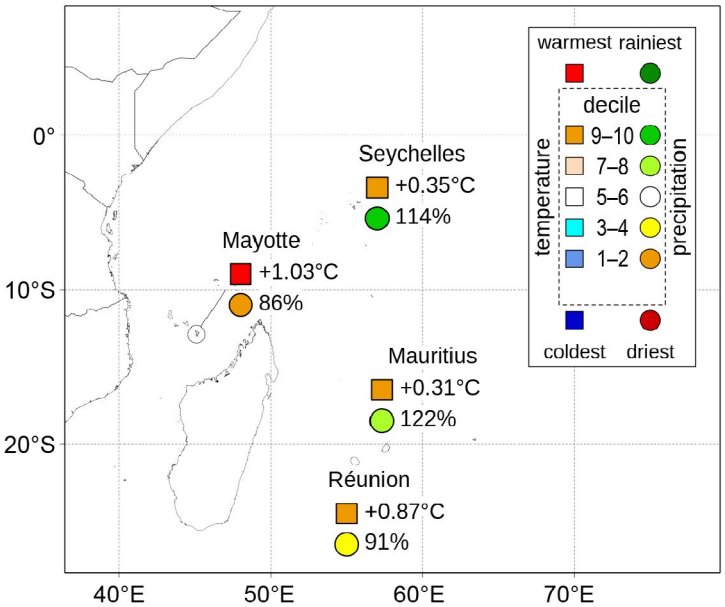

Fig. 7.32. Mean annual temperature anomalies (°C, squares), annual rainfall ratio to normal (%, circles), and their respective deciles for the western Indian Ocean island countries in 2023 (top right inset box). Base period is 1991–2020. (Sources: Météo France and meteorological services of Mauritius and Seychelles.)

(i) Temperature

In Réunion, the annual mean temperature (based on three stations) was 0.9°C above normal, the second highest since records began in 1968 (Fig. 7.33). The year started with a −0.1°C departure from normal during January–March, and then temperatures were

far above normal related to warm sea surface temperatures around the island: +1.1°C in April–June and +1.3°C in July–September (both record high), and +1.1°C in October–December (second highest).

In Mauritius, the annual mean temperature was 24.0°C, 0.3°C above normal. The highest mean temperature was in February (25.8°C) and the lowest mean temperature was in July (21.6°C; Fig. 7.34). Anomalies ranged from –1.3°C in January to +1.1°C in September. The start of the year had below-normal mean temperatures, transitioning to normal from March to June, and from July onward, with a strengthening El Nino, warm conditions were observed (+0.5°C). This warming trend persisted until the end of the year. It was the warmest September since records began in 1960.

In Mayotte (Pamandzi Airport), the annual mean temperature was the highest in the 63-year record (28.1°C, 1.0°C above normal). All months from May to December had record-high monthly mean maximum temperatures related to remarkably warm sea surface temperatures in the western Indian Ocean.

At Seychelles International Airport, the annual mean temperature anomaly for 2023 was 0.35°C above normal, the third highest since 1972. Nearly all months were above normal, except for January and February. It was the warmest December on record (anomaly of +1.0°C).

In Madagascar, annual mean temperatures were 20°C–26°C (Fig. 7.35a), with the higher temperatures observed along the west coasts and northern part of the island and lower temperatures over the central highlands. Annual mean temperatures were 0.5°C–1.0°C above average over the northern two-thirds of the country (Fig. 7.35b). These warm anomalies corresponded to the 90th–97th percentile rankings over a wide area in central and eastern Madagascar. Annual maximum temperatures were +0.5°C–1.0°C above average in central, western, eastern, and northern Madagascar. During October, the south-central region reported anomalies of +2°C to +3°C. Annual minimum temperatures also were 0.5°C–1°C above average across the northern two-thirds of the country. The warmest anomalies of +2°C to +3°C were observed in the central and eastern region during October.

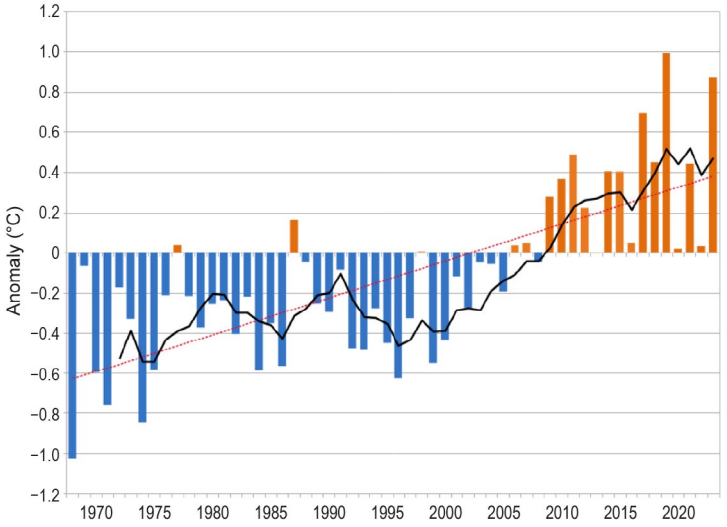

Fig. 7.33. Time series of Réunion annual mean temperature anomalies (°C; 1991–2020 base period) for the period 1968–2023. The solid black line is the five-year running mean and the dotted red line represents the linear trend. (Source: Météo-France.)

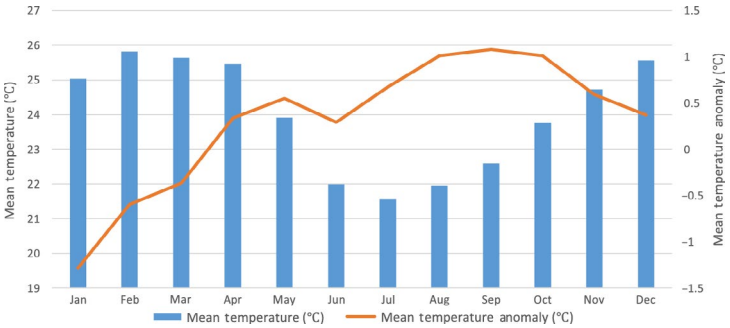

Fig. 7.34. Monthly mean temperatures for Mauritius in 2023 (blue bars, left scale) and 2023 anomalies (orange line, right scale). Base period is 1991–2020. (Source: Mauritius Meteorological Services.)

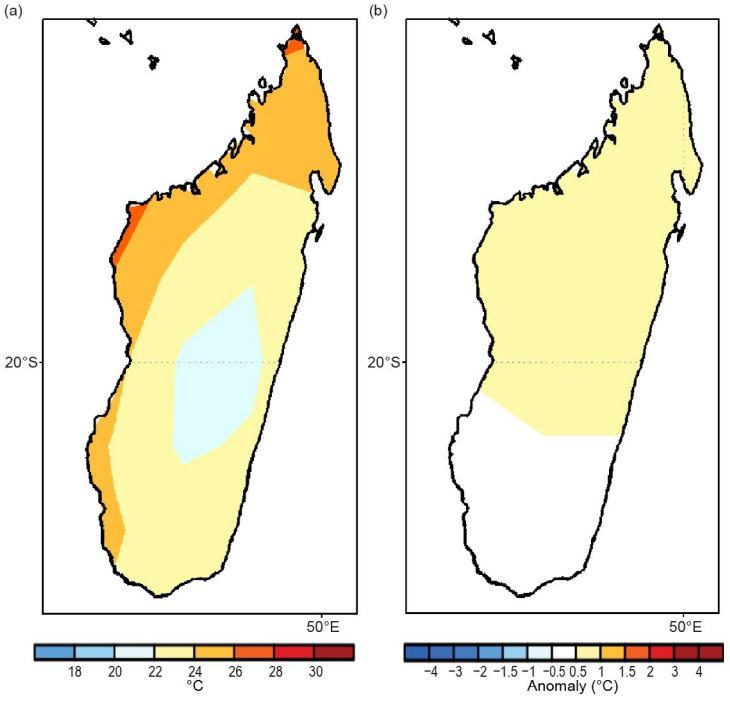

Fig. 7.35. Annual (a) mean temperatures and (b) mean temperature anomalies (°C; 1991–2020 base period) for Madagascar. (Source: NOAA National Centers for Environmental Prediction.)

(ii) Precipitation

The annual rainfall total over Réunion was 91% of normal. The rainy season (December–April) produced 71% of normal precipitation, making it the fourth-driest such period on record since records began in 1972. The dry season (May–November) was 129% of normal; this period includes the wettest November on record (289% of normal).

In Mauritius, intra-annual variability rainfall was observed throughout the year. The average cumulative annual rainfall total was 2471 mm, 122% of normal. January was wet, having seen 148% of its normal rainfall. However, February was the fifth driest on record since 1980. May was wet with 188% of rainfall, while June and July were drier than normal. August had well-above-normal rainfall, and thereafter drier conditions prevailed in September and October. November was the wettest November on record since 1905 and December had 317 mm of rainfall (192% of normal).

In Mayotte, the total annual rainfall was 86% of normal, which was the ninth-lowest on record since 1961. The rainy season (November–April) was very short, as April was the only wet month, marking the third-driest (73% of normal) such period on record. The dry season (May–October) was 67% of normal (seventh-driest). A severe drought occurred with many long-lasting water cuts. Fortunately, a wet rainy season began in December (153% of normal).

In Seychelles, the total annual rainfall (2799 mm) was 114% of normal, making 2023 the seventh-wettest year on record since 1972 (Fig. 7.36). The first half was 76% of normal (11th driest on record), and the second half was 162% of normal, the second wettest on record after 1997. The shift was related to the El Niño and the positive Indian Ocean dipole that developed in the second half of the year.

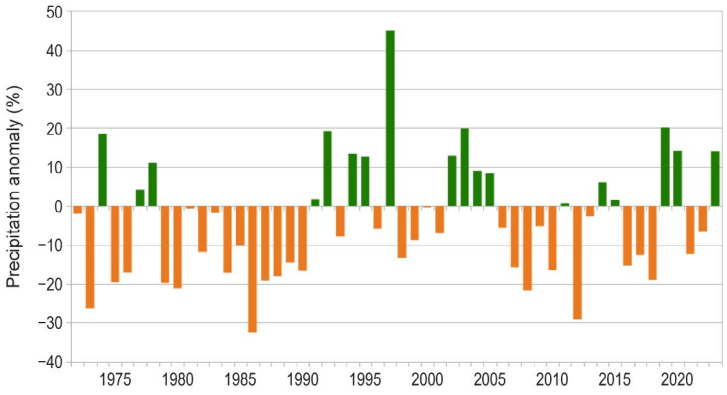

Fig. 7.36. Annual rainfall anomalies (%; 1991–2020 base period) in Seychelles for the period 1972–2023. (Source: Meteorological Services of Seychelles.)

In Madagascar, annual rainfall totals were 600 mm–2000 mm, with the highest and lowest amounts over the central highlands and southwest part of the country, respectively (Fig. 7.37a). Annual rainfall was below average in northern and southeastern Madagascar (Fig 7.37b). The driest region was near the Bay of Antongil in northeastern Madagascar, where rainfall deficits exceeded 300 mm. In contrast, annual rainfall was 50 mm–200 mm above average along the southwestern coasts of the Island.

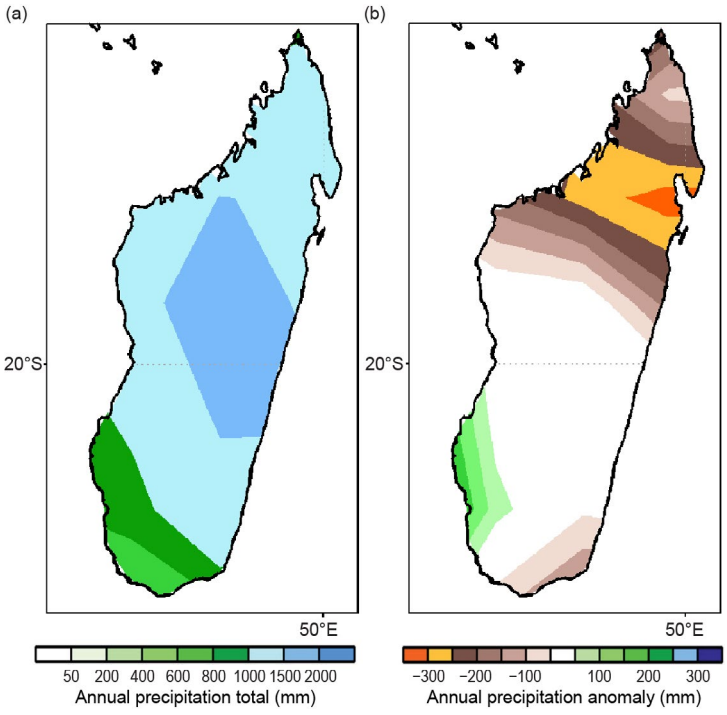

Fig. 7.37. Annual (a) rainfall totals and (b) rainfall anomalies (mm; 1991–2020 base period) for Madagascar. (Source: GPCP, NOAA National Centers for Environmental Prediction.)

(iii) Notable events and impacts

Tropical Cyclone Cheneso brought 200 mm–500 mm of rainfall, which resulted in flooding and landslides in Antalaha (Sava Region) and the Diana Region in northern Madagascar during 19–23 January, causing 53 fatalities and affecting nearly 91,000 people. During 24–25 January, Cheneso intensified and became a tropical cyclone over the Mozambique Channel but moved slowly until 26 January near the west coast of Madagascar.

In Mauritius, torrential rain was observed during 26–27 January. The most-affected regions were the central Plateau and the

eastern sector, where more than 300 mm of rainfall was recorded during 25–28 January (Fig. 7.38). The highest rainfall intensity measured was 55.1 mm h^{-1} at Wooton on the 27th.

Tropical Cyclone Freddy crossed the Indian Ocean from Australia to Mozambique during 4–24 February. Prior to landfall over Madagascar on 21 February, the center of the cyclone passed within 200 km north of Mauritius and Réunion on the 20th without causing severe damage. After entering the Mozambique Channel, the storm spent six days on land between Mozambique and Zimbabwe, then re-entered the southern Channel between 2 and 14 March. In total, Freddy hit Madagascar twice. Loss of human life and extensive material damage was reported. With winds of up to 165 km h^{-1} and rainfall totals between 100 mm and 300 mm, Freddy impacted Vatovavy, Fitovinany, Atsimo Atsinanana, Amoron'i Mania, Analamanga, Itasy, Alaotra-Mangoro, Menabe, and Atsinanana in central and eastern Madagascar during 21 February–8 March, causing 20 fatalities and affecting 299,000 people. Reports indicated one fatality and 2500 people affected in Mauritius and 25,000 people affected due to landslides in Réunion. See Sidebar 4.2 for more details on Tropical Cyclone Freddy.

In Seychelles, torrential rain in the northern part of Mahé island on 6 December caused flooding and landslides that led to power failures and three fatalities. The daily rainfall total was 360 mm at Belombre (the highest 24-hour rainfall value since records began), mainly in a five-hour period, and 310 mm at Beau Vallon.

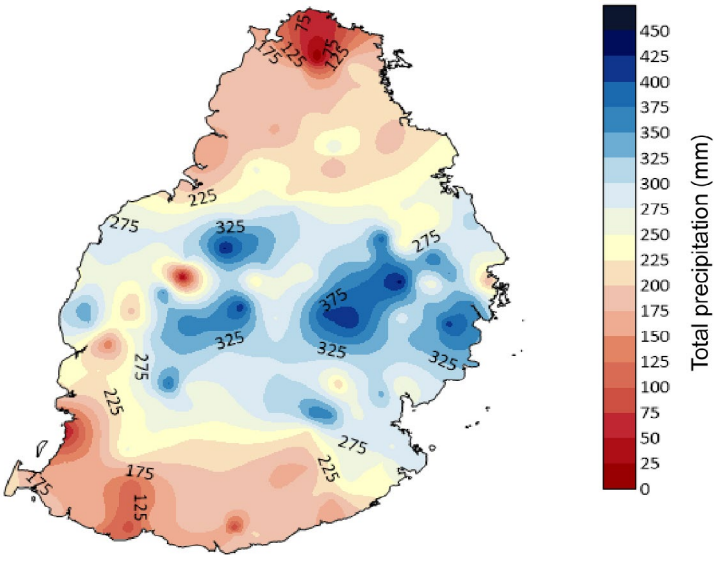

Fig. 7.38. Cumulative four-day rainfall (mm) in Mauritius during 25–28 Jan 2023. (Source: Mauritius Meteorological Services.)

f. Europe and the Middle East

—P. Bissolli (Ed.), S. Ahmadpour, C. Berne, O. Bochníček, M. Ekici, A. Gevorgyan, M. Kendon, J. Kennedy, Y. Khalatyan, V. Khan, M. Lakatos, J. Mamen, A. Orlik, A. Porat, H. Ressl, E. Rodriguez Guisado, M. Roebeling, B. Rösner, S. Sensoy, S. Spillane, K. Trachte, R. van der Linden, and G. van der Schrier

Throughout this section, 1991–2020 is the base period used for both temperature and precipitation unless otherwise specified. All seasons mentioned in this section refer to the Northern Hemisphere. More detailed information can be found in the Monthly and Annual Bulletin on the Climate in Regional Association VI (RA VI)–Europe and the Middle East, provided by the World Meteorological Organization (WMO) RA VI Regional Climate Centre on Climate Monitoring (RCC-CM; http://www.dwd.de/rcc-cm). Anomaly information has been taken from Figs. 7.40–7.43 and relevant national reports. The length of national temperature and precipitation records, annual anomalies, and rank information for each country are provided in Appendix Table 7.2. A color-coded map of the various subregions of WMO RA IV discussed in this section are shown in Fig. 7.44. Due to the high number of countries in Europe and the limited word space for each subsection, limited impact information can be provided here. More details about extreme events and impacts across Europe can be found elsewhere, e.g., https://climate.copernicus.eu/esotc/2023/key-events.

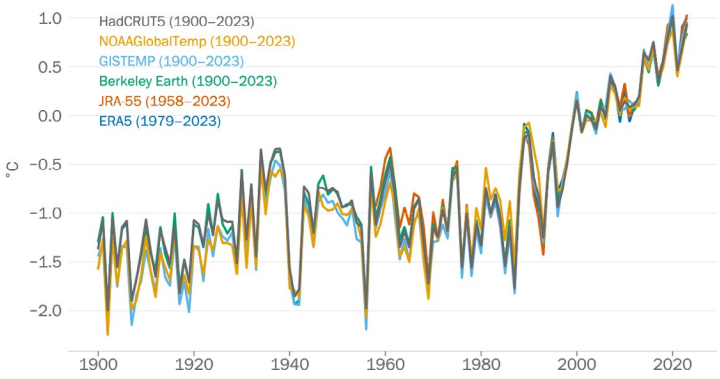

Fig. 7.39. Annual regional mean temperature for the World Meteorological Organization (WMO) Regional Association VI Europe (°C, difference from the 1991–2020 average) for the period 1900–2023. Data are from the following six datasets: Berkeley Earth, ERA5, GISTEMP, HadCRUT5, JRA-55, and NOAAGlobalTemp. (Source: WMO.)

1. OVERVIEW

Based on the WMO RA VI assessment, which utilized six datasets (Berkeley Earth, ERA5, GISTEMP, HadCRUT5, JRA-55, and NOAAGlobalTemp[1]; Fig. 7.39), the year 2023 ranked as the first or second warmest on record in Europe (here defined by the WMO RA VI Region, https://wmo.int/about-wmo/regions), depending on the dataset. The mean temperature anomaly for this year was +0.95°C (ranging from +0.84°C to +1.03°C among the six datasets).

Annual temperatures in 2023 were above average across the entire region except for some parts of the Nordic countries (Fig. 7.40). According to national data and reports, 2023 was the warmest year on record for Ireland (+1.0°C), Moldova (+1.9°C), Kazakhstan (west Kazakhstan [European part]; +1.9°C), Romania (+1.6°C), Malta (+0.7°C), Slovenia (+1.3°C), Serbia (+1.5°C), Germany (+1.3°C), Czechia (+1.4°C), Bulgaria (+1.6°C), Austria (+1.2°C), Slovakia (+1.3°C), Hungary (+1.5°C), Croatia (+1.4°C), Montenegro (+1.7°C), and the Netherlands (+1.3°C). Many other countries reported an annual temperature that was among their four highest on record.

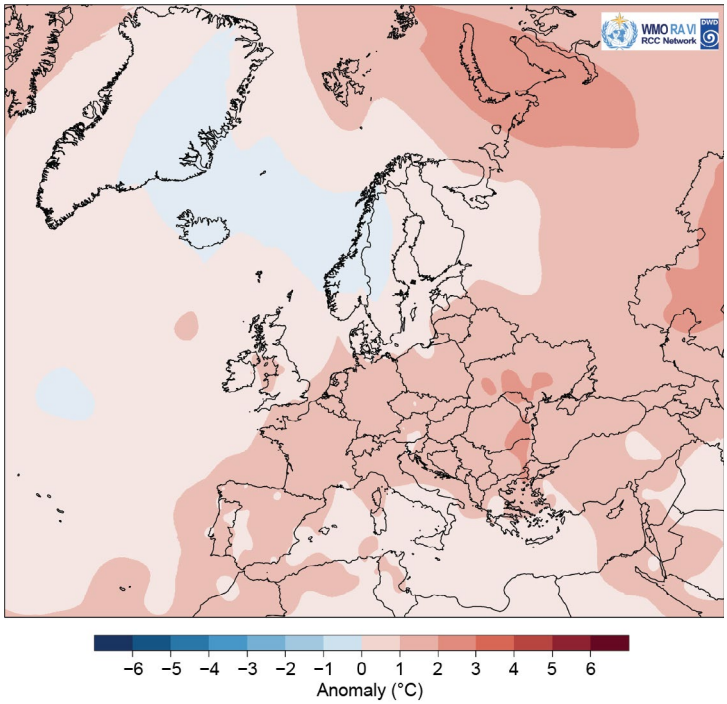

Fig. 7.40. Annual mean temperature anomalies (°C; 1991–2020 base period) for 2023. (Source: Interpolated climate station and ship data, Deutscher Wetterdienst [DWD].) The 1991–2020 anomalies were recalculated from 1981–2010 anomalies because the 1991–2020 CLIMAT data were still not available for all countries.

[1] Reference: https://jjk-code-otter.github.io/demo-dash/RegionalDashboard/wmo_ra_vi.html

According to the *European State of the Climate*—the joint report of the Copernicus Climate Change Service (C3S) and the WMO with data primarily based on the ERA5 reanalysis dataset—2023 equaled the warmest year on record, with 2020, for the WMO RA VI (Europe) domain (Copernicus and WMO 2024), with temperatures averaging 1.0°C above the 1991–2020 base period. September 2023 marked the warmest September on record, and the winter season (December 2022–February 2023) was the second warmest on record for Europe.

Based on the GHCN v4.0.1 dataset (the land component of NOAAGlobalTemp), Europe (defined here by the area 36°N–72°N, 23°W–60°E, which differs slightly from the RA VI Region) had above-average (1910–2000 base period) monthly temperatures all year, and the monthly temperature anomalies ranged between +1.05°C in May and +3.50°C in January. January and September were each the warmest on record for their respective months.

Winter 2022/23 was warmer than normal across Europe, except in Iceland and some parts of European Russia and west Kazakhstan, with positive temperature anomalies of up to +4°C. Romania (which had its warmest winter on record, with a remarkable temperature anomaly of +3.1°C) and Bulgaria were notably warmer than normal (Fig. 7.41). Armenia experienced its third-warmest winter. Spring had near-normal temperatures or was slightly cooler than normal across the region, except in the Iberian Peninsula and Eastern Europe, which were both much warmer than normal. Temperature anomalies for the season ranged from –1°C to +3°C, with the highest on the Iberian Peninsula, especially in Spain, and in European Russia and west Kazakhstan. This warmth illustrates a remarkable meridional circulation pattern in which the

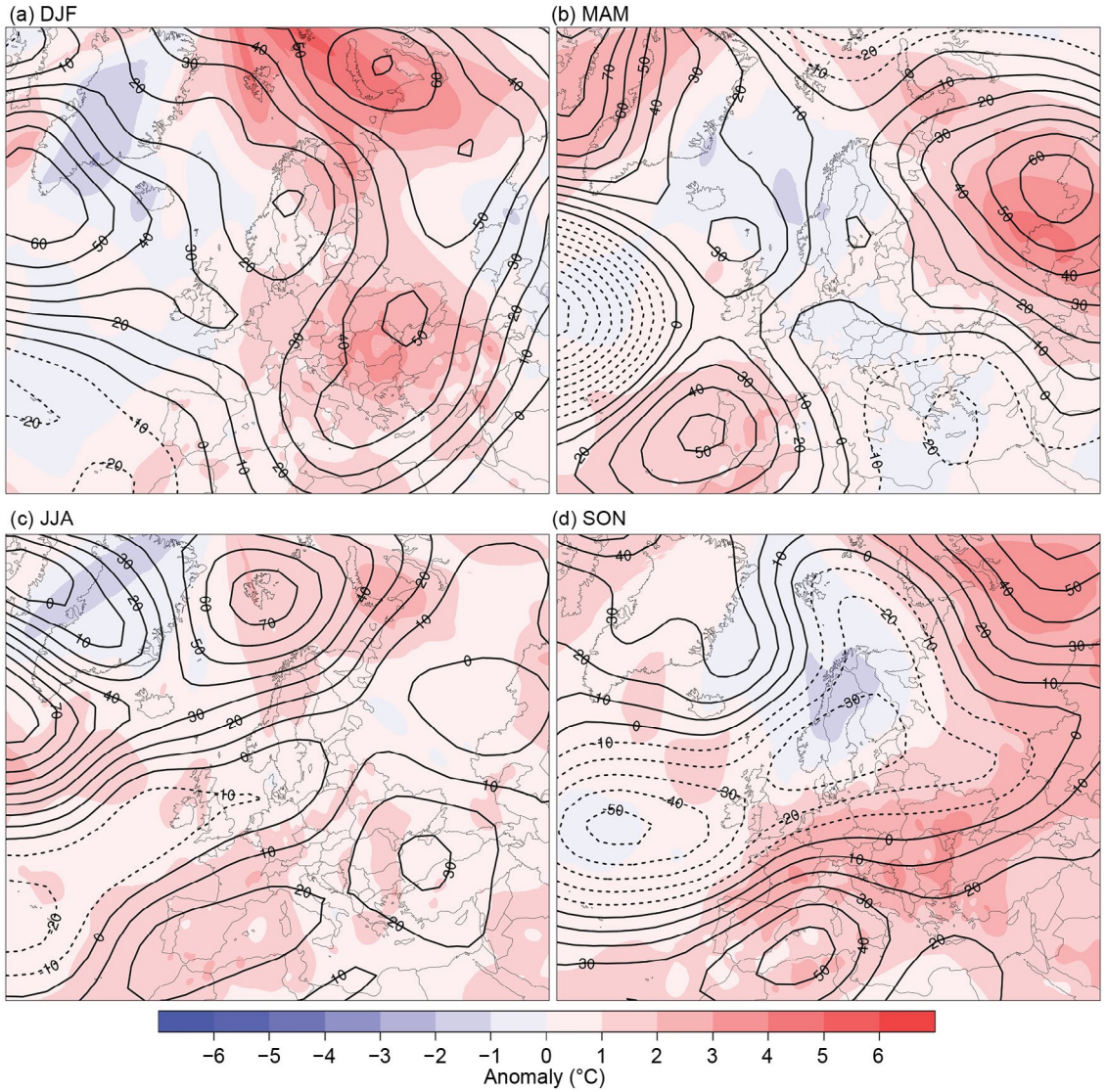

Fig. 7.41. Seasonal anomalies (1991–2020 base period) of 500-hPa geopotential height (contour; m) and surface temperature (shading; °C) using data from the NCEP/NCAR reanalysis and Deutscher Wetterdienst (DWD), respectively, for (a) Dec–Feb (DJF) 2022/23, (b) Mar–May (MAM) 2023, (c) Jun–Aug (JJA) 2023, and (d) Sep–Nov (SON) 2023.

Iberian Peninsula had anticyclonic situations while the central Mediterranean region experienced cyclonic conditions. West Kazakhstan (European part) recorded its warmest spring on record, while Ireland had its third warmest, and Portugal its second warmest. A particularly significant meridional circulation pattern was present in April, and it was warmer than normal in southwestern and northeastern parts of the region, especially in Spain, which reported its warmest April on record. In contrast, Central Europe had a cooler-than-normal April, with average anomalies of –1.0°C in Switzerland and –1.1°C in the Netherlands. May was also characterized by a strong meridional pattern, but with warmth in northwestern Europe as well. Some stations in Ireland recorded their warmest May on record. This warmth was also related to the marine heatwave in the surrounding waters (see Sidebar 3.1 for more details).

Unusually high temperatures occurred across much of Europe during summer under the influence of high pressure across much of the region, with anomalies ranging from +1°C to +2°C in large parts. The United Kingdom recorded its warmest June on record, at 2.5°C above average. The Netherlands was also record warm in June.

During autumn, except for the Nordic countries, the temperature was well above the average in the domain and was constantly influenced by a southwesterly and southerly flow of subtropical air. Parts of eastern and southeastern Europe had anomalies above +3°C. Switzerland and Denmark reported their warmest September on record at 3.8°C and +2.7°C above normal, respectively. Austria and France each reported their warmest autumn and September on record, while Italy reported its warmest autumn and October on record. Germany, Spain, Switzerland, and Poland each observed their second-warmest autumn, while Israel observed its third warmest.

Annual precipitation for 2023 was mostly near normal or wetter than normal in most parts of Europe, except for in the southern Iberian Peninsula, southern France, and Iceland, all of which were drier than normal. Precipitation totals ranged from below 60% of normal in parts of southern Europe to more than 165% of normal in various places throughout the rest of the region (Fig. 7.42). Averaged over all land areas of the RA VI Region, it was the wettest year on record according to the Global Precipitation Climatology Centre (GPCC) gridded data, but the third wettest according to ERA5 (Copernicus and WMO 2024).

Winter 2022/23 was significantly drier than normal from Iceland and western Europe to eastern Spain. In Iceland, there were large positive pressure anomalies in winter that also extended into western Europe, contributing to the dry conditions. The eastern Mediterranean region also had a dry winter. In contrast, other parts of Europe experienced a significantly wetter-than-normal winter, especially in a region extending from western Russia to the Balkans and Italy (Fig. 7.43). Spring was wetter than normal across most of Europe, with more than 125% of normal precipitation recorded in various regions, notably in parts of western Europe (southern United Kingdom and the low countries [Belgium, the Netherlands, and Luxembourg]), the central and eastern Mediterranean region, and parts of eastern Europe (Russia, Ukraine). Particularly dry were Iceland, much of the Iberian Peninsula, and a region around the Baltic Sea. The Iberian Peninsula experienced a severe drought, with areas receiving less than 40% of their spring normal (see Sidebar 7.3 for more details). Iceland was again under large high-pressure anomalies, unlike areas in southeastern parts of the domain, where low-pressure anomalies prevailed (Fig. 7.43).

Summer had mostly near-normal and wetter-than-normal precipitation in Europe. Areas with more than 125% of their normal

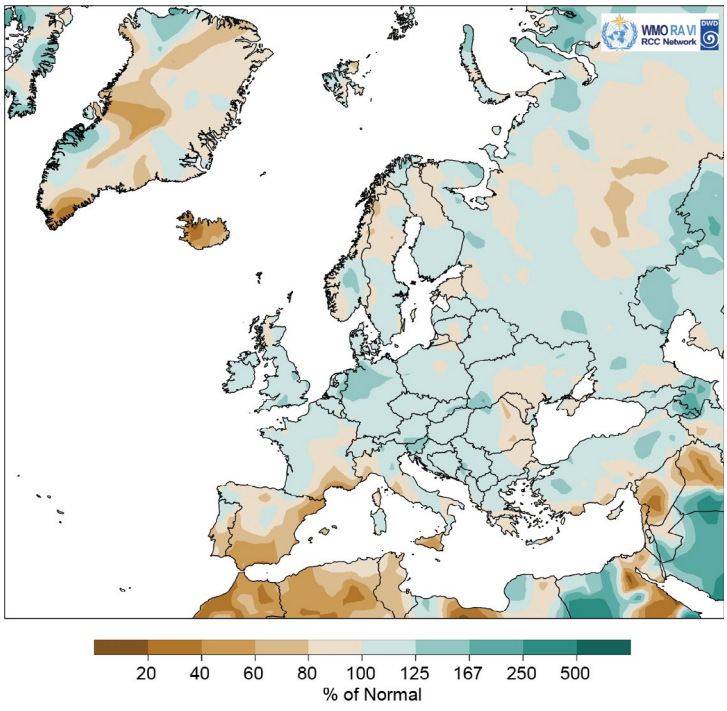

Fig. 7.42. European precipitation totals (% of 1991–2020 average) for 2023. (Source: GPCC, created by Deutscher Wetterdienst.)

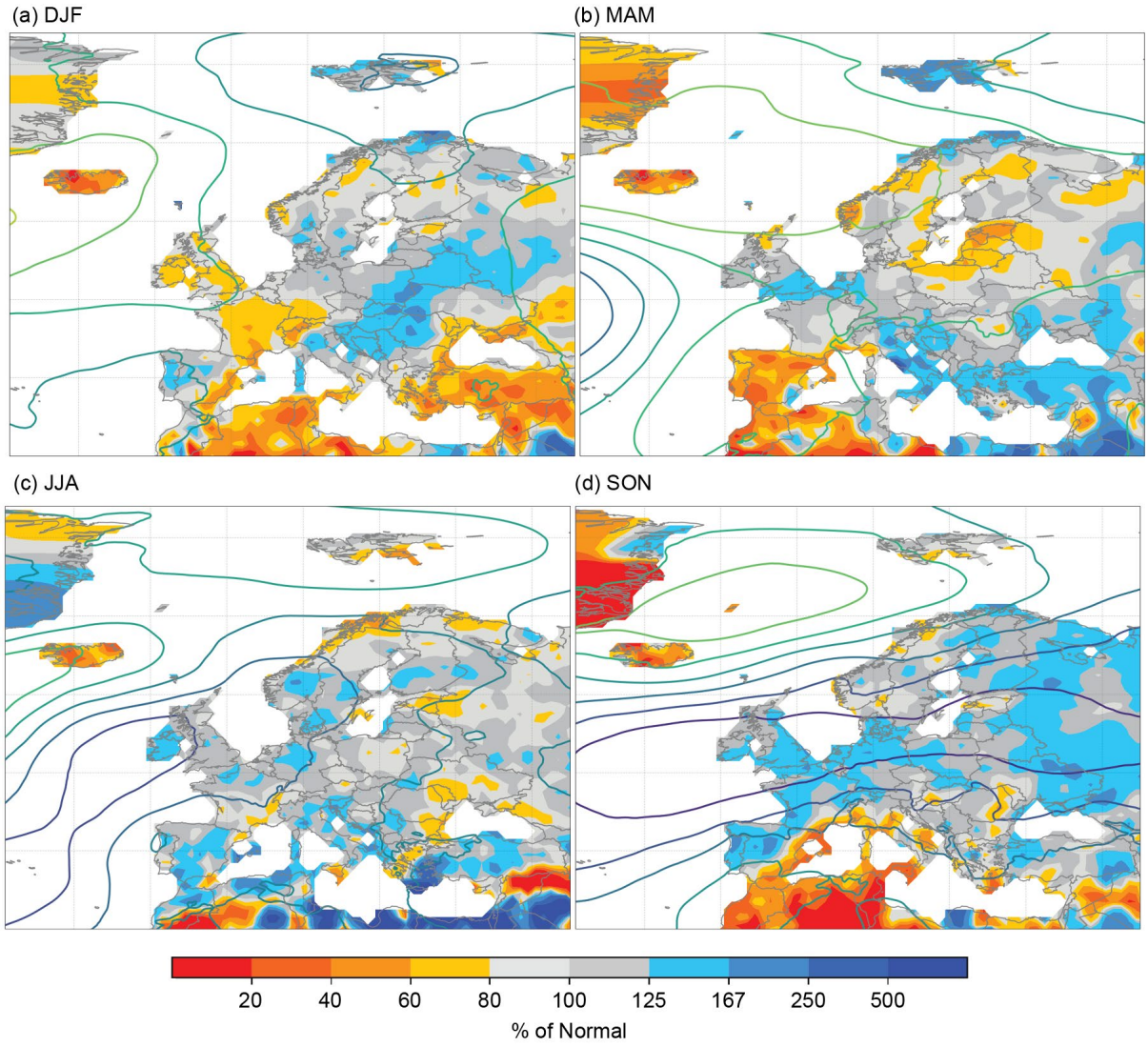

Fig. 7.43. Seasonal anomalies for 2023 (1991–2020 base period) of sea level pressure (hPa) from NCEP/NCAR reanalysis for (a) Dec–Feb (DJF) 2022/23, (b) Mar–May (MAM) 2023, (c) Jun–Aug (JJA) 2023, and (d) Sep–Nov (SON) 2023. The colored shading represents the percentage of seasonal mean precipitation for 2023 compared to 1991–2020 (Source data: GPCC, created by Deutscher Wetterdienst [DWD]).

totals were prevalent throughout the domain. Some areas in Ireland, southern Norway, northeastern Italy/Slovenia and other parts of southeastern Europe, and western Azerbaijan in the South Caucasus were particularly wet, having receiving more than 90 mm of rainfall above their respective seasonal normals. Most of the Mediterranean region had a wetter-than-normal summer, but since this part of Europe has a climatologically dry summer, anomalies were not high in absolute terms. Above-normal precipitation totals in Spain and Portugal did not compensate for the dry spring. In contrast, this season was dry again in Iceland (as the influence of high pressure continued) and in parts around the Black Sea, with seasonal totals of less than 80% of normal.

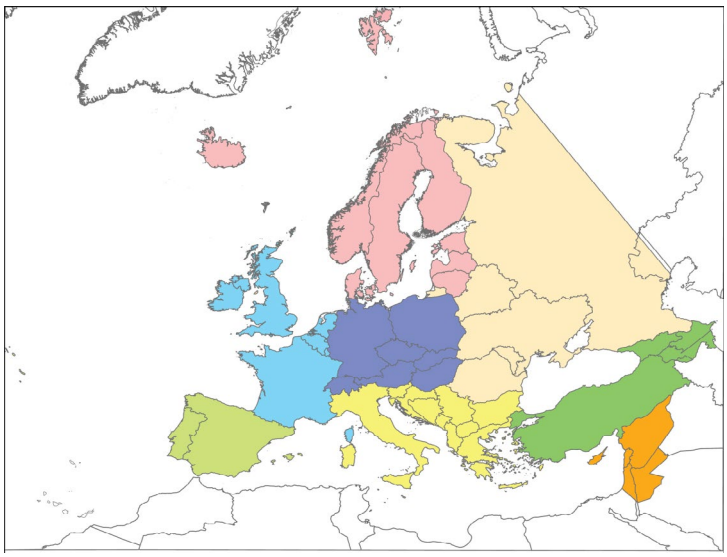

Fig. 7.44. Map of subregions in the World Meteorological Organization Regional Association VI Region of Europe

Autumn was wetter than normal across most of the region. Low-pressure systems moved over the midlatitudes from western to eastern Europe and also to the northeast and southwest. It was drier than normal again in Iceland and over the western and eastern Mediterranean basins and their coastal areas, whereas the Balkans, Greece, and Türkiye were mostly wetter than normal. However, there were large differences from month to month. In September, dry conditions prevailed over a large area of central, southeastern, and eastern Europe, but changed to a rainy period in October in central and eastern Europe and in November in southeastern Europe. In October, tropical cyclones that transitioned into midlatitude storms over the North Atlantic contributed to the wet conditions and in November, storms developed in the Black Sea region. In December 2023, some storms brought flooding in Central Europe, particularly in Germany along the Ems, Weser, and Elbe Rivers and their tributaries, while dry, cold air prevailed in northern Europe. Dryness was also prevalent in the Mediterranean region.

2. WESTERN EUROPE

This region includes Ireland, the United Kingdom, the Netherlands, Belgium, Luxembourg, and France.

(i) Temperature

In 2023, many countries in this region saw above-normal or near-normal temperatures. Ireland's mean air temperature was 1.0°C above its annual average, marking its warmest year on record. The United Kingdom recorded an annual mean temperature of 10.0°C, 0.8°C above the long-term average, marking its second-warmest year after 2022. The Netherlands experienced its warmest year since the start of its record in 1901, at 1.3°C above normal. France and Luxembourg saw their second-warmest year and Belgium its third warmest, with all three more than 1°C above normal. Across the region, all seasons experienced above-normal temperatures.

Winter 2022/23 was slightly warmer than normal in Ireland (+0.3°C anomaly) and the United Kingdom (+0.2°C). On the continent, anomalies were higher: +0.8°C in France, +0.9°C in Belgium, +1.2°C in the Netherlands, and +1.0°C in Luxembourg.

Anomalies in spring were similar to winter in the United Kingdom (+0.3°C) and higher in Ireland (+0.9°C). This was the third-warmest spring on record in Ireland; however, this overall warm period included fluctuations between colder and milder weather patterns, featuring cold spells in early March and late April. The seasonal temperature anomaly for France as a whole was +0.6°C, but up to +1°C in the west and extreme south. In contrast, spring temperatures were slightly below normal in the Netherlands (−0.2°C), Belgium (−0.3°C), and Luxembourg (−0.2°C), mainly due to a cooler April when cold air from the northeast reached the continent.

In summer, June was outstandingly warm in western Europe, while July and August were near or slightly below normal. Ireland, the United Kingdom, Belgium, and the Netherlands each experienced their warmest June on record, with anomalies of +2.5°C in Ireland and the United Kingdom, +3.2°C in the Netherlands, and +3.6°C in Belgium. Overall, the summer season was among the 10 warmest on record for all countries of western Europe except Luxembourg. Summer anomalies ranged from +0.8°C for the United Kingdom and Luxembourg to +1.4°C for France.

Anomalies in autumn were even higher than those in summer in the western European countries: Ireland (+1.0°C), the United Kingdom (+1.0°C), the Netherlands (+1.9°C), Belgium (+2.2°C), Luxembourg (+1.8°C), and France (+2.5°C). It was the warmest autumn on record in France, the second warmest in the Low countries (Netherlands, Belgium, Luxembourg), sixth warmest in the United Kingdom, and fifth warmest in Ireland. September was notable, especially for France, which saw its warmest September since the start of its record in 1900 (3.6°C above normal). The United Kingdom observed its equal warmest September in its record dating to 1884.

(ii) Precipitation

Over the year, most of western Europe received near- or above-normal precipitation. The total precipitation for the United Kingdom reached 1319 mm, which is 113% of normal. Other countries in Western Europe registered higher percentages, including Ireland (117% of normal), Belgium (121%), Luxembourg (128%), and the Netherlands (133%). The average precipitation total for France in 2023 was near normal (104%) following a very dry year in 2022. Only the southeastern

parts of France were considerably drier than normal (<60% of normal), with some parts having marked their driest year on record.

Almost all countries in western Europe received below-normal precipitation in winter 2022/23, including France (75% of normal) and Belgium (94%). The only exception was the Netherlands (102% of normal). February was extremely dry due to persistent high pressure over the area. France received only 26% of its normal monthly precipitation, marking its fourth-driest February on record since at least 1959 and the driest since 2012, while Belgium received 20% of its normal (a monthly total of just 13 mm). The Netherlands recorded 36% of its normal precipitation in February, Ireland 34%, Luxembourg 18%, and the United Kingdom 47%, its driest February since 1993.

Spring was wetter than normal across much of the region: 139% of normal in the Netherlands, 146% in Belgium, and 137% in Luxembourg. For Ireland and the United Kingdom, precipitation in spring was closer to normal (118% and 109%, respectively). France saw average rainfall across the country (102%) but below-normal precipitation in the southeast.

Summer, too, had above-normal rainfall in large parts of Western Europe. The highest national percentages were 139% of normal in Ireland and 119% in both Belgium and Luxembourg. July 2023 was the wettest July on record for Ireland, which saw 203% of its average for the month. Autumn was also wetter than normal across most of the region, with totals generally about 120%–170% of normal.

(iii) Notable events and impacts

On 17 February 2023, Storm Otto passed over western Europe. Gusts of up to 150 km h^{-1} were measured in certain regions of Scotland and northeast England.

During 21 January to 21 February (32 days), no measurable rain (>1 mm) on average fell in France, the longest such occurrence since records began in 1959 and surpassing the dry period of 17 March to 16 April 2020 (31 days).

Storm Juliette hit southern France on 26 February. In combination with cold airflow from the northeast, 5 cm–10 cm of snow fell between the Provence and Languedoc regions above 300 m altitude. In addition to the snow, the wind was strong over the south and southeast of France on 26 February, with up to 161 km h^{-1} in Cap Béar (a coastal station near the eastern Pyrenees) or 122 km h^{-1} in Avignon (Provence).

Southeastern parts of France, notably the regions close to the Mediterranean, were dry in April. Precipitation totals for the first half of April were 5 mm–20 mm on the eastern Mediterranean coast and less than 5 mm on the western Mediterranean coast.

A summer storm (Poly) impacted the Netherlands and northern Germany on 4–5 July, with heavy rainfall and strong winds, including the highest summer wind gust ever recorded in the Netherlands.

A heatwave occurred during 17–24 August across all of France. This marked the longest heatwave in the country this late in the year as well as the most intense, especially in the southern half of the country.

In late October, Storm Babet brought heavy, widespread, and persistent rain to the United Kingdom, causing serious flooding problems. The Met Office issued two red warnings for rain for eastern Scotland. November began with Storm Ciaran affecting the southern United Kingdom and western France, bringing strong winds and flooding to the region. In December, Storms Elin (Vanja), Fergus (Walter), Pia (Zoltan), Gerrit (Bodo), and Geraldine (Costa) brought strong winds, flooding, and disruption to Ireland, the United Kingdom, southern Scandinavia, the Netherlands, Belgium, and northern Germany.

3. CENTRAL EUROPE

This region includes Germany, Switzerland, Austria, Poland, Czechia, Slovakia, and Hungary.

(i) Temperature

In 2023, every country in this region reported its warmest or second-warmest year on record. Annual anomalies ranged from +1.2°C to +1.5°C.

Winter temperatures were above average, with anomalies of +2.8°C in Hungary, +2.2°C in Slovakia, +1.9°C in Czechia, +1.5°C in Germany and Austria, +2.0°C in Poland, and +1.3°C in

Switzerland. In Slovakia, 1–2 January marked the highest temperatures on record for that month. In Czechia, at the Javorník station, the maximum January temperature reached 19.6°C, the highest on record. Poland also recorded its highest January maximum temperatures.

In spring, all countries of the region had near-normal temperatures. Switzerland was the only country with a positive seasonal anomaly (+0.3°C), whereas the highest negative anomaly was in Czechia (−0.4°C). April was particularly colder than normal, with an anomaly of −2.1°C in Czechia. The average April temperatures hit record lows in Slovakia's highest mountains, notably on Lomnicky štít (−6.5°C, 1.8°C below normal), Chopek (−3.7 °C, 2.0°C below normal), and Skalnaté Pleso (−1.0°C, 2.2°C below normal).

Central European countries experienced above-normal temperatures during the summer, though in different intensity. Switzerland was 1.6°C above normal, marking its fifth-warmest summer on record. Anomalies were lower towards the north and east east of the region, and lowest in the eastern countries (Poland and Hungary: +0.8°C; Slovakia: +0.7°C). The region was affected by heatwaves originating in southwestern Europe, which weakened towards the northeast, and also by foehn effects in the Alpine region.

Autumn was the warmest or second warmest on record within Central Europe. Seasonal mean temperatures were more than 2°C above normal across almost the entire region. The highest anomaly was in Hungary at +2.6°C. September was particularly warm, with anomalies mostly between +3°C and +4°C in Central Europe and even higher locally. The anomalous warmth continued in October, particularly in the southeastern region. November had near-normal temperatures, and December 2023 was once again warmer than normal.

(ii) Precipitation

Above-average annual rainfall was observed in all parts. Germany reported 121% of its normal precipitation (especially high in the northwest), Poland 107%, Slovakia and Hungary 125%, Czechia 107%, Austria 117%, and Switzerland 112%.

During winter, the region experienced contrasting conditions. The average precipitation total for winter 2022/23 in Germany was 95% of normal, Austria received 92% of its normal, and Switzerland 69%. In contrast, winter precipitation was higher than normal in Poland (at 131%, its fourth-wettest winter on record), as it was in Slovakia (161%) and Hungary (151%), while it was near normal in Czechia (103%).

Spring precipitation was close to average or higher. Austria received 127% of its normal precipitation in spring, Germany 115%, Czechia 104%, and Slovakia 102%; Poland received 90% of its normal. April 2023 saw remarkable rainfall patterns across Austria. Precipitation was above normal in almost all regions, a phenomenon not observed since April 2017. The average precipitation total was 178% of normal, making April 2023 one of its 10 wettest April months since the mid-nineteenth century.

Summer precipitation varied across Central Europe. Switzerland was drier than normal (91% of normal). June in particular contributed to the dryness, with precipitation <61% of normal across large parts of the country and even <30% in some areas, including the Lake Constance area. Other countries experienced surpluses in summer precipitation, ranging from 103% of normal in Poland to 109% in Hungary.

Autumn was wet across the region, with rainfall totals ranging from 103% of normal in Czechia to 150% in Switzerland. Germany recorded 258.1 mm, which is 135% of its normal. Rainfall patterns varied by month. September was dry in the region, but its deficit was overcompensated by surpluses in October and November. November 2023 was the second-wettest November in Germany since the start of the record in 1881, as monthly precipitation was around 200% of normal there as well as in Czechia and Slovakia. Northern Switzerland received as much as 300% of its normal in November.

(iii) Notable events and impacts

On 4 February, a new daily average temperature record for winter was set in southern Switzerland at the Magadino/Cadenazzo station (15.1°C, measurements since 1959). Strong winds also occurred farther east in Hungary on the same day. At the Kab Mountain station in

Bakony, a gust of 129.6 km h^{-1} was measured, setting a new national daily record for maximum wind gust for 4 February.

The night of 7 February was very frosty in southern Poland after a cold front passage from the northwest; the minimum temperature dropped to –17.7°C in Zakopane. Severe frosts also occurred that same day in Slovakia, where minimum temperatures of –22°C to –23°C—the lowest temperatures of that winter—were measured in northern and central regions.

The station Rheinfelden in southwestern Germany set a new high temperature record for the first half of March, which was strongly influenced by foehn winds, with 13 March 2023 seeing 23.9°C. Several stations in Switzerland (e.g., Basel with 23.4°C) were also record warm. For the first recorded time in March, all stations below 2000-m altitude in Austria remained frost-free on the night of the 24th. The minimum temperature on 24 March was also record high in Czechia.

On 7 June, flooding in Hungary was reported due to impacts from a low-pressure system. The same system also affected southern and central Germany with up to 119 mm of precipitation falling in two hours in the Hessen region (central Germany) on 8 June. The return time for such an event is more than 100 years.

In Switzerland, new maximum temperature records for August were set at numerous measuring stations, and the 0°C level rose to a local all-time record-high altitude of 5298 meters on the night of 21 August in a balloon sounding from Payerne (measurements began in 1954). Thus, the heatwave occurred not only on the ground but also became record warm in the middle troposphere at an altitude of about 5.5 km (500-hPa level).

In early December, Storm Ciro brought snowfall across central Europe, which particularly affected southern Germany, Austria, Switzerland, Czechia, northern Italy, and Croatia and caused widespread travel disruptions in those regions. The Bavaria region (southeastern Germany) experienced its heaviest snowfall in 20 years, with approximately 50 cm accumulating in some areas.

4. IBERIAN PENINSULA

This region includes Spain and Portugal (peninsular mainland only). The reference period for Portugal is 1981–2010.

(i) Temperature

The year 2023 was the second warmest on record for Spain and Portugal, with the countries seeing anomalies of +1.3°C and +1.0°C, respectively. Spain saw above-average temperatures in winter 2022/23, marking the 10th-warmest winter since records began in 1961 and the fifth warmest in the twenty-first century. Winter was the eighth warmest in Portugal since the start of its record in 1931 (+1.1°C anomaly).

Spring 2023 was the second-warmest spring in Portugal (+1.9°C) and record warmest in Spain (+1.8°C). Spain had its third-highest summer temperature in 2023, after 2022 and 2003, at 1.3°C above normal. In Portugal, summer ranked as its sixth warmest on record, at 1.1°C above normal.

Autumn brought unusually high temperatures, with an anomaly of +1.9°C for Spain, its second-highest autumn temperature on record. In Portugal, it was the fourth-warmest autumn in the past 93 years, with an anomaly of +1.3°C. October 2023 was the second-warmest October on record in Portugal.

(ii) Precipitation

In 2023, the Iberian Peninsula had below-average rainfall. Spain recorded an average precipitation total of 536.6 mm, only 84% of its 1991–2020 normal. This marked the sixth-driest year since records commenced in 1961 and the fourth driest of the twenty-first century. Portugal recorded 735.1 mm, which was 87% of its normal.

During winter in Portugal, the total precipitation amounted to 364.2 mm (153% of normal). In mainland Spain, winter precipitation was 194.5 mm (103% of normal). Spring in Spain was drier than normal, with an average of 95.4 mm over Spain (53% of normal), its second-driest such period on record, behind 1995. Portugal observed its third-driest spring on record (99.9 mm, 49% of normal), with the driest being 2017. Throughout the season, all months saw below-normal precipitation in Portugal, particularly in April and May. April was the third driest on record.

Summer was wetter than normal, with an average precipitation total over Spain of 87.2 mm (124% of normal). This was the 16th-wettest summer on record and the third wettest of the twenty-first century, following 2010 and 2018. Summer was near normal for Portugal, receiving 54.6 mm of rain (104% of normal). June was wetter than normal, but rainfall was below average for July and August.

Autumn precipitation was above normal for both Portugal and Spain, at 410.3 mm (141% of normal) and 243 mm (121%), respectively. This marked the ninth-wettest autumn for Portugal (with a record-wet October) and the 17th wettest in mainland Spain, as well as the fifth wettest of the twenty-first century. On the Balearic Islands, however, it was the third-driest autumn since the beginning of the series, behind 1983 and 1981.

(iii) Notable events and impacts

On 28 February, Storm Juliette brought snow and wind gusts to Mallorca. The storm blocked roads, caused a power outage, and created torrents of water from melting snow.

On 11 March, Castelló de la Plana in the Valencia region of Spain set a new March record for daily maximum and minimum temperatures, reaching 30.8°C and 19.4°C, respectively. The subsequent two days were the warmest for those dates since 1950 across Spain. Record-breaking temperatures were recorded on 13 March, with Xàtiva reaching 33.1°C and Valencia Airport measuring 31.9°C. Towards the end of March, temperatures rose to over 34°C in the Murcia and Valencia regions. On 23 March, the heat triggered a large wildfire in eastern Spain, burning over 4000 hectares of land and necessitating the evacuation of more than 1800 people. The fire spread rapidly due to strong winds and dry conditions.

Three heatwaves hit Portugal's northern and central inner regions in April; 60% of the meteorological stations in the National Meteorological and Hydrological Services (NMHS) network recorded maximum air temperatures above their historical records.

Similar to other parts of Europe, northern Spain was affected by cold air in the first week of April. Several places in that region reported new local minimum temperature records as low as –8°C.

Spain saw extremely dry conditions in April. Much of the country received less than 10 mm of rainfall throughout the month, with some regions in the southeast remaining entirely dry. The monthly rainfall was less than 25% of normal in several places.

Towards the end of May, Spain received heavy rainfall following a continued spring drought, especially in the southeast. From 23 to 24 May, the areas of Andalusia, Murcia, and Valencia saw 48 hours of unprecedented rainfall that caused flash floods, which in turn forced the closure of several highways and schools.

A strong summer heatwave occurred in Spain during the final week of June, peaking at 44.4°C in El Granado (Andalusia). Extreme heat was also experienced during this time in Portugal, peaking at 42.7°C on 25 June.

On 11 July, another heatwave began and spread from southwestern Europe to the Alps. In Spain, two July maximum temperature records were broken: Albacete (air base) recorded 42.9°C, its highest since 1940, while Daroca (Zaragoza) reached 40.6°C, marking the first time that temperatures surpassed 40°C in July in over a century in this location.

August was hot, with two heatwaves occurring over the Iberian Peninsula. In Portugal, Santarém reached the highest recorded maximum temperature of 46.4°C. In several parts of mainland Spain, temperatures rose to 45.0°C and above. On 10 August, a new local all-time heat record of 46.8°C was recorded at Valencia airport, exceeding its typical August temperatures by almost 10°C.

Another heatwave occurred between 24 September and 13 October, which was the most intense heatwave in Portugal in autumn since 1941. Above-average temperatures were recorded at 26% of meteorological stations across the country.

Drought affected Portugal, with the south—particularly the Algarve and Baixo Alentejo—experiencing more severe and extreme conditions, especially from April to August.

5. THE NORDIC AND BALTIC COUNTRIES

This region includes Iceland, Norway, Denmark, Sweden, Finland, Estonia, Latvia, and Lithuania.

(i) Temperature

Annual temperatures in the northern Nordic countries were near average. Iceland and Norway had marginally below-average temperatures (–0.1°C anomaly), whereas Sweden and Finland had temperatures slightly above average (+0.2°C and +0.3°C, respectively). Anomalies were higher towards the south, with Denmark recording +0.6°C, Estonia +0.8°C, Latvia +1.0°C, and Lithuania +1.3°C. Latvia and Lithuania both experienced their third-warmest year on record.

Winter 2022/23 had above-normal temperatures across the region, particularly in its eastern parts. Finland recorded the highest anomaly at +2.1°C, whereas the other countries were mostly around 1°C warmer than normal, with Norway only 0.3°C above normal. Iceland, however, was 1°C colder than normal, marking its coldest winter since 1995. January was particularly mild in eastern parts of the region, with a monthly anomaly of +3.3°C in Lithuania and +2.0°C in Estonia.

Temperature anomalies in spring varied across the region. Normal- to below-normal temperatures occurred in the Nordic countries: Denmark saw 0.0°C, Norway –0.8°C, Finland –0.1°C, and Sweden –0.3°C. In contrast, Estonia and Latvia observed above-normal temperatures, with both recording anomalies of +0.9°C and reporting their 10th- and 11th-warmest springs, respectively. Spring in Iceland was slightly colder than normal on average due to an exceptionally cold March, which was the coldest since 1979.

Summer was warmer than normal across most of the region. It was the eighth-warmest summer on record for Norway, which had an average temperature of 1.1°C above normal. The other Nordic and Baltic countries had smaller deviations from normal, with national averages of between +0.0°C and +0.8°C. June was particularly warm (+2.5°C in Sweden, +2.6°C in Norway), as was August in the north and east of the region. July, however, was cooler than normal across the region.

Temperatures in autumn were above normal in Iceland (+0.2°C), Denmark (+0.8°C), Lithuania (+1.3°C), Estonia (+0.7°C), and Latvia (+1.1°C). Conversely, Norway, Finland, and Sweden reported below-average temperatures due to Arctic cold air outbreaks in October and November, with seasonal anomalies of –1.1°C, –0.7°C, and –0.5°C, respectively. September marked record warmth in several places, including Finland (+3.2°C anomaly), Denmark (+2.7°C), Sweden (+2.7°C), Lithuania (+3.7°C), Estonia (+3.4°C, the warmest since 1922), and Norway (+1.3°C, fifth warmest on record).

(ii) Precipitation

In 2023, precipitation varied across the region, with totals significantly above normal in most of the Nordic countries. Denmark recorded 129% of its normal precipitation, making it the wettest year on record. Sweden and Finland saw their fourth- and eighth-wettest year on record, respectively, with around 110% of normal precipitation. In Latvia, 2023 was also wetter than normal (112%). For Norway, Lithuania, and Estonia, precipitation totals were between 103% and 105% of normal, while drier-than-normal conditions occurred in Iceland (91%).

Winter 2022/23 saw mostly near-normal or above-normal precipitation across the region, except for Iceland, which received below-average amounts. Denmark experienced a significantly wetter-than-normal winter with 132% of normal precipitation, marking its eighth-wettest winter on record. January was particularly wet, with Denmark and Latvia receiving 191% and 156% of average rainfall, making it their wettest and third-wettest January on record, respectively.

Spring 2023 was mostly drier than normal across the region, particularly in the Baltic countries, which received only 72% to 78% of their normal precipitation. March was wet across most parts of the region, particularly in Finland and Latvia, which observed their second- and seventh-wettest March on record. May, in contrast, was dry. With only 28%, 31%, and 24% of normal precipitation, respectively, it was the third-driest May on record for Estonia, the second driest for Lithuania on record, and the driest on record for Latvia.

Summer was wetter than normal across most parts of the region. Denmark received 128% of its normal precipitation, mainly due to the wettest July on record for the country (215% of normal).

Norway observed its fourth-wettest August (145% of normal). In Lithuania, a wet August (168% of normal precipitation) compensated for much-drier-than-normal conditions in June and July (both 65% of normal).

Autumn was notably wet in the region, except for in Norway and Iceland. Finland experienced its fifth-wettest autumn (126% of normal), with September being its wettest on record (160% of normal precipitation). Denmark experienced its seventh-wettest autumn (132% of normal), with October seeing its fifth wettest on record (179% of normal).

(iii) Notable events and impacts

On 10 March, a high-pressure period contributed to low temperatures in the Baltic countries, with Lithuania observing a minimum of –19.4°C and Latvia experiencing its strongest frosts since December 2021. Temperatures in the interior of Estonia fell below –25°C on 10 March, with the lowest recorded at Tiirikoja (–26.3°C).

Norway experienced large snow accumulations, with some places receiving over 40 cm of snow in a single day, even in the south. Kristiansand in southern Norway recorded a remarkable snow depth increase from 3 cm to 49 cm on 17 March, marking the third-largest snowfall in March since measurements began over 100 years ago.

Another cold wave and snow storm impacted the region during 23–28 March and was most intense in Scandinavia. Tromsø in northern Norway registered a new March record for accumulated daily fresh snow depth with 179 cm, and southeastern Sweden saw significant snow accumulations, with Vattholma near Uppsala measuring 40 cm on 28 March.

Northern Norway saw snow on 1 June, with Tromsø recording –0.6°C, the first temperature below 0°C in June since 1997. Sweden and Finland also experienced some of their lowest June temperatures in decades. In early June, a countrywide cold spell hit Finland, with Saana, at an altitude of 1001 m, recording a historic low temperature of –7.7°C on 1 June, marking a new June record for the country.

A major storm passed through northern Europe on 6–8 August, bringing heavy rain, thunderstorms, and strong winds that caused floods, landslides, and casualties in Norway, Denmark, Sweden, Finland, Estonia, Latvia, and Lithuania. Record-breaking precipitation and wind speeds were reported, with significant damage to infrastructure and widespread power outages affecting thousands of households. In Estonia, a hailstorm on 7 August damaged cars, roofs, and greenhouses. The largest hailstones measured a diameter of 8 cm, the biggest on record for the country.

On 8 August, northern Europe experienced record-breaking maximum temperatures, with northern Norway reaching 30.3°C, northern Sweden observing 31.1°C in Haparanda, and Finland recording 33.2°C in Pori. On 17 August, Lithuania set a new national maximum record of 34.6°C.

In early September, northern Europe experienced a heatwave caused by an omega blocking pattern. In Norway, temperatures soared to 28.3°C in Etne, Vestland, potentially setting a new September record. Additionally, four stations in Sweden recorded new local September records (up to 27.6°C). On 12–13 September, new daily maximum temperature records were recorded at several stations in Estonia.

The nationwide average mean temperature in Denmark and Finland in September was the highest since the start of the record in 1874 and 1900, respectively; however, the period from October to December was characterized by a long cold spell in Fennoscandia, which saw below-normal temperatures during all three months. In Finland, October–December was the coldest such period since 2010. At the end of December, the sea ice extent in the Bay of Bothnia was at its largest since 2010.

6. CENTRAL MEDITERRANEAN REGION

This region includes Italy, Monaco, Malta, Slovenia, Croatia, Serbia, Montenegro, Bosnia and Herzegovina, Albania, North Macedonia, Greece, and Bulgaria.

(i) Temperature

Slovenia, Croatia, Serbia, Malta, Bulgaria, and Montenegro each experienced their warmest year on record in 2023, while Italy recorded its second warmest. All other countries in this region

experienced consistently above-average temperatures throughout the year, with many recording their highest monthly temperatures in various months.

Winter across the region was warm, with all months seeing temperatures above average. Anomalies were highest in Bulgaria (+3.0°C) and lowest in Malta (+0.3°C). Bulgaria reported its warmest winter on record, and Serbia observed its third warmest. January was particularly mild; Bulgaria's monthly average was 4.4°C above normal and Serbia's was 3.9°C above normal.

Spring saw mostly near- to below-normal temperatures across the region. Bulgaria reported its coldest May since 2005. North Macedonia, Slovenia, and Serbia recorded anomalies below normal for the season (−0.5°C, −0.05°C, and −0.3°C, respectively). Italy, Croatia, and Montenegro saw temperatures slightly above average, with anomalies ranging from +0.08°C to +0.3°C. Greece and Malta experienced above-normal temperature anomalies for spring at +1.5°C and +1.0°C, respectively, while mean temperature deviations in Bosnia and Herzegovina ranged from −0.7°C to +0.3°C.

Summer temperatures were mostly around 1°C above normal, with June and July notably warmer than average. July marked the peak of summer anomalies, with Malta and Greece reporting anomalies of +2.7°C and +3.2°C, respectively (the hottest July on record for Malta). Bulgaria experienced its third-warmest summer, at 1.2°C above normal, and its second-warmest July, with an anomaly of +2.2°C. Italy observed its third-warmest July (+2.0°C).

Italy, Malta, Slovenia, Croatia, Serbia, North Macedonia, and Bulgaria all observed their warmest autumn on record, with temperature anomalies ranging from +1.4°C to +3.3°C. September 2023 was the second warmest for Slovenia, third warmest for Italy and Serbia, and fourth warmest for Bulgaria and North Macedonia. Italy, Malta, Slovenia, and Macedonia all recorded their warmest October on record, while Serbia and Bulgaria had their second warmest. Malta reported its second-warmest November.

(ii) Precipitation

In 2023, Slovenia reported 128% of its average, making 2023 the country's third-wettest year. Other countries were closer to normal, from 96% of normal in Bulgaria and Italy to 119% of normal in Serbia.

Winter was wetter than normal in most countries. There was large variability from country to country, from 105% of normal in Slovenia to 146% in Croatia, its neighboring country. Malta received 125% of its normal precipitation. Only North Macedonia and Bulgaria received less-than-normal (85%–95%) precipitation. January was wetter than normal across almost the entire region, as was part of February. Malta observed its second-wettest February on record.

Spring also was a wet season over almost the entire region. The greatest percentages of normal were recorded in Italy (127%), Croatia (139%), and Bosnia and Herzegovina (121%). The only exception was Malta (82% of normal), which had its third-driest March on record. This contrast can be explained by the Azores High pressure zone, which expanded far into the western Mediterranean that month, while the northern Balkans were affected by midlatitude cyclonic systems.

Summer presented contrasting conditions across the region. Slovenia recorded its wettest summer on record (163% of normal precipitation), which included its second-wettest August (209%). Italy received 124% of its normal rainfall, Croatia received 141%, and Serbia 124%. Malta experienced its driest July on record, though it only saw small departures from normal for the entire season.

Autumn precipitation was below normal in Italy (77% of normal) and near normal in most of the Balkans, but with large variability from month to month. September and October were dry months, while November was much wetter than normal. Bulgaria recorded its fourth-driest October, yet its fifth-wettest November, and Serbia observed its seventh-driest October (23% of normal), yet its wettest November (162%).

(iii) Notable events and impacts

Catastrophic floods inundated several Croatian towns in May, including Obrovac, Gračac, Karlovac, Duga Resa, and Hrvatska Kostajnica, leaving numerous buildings submerged and causing contamination of drinking water, extensive damage to infrastructure such as roads

and bridges, and destruction of agricultural land and greenhouses. The floods also triggered landslides and threatened areas already flooded with additional rainfall and water waves from neighboring countries. On 15 May, 256.4 mm was measured in Gračac, which was its highest one-day total on record.

Also in May, heavy rain caused floods and landslides in northern Italy during four major events, particularly in Emilia-Romagna. The Cesena and Avellino Provinces experienced significant flooding. Within 48 hours, during 1–3 May, more than 200 mm were measured at several stations in Emilia-Romagna, marking the most intense spring precipitation event in this area since at least 1961.

On 17 June, Storm Olga's powerful winds and torrential rain caused devastation in parts of the Balkan Peninsula. Greece reported flooding, power outages, and vehicles being washed away, in addition to two fatalities. Houses in Thessaloniki flooded, and crops in western Macedonia suffered harm. Severe weather also affected Skyros Island and the Attica Region. Rivers in eastern Bosnia and Herzegovina overflowed, causing significant crop losses for farmers and prompting Tuzla to declare an emergency.

In July, central and southern Italy experienced an intense heatwave, with temperatures soaring to 8°C–10°C above average in some areas, particularly in the plains and valleys of the Alps and Apennines. Records were broken in Sardinia and Sicily, with temperatures peaking above 47°C on 24 July, reaching 48.2°C in Lotzorai and Jerzu. On 23 August, Milan saw its hottest day since 1763, with temperatures reaching 33°C.

Beginning on 19 August, a large wildfire in the Alexandroupolis municipality in Greece (the largest fire since the start of the record in 2000 in the European Union) destroyed many buildings, forced residents in 13 towns to evacuate, and killed at least 21 people. The fire burnt almost 94,000 hectares by 3 September. Overall, the total area burned in Greece in 2023 was more than four times the long-term average.

Extremely heavy precipitation during 3–6 August in Slovenia (more than 300 mm and locally more than 600 mm) led to six fatalities. The northern and central parts saw over 200 mm of rain in just 12 hours during 3–4 August. This event also caused an unprecedented flood of downstream rivers in Croatia. Koprivnica-Križevci County declared a state of natural disaster on 16 August as a result of flooding in areas including Legrand Municipality along the Drava River.

Widespread and strong thunderstorms impacted northern Italy, resulting in large hailstones 8 cm–10 cm in diameter and strong wind gusts greater than 30 m s^{-1}. On 24 July, a supercell produced record-size hail in the Friuli Venezia Giulia region; in Azzano Decimo, a 19-cm hailstone broke the European record for hail size.

In September, Greece received record rainfall from Storms Daniel and Elias, causing severe flooding in regions including Thessaly and central Greece. Zagora recorded its highest daily rainfall ever in Greece (754 mm in 21 hours, after which the station ceased reporting), resulting in significant damage to infrastructure and homes. This daily total corresponded to a normal annual total for Zagora. Heavy rains from Storm Daniel also affected southeast Bulgaria, western Türkiye, and Libya.

7. EASTERN EUROPE

This region includes Belarus, Ukraine, Moldova, Romania, the European parts of Russia, and West Kazakhstan (i.e., the country's European region).

(i) Temperature

In most places in eastern Europe, 2023 was the warmest year on record, with several individual months also recording their highest-ever temperatures. Annual temperature anomalies varied between +1.4°C in Belarus (third highest on record) and +2°C in Moldova (highest). For Romania and West Kazakhstan, it was the hottest year on record.

Except for West Kazakhstan, whose temperature was slightly below normal (–0.2°C), the region saw an overall mild winter. Romania experienced its warmest winter, with a temperature anomaly of +3.1°C. An even more notable anomaly occurred in January (+5.4°C), making it the warmest January on record in the country. The rest of the region saw seasonal temperature anomalies between +1°C and +3°C.

West Kazakhstan observed its warmest spring on record, with a temperature anomaly of +3.7°C. March was exceptionally warm (6.8°C above normal). In Belarus and Ukraine, seasonal anomalies were +0.9°C and +1.2°C, respectively. Moldova and Romania had near-normal spring temperatures. A heatwave struck many regions of European Russia in May, mainly in the east.

Summer also was warmer than normal, with anomalies of around +1°C in Belarus, Ukraine, and Romania. In Moldova, the average temperatures were 1.2°–1.7°C above normal. August was particularly warm, with maxima reaching 39.5°C and minima dropping to 10°C. Summer in European Russia started with a colder-than-normal June (≥2°C below normal in some places) and July; only August was warmer than normal.

Autumn was warmer than normal for the entire area. Romania saw its warmest autumn on record, at 2.8°C above normal. October 2023 was the country's warmest October on record, at 3.9°C above average, while September was its second-warmest September on record, at +3.4°C. Similar to Romania, Moldova saw an unusually warm autumn, with temperatures 2.8°C to 3.8°C above normal. Moldova also reported its warmest October, with temperatures 3.4°C to 5.0°C above normal. In Belarus, September was the warmest on record, with an anomaly of +3.5°C.

(ii) Precipitation

In Eastern Europe, the year as a whole had near-normal precipitation, but with locally higher annual totals. Precipitation in Belarus over the year was above average, while Moldova was characterized by below-normal precipitation, especially from August to October. Ukraine received 108% of its normal. West Kazakhstan had its sixth-wettest year, with 135% of its normal.

Winter 2022/23 was the wettest for Belarus since the start of observations in 1945, having recorded precipitation that was 152% of normal. Western Ukraine and western Romania also received above-normal precipitation, whereas winter was drier than normal around the Black Sea (Moldova, eastern Ukraine, and southwestern European Russia). Moldova received just 65% of its normal seasonal precipitation.

Spring precipitation was characterized by high spatial variability. The seasonal total in Moldova was 136% of its normal, with April 2023 being the country's wettest April on record. Its neighboring country, Romania, had a drier spring than usual, with precipitation that was 88% of its normal. May was the driest month of the season, seeing 68% of normal rainfall.

Summer was wetter than normal in Ukraine—44 mm above normal in Kyiv and 66 mm above normal in Kharkiv. West Kazakhstan received 132% of its normal precipitation for the season, as it observed its sixth-wettest July (219% of normal). Conversely, it was significantly drier than average during summer in Moldova (46% of normal); the country observed its second-driest August on record (4% of normal).

Autumn was mostly wetter than normal. Belarus experienced a rainy autumn, with a surplus of 189 mm of precipitation over the season (123% of normal). In some southern regions, totals did not exceed 5 mm, while in northern regions, 50 mm–90 mm fell (60%–100% of normal). West Kazakhstan observed its fifth-wettest autumn on record, including its second-wettest October (172% and 226% of normal, respectively).

(iii) Notable events and impacts

On 1 January, Belarus experienced its highest nationally averaged maximum January temperature on record, at 16.4°C. In the Ukraine, 1–2 January were the warmest January days since record keeping began in those countries, where several stations broke their records. Also on 1 January, Romania recorded a new monthly national high temperature of 22.5°C, surpassing its previous record set in January 2001. This "New Year warm event" occurred also in Central Europe (section 7f3). Moreover, on 19 January, the Băneasa borough of Bucharest recorded its highest daily January temperature on record (20.9°C). Average temperatures in Bulgaria, Romania, and Moldova were 15°C–17°C higher than usual.

On 13–14 June, severe weather and flooding in Krasnodar Krai, including Sochi, Russia, caused the Mzymta and Matsesta Rivers to break their banks, causing damage to four houses and dozens of roads.

On 6 July, Moldova and Ukraine experienced subtropical heat, with temperatures exceeding 38°C in Kherson and Kryvyi Rih and a daily minimum temperature of 23.4°C recorded in Odesa.

On 8 July in southern European Russia, some stations recorded daily maximum temperatures of up to 42.1°C, which was recorded at Baskuncak, close to the Kazakhstan border.

On 30 July, Russia's eastern and central regions were struck by intense rain and wind, which caused damage and at least 10 fatalities and 76 injuries. Thousands of residents in the Mari-El Region lost electricity as a result of the catastrophic weather event that happened near Lake Yalchik.

On 20 August, heavy rain (43 mm) caused flash flooding in Moscow, Russia, resulting in four fatalities.

8. MIDDLE EAST

This region includes Israel, Cyprus, Jordan, Lebanon, and Syria.

(i) Temperature

In 2023, the Middle East experienced above-normal annual temperatures. Israel and Jordan observed their third- and fifth-warmest year on record, with temperature anomalies of +1.0°C and +0.85°C, respectively. Cyprus also had its fifth-warmest year, at 1.25°C above normal.

During winter 2022/23, Israel and Cyprus experienced above-normal temperatures, with anomalies of +0.8°C and +1.2°C, respectively. In Cyprus, January was the fifth warmest on record, while February was second coldest (anomaly of −0.8°C). In February, Lebanon faced severe winter conditions, including snow in high altitudes, rain in lower regions, thunderstorms, and strong winds.

Spring was characterized by variability across the region, with temperatures having generally been slightly above normal. Israel recorded a temperature anomaly of +0.3°C, but only March was moderately warmer than normal. Cyprus recorded a spring temperature anomaly of +0.7°C, while Jordan and Syria recorded anomalies of +0.3°C and +0.4°C, respectively. Lebanon also experienced a mild spring, at 0.5°C above normal.

Jordan observed a summer temperature anomaly of +1.3°C, along with an August that was 2.4°C above normal. In Israel, summer 2023 was the fifth warmest on record, with its July and August having been second and fifth warmest, respectively. Cyprus reported a summer temperature anomaly of +0.85°C.

Autumn was notably warmer than usual across the region, with anomalies surpassing +1.0°C. In most regions, November had the highest monthly anomaly, exceeding +2°C. Israel recorded its third-warmest autumn and third-warmest September, while Cyprus had its second-warmest October, along with a September and November that were both fourth warmest. In the remaining areas of the region, November also had the highest temperature departures from normal among the autumn months.

(ii) Precipitation

Overall, precipitation totals in 2023 for most places and months were near or below normal. Israel received 521 mm of precipitation in 2023 (98% of normal). Total precipitation in Cyprus was 414 mm (82% of normal). Lebanon and Syria were also drier than normal (numbers were not available).

Winter 2022/23 was dry in the Middle East, with all regions recording below-normal rainfall. Israel and Cyprus received 75% and 64% of their seasonal averages, respectively. January was notably dry in Israel, with just 54% of average precipitation, marking its eighth-driest January on record. The total precipitation in winter was 65% of normal in Jordan, 53% in Syria, and 58% in Lebanon.

Spring was significantly wetter than normal in Israel, with 161% of normal precipitation, marking the eighth-wettest spring on record along with the fifth-wettest April. The total precipitation in Cyprus was normal (101%). Jordan experienced particularly high rainfall totals during spring, recording 289% of its normal for the season, with all months much wetter than normal. Syria received 131% of its normal spring precipitation, while Lebanon recorded slightly below-normal precipitation (96% of normal).

Summer was wetter than normal in Cyprus, with 108% of the seasonal normal precipitation. Total precipitation was 150% of normal in Syria, 204% in Lebanon, 263% in Israel, and 334% in Jordan; however, summer is the dry season in the eastern Mediterranean, and typical rainfall

amounts are low. In Israel, for example, the long-term average for June is 0.5 mm–3 mm. For July and August, it is less than 0.5 mm.

In general, the wet weather pattern continued into autumn, with September experiencing normal to above-average rainfall in the region. Most areas recorded precipitation levels above the seasonal average. Israel reported 110% of its normal precipitation, and Cyprus experienced 159% of its normal. Particularly noteworthy were Jordan and Syria, which recorded 272% and 294% of their normals, respectively.

(iii) Notable events and impacts

In January, Cyprus set a new record as the temperature at the Tepak station rose to 25.5°C due to foehn winds from the Troodos Mountains. This marked the highest temperature recorded for January in Cyprus.

In early February, Israel experienced the impact of Storm Barbara, which brought strong winds, heavy rains, and snow to the region. Wind speeds peaked at 50 km h^{-1} to 70 km h^{-1}, with gusts surpassing 100 km h^{-1}, notably reaching 119 km h^{-1} in Zefat Har Kena'an. Rainfall totals ranged from 80 mm to 150 mm in northern and central Israel. Snowfall was concentrated in the northern and central mountains, with depths exceeding 2 m on Mount Hermon and over 20 cm in the high peaks of the Golan Heights.

During 8–11 February, a massive flooding disaster occurred close to Idlib in northwest Syria. After heavy rainfall, the river's water level was high. Approximately 7000 individuals were forced to evacuate their homes as flooding submerged them.

In late March, a heatwave hit Jordan, particularly the Jordan Valley, resulting in maximum temperatures surpassing 35°C for 13 consecutive days. Ten station records were broken during this period.

During 10–12 April, heavy rain fell in the extreme south of Israel, namely in the southern Negev region. This led to river overflows and flash floods, which caused fatalities and property damage. The cities of Eilat and Paran as well as the Aravah region were the most severely hit, with at least two fatalities recorded.

On 30 May, heavy rain and hailstorms affected various parts of Jordan, causing fatalities, destruction, and flash floods. The capital city, Amman, along with Salt, Madaba, and Irbid experienced significant hailstorms that caused extensive damage.

In July, a heatwave impacted the Middle East, with Israel's Jordan Valley experiencing maximum temperatures of 43°C–46°C. It was unusual for the Middle East region to see a heatwave lasting longer than two weeks. Another noteworthy summer heatwave occurred during 12–20 August. The nights were very warm, especially in the coastal plain and the northern valleys, with an unprecedented consecutive seven to eight nights with minimum temperatures of 26°C–29°C. The Euphrates River's water level reached a historic low at Tabqa Dam in Syria, affecting nearly one million residents in the Hassakeh governorate. As a significant hydroelectric dam, it is crucial for water regulation and electricity production. The crisis impacted daily life, agriculture, and health, and increased occurrences of waterborne diseases.

A heatwave impacted Israel during 5–8 September; temperatures peaked on 8 September with 40°C recorded across the country: 40°C–42°C in the coastal plain, 42°C–44°C in the northern Negev, and 45°C–46°C in some locations of the Jordan Valley and the Arava. Several stations broke their September records, including Besor Farm (44.3°C), which surpassed its previous high of 43.6°C, and Negba (42.8°C), which exceeded its previous record of 42.4°C.

On 20 October, a warming trend began, leading to a heatwave from 21 October to 13 November. Temperatures reached 32°C–35°C in the coastal plain, northern Negev, and valleys, 35°C–39°C in the Arava, and 28°C–32°C in the mountains. Such a long heatwave that late in the year has only occurred two to three times since the early 1900s.

9. TÜRKIYE AND SOUTH CAUCASUS

This region includes Türkiye, Armenia (which has a reference period of 1961–90), Georgia, and Azerbaijan.

(i) Temperature

In Armenia, 2023 was the third-warmest year since 1935, with a temperature that was 2.2°C above the 1961–90 normal. This year was also the third warmest in Türkiye since 1971, surpassing its normal by 1.2°C.

Winter 2022/23 in Armenia was the third warmest since 1935. The average winter temperature of –3.9°C was 1.6°C above average. Türkiye's winter mean temperature was 5.5°C, 1.6°C above normal; the January mean temperature was 5.3°C, surpassing its monthly normal by 2.4°C, making it the second-warmest January for the country since 1971.

In Türkiye, the average spring temperature was 12.8°C, which was slightly above normal (+0.4°C). In Armenia, it was the second-warmest spring on record, behind only 2018. The average temperature was 7.1°C, 2.8°C above normal.

Summer 2023 in Armenia was one of the warmest on record. The average seasonal temperature reached 17.3°C, which was 1.5°C above normal. August was particularly warm, with the average monthly temperature having been 3.1°C above normal, marking the third-warmest August following 2006 and 2017. In Türkiye, the summer mean temperature was 24.7°C, 0.7°C above normal.

Autumn in Armenia was the fifth warmest since 1935. The average seasonal temperature was 9.3°C, which was 2.1°C above normal. November was the warmest on record, with the average monthly temperature 3.7°C above normal. The average autumn temperature in Türkiye was 17.4°C, which was 2.1°C above normal. November 2023 was also the warmest November on record for the country.

(ii) Precipitation

In Armenia, the total annual precipitation for 2023 was 577 mm (97% of its normal). The mean precipitation for Türkiye was 641.5 mm (112% of its normal). In Türkiye, precipitation was below average in the Marmara region, west of Ankara, Çankırı, Kırıkkale, Muğla, eastern and western parts of Antalya, Mersin, Adana, Osmaniye, Hatay, southeastern Anatolia, and eastern parts of eastern Anatolia. Total precipitation was just 40% of normal in Hatay.

During winter in Armenia, precipitation levels were 34%, 22%, and 97% of normal for December, January, and February, respectively. Türkiye also experienced below-normal precipitation throughout the winter, with all months receiving below-normal precipitation.

In Armenia, spring precipitation was near-normal, with May being the exception (81% of normal). Conversely, spring precipitation for Türkiye was above average. In March, Türkiye recorded 95.5 mm of rain (165% of normal). Additionally, precipitation totals for April and May were 151% and 127% of normal, respectively.

Summer 2023 was wet in Armenia, with seasonal precipitation reaching 169.7 mm (114% of normal). June and July had above-normal precipitation totals at 135% and 117% of normal, respectively. However, August saw a dry spell, with a monthly precipitation that was only 68% of normal. In Türkiye, June and July also had significant above-normal precipitation. The average June rainfall total was 58.1 mm (173% of normal).

The seasonal precipitation in autumn was 122.7 mm in Armenia (103% of normal). Only September had above-normal precipitation (153% of normal). Precipitation was below average in October and November, at 89% and 86% of normal, respectively. Across Türkiye, autumn precipitation exceeded the normal by 23% and by 69% compared to the previous year's autumn season.

(iii) Notable events and impacts

On 20 January, new local monthly records were set in Türkiye in high elevations at Bingol (1120 m a.s.l.; 13.8°C) and Erzurum (1800 m a.s.l.; 9.1°C), as well as in Samsun on the Black Sea coast (24.2°C) on 22 January.

On 15 August, a new national high-temperature record for Türkiye was set at 49.5°C in Eskisehir, northwestern Türkiye.

The province of Canakkale in northwest Türkiye was impacted by a wildfire on 22–23 August, which led to damage and evacuations. There were around 4080 hectares of burned land.

During 8–10 July, heavy rain in Türkiye's western and central Black Sea area resulted in flash floods and over 1000 landslides. Over 250 mm of rain fell in one day in the province of Düzce, which is near the western shore of the Black Sea.

Convective hailstorms at Ijevan station in northeastern Armenia resulted in unusually high wind gusts of up to 37 m s^{-1}. Hail diameters reached 3 cm, and rain totals of 30 mm were measured.

On 3 August, a significant landslide in a mountain resort town in northern Georgia (Kvemo Svaneti region) claimed the lives of at least 18 individuals. For many days, more than 400 firemen, helicopters, and drones were used for evacuations and the search for missing persons.

Azerbaijan recorded a temperature of 36.9°C in Baku on 30 May, making it the warmest May day in the city's measuring history.

On 4–5 June, heavy rains in many provinces in Türkiye's Black Sea region including Kastamonu, Samsun, Amasya, and Sinop caused considerable river floods and landslides.

Except for the northern and mountainous areas, most of Armenia experienced drought conditions and a dry spell toward the end of August.

Sidebar 7.3: European drought conditions in 2023

Various parts of Europe were severely impacted by dry conditions in 2023. The incidence and severity of drought varied significantly across different regions and months throughout the year, and each region faced distinct signs of drought and the ensuing effects.

The Combined Drought Indicator (CDI; Fig. SB7.5) shows severe and possibly critical European drought conditions at various times and locations. Southern and eastern Spain, southern France, most of Italy, Malta, eastern Poland, central Romania, southern Greece, Cyprus, and southern Türkiye consistently experienced warning-level drought conditions throughout most months of 2023.

Figure SB7.5a illustrates that France, the United Kingdom, and Ireland were in the warning zone in February. By April, Spain faced severe dry conditions, which were marked as a warning and alert condition (Fig. SB7.5b). This drought persisted into May for Spain, with some parts of Eastern Europe also experiencing drought conditions (Fig. SB7.5c). Drought spread across much of Europe by June, with Spain being notably dry (Fig. SB7.5d); however, July brought wetter conditions to Spain, as drought began shifting towards Central and Eastern Europe (Fig. SB7.5e). In October, Eastern and southeastern Europe, Italy, and France were all under a drought warning, while other regions did not experience drought during this time (Fig. SB7.5f).

Soil moisture indicators show that in April and May (Figs. SB7.6a,b, respectively), soil moisture anomalies in Spain were negative, indicating drier-than-normal conditions due to a combination of low precipitation and high temperatures. However, in other parts of the region, although precipitation

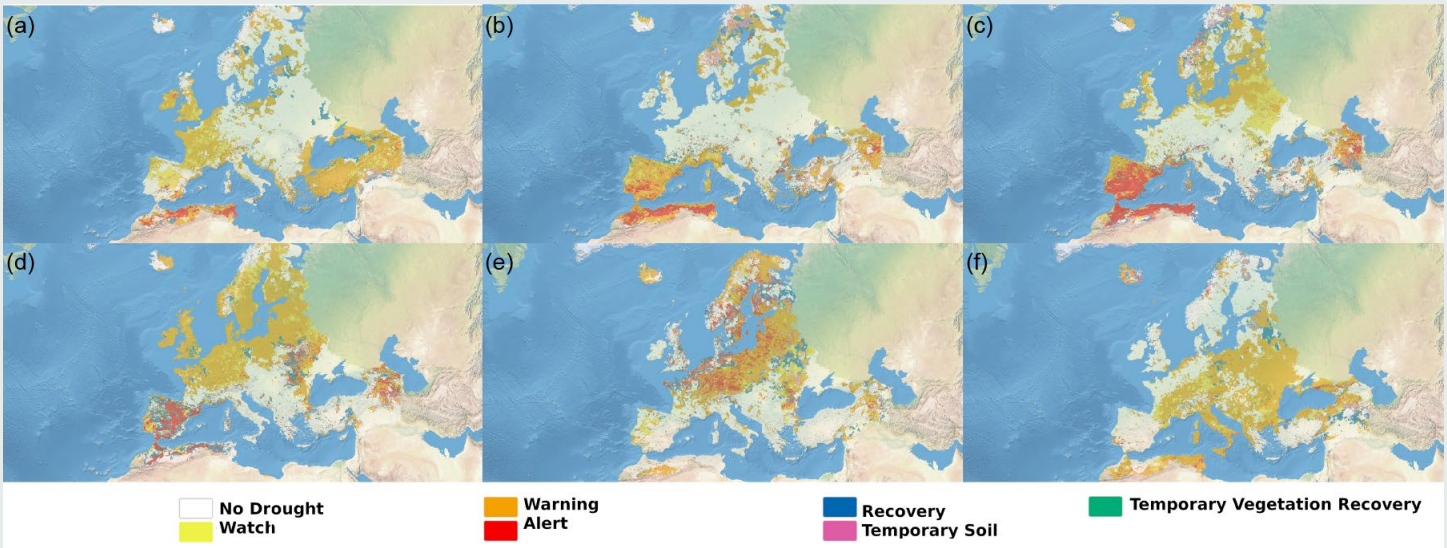

Fig. SB7.5. The Combined Drought Indicator shows drought status based on a combination of indicators of precipitation, soil moisture, and vegetation conditions for (a) mid-Feb, (b) third 10-day period of Apr, (c) third 10-day period of May, (d) mid-Jun, (e) third 10-day period of Jul, and (f) first 10-day period of Oct in 2023. (Source: European Drought Observatory of the Copernicus Emergency Management Service.)

was below normal, soil moisture anomalies remained normal or near normal. By June, the situation shifted: Spain had notably higher soil moisture anomalies, while the United Kingdom as well as Central, Eastern, and Northern Europe experienced negative, dry conditions (Fig. SB7.6c), attributed to lower precipitation in these areas and above-normal precipitation in Spain. In October, southeastern Europe in particular faced drier-than-normal soil moisture (Fig. SB7.6d). December 2023 saw near-normal or wetter-than-normal conditions across most regions except for eastern and southern Spain, which remained dry (Fig. SB7.6e), having received lower precipitation than usual for this month.

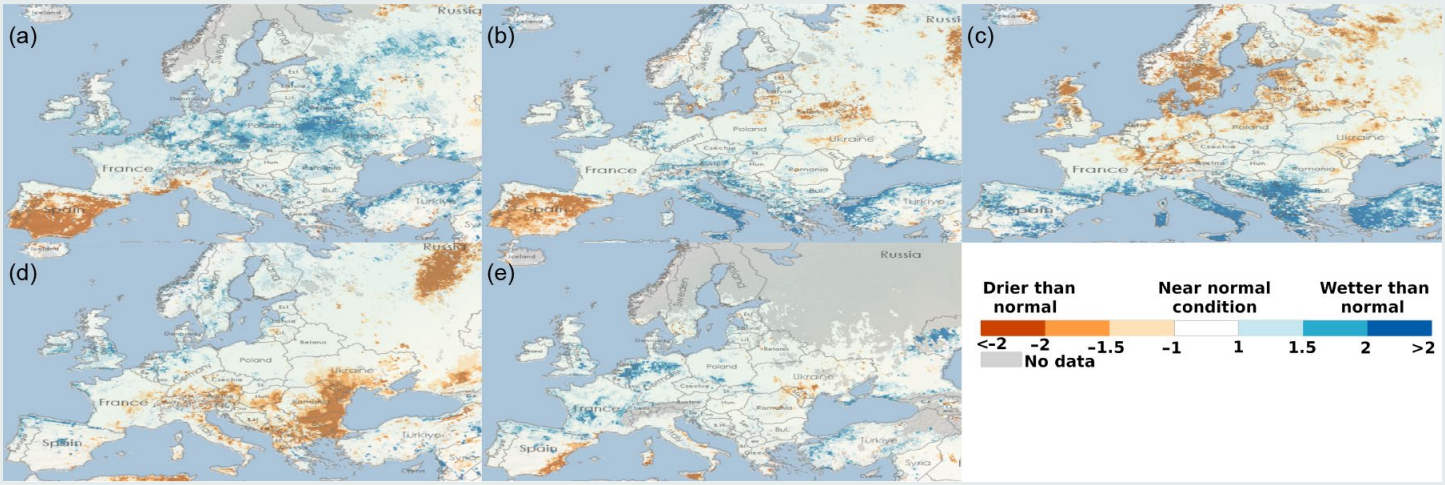

Fig. SB7.6. Soil moisture anomalies for (a) Apr, (b) May, (c) Jun, (d) Oct, and (e) Dec 2023. (Source: European Drought Observatory of the Copernicus Emergency Management Service.)

g. Asia

—Z. Zhu, Ed.

Throughout this section, the base period for the climatological normal and anomalies is 1991–2020. All seasons in this section refer to the Northern Hemisphere, with winter referring to December–February 2022/23, unless otherwise noted.

1. OVERVIEW

—Z. Zhu, P. Zhang, T.-C. Lee, R. Muharsyah, K. Takemura, A. Moise, Y. Okunaka, K. Takahashi, J. I. Seong, D. Dulamsuren, M.-V. Khiem, and H.-P. Lam

Annual mean surface air temperatures during 2023 were above normal across most of Asia and Siberia, except for northwestern South Asia and parts of Eastern Siberia, with anomalies of more than +1°C from Japan to northern China, in eastern Central Siberia, and from Western Siberia to the eastern Middle East (Fig. 7.45). In Central Asia and the Siberian plain, the anomalies were even greater than +2°C. Annual precipitation totals were above normal (>120% of normal) in central Mongolia, in western Central Asia, in and around Pakistan, and in the Arabian Peninsula, and below normal (<80% of normal) in northwestern China and from southern Central Asia to the central Middle East (Fig. 7.46).

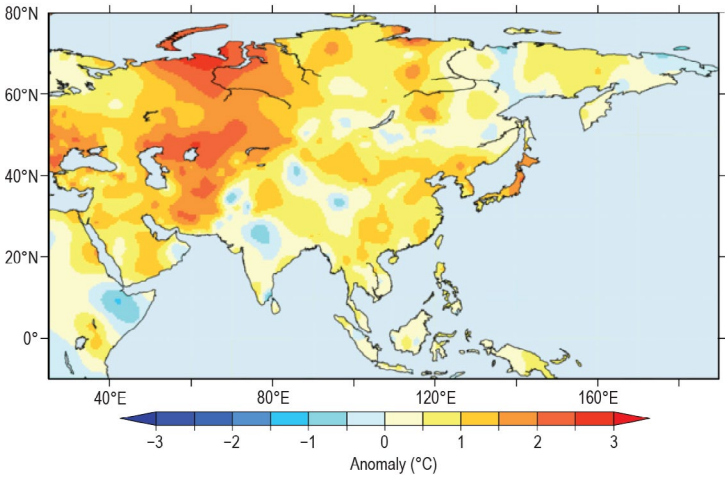

Fig. 7.45. Annual mean surface temperature anomalies (°C; 1991–2020 base period) over Asia in 2023. (Source: Japan Meteorological Agency.)

In winter, positive temperature anomalies were observed in the eastern part of Eastern Siberia, from southern Central Siberia to northern Mongolia, in northern Western Siberia, and from northwestern Southeast Asia to the southeastern Arabian Peninsula, while temperatures were below normal in and around western Eastern Siberia and from western China to southern Central Asia (Fig. 7.47a). Seasonal precipitation was above normal in northeastern Central Siberia, northwestern China, the eastern Indochina Peninsula, southern India, and the central and southern Arabian Peninsula, but below normal from the northern Indochina Peninsula to southwestern Central Asia (Fig. 7.47b).

In spring, temperatures were above normal from central East Siberia to the eastern part of East Asia and northern Western Siberia to the eastern Middle East, while temperatures were below normal in the eastern part of Eastern Siberia, from western Mongolia to western China, and from India to Pakistan (Fig. 7.47c). Seasonal precipitation was above normal in northern and western China and from southern India to Pakistan and below normal from southern China to the Indochina Peninsula, in southern Western Siberia, and from southern Central Asia to the central Middle East (Fig. 7.47d).

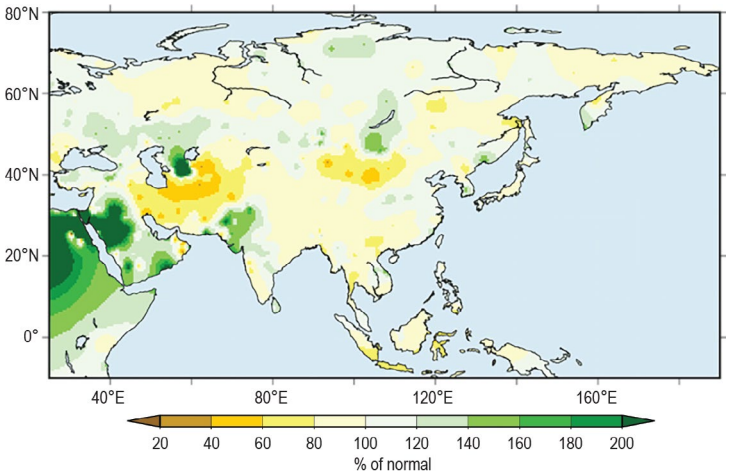

Fig. 7.46. Annual precipitation (% of normal; 1991–2020 base period) over Asia in 2023. (Source: Japan Meteorological Agency.)

In summer, positive temperature anomalies exceeding +1°C were observed from Japan to the northern Arabian Peninsula and from the western part of Eastern Siberia to northern Western Siberia, with some areas reaching +2.5°C. However, temperature anomalies were below –1°C in the northeastern part of Eastern Siberia and in and around Pakistan, with some areas below –2.5°C (Fig. 7.47e). Seasonal precipitation was above normal around Lake Baikal, from Pakistan to Turkmenistan, and in the western

Middle East, and below normal from northern to western China, in the central part of Central Asia, and in and around the eastern Arabian Peninsula (Fig. 7.47f).

In autumn, above-normal temperatures dominated in most of Asia and Siberia, with anomalies of more than +2.0°C from Central Siberia to the Middle East and from North China to Japan (Fig. 7.47g). Seasonal precipitation was much above normal from central Mongolia to western Central Asia and from the eastern to southern Middle East, and below normal in Indonesia, northwestern China, southern Japan, and the Korean Peninsula (Fig. 7.47h).

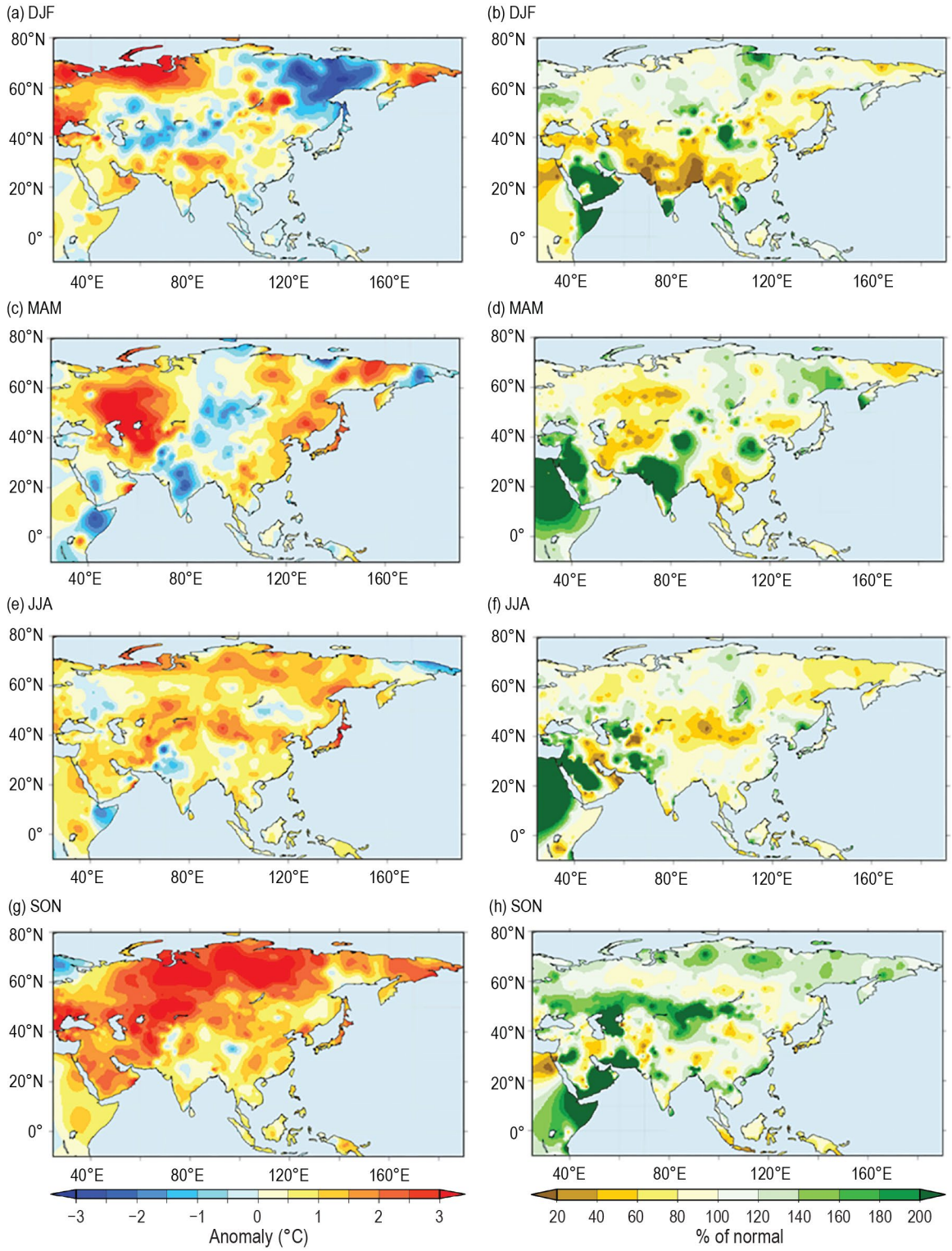

Fig. 7.47. Seasonal mean surface temperature anomalies (°C, left column) and seasonal precipitation ratios (% of normal, right column) over Asia in 2023 for (a),(b) winter, Dec–Feb (DJF); (c),(d) spring, Mar–May (MAM); (e),(f) summer, Jun–Aug (JJA); and (g),(h) autumn, Sep–Nov (SON). Anomalies and ratios are relative to 1991–2020. (Source: Japan Meteorological Agency.)

In winter, negative 500-hPa geopotential height anomalies and 850-hPa temperature anomalies were observed from Central Asia to northern East Asia, with the negative center located over eastern Siberia (Fig. 7.48a). Convective activity was enhanced near Indonesia, accompanied by 850-hPa cyclonic circulation anomalies straddling the equator from the eastern Indian Ocean to the western Pacific (Fig. 7.48b). In spring, positive 500-hPa geopotential height anomalies and 850-hPa temperature anomalies were observed over Central Asia and from the eastern part of East Asia to the midlatitude North Pacific (Fig. 7.48c). Convective activity was enhanced over India and to the east of the Philippines (Fig. 7.48d). In summer, positive 500-hPa geopotential

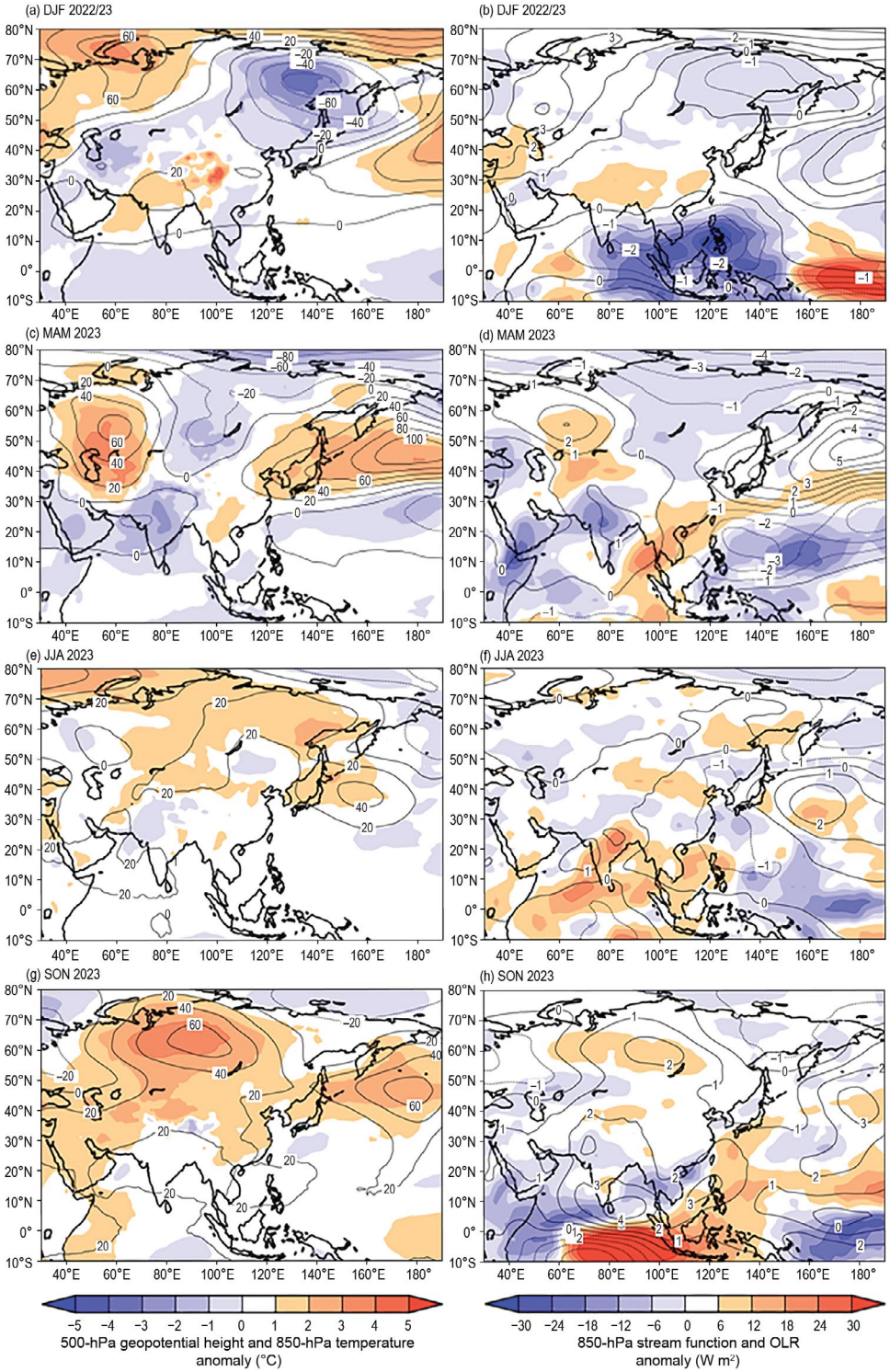

Fig. 7.48. Seasonal mean anomalies of atmospheric circulation variables in 2023 for (a),(b) winter, Dec–Feb (DJF); (c),(d) spring, Mar–May (MAM); (e),(f) summer, Jun–Aug (JJA); and (g),(h) autumn, Sep–Nov (SON). Left column: 500-hPa geopotential height (contour, gpm) and 850-hPa temperature (shading, °C). Right column: 850-hPa stream function (contour, 1 × 10^6 m^2 s^{-1}) using data from the JRA-3Q and CPC blended outgoing longwave radiation (OLR; shading, W m^{-2}) using data originally provided by NOAA. Anomalies are relative to 1991–2020. (Source: Japan Meteorological Agency.)

height anomalies accompanying positive 850-hPa temperature anomalies were observed over a wide region from Central Asia to Northeast Asia (Fig. 7.48e). Convective activity was suppressed over the northern Indian Ocean and enhanced over the tropical western and central Pacific, accompanied by 850-hPa cyclonic circulation anomalies near the Philippines (Fig. 7.48f). In autumn, positive 500-hPa geopotential height anomalies and 850-hPa temperature anomalies were dominant in the midlatitudes from Eurasia to the North Pacific, with positive geopotential height centered over the midlatitude Eurasian continent and the North Pacific Ocean (Fig. 7.48g). Convective activity was enhanced from the western Indian Ocean to South China, and suppressed from the central equatorial Indian Ocean to the Maritime Continent, accompanied by 850-hPa anticyclonic circulation anomalies straddling the equator over the Indian Ocean (Fig. 7.48h).

2. RUSSIA

—M. Yu. Bardin and N. N. Korshunova

Estimates of climate features for Russia were obtained from the hydrometeorological observations of the Roshydromet Observation Network. Anomalies are relative to the 1991–2020 base period, and national rankings and percentiles reflect the 1936–2023 period of record. Note that the temperature database was extended significantly, which in some cases changed previous ranking. The boundary between Asian Russia and European Russia is considered to be 60°E.

(i) Temperature

The year 2023 in Russia was the third warmest on record with an annual mean temperature 0.99°C above normal (Fig. 7.49a), after 2020 (+2.02°C; record warmest) and 2007 (+1.00°C; second warmest). Annual and seasonal trends are statistically significant at 1%, except for those of winter, both in Asian and European Russia. Anomalies above the 95th percentile were observed at most stations in southern European Russia, the Urals, and Western Siberia; the largest anomalies above +2°C were located around the Yenisei Bay.

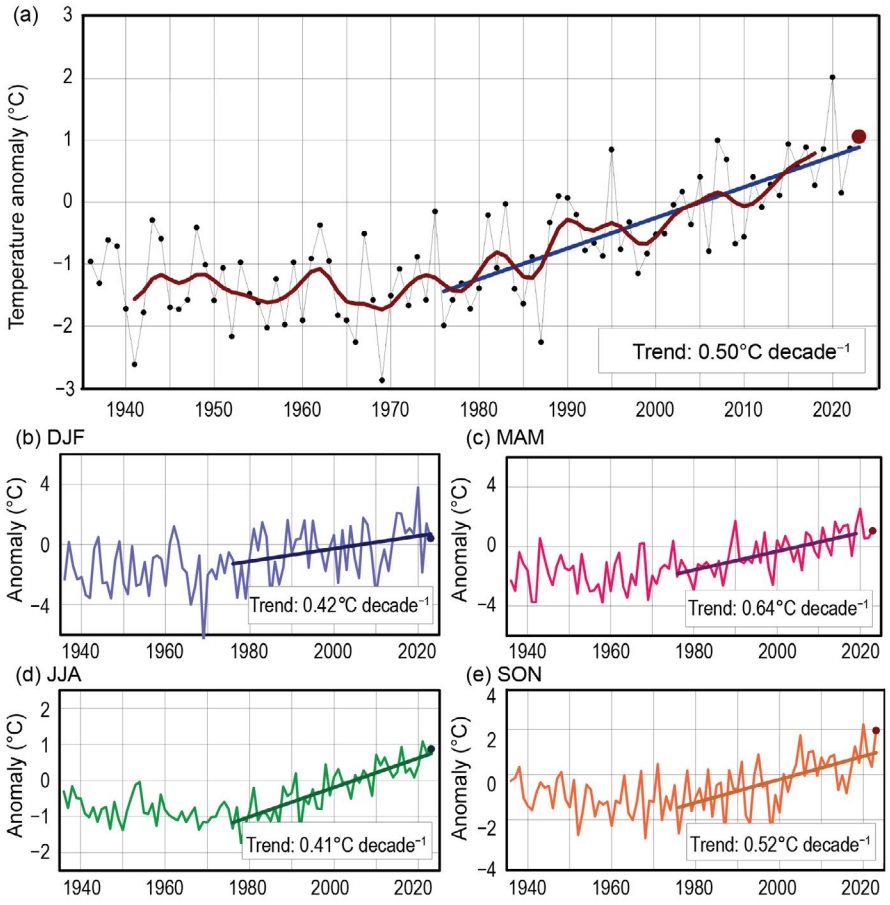

Fig. 7.49. Annual and seasonal mean temperature anomalies (°C; 1991–2020 base period) averaged over the territory of Russia for the period 1936–2023: (a) annual, (b) winter, (c) spring, (d) summer, and (e) autumn. The dark red line on the annual mean time series is an 11-point binomial filter. The linear trend (°C decade^{-1}) is calculated for the period 1976–2023.

Winter was the 23rd warmest since 1936, with a seasonal anomaly of +0.42°C (Fig. 7.49b). Negative anomalies reaching –5°C were observed across large parts of Asian Russia east of 110°E. During January, in northern Eastern Siberia and western Yakutia, an extensive cold center formed with an average monthly temperature anomaly of –8°C to –10°C (Fig. 7.50). During the second 10-day period, in the north of the Krasnoyarsk Territory, frost temperatures reached –50°C, and in Yakutia –60°C and below. At the Agata station, the second 10-day period was especially cold, as the maximum temperature was significantly lower than the normal minimum temperature. On 14 and 15 January, daily minimum air temperature records were broken. In southern Yakutia, the second 10-day period was also the coldest on record. On 15 and 18 January, the minimum air temperature dropped below –60°C, and the mean daily temperature was below the minimum normal for these days.

Spring was 1.06°C above normal, ranking 13th warmest on record (Fig. 7.49c). The European Russia spring temperature was the fourth highest, at 1.91°C above normal; all stations in southeast European Russia observed temperatures that exceeded the 95th percentile.

Summer was third warmest on record for Russia as a whole (0.87°C above normal; Fig. 7.49d), with Asian Russia record warm (1.03°C above normal). July and August were both record warm in this region, at 1.08°C and 1.40°C above normal, respectively.

Autumn was the second warmest on record, at 1.96°C above normal, following +2.24°C in 2020 (Fig. 7.49e). Asian Russia had its second warmest autumn on record (2.10°C above normal),

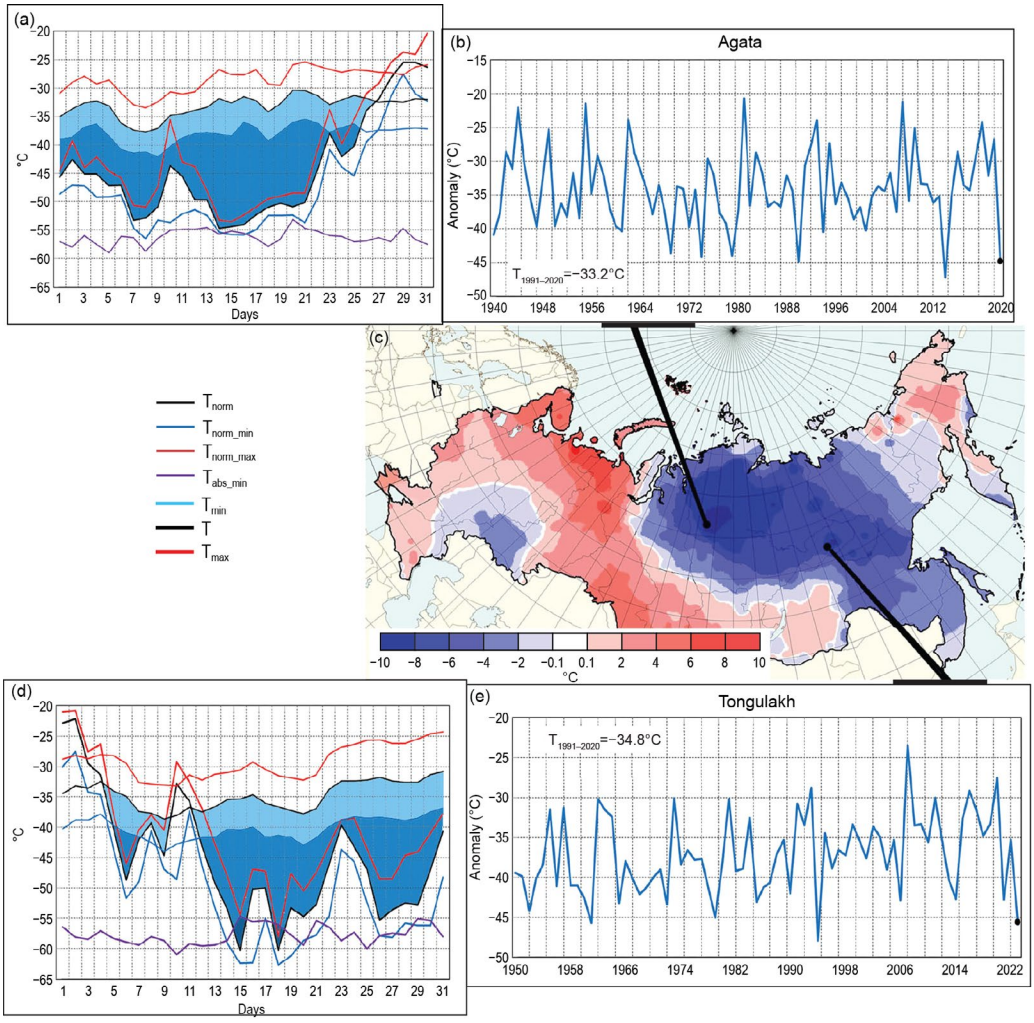

Fig. 7.50. Map of temperature anomalies across Russia (shading) in Jan 2023. Insets are of mean monthly temperature (°C) time series in Agata for the period 1940–2023 and Tongulakh for the period 1950–2023, and mean, minimum, and maximum daily temperatures (°C) in Jan 2023 at these stations. T1991-2020 on plots of monthly temperatures is the 1991–2020 mean. Plots of daily temperature show observed daily mean (T, black line), daily minimum (Tmin, blue line), and daily maximum (Tmax, red line) temperatures along with their climatological values (three uppermost curves: Tnorm, black; Tnorm_min, blue; Tnorm_max, red) and absolute minimum temperature (Tabs_min, violet). The area between the normal daily mean curve, Tnorm, and the observed daily mean curve is shaded light blue where T < Tnorm, and is shaded deep blue if T was below the normal daily minimum Tnorm_min.

and European Russia had its fourth (1.56°C above normal). September was record warm in European Russia (2.63°C above normal). October was second warmest in Asian Russia (2.81°C above normal) with temperatures above the 95th percentile at most stations between 80°E and 140°E. In European Russia, the temperature was near normal, with negative anomalies in the northwest.

(ii) Precipitation

Across Russia as a whole, the 2023 average precipitation total equaled the third highest on record, at about 106% of normal (Fig. 7.51). European Russia had 111% of normal precipitation, its fourth highest, while Asian Russia had 103% of its normal precipitation. Autumn was record wet (117% of normal) across Russia and was the second wettest for both European and Asian Russia (125% and 112%, respectively). Winter and spring were moderately wet (105% for both seasons), while summer was moderately dry (97%). Record precipitation fell in March over almost all of Russia (140% of normal), notably in Yakutia where four times the monthly normal was observed in Yakutsk. This anomalous precipitation was due in part to a vast persistent depression over the Arctic basin near the coast of Eurasia that occasionally expanded southward as far as Baikal.

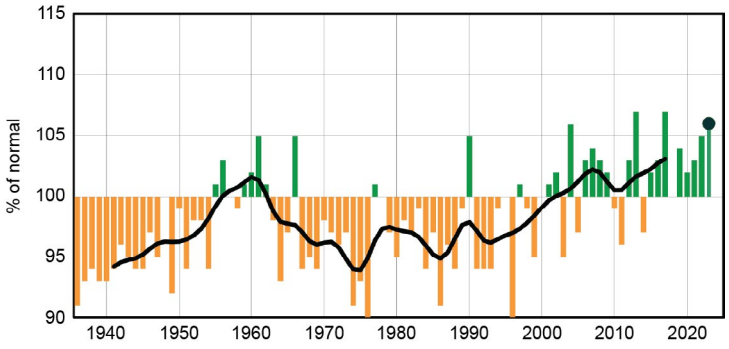

Fig. 7.51. Annual precipitation (% of normal; 1991–2020 base period) averaged over the Russian territory for the period 1936–2023. The smoothed time series (11-point binomial filter) is shown by the black line.

Precipitation in Russia has increased during the period of warming since the mid-1970s by about 1.8% per decade, mainly in spring when the rate is about 6% per decade. However, there is a vast area of decreasing precipitation in southern European Russia; the high rate of warming and increase in heatwave occurrence and duration together enhance the risk of drought in this principal grain-producing region (Fig. 7.49).

(iii) Notable events and impacts

During 6–8 February, strong northeast winds of up to 37 m s^{-1} raged in Novorossiysk and Gelendzhik. Building rooftops were damaged, shopping pavilions, fences, and bus stops were overturned, and trees, road signs, and lamp posts were toppled.

On 11–12 July, heavy rain fell in the Tuapse region of the Krasnodar Territory: Defanovka, 282.2 mm; Tuapse, 51mm; Dzhugba, 57.2 mm. In 13 settlements, 650 household plots and 39 apartment buildings were flooded, four pedestrian bridges and one road bridge were damaged, and power and water supplies were disrupted at several children's health camps. One fatality was reported, along with four missing persons.

On 10–11 August, 94 mm–190 mm of rain fell in the Primorsky Territory, which caused rivers to rise by 1 m–3.9 m (up to 5 m–8 m for the Spasovka and Razdolnaya Rivers). States of emergency were introduced in 14 municipalities. Bridges and sections of roads were destroyed, about 600 residential buildings, 1400 houses, and multi-story buildings in Ussuriysk were flooded, and dozens of settlements were cut off. More than 2000 residents were evacuated, and three fatalities were reported.

On 6 September, heavy thunderstorms accompanied by high winds of up to 32 m s^{-1} and hail with diameters between 20 mm and 23 mm impacted the Chechen Republic. More than 30 roofs were torn off or damaged, a road tunnel and nine houses were flooded, trees were knocked down, cars and power lines were damaged, and a tower crane was toppled. One fatality was reported.

On 19 November, in the Novosibirsk, Tomsk, and Kemerovo regions and the Altai Territory, a blizzard with wind speeds of up to 26 m s^{-1} (up to 37 m s^{-1} in the Altai Territory) caused significant damage to infrastructure. Four fatalities and 22 injuries were reported.

On 26 November, hurricane-force winds of up to 40 m s^{-1} were observed in the Republic of Crimea. Electricity was cut off in 273 settlements, roofs were damaged, 195 houses in the Saki district and Yevpatoria were flooded, and more than 300 people were evacuated. Seven people were injured, and one fatality was reported.

3. EAST AND SOUTHEAST ASIA

—P. Zhang, T. C. Lee, R. Muharsyah, A. Moise, K. Takemura, K. Takahashi, J. I. Seong, D. Dulamsuren, M.-V. Khiem, and H.-P. Lam

Countries considered in this section include China, Hong Kong (China), Indonesia, Japan, Republic of Korea (ROK, South Korea), Mongolia, and Vietnam. Unless otherwise noted, anomalies refer to the 1991–2020 base period.

(i) Temperature

Annual mean temperatures for 2023 across East and Southeast Asia are shown in Fig. 7.45. In 2023, the annual mean air temperature for China was 0.82°C above normal, the highest since the start of the record in 1951. In Hong Kong, 2023 was the second-warmest year since records began in 1884 with an annual mean temperature of 24.5°C, which was 1.0°C above normal.

In Japan, annual mean temperatures were above normal nationwide and significantly above normal in northern and eastern Japan. The regional average of annual mean temperature anomalies was the highest on record since 1946 in northern and eastern Japan, and tied with 1998 as the highest on record in western Japan.

The annual mean temperature for ROK was 13.7°C, 1.2°C above normal, the highest on record since 1973. March and September were 3.3°C and 2.1°C above normal, respectively, significantly contributing to the high annual mean temperature.

The annual mean temperature for Mongolia was 1.3°C above normal, its seventh-warmest year since 1940. October was record warm, with average temperatures 3.8°C above normal, and March was fourth warmest, at 3.5°C above normal.

The average temperature for Indonesia in 2023 was 27.2°C, which was 0.5°C above normal, marking the country's second-warmest year on record since 1981.

Singapore reported its fourth-warmest year, with an annual mean temperature of 28.2°C, which was 0.4°C above the long-term average. Most of the high heat stress days occurred in April, May, June, and October.

The observed annual mean temperature of Vietnam in 2023 was 1.09°C above normal. This marks the second-warmest year on record after 2019 (1.21°C above normal).

(ii) Precipitation

Annual precipitation for 2023 as a percentage of normal over East and Southeast Asia is shown in Fig.7.46. The annual mean precipitation total for China was 615.0 mm, which was 96.1% of normal and the second-lowest total of the past decade. The Meiyu over the Yangtze River basin started and ended later than normal and was six days longer than normal overall, with 364.6 mm of rainfall (14.6% above normal). The total rainfall for Hong Kong (China) in 2023 was 2774.5 mm, which was about 14% above normal.

In Japan, annual precipitation amounts were above normal on the Sea-of-Japan side of northern Japan and below normal on the Pacific side of northern and eastern Japan and in Okinawa and the Amami islands.

The annual precipitation for ROK reached 1746.0 mm, which was 131.8% of its normal of 1331.7 mm, marking the third-highest amount on record. May, July, and December experienced heavy precipitation, amounting to 188% (third wettest), 172.6% (second wettest), and 382.1% (wettest) of their respective normals.

For Indonesia, 2023 was the 10th-driest year since 1991, at 95% of normal. About 51% of the country, particularly the southern part, experienced below-normal rainfall (less than 85% of normal). The lowest rainfall total was recorded at Situbondo district, East Java, with annual rainfall of only 871 mm (67% of its normal).

Singapore's annual total rainfall averaged across the island-wide stations (2866.1 mm) was 13.1% above its long-term average of 2534.3 mm, making 2023 Singapore's seventh-wettest year since 1980. Although 2023 was generally wet, April, May, August, and October were drier than normal.

Average total annual rainfall in 2023 for Vietnam was 10%–20% below normal. However, Da Nang and Thua Thien Hue received annual rainfall 50%–60% above their normals due to a heavy rain event.

(iii) Notable events and impacts

In summer 2023, there were extreme dry and wet events that occurred in North China. From 1 June to 28 July, precipitation was 50% to 80% below normal in south-central North China and the northern Hebei province. The dryness was combined with high temperatures in the same areas. On 20 July, the area of meteorological drought above the moderate level reached its maximum area of 189,000 km^2. From 29 July to 1 August, the Beijing-Tianjin-Hebei region experienced a historically rare torrential rainfall induced by Typhoon Doksuri, with maximum rainfall of 1003 mm measured at Lincheng County in Xingtai, Hebei province.

A major and prolonged heatwave affected much of north Vietnam in May; an all-time national maximum temperature record of 44.2°C was observed at Tuong Duong on 7 May, surpassing the previous historical value of 43.4°C at Huong Khe on 20 April 2019. Heavy rain fell during 8–18 October in central Vietnam, from Nghe An to the Quang Ngai region, with total rainfall ranging from 300 mm to 600 mm; Thua Thien Hue and Da Nang received 1194 mm and 1442 mm, respectively. On 13 October, the daily rainfall in Da Nang was 409 mm, which exceeded its previous record of October rainfall (396 mm in October 2022).

Autumn precipitation was significantly below normal on the Pacific side of eastern and western Japan and in Okinawa and the Amami islands. The regional seasonal precipitation was the lowest on record for autumn since 1946 on the Pacific side of western Japan.

In the middle of the Changma season (13–18 July), a stationary front moved up and down the southern part of ROK for an extended period, dropping more than 500 mm of rain over six days. Throughout the season, approximately $560 million (U.S. dollars) in property damage was recorded and about 50 people were killed due to the intense rains.

The northern part of Lombok, West Nusa Tenggara, in Indonesia had 222 dry spell days in 2023, which was the longest dry spell on record. The drought triggered a clean water crisis for more than 13,000 people in the region.

Tropical Cyclone Koinu skirted to the south of Hong Kong (China) and brought heavy rain to the territory on 8–9 October. Rainfall on 9 October reached 369.7 mm, the highest daily rainfall on record for October.

The only typhoon that affected ROK in 2023 was Khanun. After the typhoon made landfall on the Korean Peninsula, it crossed ROK almost in a straight line from south to north. Heavy rain and strong winds resulted in $42 million (U.S. dollars) in property damage and the displacement of 15,000 people.

4. SOUTH ASIA

—O. P. Sreejith, A. K. Srivastava, and C. T. Sabeerali

Countries in this section include Bangladesh, India, Pakistan, and Sri Lanka.

(i) Temperature

In 2023, South Asia generally experienced above-normal temperatures. The annual mean land surface air temperature averaged over India was 0.65°C above the 1981–2010 average, making it the second-warmest year on record since nation-wide records commenced in 1901 (Fig. 7.52). The country-averaged seasonal mean temperatures were above normal for all seasons except the pre-monsoon season. The mean temperature anomaly was +0.83°C for winter (January–February), +0.74°C for the monsoon season (June–September), and +1.00°C for the post-monsoon season (October–December). Overall, the five warmest years on record in order are: 2016 (anomaly of +0.71°C), 2023 (+0.65°C), 2009 (+0.55°C), 2017 (+0.54°C), and 2010 (+0.54°C).

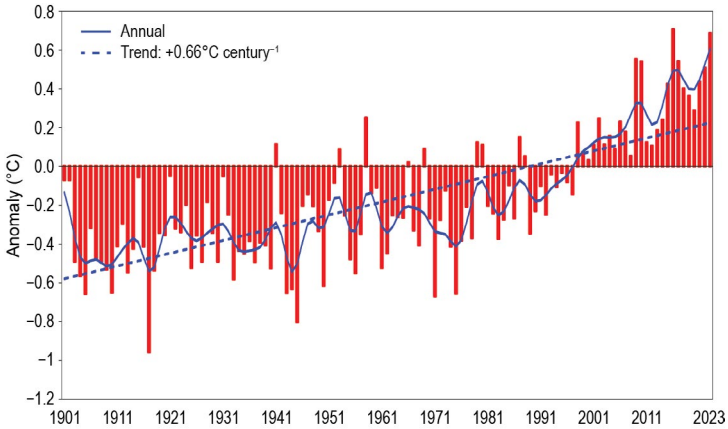

Fig. 7.52. Annual mean temperature anomalies (°C; 1981–2010 base period) averaged over India for the period 1901–2023. The smoothed time series (nine-point binomial filter) is shown as a continuous blue line, and the trend is shown by the dashed blue line.

(ii) Precipitation

The summer monsoon season (June–September) contributes about 75% of the annual precipitation over South Asia. The 2023 summer monsoon set in over Kerala (southwestern parts of peninsular India) on 8 June (the normal date is 1 June). The monsoon covered the entire country on 2 July, six days ahead of its normal date (8 July).

For India, the long-term average (LTA) value of the summer monsoon rainfall, calculated using data from 1971 to 2020, is 869 mm with a standard deviation of about ±10%. However, over smaller regions, the standard deviation is much larger (around ±19%). During 2023, the summer monsoon seasonal rainfall averaged over India was 95% of its LTA. Rainfall was fairly well distributed over the country, except over parts of the east and northeast (Fig. 7.53a). Seasonal rainfall over the homogeneous regions of northwest India, central India, South Peninsula, and east and northeast India was 101%, 100%, 92%, and 81% of their LTAs, respectively (Figs. 7.53b,c). On a monthly scale, rainfall for the country as a whole was above normal during July and September (both 113% of LTA) and below normal during June and August (91% and 64% of LTA, respectively). For August, country-wide rainfall was 162.7 mm, the lowest on record since 1901. Over the core monsoon region, the southwest monsoon was active on some days in June, July, and September, while it was significantly subdued on most days in August (Fig. 7.54).

During the winter season (January–February), rainfall over India was below normal (55% of its LTA). It was above normal (113%) during the pre-monsoon season (March–May) and below normal again (91%) during the post-monsoon season (October–December).

Pakistan, which is at the western edge of the pluvial region of the South Asian monsoon, receives 60% to 70% of its annual rainfall during the summer monsoon season (July–September). The summer monsoon sets in over eastern parts of Pakistan around 1 July with a standard deviation of five days. During 2023, the monsoon set in on 3 July. Monsoon rainfall over Pakistan was normal (104% of the LTA); however, there was large seasonal variability as July had significantly

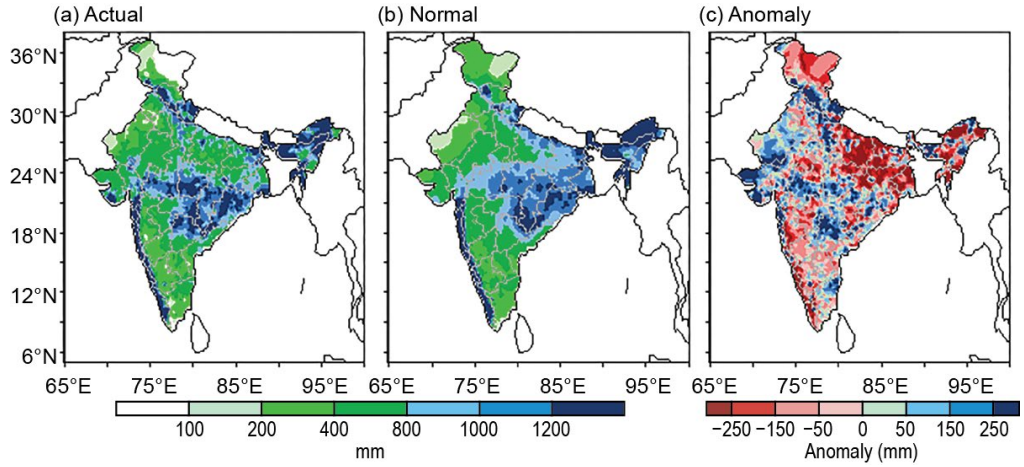

Fig. 7.53. Spatial distribution of monsoon seasonal (Jun–Sep): (a) actual, (b) normal (1971–2020 average), and (c) anomalous rainfall (mm) over India in 2023.

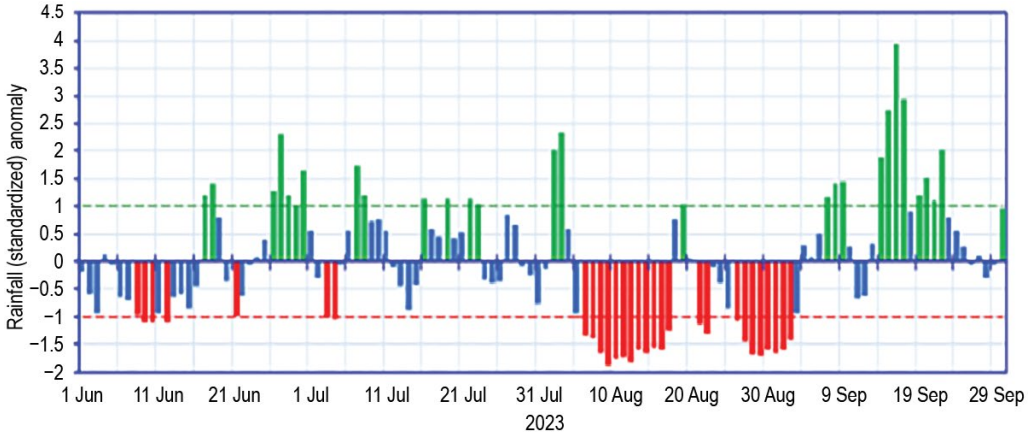

Fig. 7.54. Daily standardized rainfall anomaly time series averaged over the core monsoon zone of India for the period 1 Jun–30 Sep 2023.

above-normal (170% of the LTA) rainfall, followed by below-normal rainfall in August (34%) and near-normal rainfall in September (93%).

Bangladesh received normal rainfall during its summer monsoon season in 2023, while Sri Lanka received above-normal rainfall during its summer monsoon season (May–September).

The northeast monsoon (NEM) sets in over southern peninsular India during October and over Sri Lanka in late November. The NEM contributes 30%–50% of the annual rainfall over southern peninsular India and Sri Lanka as a whole. In 2023, the NEM set in over southern peninsular India on 21 October, and the seasonal rainfall was near normal (94%). However, many stations reported extremely heavy rain on 18 December, resulting in floods in the Thoothukudi and Tirunelveli districts of Tamil Nadu. Several stations reported more than 500 mm of precipitation: Kayalpattinam (946 mm); Tiruchendur (689 mm); Srivaikuntam (621 mm); and Kovilpatti (525 mm). Sri Lanka received above-normal rain totals during the NEM.

(iii) Notable events and impacts

Extremely Severe Cyclonic Storm Mocha, which developed in May during the pre-monsoon season, was one of the most intense cyclones ever formed over the Bay of Bengal, reaching peak 10-minute sustained winds of 115 kt (59 m s^{-1}). The storm formed on 11 May and intensified as it moved north, reaching its peak intensity early on 14 May before making landfall near the Bangladesh-Myanmar border (Fig. 7.55). There were at least five fatalities, and thousands of people were forced to seek shelter.

In recent years in India, thunderstorms accompanied by lightning strikes have been among the most common cause of fatalities. In 2023, thunderstorms and lightning claimed around 1280 lives across the country. On 4 July, approximately 43 people died due to lightning strikes associated with a severe thunderstorm that occurred in parts of Bihar, Jharkhand, Uttar Pradesh, and Madhya Pradesh.

Heavy rainfall and flood-related incidents claimed around 880 lives in different parts of India in 2023. Among these, more than 130 lives were lost in Madhya Pradesh, more than 120 in Himachal Pradesh, and more than 100 in Sikkim (mainly due to cloudburst and flooding in the Teesta basin due to a glacial lake outburst flood on 4 October). Additionally, 81 lives were lost in Uttar Pradesh, along with 75 in Uttarakhand, 71 in Maharashtra, and 56 in Rajasthan, with the remaining fatalities occurring in other states of India. A massive landslide, associated with heavy

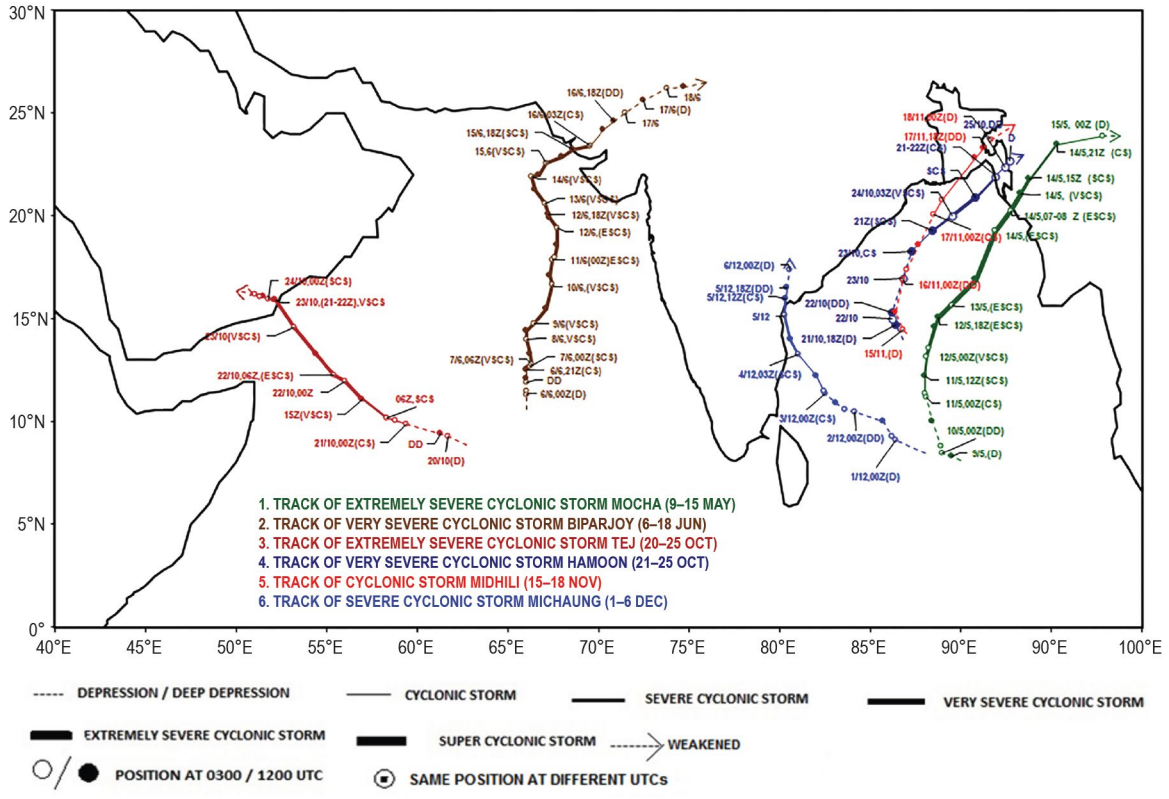

Fig. 7.55. Cyclonic storm tracks during 2023 over the North Indian Ocean.

rainfall, occurred on 19 July in the Raigad district of Maharashtra state, India, claiming 84 lives. On 14 August, a landslide in the Shimla district of Himachal Pradesh resulted in 25 fatalities.

A heatwave in June 2023 claimed more than 160 lives in various parts of India. While June is normally hot for the region, the heatwave had driven temperatures as high as 43.3°C. More than 85 lives were lost in the adversely affected state of Uttar Pradesh, along with 45 in Odisha, 25 in Jharkhand, and the remaining in Maharashtra and Chhattisgarh.

Extremely Severe Cyclonic Storm Biparjoy formed over the northeast Arabian Sea in the monsoon season during 6–19 June. Seven fatalities were reported in Rajasthan. The Bhavnagar, Banaskantha, Devbhoomi Dwarka, Gandhinagar, Jamnagar, Junagadh, and Kutch districts of Gujrat were also affected.

Severe Cyclonic Storm Michaung (1–6 December) formed in the post-monsoon season over the Bay of Bengal and crossed the south Andhra Pradesh coast close to Bapatla on 5 December as a severe cyclonic storm, claiming 24 lives in Tamil Nadu, Andhra Pradesh, and Telangana. The Malkangiri district of Odisha was also affected.

Bangladesh received very heavy rain during 5–10 August that affected 2.4 million people in four districts: Chittagong, Bandarban, Ragamati, and Cox's Bazar.

5. SOUTHWEST ASIA

—A. Vazife, A. F. Kazemi, and M. Mohammadi

This section covers the Middle East region including Iran. Unless otherwise noted, anomalies refer to the 1991–2020 base period.

(i) Temperature

Generally, 2023 was dry and warm in Iran. The data presented in Fig. 7.56 illustrate the mean surface temperature anomalies for winter, spring, summer, and autumn 2023. During winter (Fig. 7.56a), temperatures were either normal or slightly below normal in most of Iran, but notably

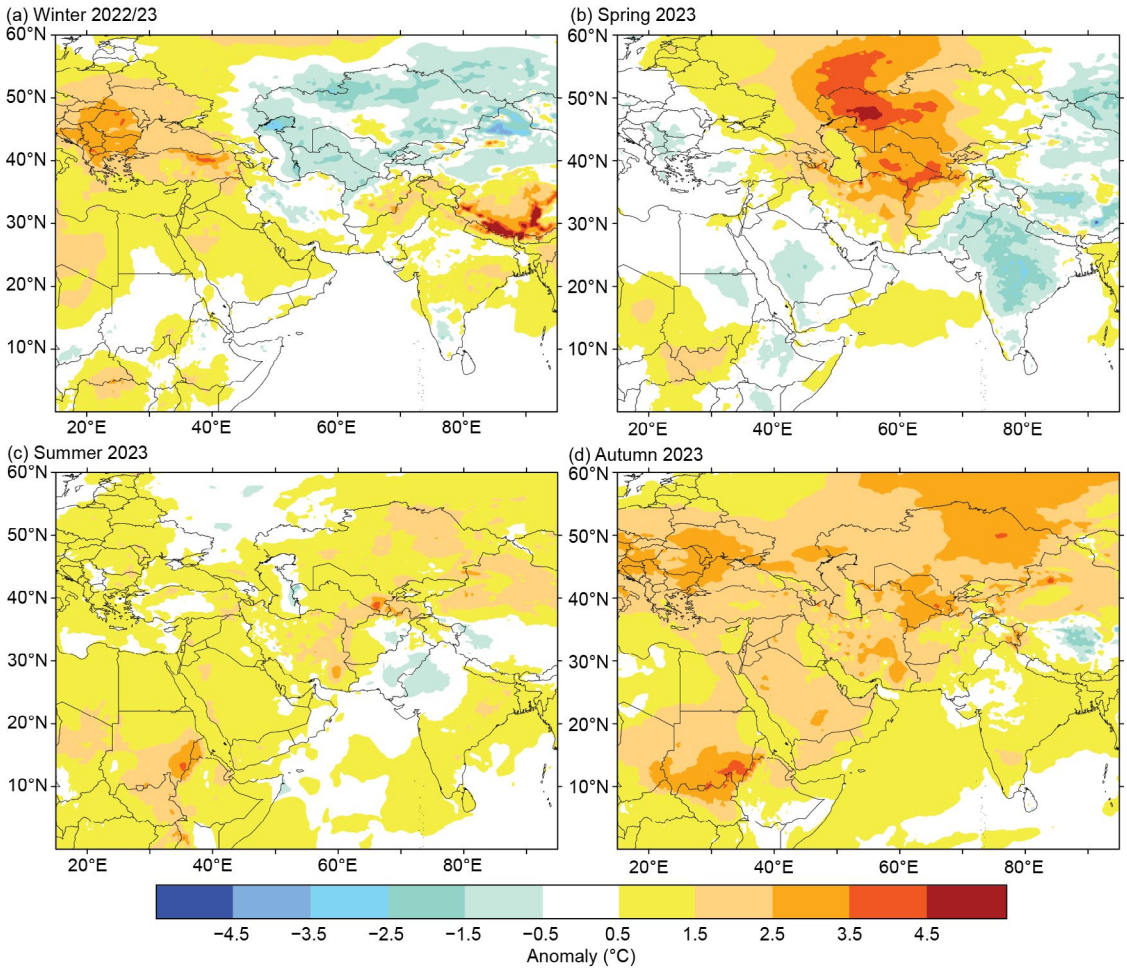

Fig. 7.56. The seasonal mean 2-m temperature anomaly (°C) in (a) winter 2022/23, (b) spring 2023, (c) summer 2023, and (d) autumn 2023.

above normal in the south. All other seasons experienced significant warmth, with spring and autumn temperatures (Figs. 7.56b,d, respectively) notably higher than usual. November 2023 was the warmest on record for the country in the past 70 years. The seasonal temperature anomalies, as depicted on the map, ranged from +0.5°C to +4.5°C.

(ii) Precipitation

Precipitation during the main rainy seasons (winter, spring, and autumn) was below normal, and severe rain deficits were observed in central, north-northwest, and northeast and east Iran.

The December 2022–February 2023 period was drier than normal in Iran. Southwest Iran received above-normal precipitation only during January. Other regions faced their third consecutive year with below-normal rain during the winter period.

Figure 7.57a shows that most of southwest Asia was drier than normal during winter, as was northern to eastern Iran and the Caspian Sea region. Moderate to severe drought occurred in vast regions of southwest Asia, including the Caspian Sea and the north and eastern half of Iran.

Spring 2023 was drier than normal (Fig. 7.57b). Eastern Saudi Arabia, eastern Iraq, and southwest Iran received above-normal rain, while vast areas of central to eastern Iran and the Caspian Sea region received normal to severely-below-normal rain during the season.

The summer season in southwest Asia typically experiences minimal rainfall; occasional thunderstorms originating from easterly monsoonal currents are the primary source of moisture. Pakistan and at times southeastern Iran also benefit from monsoonal rains through afternoon thunderstorm activity. However, there was weaker monsoonal and thunderstorm activity in summer 2023 compared to previous years, as depicted in Fig. 7.57c. This contrasts sharply with the humid conditions and above-normal monsoon activity observed in 2022, which led to significant flash floods in Iran. Autumn 2023 were also drier than normal for many parts of Iran (Fig. 7.57d).

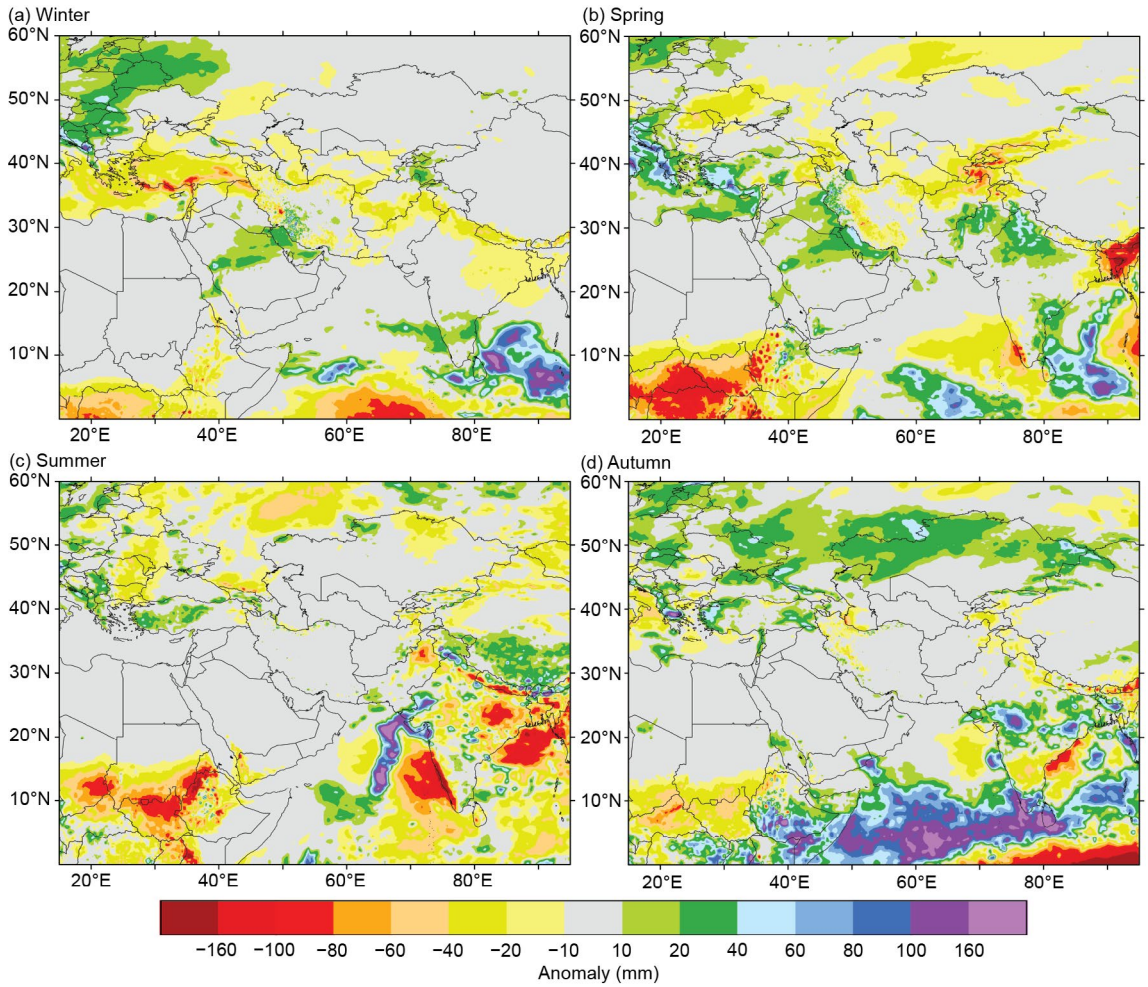

Fig. 7.57. The seasonal mean precipitation anomaly (mm) in (a) winter 2022/23, (b) spring 2023, (c) summer 2023, and (d) autumn 2023.

(iii) Notable events and impacts

The most pressing weather hazard in Iran in 2023 was persistent drought that resulted in substantial financial losses for the agricultural sector and produced severe hydrological challenges. Lake beds dried up, notably in the northwestern and eastern regions of the country. Lake Urmia in northwestern Iran nearly completely dried up, while Lake Hamoon in the east has been completely dry since 2021. The dried lake beds have become a significant source of rising dust during late spring and summer wind storms, leading to adverse health effects on the local population.

Most of Iran and the Caspian Sea region were affected by severe drought in the spring following the dry winter. Spring holds immense importance for agriculture in this region as it marks the primary growing season, with rainfall playing a pivotal role in supporting rain-fed agriculture. The dry spell that persisted through winter had a detrimental impact on crop yields, particularly affecting staple grains such as wheat, barley, and other essential rain-fed agricultural produce in the area. Summer 2023 also had below-average precipitation in most parts of southwest Asia, including Iran. The persistent dry conditions over the past three years have intensified water stress levels across many countries in the region.

6. CENTRAL ASIA

—R. Shukla and W. M. Thiaw

This section covers the Central Asia (CA) region, including the countries of Afghanistan to the south, Turkmenistan, Uzbekistan, Tajikistan, Kyrgyzstan (from west to east) in the central part of the region, and Kazakhstan to the north. Unless otherwise specified, the climatological base period is 1991–2020.

(i) Temperature

During 2023, annual mean temperatures featured a strong meridional gradient near 50°N, with temperatures ranging between 0°C and 5°C in the northern and eastern Kazakhstan regions, between 10°C and 20°C in southern and southwestern Kazakhstan, Uzbekistan, Turkmenistan, and northern, western, southern, and southeastern Afghanistan, and between 20°C and 25°C farther south in Afghanistan (Fig. 7.58a). Annual mean temperatures were lowest at around –10°C–0°C in eastern Tajikistan, southeastern Kyrgyzstan, and some parts of eastern Kazakhstan and the northeastern high-elevation region of Afghanistan (Fig. 7.58a). The magnitude of annual mean temperatures was higher (lower) than normal in many parts of Kazakhstan and western and central parts of Uzbekistan and Turkmenistan (northern and eastern Kyrgyzstan, Tajikistan,

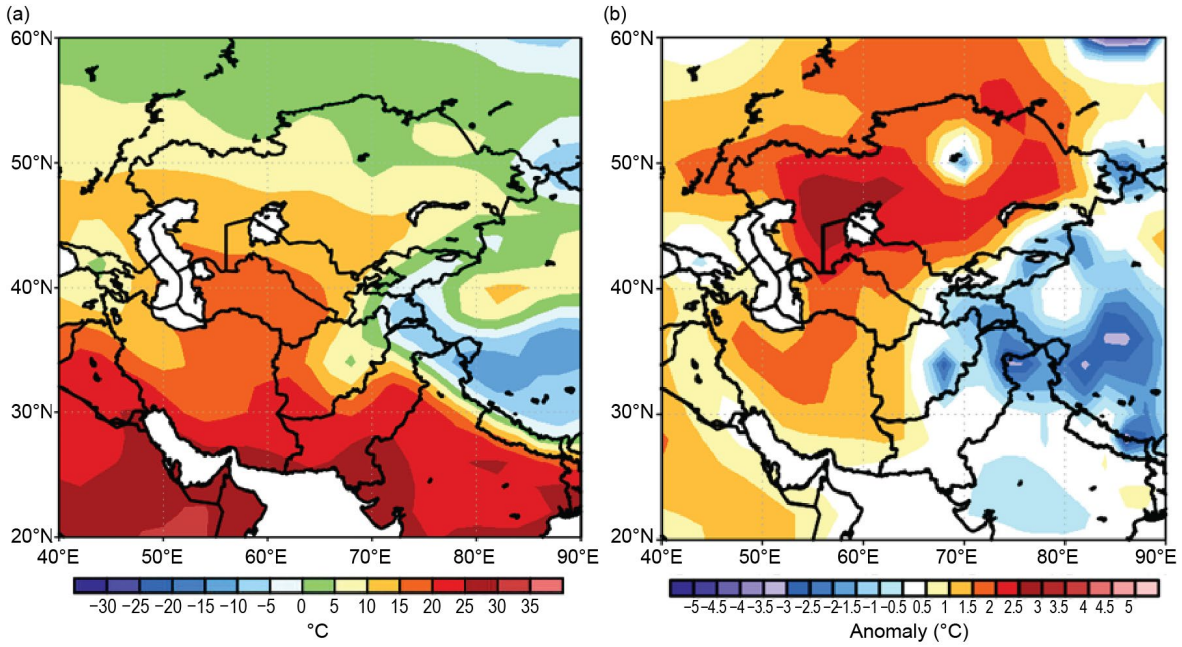

Fig. 7.58. Annual (a) mean temperature (°C) and (b) mean temperature anomalies of 2023 (°C, 1991–2020 base period) for Central Asia. (Source: NOAA National Centers for Environmental Prediction.)

and northeastern and eastern Afghanistan). Annual mean temperature anomalies were +0.5°C to +3.0°C in many parts of western, southern, central, northern, and northeastern Kazakhstan, western and central Uzbekistan, Turkmenistan, and the western and southern Afghanistan regions (Fig. 7.58b), placing 2023 in the 90th to 97th percentiles of warmest years on record in many places. The highest temperature anomalies were around +2.5°C to +3.0°C in Aktobe province in western Kazakhstan and some parts of northwestern Uzbekistan. By contrast, annual mean temperature anomalies were around –2.0°C to –0.5°C in northern, central, and eastern Kyrgyzstan, Tajikistan, northeastern, eastern, and southeastern Afghanistan, and some parts of east Kazakhstan and the country's Almaty region (Fig. 7.58b), placing 2023 in the 3rd to 10th percentiles of coldest years on record in eastern Kazakhstan.

(ii) Precipitation

Annual total precipitation for 2023 depicted a large variation across the Central Asia regions (Fig. 7.59a). The lowest precipitation totals, around 50 mm–200 mm, were received in western and southern Afghanistan, Turkmenistan, and central Uzbekistan in 2023. About 200 mm–500 mm of precipitation were received across southwestern, southern, central, and southeastern Kazakhstan, as well as Kyrgyzstan, Tajikistan, eastern and northwestern Uzbekistan, and northeastern, northern, central, southeastern, and eastern Afghanistan. Larger precipitation totals of around 500 mm–700 mm were observed in northwestern, northern, and eastern Kazakhstan (Fig. 7.59a). Seasonally, large precipitation deficits (–100 mm to –20 mm, not shown) were observed across Afghanistan, central and eastern regions of Turkmenistan, and Uzbekistan during the January–March and March–May (MAM) periods, as well as across Tajikistan and Kyrgyzstan during MAM and April–June (AMJ). The seasonal total precipitation was 20 mm–100 mm below average (lowest 3rd to 10th percentiles of driest years) across the northern, eastern, and southeastern regions of Kazakhstan during AMJ and May–July. The seasonal total precipitation was 20 mm–150 mm above average (highest 90th to 97th percentiles of wettest years) across the western, northern, central, and eastern regions of Kazakhstan during the August–October and October–December periods.

Most regions in Central Asia received maximum precipitation (rain and snowfall) during winter and spring, while northern and eastern regions of Kazakhstan received precipitation throughout the year. The annual precipitation totals were 25 mm–200 mm below normal (lowest 3rd–10th percentiles of driest years) in many parts of Afghanistan, southwestern, central,

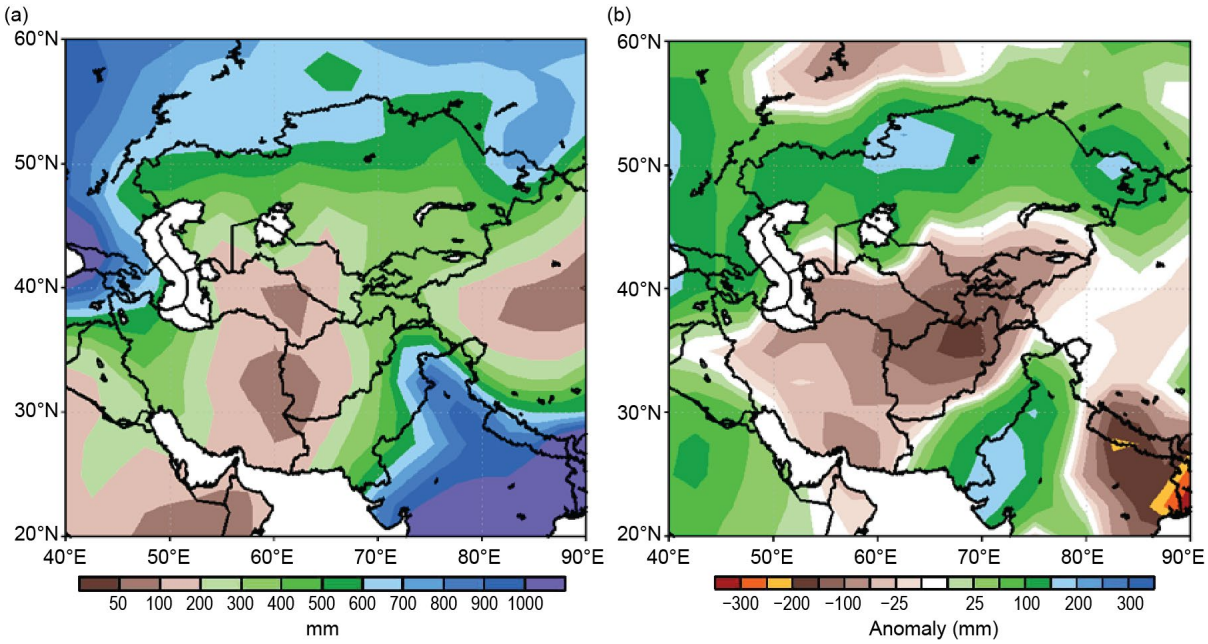

Fig. 7.59. Cumulative annual (a) precipitation (mm) and (b) precipitation anomalies (mm; 1991–2020 base period) of 2023 for Central Asia. (Source: NOAA National Centers for Environmental Prediction GPCP data.)

northern, and eastern Turkmenistan, central and eastern Uzbekistan, Kyrgyzstan, Tajikistan, and some parts of southern and southeastern Kazakhstan (Fig. 7.59b). Precipitation was below average by about 150 mm–200 mm in some parts of northern and central Afghanistan this year. By contrast, the annual total precipitation was 25 mm–200 mm above normal in many parts of western, northern, central, and eastern Kazakhstan and northwestern Uzbekistan (highest 90th–97th percentiles of wettest years in the northwestern, northern, and eastern Kazakhstan regions). About 150 mm–200 mm of above-average precipitation was observed in the Kostanay and Akmola provinces in northern Kazakhstan and some parts of the eastern Kazakhstan regions in 2023 (Fig. 7.59b).

(iii) Notable events and impacts

According to Afghanistan's minister of Disaster Management, at the start of 2023, the country experienced one of its coldest Januarys on record due to a disrupted polar vortex. Temperatures during the month reached –28°C and resulted in 162 fatalities. Based on the NOAA Climate Prediction Center Unified Gauge minimum temperature records, extreme minimum temperatures of around –35°C to –20°C were observed in many parts of Afghanistan during 9–15 January. At the end of the year, extreme minimum temperatures during 10–13 December were around –35°C to –25°C across the Zhambyl region of Kazakhstan. The state news agency Kazinform reported that the cold temperatures damaged gas pipelines in the Zhambyl region, leaving at least 1200 homes without fuel.

According to the Taliban official for Natural Disasters Management, around 10 mm–50 mm of rain fell during 20–26 March, causing flooding in 23 provinces of Afghanistan and resulting in nine fatalities, 74 injuries, and 1778 destroyed houses. According to reports from various sources including the Afghan Red Crescent Society and the Afghan National Disaster Management Authority, around 10 mm–75 mm of rain in eastern, central, southeastern, and southern Afghanistan during 21–31 July led to flash flooding and affected 6193 people across eight provinces (Kabul, Kunar, Laghman, Maidan Wardak, Nangarhar, Nuristan, Parwan, and Zabul). According to the United Nations Office for the Coordination of Humanitarian Affairs, 61 people lost their lives, 30 others were injured, 1360 houses were damaged or destroyed, and ~13,000 hectares of agricultural land were destroyed. According to Tajikistan's emergency authorities, around 10 mm–50 mm of precipitation during 26–28 August in western and eastern Tajikistan caused severe flooding and landslides across wide areas and resulted in 13 fatalities.

Sidebar 7.4: **Record-breaking high temperatures over North China in October 2023**

—Z. ZHU, H. HUANG, K. TAKAHASHI, AND K. TAKEMURA

During October 2023, extreme high temperatures swept through northeast Asia. Northern China was affected in a wide range of areas and set a record for its hottest October since the start of the record in 1961. Winter started more than five days late across most regions, with Shenyang marking its latest start to winter on record and Beijing marking its latest in the last decade.

The high daily maximum temperature (Tmax) anomalies in October were widespread, extending from Siberia to North China (32.5°N–54°N, 107°E–135°E), where the average temperature was 3°C higher than the 1991–2020 normal, with a northwest to southeast decline pattern (Fig. SB7.7a). The above-normal temperatures averaged over North China lasted 26 days, with a maximum anomaly of +8°C on 25 October (Fig. SB7.7b). A total of 14 extreme high-temperature days (defined as those in which daily maximum temperatures exceeded the 90th percentile) were recorded during mid- to late October. The normalized October Tmax averaged over North China (referred to as NCT hereafter) in 2023 exceeded 2.5 standard deviations, the highest since the start of the record there in 1979 (Fig. SB7.7c) and well above the second highest in 1990.

The extreme high temperatures in North China were related to a local anomalous barotropic anticyclone (i.e., heat dome). The deep high-pressure system tilted westward with height, and the center of the high-pressure anomaly at 200 hPa was

located over Lake Baikal (Fig. SB7.7d) and extended eastward to southeastern Mongolia at 500 hPa and to northeastern China at 850 hPa (Figs. SB7.7e,f). Under upper- and lower-level anomalous anticyclones, persistent descent motions and strong solar radiation from clear skies caused the high surface temperatures in North China.

The heat dome above North China was one lobe of the Rossby wave train over the Eurasian continent. As indicated by the 200-hPa wave activity flux (Fig. SB7.8a), significant wave energy propagated downstream from the North Atlantic to northeast Asia, leading to the large-scale anomalous high pressure over and around Lake Baikal. Comparing the October 2023 anomaly fields with the regression fields onto the NCT during 1979–2022, two potential universal factors for the extreme high temperatures over North China were proposed: 1) the enhanced convection anomalies over the tropical Atlantic (TAP; Fig. SB7.8b), and 2) the dipole sea surface temperature anomalies in the tropical Indian Ocean (TIS; Fig. SB7.8c). The

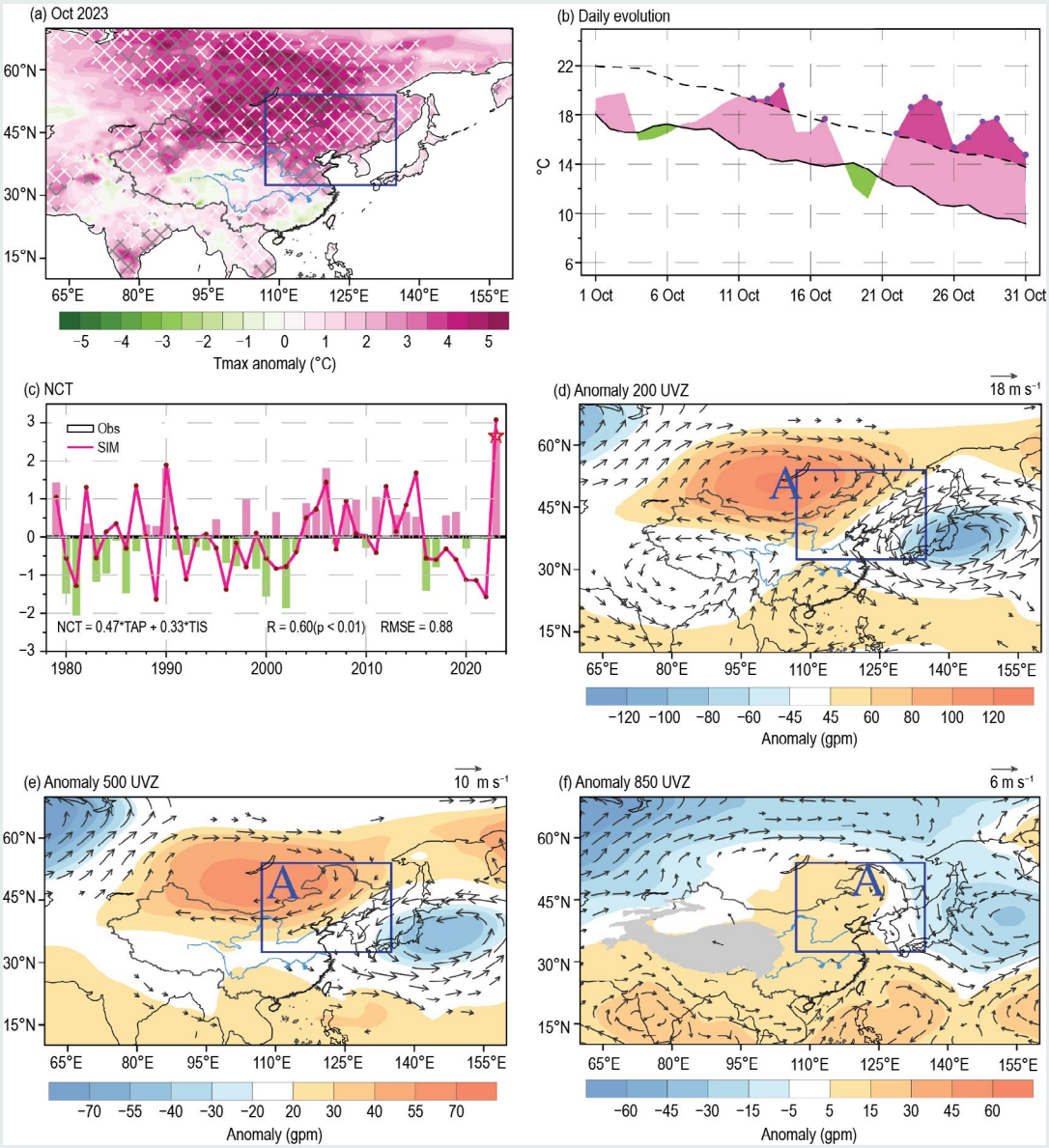

Fig. SB7.7. (a) Maximum surface temperature anomalies (Tmax, shading, °C) in Oct 2023. Areas with extreme high-temperature days (EHDs) 20% more than normal (1991–2020) are slashed with white, and areas with EHDs 30% more than normal are slashed with gray. (b) Daily evolution of Tmax averaged over North China in Oct 2023. The dashed (solid) curve represents the 90th percentile (climatological mean) of the temperature records, and the EHDs are marked with purple dots. (c) Time series of the normalized October Tmax averaged over North China (NCT) during 1979–2023 from observations (bar) and reconstructions by the multiple linear regression model (curve). The legend in the bottom left shows the linear regression equations, and the bottom right legend presents the correlation coefficients (R) and root-mean-square error (RMSE). (d) Local anomalous 200-hPa geopotential height (shading, gpm) and wind (vectors, m s^{-1}). (e),(f) As in (d) but for 500-hPa and 850-hPa, respectively. In (a) and (d)–(f), the blue frame outlines NCT and the letter "A" in (d)–(f) represents the center of the anomalous anticyclone. In (f), the Tibetan Plateau is denoted by gray shading.

diabatic heating anomaly associated with the TAP could trigger a midlatitude Rossby wave train over the Eurasian continent and end with an anomalous anticyclone over North China (Fig. SB7.8b). The TIS favored the anomalous convection in situ and excited another poleward wave train, strengthening the anomalous anticyclone over North China and increasing the local temperature (Figs. SB7.8b,c).

Using a multiple regression model, the above two factors simulate the NCT index with a correlation coefficient of 0.60 ($p<0.01$) and a root mean square error of 0.88 (Fig. SB7.7c). The model also reproduced the extremity in 2023 well, suggesting that the tropical Atlantic and Indian Oceans had significant impacts on the extreme high temperatures over North China during this period.

In addition to this high temperature record in North China, unprecedented high temperatures were also observed in northern and eastern Japan from mid-July 2023 onward. The national average temperature in Japan for summer 2023 was 1.76°C above normal, making it the warmest summer since the start of the record in 1898. From 16 July to 23 August, 106 of 915 observation stations across the country observed record-high maximum temperatures. These extreme high temperatures are associated with several factors, including tropical convection over the western North Pacific and an abnormal Pacific-Japan pattern and northward shift of the upper-level westerly jet, along with the worldwide warming tendency associated with persistent global warming.

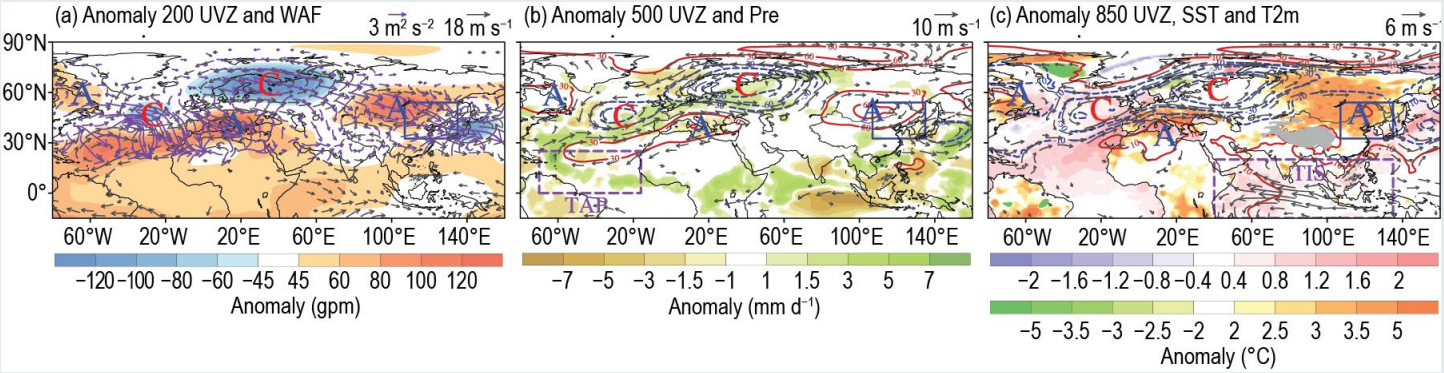

Fig. SB7.8. Oct 2023 (a) 200-hPa geopotential height (shading, gpm), wind (vectors, m s^{-1}), and wave activity flux (purple vectors, m^2 s^{-2}) anomalies, (b) 500-hPa geopotential height (contours, gpm), wind (vectors, m s^{-1}), and precipitation (shading, mm d^{-1}) anomalies, and (c) 850-hPa geopotential height (contours, gpm), wind (vectors, m s^{-1}), and sea surface temperature (SST)/maximum surface temperature (shading, °C) anomalies. The letters "A"/"C" denote the centers of anomalous anticyclones/cyclones. The blue frame outlines the domain of North China. The gray shading in (c) denotes the Tibetan Plateau. In (b),(c), the purple boxes are the domains for calculating the tropical Atlantic precipitation (TAP) and tropical Indian Ocean SST (TIS) indices.

h. Oceania

—C. Ganter, Ed.

1. OVERVIEW

—C. Ganter

The region of Oceania (Fig. 7.60) began the year affected by La Niña, which gave way to an El Niño later in the year (see section 4b for details). While the decaying La Niña provided more typical effects across the area, many regions of Oceania saw atypical effects from their usual El Niño conditions. In addition to the El Niño–Southern Oscillation (ENSO), a positive Indian Ocean dipole (IOD) also affected the region (see section 4g for details), as well as the long-term warming trend.

The year 2023 was New Zealand's second-warmest since the start of its record in 1909; Australia had its eighth-warmest year since 1910.

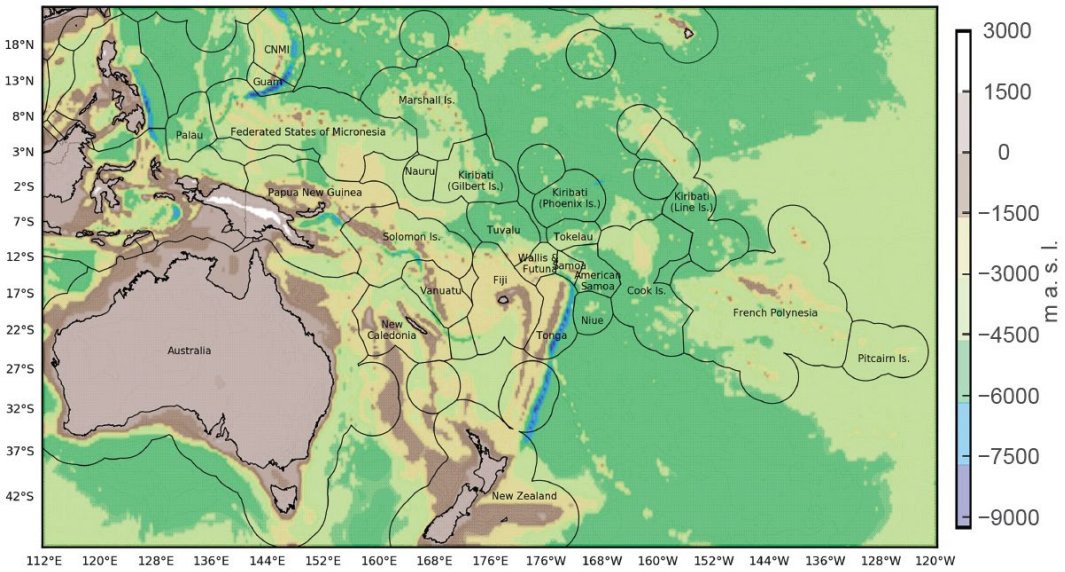

Fig. 7.60. The islands of Oceania. The colors represent topographical heights, with white and browns colors ranging from around 3000 m a.s.l to around –1500 m a.s.l. The yellow/green/blue indicates greater depths of up to 9000 m below sea level, with blue indicating the lowest depths.

2. NORTHWEST PACIFIC AND MICRONESIA

—B. Bukunt

This assessment covers the area from the dateline west to 130°E, between the equator and 20°N. It includes the U.S.-Affiliated Pacific Islands of Micronesia, but excludes the western islands of Kiribati and nearby northeastern islands of Indonesia (Fig. 7.60). The temperature analysis is based on data from ERA5 (Hersbach et al. [2020]) and scripts developed by the NWS, Alaska Region. Anomalies are calculated with respect to the 1991–2020 base period. Rainfall data is a combination of NWS station data and the MSWEP (Beck et al. [2019]) analyses as presented by the Bureau of Meteorology Pacific Climate Monitoring and the Climate And Oceans Support Program In The Pacific (COSPPac) Online Climate Outlook Forum. The base period for the precipitation station data is 1991–2020 while the maps are 1980–2021.

While the past few years followed a relatively conventional La Niña pattern that began in mid-2020, 2023 was a year of marked change as a canonical (east-based) El Niño developed during the boreal spring and summer. Meanwhile, oceanic warmth persisted at higher latitudes east of Japan and north of Hawaii, reinforcing the strongly negative Pacific Decadal Oscillation (PDO). Although the strengthening El Niño pushed the Southern Oscillation Index (SOI) into negative values by August 2023, the SOI struggled to reach negative values on par with strong El Niño events of the past (see *Notable events and impacts* for more information).

(i) Temperature

Along the equator, air temperatures were slightly (0.25°C–0.75°C) below normal to the east of the dateline during January–March (JFM). This was linked to the fading La Niña sea surface

temperature (SST) pattern. Temperatures were slightly above normal across the Republic of Palau, the western portion of the Federated States of Micronesia, Guam, and the Commonwealth of the Northern Mariana Islands (CNMI) during JFM (Fig. 7.61a). ERA5 data indicated a

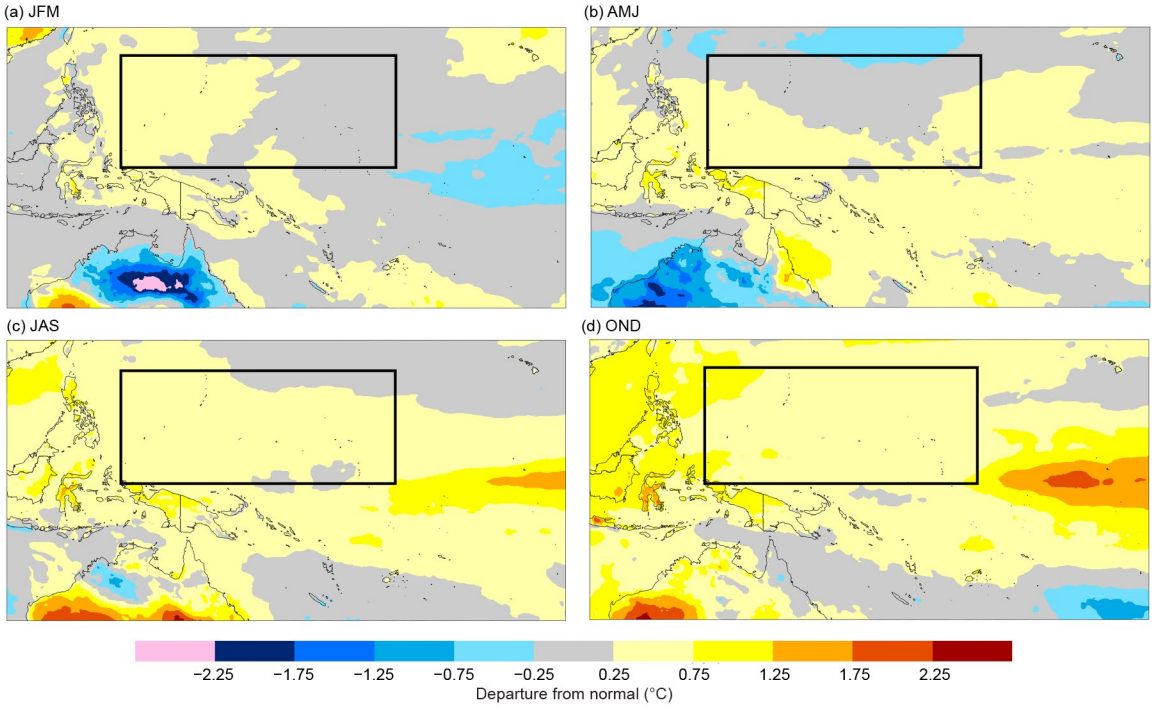

Fig. 7.61. Seasonal air temperature surface anomalies (°C) in 2023 across the west-central Pacific for (a) Jan–Mar, (b) Apr–Jun, (c) Jul–Sep, and (d) Oct–Dec. The black box defines the northwest Pacific and Micronesia region. (Source: ERA5 and Brettschneider.)

crescent-shaped region of record-high SSTs from west of Palau extending northeastward to Yap proper and waters south of Guam during the first half of 2023 (Fig. 7.62a).

The swath of slightly above-normal air temperatures across western Micronesia expanded to the rest of the region during the remainder of the year (Figs. 7.61b–d), with pockets of above-normal (0.75°C–1.25°C) air temperatures along the equator to the southeast of the Republic of the Marshall Islands (RMI) and portions of far western Micronesia (Republic of Palau [ROP] and western Yap State). Increasing air temperature anomalies to the southeast of the Marshall Islands were likely due to the growing El Niño signal. SSTs in the Niño-4 region reached record levels for the July–December period, according to ERA5 data (Fig. 7.62b). Fragments of this record-warm SST pool expanded northward to Majuro at times: Majuro tied its all-time highest minimum temperature of 28.9°C on 8 September and its highest minimum temperature in December of 28.3°C on both 2 and 22 December (records since 1946).

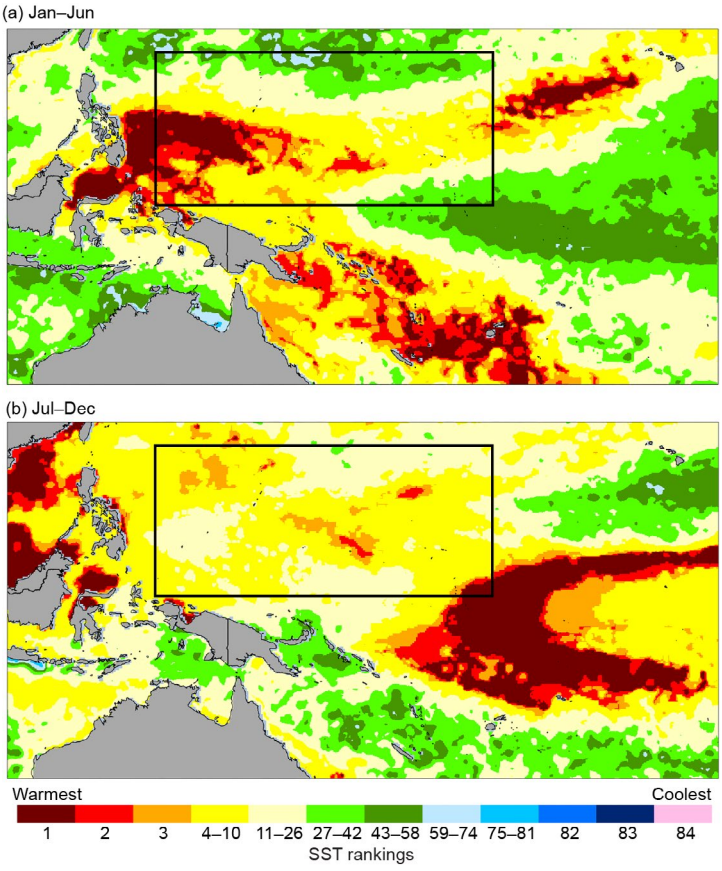

Fig. 7.62. Sea surface temperature rankings for (a) Jan–Jun and (b) Jul–Dec 2023. Ranking are based on 83 years of reanalysis data. The black box defines the northwest Pacific and Micronesia region. (Source: ERA5 and Brettschneider.)

(ii) Precipitation

Precipitation during the first half of the year followed the traditional expectations of El Niño onset with above-normal rainfall observed across Micronesia (Table 7.2; Fig. 7.63). Stations saw well-above-normal rainfall in Guam, Saipan, and Kwajalein during this time.

Patches of drier-than-normal conditions were observed during the second half of the year, particularly in portions of the central and northern Marshall Islands, far southern portions of the ROP, and the northern reaches of the CNMI (Fig. 7.63). Equatorial locations near and east of 150°E experienced very-wet conditions from July to December in response to the strengthening El Niño. Conversely, slightly drier-than-normal conditions were observed across the central and northern RMI. The dry pattern across the northern portion of the Marshall Islands can be attributed to the consolidation of tropical convection closer to the equator, as well as the absence of nascent tropical systems that have typically accompanied strong El Niño events in the past.

Guam, Pohnpei, and Kapingamarangi all experienced their second-wettest year on record, with records stretching back 75, 72, and 21 years, respectively. Saipan ended the year at fourth wettest on record. Although the above-normal rainfall statistics matched expectations of a traditional El Niño, the mechanisms for this above-normal rainfall differed significantly from other notable El Niño years, with one of the main differences this year including a retracted (westward-displaced) monsoon.

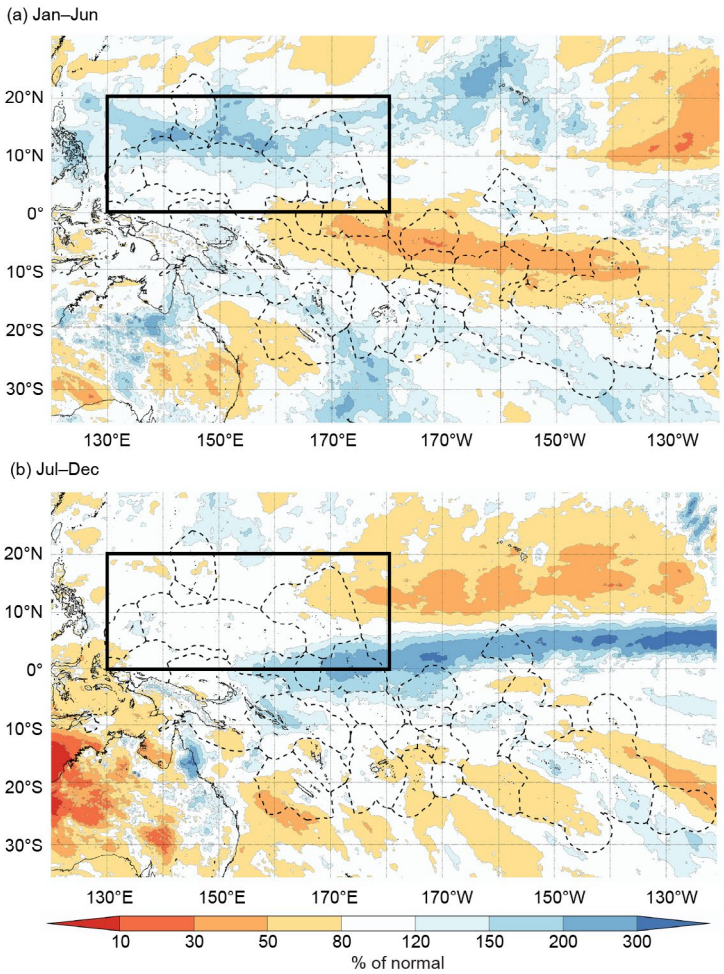

Fig. 7.63. Six-month percent of normal rainfall (%) across the central and western Pacific for (a) Jan–Jun and (b) Jul–Dec 2023. The black box defines the northwest Pacific and Micronesia region. (Source: MSWEP.)

(iii) Notable events and impacts

Typhoon Mawar was the strongest tropical cyclone (TC) to impact Guam since Super Typhoon Pongsona on 8 December 2002. Mawar gathered in Chuuk State during mid-May 2023 before curling northward and rapidly intensifying to a Category 5 super typhoon on approach to Guam. The system weakened to Category 4 and slowed its forward speed considerably as it drifted over the northern tip of Guam on 24 May. As Mawar pulled away, it underwent another period of rapid intensification that kept typhoon-force winds blowing over Guam for a total of 8–10 hours and tropical-storm force winds persisting for roughly 14 hours. Mawar dropped over 600 mm of rain in less than 24 hours, with maximum sustained winds of 210 km h^{-1} to 225 km h^{-1} across far-northern Guam. Damage estimates exceeded $4 billion U.S. dollars.

Mawar was eerily similar to Typhoon Pamela in 1976. Both 1976 and 2023 were developing El Niño years after three years of La Niña. Pamela (1976) and Mawar (2023) spawned in Chuuk State before curving northward during the month of May. Both systems delivered a hefty blow of lengthy typhoon-force winds, bringing torrential rains exceeding 600 millimeters to Guam. While the year 1976 was the wettest year on record at the Guam International Airport (3613.91 mm), 2023 became the second wettest (3556.25 mm). Nearly 20% of the annual rainfall fell in two days during both years, highlighting the importance of these infrequent but high-impact events for the island's water budget and climatology. See the NWS Guam Super Typhoon Mawar Meteorological Assessment for a more detailed examination.

Table 7.2. Average rainfall total (AVG; mm) compared to rainfall total (mm) and percent of average values (%) for select Micronesia locations in 2023 (1991–2020 base period) for Jan–Jun, Jul–Dec, and annual (Jan–Dec). Latitudes and longitudes are approximate. "Kapinga" stands for Kapingamarangi Atoll in Pohnpei State, Federated States of Micronesia. Green-filled cells with an up arrow icon (↑) indicate above-average rainfall and yellow-filled cells with a down arrow icon (↓) represent below-average rainfall. (Source: NOAA's National Weather Service.)

Location	Jan–Jun AVG Rainfall (mm)	Jan–Jun 2023 Rainfall (mm)	Jan–Jun % of Normal Rainfall	Jul–Dec AVG Rainfall (mm)	Jul–Dec 2023 Rainfall (mm)	Jul–Dec % of Normal Rainfall	Jan–Dec AVG Rainfall (mm)	Jan–Dec 2023 Rainfall (mm)	Jan–Dec % of Normal Rainfall
Saipan 15°N, 146°E	462.8	779.3 ↑	168.4 ↑	1306.1	1450.1 ↑	111.0 ↑	1768.9	2229.4 ↑	126.0 ↑
Guam 13°N, 145°E	678.7	1768.1 ↑	263.2 ↑	1813.6	1770.1 ↓	97.6 ↓	2492.3	3556.3 ↑	142.7 ↑
Palau 7°N, 134°E	1798.1	2034.3 ↑	113.1 ↑	2279.4	2256.5 ↓	99.0 ↓	4077.5	4290.8 ↑	105.2 ↑
Yap 9°N, 138°E	1191.5	1310.6 ↑	110.0 ↑	1943.4	1967.5 ↑	101.2 ↑	3134.9	3278.1 ↑	104.6 ↑
Chuuk 7°N, 152°E	1678.2	2145.5 ↑	127.8 ↑	1917.7	2100.8 ↑	109.5 ↑	3595.9	4246.4 ↑	118.1 ↑
Pohnpei 7°N, 158°E	2361.2	3024.6 ↑	128.1 ↑	2308.4	3058.2 ↑	132.5 ↑	4669.6	6082.8 ↑	130.3 ↑
Kapinga 1°N, 155°E	1880.6	2252.0 ↑	119.7 ↑	1485.1	2265.7 ↑	152.6 ↑	3365.7	4517.6 ↑	134.2 ↑
Kosrae 5°N, 163°E	2635.8	3066.5 ↑	116.3 ↑	2354.8	2548.1 ↑	108.2 ↑	4990.6	5614.7 ↑	112.5 ↑
Kwajalein 9°N, 168°E	898.4	1417.6 ↑	157.8 ↑	1553.7	1408.2 ↓	90.6 ↓	2452.1	2825.8 ↑	115.2 ↑
Majuro 7°N, 171°E	1459.0	1750.3 ↑	120.0 ↑	1875.0	1464.6 ↓	78.1 ↓	3334.0	3214.9 ↓	96.4 ↓

The biggest event of 2023 was arguably the unique El Niño that developed. There were a number of aspects that did not follow a "traditional" El Niño year for Micronesia, including westerly wind bursts (WWBs), regional TC activity, sea level heights, SST patterns, and other oscillations on longer time scales, including the PDO. Whereas strong El Niño events of the past featured flurries of WWBs and an anomalous eastward extension of the monsoon trough into far eastern Micronesia, 2023 was characterized by weaker WWBs and an abbreviated monsoon trough. Only 11 typhoons occurred in the western North Pacific basin during 2023, well below the average of 16 (see section 4g4). The number of named storms in 2023 was also extremely low (17 total), and the overall distribution was shunted west and north. While this TC activity and distribution was atypical from an El Niño standpoint, it closely followed the trends observed during the negative phase of the PDO and Pacific Meridional Mode (PMM)—both of which are linked to reduced TC activity across much of Micronesia (PDO: Scoccimarro et al. 2021; Lee et al. 2021; PMM: Zhang et al. 2016). Overall, 2023 TC statistics better matched strong post-El Niño years transitioning to La Niña (e.g., 1998 and 2010) rather than strong El Niño onset years.

Sea level heights also diverged from past strong El Niño events. While sea levels did decrease as one would anticipate during El Niño, the region of below-normal sea level heights was confined to a much smaller area, mainly south of 8°N, with lower magnitudes when compared to previous El Niño events. Sea levels at Guam and Yap typically fall below normal late in the year linked to the peak of El Niño, but tide gauges on both islands remained near or even slightly above normal.

The SOI, a measure of the atmospheric response to the ENSO, did not transition to negative values associated with El Niño until August. This was somewhat delayed compared to other prominent El Niño events. While the SOI remained negative during the second half of 2023, it was weak in magnitude. It is conceivable that the above-normal SSTs observed across much of the tropical Pacific basin during this period, along with the expansion of record SST warmth in the North Atlantic Ocean, disrupted the classic eastward El Niño shift of tropical convection into the central Pacific.

3. SOUTHWEST PACIFIC

—E. Chandler

Countries considered in this section include American Samoa, the Cook Islands, Fiji, French Polynesia, Kiribati, Nauru, New Caledonia, Niue, Papua New Guinea (PNG), Samoa, the Solomon Islands, Tokelau, Tonga, Tuvalu, Vanuatu, and Wallis and Futuna (Fig. 7.60). The temperature analysis is based on the Climate Anomaly Monitoring System (CAMS) monthly surface air temperature anomalies (https://iridl.ldeo.columbia.edu/maproom/Global/Atm_Temp/Anomaly.html). Anomalies are calculated with respect to the 1991–2020 base period. The precipitation analysis is based on the MSWEP monthly analyses as presented for the South Pacific (http://www.bom.gov.au/climate/pacific/outlooks/) and the COSPPac Online Climate Outlook Forum (https://www.pacificmet.net/products-and-services/online-climate-outlook-forum). The base period for precipitation is 1980–2021.

With the transition from La Niña at the beginning of 2023 to El Niño by mid-year, SSTs warmed quickly through the first quarter, with above-normal SSTs widespread by the second quarter across the Pacific, particularly evident in the South Pacific off-equatorial regions (see Figs. 3.2a,b). Atmospheric indicators of El Niño lagged the changes seen in the ocean, with changes to wind and cloud patterns emerging during September and October that were more typical of El Niño. These changes in the atmosphere combined with a strengthening of the warm SSTs along the equator led to a consolidation of El Niño in the Pacific through the last quarter of 2023.

In the early months of 2023, air temperatures and rainfall patterns were both typical of a La Niña event transitioning to ENSO-neutral, with atmospheric patterns more typical of El Niño becoming apparent by the last quarter of the year. Rainfall was suppressed along the equator through the first quarter of 2023, as is typical with La Niña, with the region south of 10°S and west of the Cook Islands tending to receive more rainfall than normal. The La Niña-like rainfall pattern present in early 2023 broke down during the second quarter of the year as the South Pacific transitioned into the dry season. There was a mixed rainfall pattern over the third quarter as the Pacific transitioned towards El Niño, with a more zonal South Pacific Convergence Zone (SPCZ) becoming evident towards the equator by September. Through the last quarter of 2023, enhanced rainfall was present along the equator extending the width of the Pacific. Suppressed rainfall became increasingly evident over the South Pacific from September onwards, reaching a peak in terms of magnitude and spatial extent over November and December. This pattern of rainfall across the South Pacific is often associated with El Niño.

(i) Temperature

Along the equator, air temperatures were up to 1°C below normal on and to the east of the dateline through to Kiribati during January and February, associated with warmer SSTs in the same region. A small region of below-normal air temperatures (anomalies of up to –1°C) was located near Tonga during January; however, that region weakened to near-normal levels by February, with March air temperatures having been close to normal across the Pacific (Fig. 7.64a).

Warm air temperature anomalies near the South American coast were present and extended westwards along the equator though the second quarter of the year (Fig. 7.64b), and were associated with increasing SST anomalies. Though a small region of cooler air temperatures up to 1°C below normal was located to the south of the Cook Islands during May, it warmed to near-normal by June.

During July–September (JAS), the area of +1°C to +3°C anomalies continued to expand westward along the equator in the South Pacific (Fig. 7.64c), reaching western Kiribati (Gilbert

Island group) by September with air temperature anomalies of up to +1°C. Off-equatorial air temperatures were near normal across the South Pacific.

During October–December (OND), the region of positive air temperature anomalies along the central equatorial region persisted (Fig. 7.64d). Anomalies of up to +2°C were present over much of Kiribati by December. Small regions of below-normal air temperatures were present in the off-equatorial South Pacific to the east of the dateline near Tonga and Niue during October. This region expanded during November and December eastwards to French Polynesia, with temperature anomalies reaching up to –1°C.

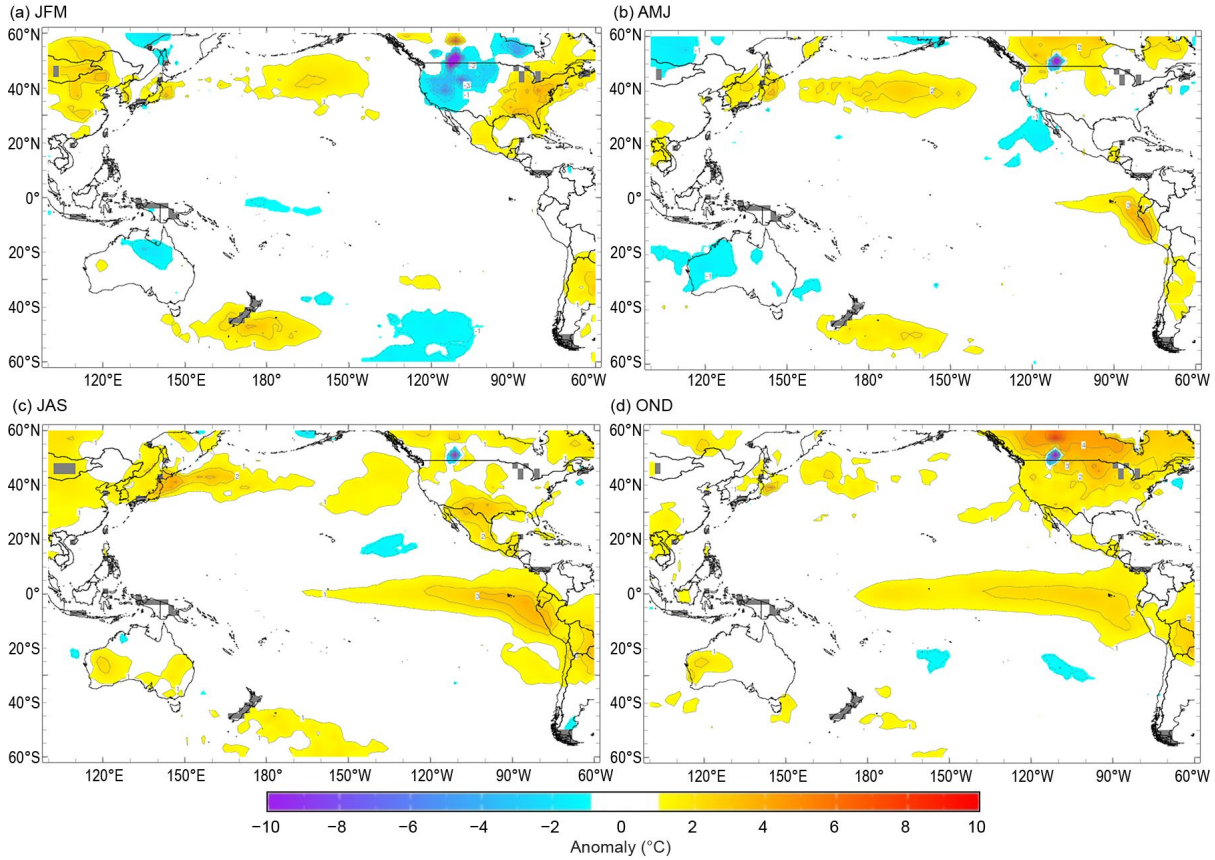

Fig. 7.64. Seasonal air temperature surface anomalies (°C) across the Pacific for (a) Jan–Mar, (b) Apr–Jun, (c) Jul–Sep, and (d) Oct–Dec. (Source: CAMS.)

(ii) Precipitation

The year began with suppressed rainfall along the equator over Kiribati, Nauru, Tuvalu, Tokelau, northern American Samoa, the northern Cook Islands, and northern French Polynesia, in a pattern typically associated with an established La Niña (Fig. 7.65a). In Tuvalu, Niulakita recorded its driest JFM on record with 358 mm (70-year climatology). The suppressed rainfall over the quarter led to several locations in Tuvalu and the northern Cook Islands receiving rainfall in their bottom 10th percentiles. The rainfall pattern south of 10°S was closer to normal with regions of enhanced rainfall. The southern Solomon Islands, Vanuatu, New Caledonia, Fiji, Wallis and Futuna, the southern Cook Islands, and southern French Polynesia experienced enhanced rainfall during January; however, through February and March, suppressed rainfall was evident over parts of the southern Solomon Islands and Fiji as rainfall patterns began to transition towards an ENSO-neutral pattern for the Pacific. Parts of Fiji recorded rainfall in their top 10th percentile during this period.

Through the second quarter of the year, the Pacific rainfall pattern was mixed as rainfall over the region continued to transition from La Niña to ENSO-neutral (Fig. 7.65b). April–June (AMJ) rainfall was near or slightly below normal over most of the region north of 10°S, although in a narrower band than during the first quarter of the year. The region of suppressed rainfall covered Kiribati (excluding the northern Line Islands), the northeastern Solomon Islands, Tuvalu and Tokelau, northern American Samoa, the northern Cook Islands, and northern French Polynesia. Another region of suppressed rainfall was present covering New Caledonia and extending to the

Australian coast. Regions of enhanced rainfall were present over most of PNG, Samoa, Tonga, Niue, the southern Cook Islands, and western and central French Polynesia. Niuatoputapu (Tonga) recorded its third-wettest AMJ on record (75 years) with 914 mm, and Faleolo (Samoa) recorded 622 mm of rainfall during AMJ, making 2023 the seventh-wettest year in its 58-year record.

Positive rainfall anomalies were present along the equator during JAS, reflecting a developing El Niño (Fig. 7.65c). The region of enhanced rainfall covered Nauru and Kiribati, causing the precipitation totals of both countries to reach their top 10th percentiles during JAS. Rainfall was also enhanced in a band from eastern PNG to Vanuatu and southern Fiji. Rainfall in this region during September was associated with an enhanced SPCZ, which was evident close to the northern Solomon Islands and in a band stretching eastward across to the northern Cook Islands. The Solomon Islands had several stations record rainfall in their top 10th percentile. Taro (Solomon Islands) and Tarawa (Kiribati) saw their second-wettest JAS on record (45- and 74-year records, respectively), with the former recording 1254 mm and the latter recording 1080 mm. In contrast, patches of suppressed rainfall covered much of the southern half of PNG and the far southern Solomon Islands into western New Caledonia. There were other isolated patches of suppressed rainfall over northern Tuvalu, the southern Phoenix Islands (Kiribati), southern Tonga, American Samoa, the central Cook Islands, and western French Polynesia.

Rainfall patterns during October–December (OND) reflected the emergence of El Niño. Rainfall was enhanced across the width of the Pacific, extending westwards over Kiribati, Nauru, and parts of PNG (Fig. 7.65d). Off the equator, rainfall was also enhanced over parts of the Solomon Islands, Nauru, northern Tuvalu, northern Tokelau, and the northern Cook Islands. Nauru recorded its wettest OND in the 80-year record with 1461 mm of rainfall, while stations across Tuvalu, Kiribati, and the Solomon Islands all recorded rainfall in their top 10th percentiles. In a typical El Niño rainfall response, rainfall across New Caledonia, Vanuatu, Fiji, Tonga, parts of Samoa and Niue, the southern Cook Islands, and southern French Polynesia was suppressed. Tonga, Fiji, and the southern Cook Islands all recorded rainfall in their lowest 10th percentiles on record, with Rarotonga (the Cook Islands) recording its second-lowest OND in its 125-year record with 209 mm.

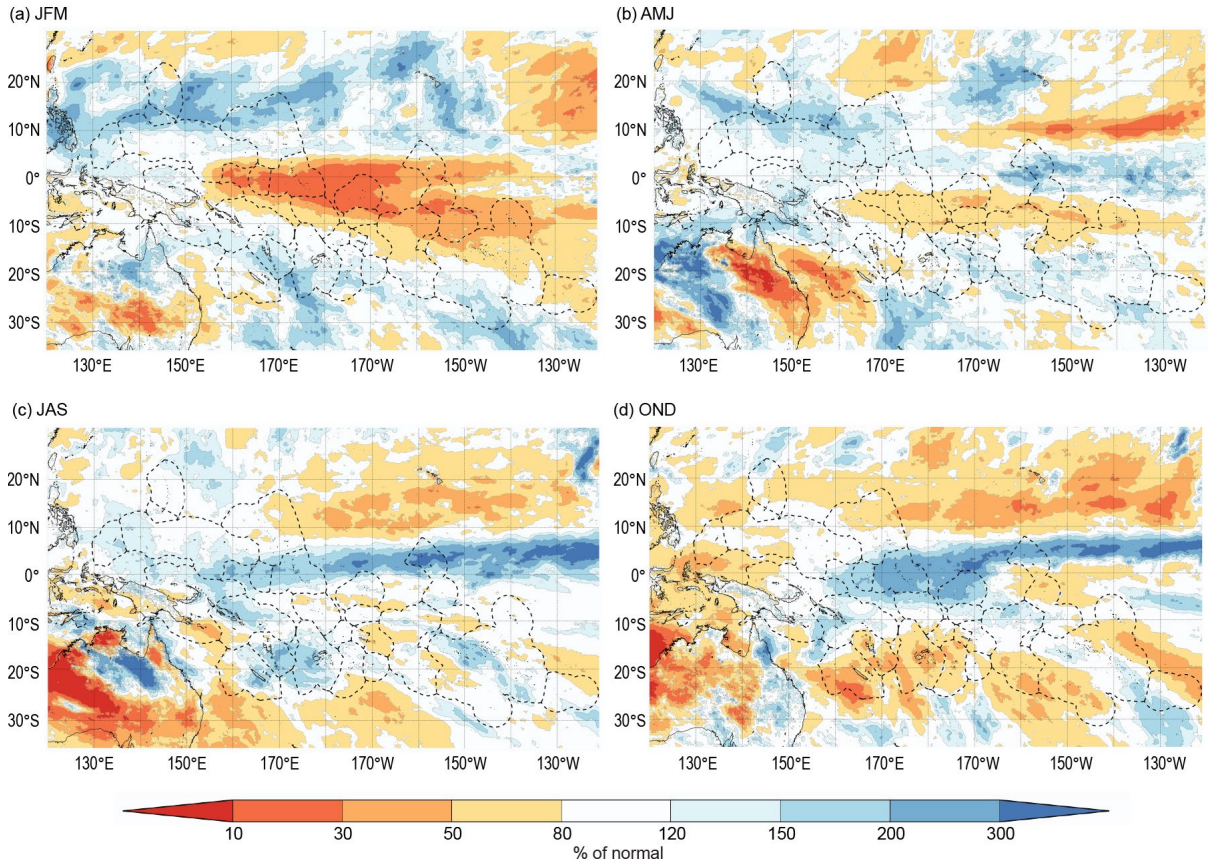

Fig. 7.65. Seasonal percentage of normal rainfall (%) across the southwest Pacific for (a) Jan–Mar, (b) Apr–Jun, (c) Jul–Sep, and (d) Oct–Dec. (Source: MSWEP.)

(iii) Notable events and impacts

The most devastating TCs to affect the South Pacific in 2023 were severe TCs Kevin and Judy, which both impacted Vanuatu within 48 hours of each other in early March. TC Judy formed north of Fiji and tracked to the west, passing to the south of the Solomon Islands in late February as the cyclone intensified. Judy then tracked southward directly over many of the central and southern islands of Vanuatu. At its peak, Judy's 10-minute sustained winds reached 175 km h^{-1} (Category 4) and a lowest central pressure of 941 hPa. Conversely, TC Kevin formed off the Australian coast in late February and tracked southeastward and, influenced by a subtropical ridge, passed over the southern islands of Vanuatu. The lowest central pressure recorded was 918 hPa, while 10-minute sustained winds peaked at 215 km h^{-1} (Category 5) as it passed away from Vanuatu.

All islands of Vanuatu were influenced by one or both cyclones over a four-day period, with approximately 80% of the population being affected by at least Category 2 winds. There were extensive interruptions to running water and power in various regions, including the capital Port Vila on 4 March, where the international airport sustained wind damage. Central Vanuatu provinces of Shefa, Tafea, Penama, and Malapa were the worst impacted in terms of damage to infrastructure and loss of communications. Fortunately, there were no reported deaths associated with either cyclone.

4. AUSTRALIA

—C. Minney

For this section, monthly area-averaged temperatures are based on the ACORN-SAT dataset (Trewin 2018), while mapped temperature analyses are based on the AWAP dataset (Jones et al. 2009), both of which begin in 1910. Area-averaged rainfall values and mapped analyses use the AGCD dataset (Evans et al. 2020), which begins in 1900. Anomalies are based on the 1991–2020 average.

(i) Temperature

The year 2023 was Australia's equal eighth-warmest year on record since 1910, with the area-averaged mean temperature having been 0.34°C above the 1991–2020 average. The area-averaged annual mean maximum temperature (Fig. 7.66) was 0.58°C above the 1991–2020 average. The area-averaged annual mean minimum temperature (Fig. 7.67) was 0.10°C above the 1991–2020 average. Maximum temperature anomalies were positive across most of Australia, excluding some areas across the tropical north and southern mainland coastal regions. Anomalies of +1°C to +2°C were recorded in Western Australia and across the Queensland–New South Wales border, extending into South Australia; anomalies of −0.5°C to −1.0°C below average were mostly observed in central parts of the Northern Territory. Minimum temperature anomalies varied across Australia; negative anomalies were recorded across much of the northern half of Australia, extending into New South Wales and eastern South Australia. Positive minimum temperature anomalies of up to +1.5°C were recorded in central Western Australia, northern South Australia, and southwest Queensland.

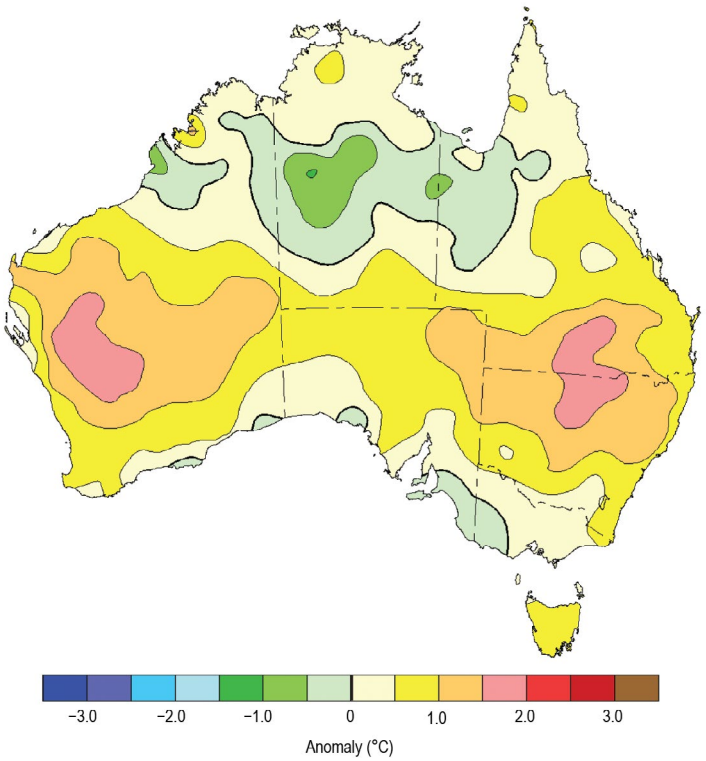

Fig. 7.66. Maximum temperature anomalies (°C) for Australia, averaged over 2023, relative to a 1991–2020 base period. Australian States/Territories are as follows, starting clockwise from the west: Western Australia, the Northern Territory, Queensland, New South Wales, Victoria, and South Australia, with the island of Tasmania in the southeast. (Source: Australian Bureau of Meteorology.)

Nationally, January was the coldest since 2002 and cool conditions continued into February for much of northern Australia, while the month was warmer for much of Western Australia. The autumn (March–May) area-averaged mean temperature was close to average.

The remainder of the year saw a shift towards warmer-than-usual temperatures. It was Australia's warmest June–November on record (since 1910). Record-high temperatures aligned with a developing El Niño and positive Indian Ocean dipole (IOD), both of which are known to increase maximum/minimum temperatures in the austral winter and spring (McKay et al. 2022). It was the warmest June on record for much of Queensland, and most of Tasmania and the eastern parts of southeast Australia had their warmest July on record. The national mean temperatures for June, July, August, September, November, and December were among their respective 10 warmest on record. The year finished up with the fourth-warmest December on record nationally.

(ii) Precipitation

Nationally, the area-averaged annual rainfall total for Australia during 2023 was 472.5 mm. This was 2.78% below the 1991–2020 average of 486.0 mm. Compared to the distribution across all years of observation from 1900 to 2023, rainfall in 2023 (Fig. 7.68) was above to very much above average across much of northern Australia and below average for much of Tasmania, northern New South Wales, southern Queensland, eastern South Australia, and western and southern Western Australia. Some small isolated areas of Cape York Peninsula in Queensland had their wettest year on record, while some localized parts of the western Australian coastline had their driest year on record.

A number of climate influences affected Australia's rainfall during 2023. These included a La Niña, which weakened and dissipated at the start of the year, and an El Niño and positive IOD that developed during the latter half of the year (Ashok et al. 2003; Hendon et al. 2007; McKay et al. 2023; see sections 4b and 4f for more details on the El Niño–Southern Oscillation and the IOD, respectively). During November and December, much of eastern Australia

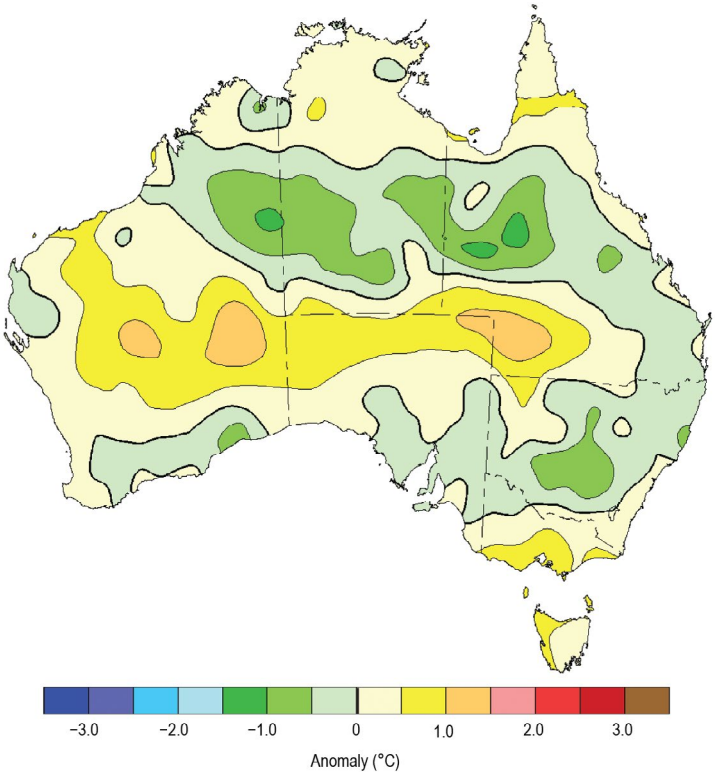

Fig. 7.67. Minimum temperature anomalies (°C) for Australia, averaged over 2023, relative to a 1991–2020 base period. (Source: Australian Bureau of Meteorology.)

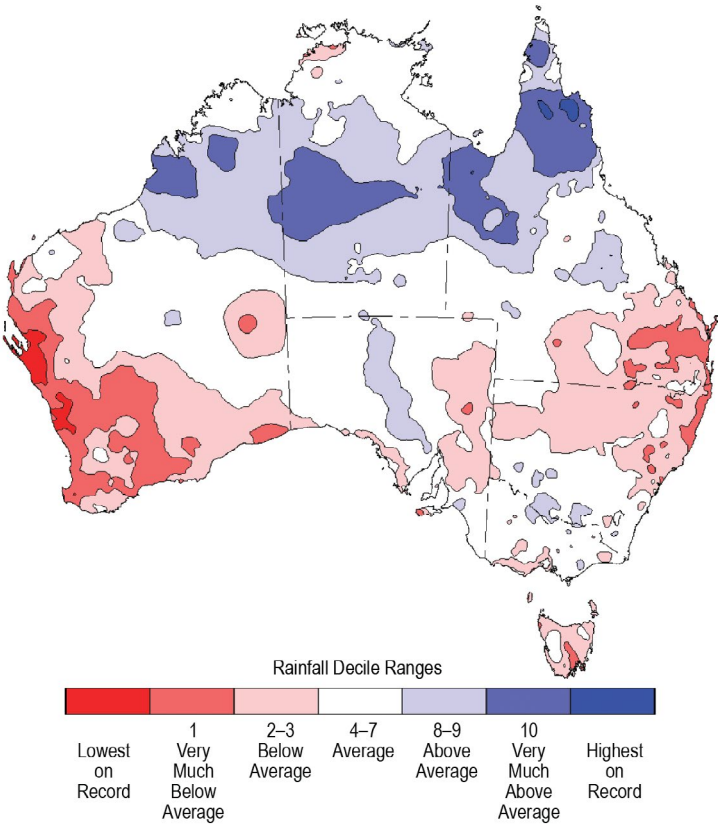

Fig. 7.68. Rainfall deciles for Australia for 2023, based on the 1900–2023 distribution. (Source: Australian Bureau of Meteorology.)

experienced widespread and at times heavy rainfall, along with isolated severe thunderstorms. A positive Southern Annular Mode (SAM) during December likely contributed to above-average rainfall over much of eastern Australia (Hendon et al. 2007). The positive SAM was influenced by a stronger-than-normal winter polar vortex (Thompson et al. 2005; see section 6b for details). Warm ocean temperatures surrounding Australia, particularly in the Tasman and Coral Seas located to the southeast and northeast of Australia, respectively, likely contributed to changes in the expected El Niño influence on rainfall patterns during November and December. The 2023 El Niño was unusual due to above-average SSTs persisting in the western Pacific. These changed SST patterns likely contributed to a delayed atmospheric Southern Oscillation Index response to SSTs and a weak response in cloudiness and wind patterns and, therefore, reduced drying impact across Australia (see http://www.bom.gov.au/climate/current/season/aus/summary.shtml).

January–April generally saw above-average rainfall across northern Australia. Rainfall was very much above average (top 10% of January–April periods) for parts of the northern Kimberley in Western Australia, which was impacted by Tropical Cyclones Ellie and Ilsa. While rainfall is typically high during the wet season in these regions, very-much-above-average rainfall for the season was also recorded in northern Queensland, which was associated with monsoonal rain and brought significant flooding to some parts. Rainfall was mostly near average farther south; however, some parts of southern Queensland, northern New South Wales, and Tasmania were below average for the four months, as was coastal western Australia, which typically receives low warm-season rainfall.

May–July mostly saw drier conditions for parts of southern and eastern Australia, with unseasonable rain events in June and July for much of the north, particularly northwestern Australia. August–October 2023 was the driest three-month period in Australia on record (since 1900), with a national area-averaged rainfall total of 22.63 mm. Most of Australia recorded below-average rainfall during this period; rainfall was the lowest on record across much of southern Queensland. Soil moisture was below to very much below average for much of southern Australia during this period.

High rainfall totals preceding 2023 meant water storages and soil moisture were high at the beginning of the year. Dry conditions during 2023 reduced overall water storages; however, storages remained high at the end of the year (74.1% accessible capacity). Rainfall deficits emerged, with May–December experiencing severe and serious deficiencies (lowest 5% and 10% of rainfall records, respectively) over much of the west of Western Australia and northern New South Wales.

(iii) Notable events and impacts

The year started with heavy rainfall, flooding, and storms across much of northern Australia. Ex-Tropical Cyclone Ellie caused significant flooding in January with the Fitzroy River in north-west Australia exceeding its major flood level and significantly impacting local communities.

Heatwaves affected many areas across Australia during February and March. Severe-intensity heatwaves affected southern Victoria and much of Western Australia during February, as well as the Pilbara district of Western Australia during March. Tropical Cyclone Ilsa made landfall as a Category 5 system on 14 April on the Pilbara Coast of Western Australia. Prior to making landfall on the Australian mainland, the highest 10-minute sustained wind speed on record across the Bureau's observation network, at 219 km h^{-1}, was recorded over Bedout Island on 13 April as Ilsa passed directly over.

Heatwaves and unusually warm conditions were experienced from September to December. Unusually warm conditions during September and October led to elevated fire risk in the Northern Territory, Queensland, and New South Wales due to the dry landscape and warm winter and spring conditions. Bushfires burned for weeks in the Northern Territory, including an estimated 1 million hectares burned by a large bushfire east of Tennant Creek, 2.8 million hectares burned in the Barkly region, and millions of hectares burned across the Tanami and central Australia (Northern Australian Fire Information 2024). Northern, central, and western Australia continued to be affected by heatwaves throughout November and December, including extreme heatwave conditions in northwest Western Australia at the end of December. Drought conditions developed along the east coast between January and October, easing with high rainfall during

November and December. Serious to record-low rainfall deficiencies also developed between May and October for much of southern Western Australia.

Significant rainfall from a series of low-pressure troughs impacted eastern Australia during the latter half of December. Severe thunderstorms impacted areas of southern and central Queensland between the 24th and 31st. Impacts included large hail, reports of a tornado between Queensland's Gold Coast and Scenic Rim, flash flooding, and damaging winds. November and December rainfall eased the rapidly developing drought conditions along most of the east coast.

Tropical Cyclone Jasper made landfall near Wajul Wajul on the Queensland north-east coast on 13 December as a Category 2 system. As the storm moved inland, it stalled over the Cape York Peninsula, bringing several days of heavy rainfall and major flooding, landslides, road closures, and damage to businesses and crops. The stalling of the system inland as well as the formation of a trough significantly contributed to the heavy rainfall totals and associated impacts.

5. AOTEAROA NEW ZEALAND

—T. Meyers

(i) Temperature

The year 2023 was New Zealand's second warmest on record, based on the mean temperature from the National Institute of Water and Atmospheric Research's (NIWA) seven-station series, which began in 1909. Annual temperatures were above average (defined as 0.51°C–1.20°C above the 1991–2020 average) or well above average (>1.20°C above average) for much of Aotearoa New Zealand (Fig. 7.69a). Small pockets of near-average temperatures (−0.50°C to +0.50°C of average) were observed around Northland, Auckland, Bay of Plenty, Gisborne, Hawke's Bay, eastern Wairarapa, southern Marlborough, Canterbury high country, and Otago.

Data from NIWA's seven-station series shows that eight months of 2023 had temperatures that were above or well above average. May and September were both the warmest on record at an astounding 1.10°C and 2.00°C above their 1991–2020 monthly averages, respectively. Meanwhile, August was relatively cool, having seen a mean temperature of −0.55°C below average and becoming the first month to have below-average national temperatures (0.51°C–1.20°C below average) since May 2017.

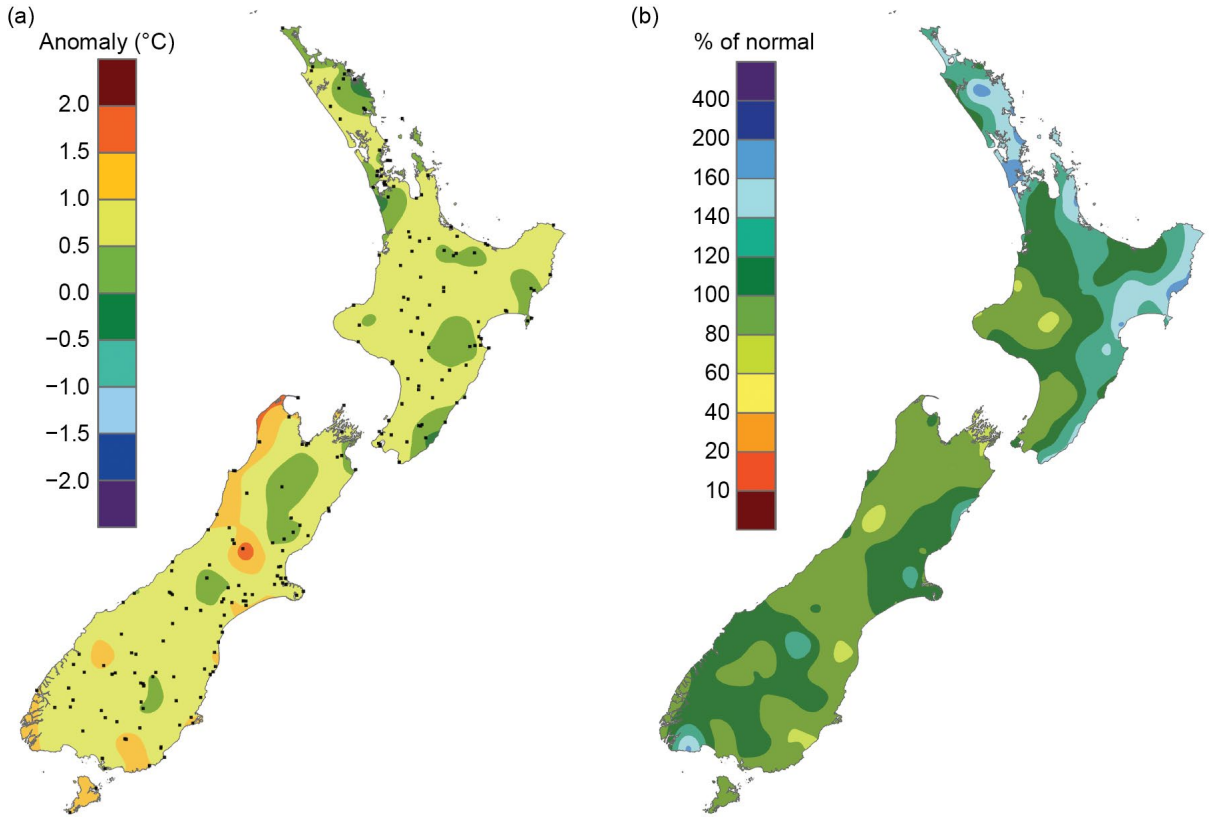

Fig. 7.69. Annual (a) average temperature anomaly (°C) and (b) total rainfall (% of normal) for 2023, relative to 1991–2020. The black dots in (a) represent the locations of climate stations used to create both the temperature and rainfall maps.

In terms of annual minimum and maximum temperatures, it was also the second-warmest year on record for both. Across the country, 58 locations observed a record or near-record annual mean temperature, 43 locations observed a record or near-record annual mean maximum temperature, and 52 locations observed a record or near-record annual mean minimum temperature. For the eighth consecutive year, no locations experienced a record or near-record cold year.

The record or near-record heat experienced around the country throughout 2023 and in recent years is consistent with expectations of a warming planet caused by anthropogenic climate change. Coastal sea surface temperatures (SSTs) also influenced terrestrial temperatures in New Zealand during 2023, with SSTs near the coasts exhibiting record or near-record warmth in all regions but the northern North Island. Coastal SSTs were average or above average nearly every month, with February ranking as the most unusually warm month as monthly SSTs off the west of the South Island peaked at 3.19°C above average, according to NOAA's OISSTv2. Averaged across 2023, SSTs were the highest on record near the eastern South Island, second highest on record near the western North Island, northern South Island, and western South Island, and third highest on record in the eastern North Island since records began in 1981.

Farther afield, SSTs around the Tasman Sea and Coral Sea were also above average for the majority of the year, and thus added to an increase in the atmospheric water vapor content around New Zealand. This in turn contributed to higher-than-average humidity, which resulted in warmer-than-average nights.

La Niña also influenced New Zealand's climate, which tends to be associated with higher-than-normal air pressure near and to the east of the country, with lower pressures to the north. This contributes to more sub-tropical, northeasterly winds than normal, which increases air temperatures, sea temperatures, and humidity. This air flow was common in the first half of the year. Meanwhile, El Niño tends to be associated with lower-than-normal air pressure to the south and southeast of the country and higher-than-normal air pressure to the north. This can lead to an increased north-to-south pressure gradient, intensifying spring-time westerly winds and fronts as they move across the county. This air flow occurred more consistently during the second half of 2023, as the ocean–atmosphere system transitioned to El Niño. However, one atypical element of the building El Niño was a persistent blocking high-pressure system to the southeast of New Zealand, which was a holdover from La Niña. This high-pressure system slowed the typical progression of weather patterns from west to east across the country and led to more northerly winds than what is usually associated with a classical El Niño circulation regime.

(ii) Precipitation

As shown in Fig. 7.69b, rainfall was well above normal (>149% of the annual normal) for parts of Northland, Auckland, Coromandel, Gisborne, and Hawke's Bay, while above-normal rainfall (120%–149% of normal) was observed throughout these same areas, as well as much of eastern Wairarapa, the eastern Tararua District, and the Bay of Plenty. Near-normal rainfall (80%–119% of normal) was observed for the rest of the country, except for small and isolated areas of below-normal rainfall (50%–79% of normal) in the Central Plateau, the West Coast, South Canterbury, and eastern Otago.

Despite the several extreme rainfall events that occurred throughout the first part of the year, 2023 was only New Zealand's 21st-wettest year on record, based on an analysis of areal-averaged rainfall anomalies from NIWA's Virtual Climate Station Network (VCSN) dating back to 1961. The nationwide rainfall anomaly in the VCSN was 104% of normal compared to the 1991–2020 normal. Of all the regularly reporting gauges, the wettest location in 2023 was Cropp River (West Coast), at 975 m a.s.l with 11,717 mm. The driest of the regularly reporting rainfall sites in 2023 was Ranfurly in the Otago region of the South Island, which reported only 359 mm.

(iii) Notable events and impacts

On 27 January, a highly localized convective weather system delivered unprecedented rainfall amounts in an event dubbed the "Auckland Anniversary Floods." Within 12 hours, over 200 mm was observed at Māngere and Auckland Airport, with hourly rainfall rates as high as 73 mm recorded. Auckland Airport was severely flooded, with floodwaters throughout the terminal buildings forcing the airport to temporarily close. Tens of thousands of travelers were impacted

by canceled and diverted flights. A state of emergency was declared in Auckland. Largely due to this event, the homogenized central Auckland rainfall series (Fowler 2021) recorded a January total of 539 mm at Albert Park, shattering the previous all-months record of 420 mm from February 1869. Rainfall data from this series began in 1853.

From 12 to 15 February, Post-Tropical Cyclone Gabrielle hit New Zealand, resulting in 11 fatalities, widespread flooding, and extensive damage to key infrastructure in the east coast of the North Island, including roads, electricity, telecommunication, and water infrastructure. A National State of Emergency was declared for only the third time in New Zealand's history. At the height of the cyclone's impact, around 225,000 homes were without power, and thousands of people were displaced as flood waters rose. In the worst-affected areas, there was significant damage to agricultural land, property, and livelihoods. Gabrielle ranks as one of the costliest natural disasters in New Zealand history, with over $16 billion New Zealand dollars ($9.5 billion U.S. dollars) of costs to the insurance industry.

Powerful winds associated with Gabrielle brought considerable damage to forestry areas in the central North Island. Nine sites recorded their strongest gust on record during 12 and 13 February, including a 124 km h^{-1} gust at Mount Ruapehu Chateau. Over 6000 hectares of pine was destroyed due to these powerful winds, possibly by a sting jet (a narrow, transient, and mesoscale airstream that descends from the mid-troposphere to the surface in some extratropical cyclones).

Exceptional flooding was seen in Hawke's Bay due to Gabrielle, particularly in Esk Valley, Hastings, where floodwater levels reached nearly to the roofs of homes and trapped dozens of people. Tareha recorded 561 mm in 24 hours on 13 February, the highest 24-hour rainfall total to be recorded in 2023 from a low-elevation station. During the event, 22 stations set new February daily rainfall records, including Whangārei (216 mm), parts of Auckland (147 mm), Napier (176 mm), and Hastings (126 mm). Entire communities were cut off due to floodwaters in Hawke's Bay and Gisborne.

Auckland, Gisborne, and Napier all experienced their wettest year on record as a result of these major rainfall events. The record for Napier is particularly noteworthy, as rainfall observations began in 1870.

Acknowledgments

Europe

Much of the information in this section is based on national climate reports kindly provided by the National Meteorological and Hydrological Services (NMHSs) of the World Meteorological Organization (WMO) Regional Association (RA) VI region. The information has been compiled at the WMO RA VI Regional Climate Centre (RCC) Node on Climate Monitoring, located at Deutscher Wetterdienst (DWD) in Germany. National contributions have been made to the cooperation between NMHSs and the RCC. https://rcccm.dwd.de/DWD-RCCCM/EN/products/reports/monthlyreports_national.html?nn=500112

Oceania

The editors wish to thank the numerous NMHSs for collecting and providing data for this report. Special thanks to all the authors in this section for their timely contributions, and the thoughtful and constructive comments from the internal and external reviewers and document editors. Data centers such as NCEP/NCAR, ECMWF-ERA, and CHIRPS are also acknowledged for making their data freely available.

The Oceania editor would like to acknowledge and thank Nava Fedaeff of the National Institute of Water and Atmospheric Research for stepping in and assisting with reviewer comments while her colleague was on leave welcoming his first child into the world.

Appendix 1: Acronyms

ANDMA	Afghanistan National Disaster Management Authority
ARCS	Afghan Red Crescent Society
C3S	Copernicus Climate Change Service
CA	Central America
CA	Central Asia
CAMS	Climate Anomaly Monitoring System
CA-NWS	Central America National Weather Service
CAR	Central African Republic
CDI	Combined Drought Indicator
CNMI	Commonwealth of the Northern Mariana Islands
CONUS	contiguous United States
DMH	Dirección de Meteorologia e Hidrologia
DRC	Democratic Republic of the Congo
DWD	Deutscher Wetterdienst
ECCC	Environment and Climate Change Canada
EHD	extreme high-temperature days
ENSO	El Niño–Southern Oscillation
FWI	Fire Weather Index
GPCC	Global Precipitation Climatology Centre
IOD	Indian Ocean dipole
LPB	Parana-La Plata basin
LTA	long-term average
LTM	long-term mean
NAO	North Atlantic Oscillation
NCEP/NCAR	National Centers for Environmental Prediction/National Center for Atmospheric Research
NCT	Tmax averaged over North China
NEM	northeast monsoon
NIWA	National Institute of Water and Atmospheric Research
NMHS	National Meteorological and Hydrological Service
NS	Nova Scotia
OCHA	Office for the Coordination of Humanitarian Affairs
OLR	outgoing longwave radiation
PM2.5	fine particulate matter
PMM	Pacific Meridional Mode
PNG	Papua New Guinea
RA VI	Regional Association VI
RCC-CM	Regional Climate Centre on Climate Monitoring
RFE2	satellite rainfall estimates version 2
RMI	Republic of the Marshall Islands
ROK	Republic of Korea
ROP	Republic of Palau
SAM	Southern Annular Mode
SOI	Southern Oscillation Index
SPCZ	South Pacific Convergence Zone
SSA	southern South America
SST	sea surface temperature

TAP	tropical Atlantic
TC	tropical cyclone
TIS	tropical Indian Ocean SST
Tm	mean temperature
Tmax	daily maximum
VCSN	Virtual Climate Station Network
WMO	World Meteorological Association
WWB	westerly wind burst

Appendix 2: Supplemental materials

Appendix Table 7.1. Maximum temperatures (TMax; °C) observed in central South America during heatwaves from August to November 2023. Long-term mean (LTM) is 1991–2020. (Sources: Peru: Servicio Nacional de Meteorología e Hidrología del Perú [SENAMHI]; Bolivia: Servicio Nacional de Meteorología e Hidrología del Bolivia [SENAMHI]; Brazil: Instituto Nacional de Meteorlogia [INMET]; Paraguay: Dirección de Meteorología e Hidrología [DMH].) A standalone dash indicates the information was not available.

August Heatwave 2023			
Location	Date	TMax	LTM
BRAZIL, Cuiabá	08/20	41.8	34.7
BRAZIL, São Paulo	08/23	32.3	24.5
BRAZIL, Rio de Janeiro	08/22	38.7	27.0
BOLIVIA, Magdalena	08/22	39.2	33.7
BOLIVIA, Guajaramirim	08/24	39.0	33.7
BOLIVIA, Ascensión de Guarayos	08/31	39.7	30.8

September Heatwave 2023			
Location	Date	TMax	LTM
BRAZIL, São Paulo	09/24	36.5	25.2
BRAZIL, São Paulo	09/23	34.8	25.2
BRAZIL, Curitiba	09/23	31.8	22.3
BRAZIL, Goiania	09/23	38.0	34.0
BRAZIL, Cuiabá	09/23	41.2	35.6
BRAZIL, Rio Branco	09/23	37.1	33.7
BRAZIL, Belém	09/23	36.3	33.2
BRAZIL, Belo Horizonte	09/25	37.5	29.9
BRAZIL, Brasília	09/25	34.8	29.1
BOLIVIA, Cobija	09/24	**39.8**	33.2
BOLIVIA, San Borja	09/24	40.4	32.8
BOLIVIA, Magdalena	09/25	**40.3**	34.1
BOLIVIA, San Joaquin	09/25	40.2	33.9
BOLIVIA, Puerto Suarez	09/26	41.3	31.9

Location	Date	TMax	LTM
BOLIVIA, San José de Chiquitos	09/26	42.7	33.7
BOLIVIA, La Paz-Laykacota	09/26	**27.5**	19.7
BOLIVIA, San Ramón	09/27	39.8	28.9
PARAGUAY, Mariscal Estigarribia	09/24	43.6	32.7
PARAGUAY, Paraguari	09/24	39.6	27.3
PARAGUAY, Villarica	09/24	38.6	27.3
PARAGUAY, Aer. Int Guarani	09/24	39.6	27.5
PARAGUAY, Caazapá	09/24	38.5	26.4
PARAGUAY, Capitan Meza	09/24	38.8	25.7
PARAGUAY, Encarnación	09/24	37.6	26.1
PARAGUAY, Pedro Juan Caballero	09/24	38.6	28.6
PARAGUAY, Puerto Casado	09/24	42.0	31.7
PERU, Papayal	09/25	35.8	28.6
PERU, Tingo de Ponaza	09/27	41.4	33.5
PERU, Chichas	09/24	28.3	–
PERU, Tabaconas	09/27	28.5	–
PERU, San Ignacio	09/28	33.4	–
PERU, Chichas	09/24	28.3	–

October Heatwave 2023

Location	Date	TMax	LTM
BRAZIL, Manaus	10/10	40.0	33.4
BRAZIL, Tarauaca	10/04	39.4	–
BRAZIL, Codajas	10/09	38.8	–
BRAZIL, Benjamin Constant	10/01	40.0	–
BRAZIL, Goiania	10/07	41.2	–
BRAZIL, Cuiaba	10/19	44.2	–
BOLIVIA, La Paz-Laykacota	10/08	**28.9**	20.5
BOLIVIA, Villamontes	10/16	46.5	34.3

Location	Date	TMax	LTM
BOLIVIA, Ascensión de Guarayos	10/19	41.5	32.7
BOLIVIA, Magdalena	10/19	**40.6**	33.8
BOLIVIA, San José de Chiquitos	10/19	**43.7**	34.7
BOLIVIA, Trinidad	10/22	41.5	33.1
PARAGUAY, Pedro Juan Caballero	10/17	38.0	29.8
PARAGUAY, Mariscal Estigarribia	10/23	43.6	35.1
PERU, Iñapari	10/24	39.0	33.2
PERU, Trujillo	10/22	27.2	21.8
PERU, Yungay	10/24	28.8	–
PERU, Rincon de la Cruz	10/28	21.6	–
PERU, Tahuaco-Yunguyo	10/11	21.0	–
PERU, Ayabaca	10/17	23.2	–

November Heatwave 2023

Location	Date	TMax	LTM
BRAZIL, Itacoatiara	11/08	39.2	–
BRAZIL, Rio de Janeiro	11/12	40.4	29.4
BRAZIL, Cuiaba	11/12	39.6	33.6
BRAZIL, Teresina	11/12	38.9	36.2
BRAZIL, Belo Horizonte	11/12	35.3	27.7
BRAZIL, Florianopolis	11/12	30.8	26.0
BRAZIL, Brasilia	11/12	32.9	26.7
BRAZIL, São Paulo	11/12	37.1	26.9
BRAZIL, Porto Murtinho	11/11	42.3	33.0
BRAZIL, Araçuaí	11/20	44.8	32.0
BRAZIL, Lavras	11/14	38.2	–
BRAZIL, Salinas	11/18	41.8	–
BOLIVIA, San Borja	11/10	41.2	32.5
BOLIVIA, Yacuiba	11/12	**44.9**	30.9

Location	Date	TMax	LTM
BOLIVIA, San Matias	11/13	42.8	34.3
BOLIVIA, Puerto Suarez	11/16	**43.5**	33.3
BOLIVIA, Cochabamba Aero	11/17	**36.2**	28.9
BOLIVIA, Santa Ana de Yacuma	11/18	39.5	32.5
BOLIVIA, Trinidad	11/18	41.3	32.3
BOLIVIA, San Ramón	11/17	39.5	32.6
BOLIVIA, San José de Chiquitos	11/08	44.1	33.7
BOLIVIA, Pto Suarez	11/16	43.5	33.3
BOLIVIA, Riberalta	11/17	39.3	32.6
BOLIVIA, San Ignacio de Moxos	11/17	38.9	32.2
PARAGUAY, Mariscal Estigarribia	11/8, 11/12	44.5	35.7
PARAGUAY, Perto Casado	11/12	42.0	32.4
PARAGUAY, Pedro Juan Caballero	11/12	39.2	29.9
PARAGUAY, Concepción	11/17	42.2	32.4
PERU, Cajatambo	11/10	20.6	–
PERU, Palca	11/14	24.6	–

Appendix Table 7.2. Temporal coverage of nationally averaged temperature and precipitation in situ observations for Europe / World Meteorological Organization (WMO) Regional Association (RA) VI region. For some countries, only one station (preferably with a long time series) has been used (name of the location in brackets). A standalone dash indicates that the information was not available.

Nation	Temperature start of record	Precipitation start of record	Source	Temperature anomaly (°C)	Rank (ordered from warmest [1] to coldest)	Precipitation anomaly (annual total in % of normal)	Rank (ordered from wettest [1] to driest)
European average	1950	1881	GHCN data (temperature), GPCC (precipitation)	+0.95	1–2	95%	91
Albania (Korce)	1963	1963	–	–	–	–	–
Andorra	1950	1950	NMHS[1]	–	–	–	–
Armenia	1935	1935	NMHS	+2.2	3	97%	49
Austria	1767	1858	NMHS	+1.2	1	117%	7
Azerbaijan (Astara)	1991	1991	–	–	–	–	–
Belarus	1881	1945	NMHS	+1.4	3	–	–
Belgium	1981	1981	NMHS	+1.1	3	174%	11
Bosnia & Herzegovina (Sarajevo)	1961	1961	NMHS	+1.3	1	116%	10
Bulgaria	1930	1930	NMHS	+1.0	1	96%	52
Croatia (Nicosia)	1961	1961	NMHS	–	1	116%	–
Cyprus	1899	1916	NMHS	+1.2	5	82%	102
Czechia	1961	1961	NMHS	+1.4	1	107%	15
Denmark	1873	1874	NMHS	+1.2	3	129%	1
Estonia	1922	1961	NMHS	+0.8	6–9	104%	20
Finland (Helsinki)	1900	1961	NMHS	+0.3	22	112%	8
France	1900	1959	NMHS	+1.4	2	104%	24
Georgia	1956	1881 (Tbilisi)	NMHS	+1.3	3	113%	11
Germany	1881	1881	NMHS	+2.4	1	169%	6
Greece	1960	1960	NMHS	+1.3	1	91%	54
Hungary	1901	1901	NMHS	+1.5	1	125%	8

Nation	Temperature start of record	Precipitation start of record	Source	Temperature anomaly (°C)	Rank (ordered from warmest [1] to coldest)	Precipitation anomaly (annual total in % of normal)	Rank (ordered from wettest [1] to driest)
Iceland	1900 (Stykkishólmur)	1921 (Reykjavik)	NMHS	–0.1	–	91%	–
Ireland	1900	1900	NMHS	+1.0	1	117%	3
Israel	1951	1935 (Deganya)	NMHS	+1.0	3	90%	34
Italy	1961	1961	NMHS	+1.1	2	96%	28
Jordan (Amman)	1923	1923	NMHS	+1.0	5	135%	20
Kazakhstan	1941	1941	NMHS	+1.9	1	85%	6
Latvia	1924	1924	NMHS	+1.0	3	112%	13
Lebanon (Beirut)	1949	1949	–	–	–	–	–
Lithuania	1961	1887 (Vilnius)	NMHS	+1.3	3	103%	20
Luxembourg (Findel)	1838	1854	NMHS	+1.0	2	234%	8
Malta (Luqa)	1923	1949	NMHS	+0.7	1	99%	97
Moldova (Chisinau)	1886	1891	NMHS	+1.9	1	78%	–
Monaco	1966	1966	NMHS	+1.2	2	55%	53
Montenegro (Podgorica)	1949	1949	NMHS	+2.34	2	109%	2
Netherlands	1901	1901	NMHS	–	1	–	–
North Macedonia	1981	1981	NMHS	+1.2	4	112%	13
Norway	1900	1900	NMHS	–0.1	37	105%	13
Poland	1951	1951	NMHS	+1.3	2	145%	17
Portugal	1931	1931	NMHS	+1.0	2	87%[5]	25
Romania	1961	1961	NMHS	+1.6	1	99%	31
Russia, European part	1936	1936	NMHS	+1.3	1	111%	4
Serbia	1951	1951	NMHS	+1.5	1	119%	6

Nation	Temperature start of record	Precipitation start of record	Source	Temperature anomaly (°C)	Rank (ordered from warmest [1] to coldest)	Precipitation anomaly (annual total in % of normal)	Rank (ordered from wettest [1] to driest)
Slovakia	1951	1961	NMHS	+1.3	2	125%	2
Slovenia	1961	1961	NMHS	+1.3	1	410%	3
Spain	1961	1961	NMHS	+1.3[3]	2	84%	57
Sweden	1860	1880	NMHS	+0.2	22	113%	4
Switzerland	1864	1864	NMHS	+1.4	2	112%	20
Syrian Arab Republic (Aleppo)	1960	1960	–	–	–	–	–
Türkiye	1971	1991	NMHS	+1.2	3	112%	–
Ukraine (Kyiv and Kharkiv)	1891	1891	NMHS	+1.8	2	108%	19
United Kingdom	1884	1836	NMHS	+0.8	2	111%	11

[1] NMHS = National Meteorological and Hydrological Service; for individual names of NMHSs see https://public.wmo.int/en/about-us/members

[2] reference period 1961–1990

[3] reference period 1981–2010

References

Alvala, R., D. F. Ribeiro, J. A. Marengo, M. E. Seluchi, D. A. Gonçalves, L. Antunes da Silva, L. A. Cuartas Pineda, S. M. Saito, 2024: Analysis of the hydrological disaster that occurred in the state of Rio Grande do Sul in September 2023: Vulnerabilities and risk management capabilities. *Int. J. Disaster Risk Reduct.*, **110**, 104645, https://doi.org/10.1016/j.ijdrr.2024.104645.

Amador, J. A., 1998: A climatic feature of the tropical Americas: The trade wind easterly jet. *Top. Meteor. Oceanogr.*, **5**, 91–102.

—— , 2008: The Intra-Americas Seas Low-Level Jet (IALLJ): Overview and future research. *Ann. N. Y. Acad. Sci.*, **1146**, 153–188, https://doi.org/10.1196/annals.1446.012.

—— , E. J. Alfaro, H. Hidalgo, and B. Calderon, 2011: Central America and the Caribbean [in "State of the Climate in 2010"]. *Bull. Amer. Meteor. Soc.*, **92** (6), S182–S183, https://doi.org/10.1175/1520-0477-92.6.S1.

—— , E. R. Rivera, A. M. Durán-Quesada, G. Mora, F. Sáenz, B. Calderón, and N. Mora, 2016a: The easternmost tropical Pacific. Part I: A climate review. *Rev. Biol. Trop.*, **64** (Suppl. 1), S1–S22, https://doi.org/10.15517/rbt.v64i1.23407.

—— , A. M. Durán-Quesada, E. R. Rivera, G. Mora, F. Sáenz, B. Calderón, and N. Mora, 2016b: The easternmost tropical Pacific. Part II: Seasonal and intraseasonal modes of atmospheric variability. *Rev. Biol. Trop.*, **64** (Suppl. 1) S23–S57, https://doi.org/10.15517/rbt.v64i1.23409.

Arias, P. A., and Coauthors, 2024: Interplay between climate change and climate variability: The 2022 drought in Central South America. *Clim. Change*, **177**, 6, https://doi.org/10.1007/s10584-023-03664-4.

Ashok, K., Z. Guan, and T. Yamagata, 2003: Influence of the Indian Ocean dipole on the Australian winter rainfall. *Geophys. Res. Lett.*, **30**, 1821, https://doi.org/10.1029/2003GL017926.

Beck, H. E., E. F. Wood, M. Pan, C. K. Fisher, D. G. Miralles, A. I. J. M. van Dijk, T. R. McVicar, and R. F. Adler, 2019: MSWEP V2 global 3-hourly 0.1° precipitation: Methodology and quantitative assessment. *Bull. Amer. Meteor. Soc.*, **100**, 473–500, https://doi.org/10.1175/BAMS-D-17-0138.1.

Beltrando, G., and P. Camberlin, 1993: Interannual variability of rainfall in the eastern Horn of Africa and indicators of atmospheric circulation. *Int. J. Climatol.*, **13**, 533–546, https://doi.org/10.1002/joc.3370130505.

CatIQ, 2024: CatIQ: Canada's loss and exposure indices provider. Accessed 29 February 2024, https://public.catiq.com/.

CCRIF SPC, 2023a: Covered area rainfall event (08/06/2023 to 13/06/2023) excess rainfall event briefing the Bahamas central. Caribbean Catastrophe Risk Insurance Facility, 14 pp., https://www.ccrif.org/sites/default/files/publications/eventreports/20230622_CCRIF_XSR_EventBriefing_BHS_C_CARE_20230608-13_Final.pdf.

—— , 2023b: Tropical cyclone Bret (AAL032023) final event briefing reportable event St. Lucia electricity services limited. Caribbean Catastrophe Risk Insurance Facility, 6 pp., https://www.ccrif.org/sites/default/files/publications/eventreports/20230703_CCRIF_FinalEventBriefing_TC_Bret_CPU_LCA_Final.pdf.

—— , 2023c: Covered area rainfall event (02/10/2023 to 05/10/2023) Dominica excess rainfall event briefing. Caribbean Catastrophe Risk Insurance Facility, 12 pp., https://www.ccrif.org/sites/default/files/publications/eventreports/20231012_CCRIF_XSR_EventBriefing_DMA_CARE_2-5October2023_Final.pdf.

—— , 2023d: Covered area rainfall event (3/10/2023 to 4/10/2023) Antigua and Barbuda excess rainfall event briefing. Caribbean Catastrophe Risk Insurance Facility, 14 pp., https://www.ccrif.org/sites/default/files/publications/eventreports/20231010_CCRIF_XSR_EventBriefing_ATG_CARE_20231010_Final.pdf.

—— , 2023e: Covered area rainfall event (16/11/2023 to 19/11/2023) excess rainfall event briefing Jamaica. Caribbean Catastrophe Risk Insurance Facility, 12 pp., https://www.ccrif.org/sites/default/files/publications/eventreports/20231128_CCRIF_XSR_EventBriefing_JAM_CARE_16Nov2023_Final.pdf.

Chen, J., K. Anderson, R. Pavlovic, M. D. Moran, P. Englefield, D. K. Thompson, R. Munoz-Alpizar, and H. Landry, 2019: The FireWork v2.0 air quality forecast system with biomass burning emissions from the Canadian Forest Fire Emissions Prediction System v2.03. *Geosci. Model Dev.*, **12**, 3283–3310, https://doi.org/10.5194/gmd-12-3283-2019.

CIFFC, 2023: Canadian Interagency Forest Fire Centre. https://ciffc.net/.

Costa, F., and J. Marengo, 2023: Statement on the 2023 Amazon drought and its unforeseen consequences. SPA Scientific-Technical Secretariat, 8 December, https://www.theamazonwewant.org/spa_publication/statement-on-the-2023-amazon-drought/.

Delforge, D., V. Wathelet, R. Below, C. L. Sofia, M. Tonnelier, J. van Loenhout, and N. Speybroeck, 2023: EM-DAT: The Emergency Events Database. https://doi.org/10.21203/rs.3.rs-3807553/v1.

DGE, 2023: Temperaturas naturales extremas (Temporada de calor 2023). Dirección General de Epidemiología, 11 pp., www.gob.mx/cms/uploads/attachment/file/847069/TNE_2023_SE30.pdf.

ECCC, 2024: Canada's top 10 weather stories of 2023. Accessed 29 February 2024, https://www.canada.ca/en/environment-climate-change/services/top-ten-weather-stories/2023.html.

EPA, 2023: Canadian wildfires prompt poor air quality alert for parts of New England on June 7, 2023. United States Environmental Protection Agency, accessed 13 February 2024, https://www.epa.gov/newsreleases/canadian-wildfires-prompt-poor-air-quality-alert-parts-new-england-june-7-2023.

Espinoza, J. C., J. C. Jimenez, J. Á. Marengo, J. Schongart, J. Ronchail, W. Lavado, and J. B. M. Ribeiro, 2024: The new record of drought and warmth in the Amazon in 2023 related to regional and global climatic features. *Sci. Rep.*, **14**, 8107, https://doi.org/10.1038/s41598-024-58782-5

Evans, A., D. Jones, R. Smalley, and S. Lellyett, 2020: An enhanced gridded rainfall analysis scheme for Australia. Bureau of Meteorology Research Rep. 41, 38 pp., http://www.bom.gov.au/research/publications/researchreports/BRR-041.pdf.

Fowler, A. M., 2021: Central Auckland rainfall, 1853-2020: Towards a homogenous record. *J. Hydrol.*, **60** (1), 25–47, https://www.hydrologynz.org.nz/journal/volume-60-2021.

Funk, C., and Coauthors, 2015: The Climate Hazards Infrared Precipitation with Stations —— A new environmental record for monitoring extremes. *Sci. Data*, **2**, 150066, https://doi.org/10.1038/sdata.2015.66.

Guardamino Soto, B., 2023: Puno: Continuo descenso del lago Titicaca y sequía del 84% de totorales causan preocupación en la region. Infobae, 26 September, https://www.infobae.com/peru/2023/09/26/puno-continuo-descenso-del-lago-titicaca-y-sequia-del-84-de-totorales-causan-preocupacion-en-la-region/.

Gutierrez, R. A., J. C. Espinoza, W. Lavado, C. Junquas, J. Molina-Carpio, T. Condom, and J. A. Marengo, 2024: The 2022-23 drought in the South American Altiplano: ENSO effects on moisture flux in the western Amazon during the pre-wet season. *Wea. Climate Extremes*, **45**, 100710. https://doi.org/10.1016/j.wace.2024.100710.

Hendon, H. H., D. W. Thompson, and M. C. Wheeler, 2007: Australian rainfall and surface temperature variations associated with the Southern Hemisphere annular mode. *J. Climate*, **20**, 2452–2467, https://doi.org/10.1175/JCLI4134.1.

Hersbach, H., and Coauthors, 2020: The ERA5 global reanalysis. *Quart. J. Roy. Meteor. Soc.*, **146**, 1999–2049, https://doi.org/10.1002/qj.3803.

Hidalgo, H., E. Alfaro, J. Amador, and A. Bastidas, 2019: Precursors of quasi-decadal dry-spells in the Central America Dry Corridor. *Climate Dyn.*, **53**, 1307–1322, https://doi.org/10.1007/s00382-019-04638-y.

Jain, P., and Coauthors, 2024: Canada under fire – Drivers and impacts of the record-breaking 2023 wildfire season. *ESS Open Archive*, https://doi.org/10.1038/s41467-024-51154-7.

Jones, D. A., W. Wang, and R. Fawcett, 2009: High-quality spatial climate data-sets for Australia. *Aust. Meteor. Oceanogr. J.*, **58**, 233–248, https://doi.org/10.22499/2.5804.003.

Lee, M., T. Kim, D. H. Cha, S. K. Min, D. S. R. Park, S. W. Yeh, and J. C. Chan, 2021: How does Pacific decadal oscillation affect tropical cyclone activity over far East Asia? *Geophys. Res. Lett.*, **48**, e2021GL096267, https://doi.org/10.1029/2021GL096267.

Lowe, S. R., and D. R. Garfin, 2023: Crisis in the air: The mental health implications of the 2023 Canadian wildfires. *Lancet Planet. Health*, **7**, e732–e733, https://doi.org/10.1016/S2542-5196(23)00188-2.

Mao, W., R. Shalaby, B. Agyapong, G. Obuobi-Donkor, R. Da Luz Dias, and V. I. O. Agyapong, 2024: Devastating wildfires and mental health: Major depressive disorder prevalence and associated factors among residents in Alberta and Nova Scotia, Canada. *Behav. Sci.*, **14**, 209, https://doi.org/10.3390/bs14030209.

Marengo, J. A., and Coauthors, 2024: Heavy rains and hydrogeological disasters on February 18th–19th, **2023**, in the city of São Sebastião, São Paulo, Brazil: From meteorological causes to early warnings. *Nat. Hazards*, **120**, 7997–8024, https://doi.org/10.1007/s11069-024-06558-5.

Magaña, V., J. A. Amador, and S. Medina, 1999: The mid-summer drought over México and Central America. *J. Climate*, **12**, 1577–1588, https://doi.org/10.1175/1520-0442(1999)012<1577:TMDOMA>2.0.CO;2.

Matz, C. J., M. Egyed, G. Xi, J. Racine, R. Pavlovic, R. Rittmaster, S. B. Henderson, and D. M. Stieb, 2020: Health impact analysis of $PM_{2.5}$ from wildfire smoke in Canada (2013–2015, 2017–2018). Sci. *Total Environ.*, **725**, 138506, https://doi.org/10.1016/j.scitotenv.2020.138506.

National Drought Mitigation Center, 2024: North American Drought Monitor: Maps. Accessed 10 May 2024, https://droughtmonitor.unl.edu/NADM/Maps.aspx.

NOAA/NCEI, 2024: Billion-dollar weather and climate disasters: Overview. Accessed 2 February 2024, https://www.ncei.noaa.gov/access/billions/.

Public Health Agency of Canada, 2023: Public health risk profile: Wildfires in Canada, 2023. Accessed 8 May 2024, https://www.canada.ca/en/public-health/services/emergency-preparedness-response/rapid-risk-assessments-public-health-professionals/risk-profile-wildfires-2023.html.

SENAMHI, 2023: Boletín hidrológico mensual a nivel nacional: Septiembre 2023. SENAMHI, 12 pp., https://www.senamhi.gob.pe/load/file/02609SENA-147.pdf.

McKay, R. C., J. M. Arblaster, and P. Hope, 2022: Tropical influence on heat-generating atmospheric circulation over Australia strengthens through spring. *Wea. Climate Dyn.*, **3**, 413–428, https://doi.org/10.5194/wcd-3-413-2022.

—— , and Coauthors, 2023: Can southern Australian rainfall decline be explained? *A review of possible drivers. Wiley Interdiscip. Rev.: Climate Change*, **14**, e820, https://doi.org/10.1002/wcc.820.

NAFI, 2024: Fire maps. North Australia and Rangelands Fire Information, https://firenorth.org.au/nafi3/.

Scoccimarro, E., G. Villarini, S. Gualdi, and A. Navarra, 2021: The Pacific Decadal Oscillation modulates tropical cyclone days on the interannual timescale in the North Pacific Ocean. *J. Geophys. Res. Atmos.*, **126**, e2021JD034988, https://doi.org/10.1029/2021JD034988.

Singh, D., and Coauthors, 2023: Focus on compound events. *Fifth National Climate Assessment*, A. R. Crimmins et al., Eds., U.S. Global Change Research Program, https://doi.org/10.7930/NCA5.2023.F1.

Skakun, R., G. Castilla, J. Metsaranta, E. Whitman, S. Rodrigue, J. Little, K. Groenewegen, and M. Coyle, 2022: Extending the National Burned Area Composite time series of wildfires in Canada. *Remote Sens.*, **14**, 3050, https://doi.org/10.3390/rs14133050.

Smith, A. B., 2024: 2023: A historic year of U.S. billion-dollar weather and climate disasters. NOAA/NCEI, accessed 2 February 2024, https://www.climate.gov/news-features/blogs/beyond-data/2023-historic-year-us-billion-dollar-weather-and-climate-disasters.

SPC, 2024: Tornado totals and related deaths. NOAA/National Weather Service, accessed 2 February 2024, https://www.spc.noaa.gov/climo/torn/STAMTS23.txt.

Thompson, D. W. J., M. P. Baldwin, and S. Solomon, 2005: Stratosphere–troposphere coupling in the Southern Hemisphere. *J. Atmos. Sci.*, **62**, 708–715, https://doi.org/10.1175/JAS-3321.1.

Toreti, A., and Coauthors, 2023: Drought in the Amazon basin November 2023. JRC Tech. Rep. 136439, European Commission, 28 pp., https://doi.org/10.2760/756827.

Trewin, B., 2018: The Australian Climate Observations Reference Network–Surface Air Temperature (ACORN-SAT) version 2. Bureau of Meteorology Research Rep. 032, 67 pp., http://www.bom.gov.au/research/publications/researchreports/BRR-032.pdf.

Zhang, W., G. A. Vecchi, H. Murakami, G. Villarini, and L. Jia, 2016: The Pacific meridional mode and the occurrence of tropical cyclones in the western North Pacific. *J. Climate*, **29**, 381–398, https://doi.org/10.1175/JCLI-D-15-0282.1.